Universidade do Minho
Escola de Engenharia

Duarte Manuel Azevedo Fernandes

Power Saving Mechanisms for firefighters monitoring Wireless Body Networks

June, 2018

Power Saving Mechanisms for firefighters monitoring Wireless Body Networks
Duarte Manuel Azevedo Fernandes
UMinho | 2018

FCT
Fundação para a Ciência e a Tecnologia
MINISTÉRIO DA EDUCAÇÃO E CIÊNCIA

POPH
QUALIFICAR É CRESCER.

QREN
QUADRO DE REFERÊNCIA ESTRATÉGICO NACIONAL
PORTUGAL 2007.2013

Governo da República Portuguesa

UNIÃO EUROPEIA
Fundo Social Europeu

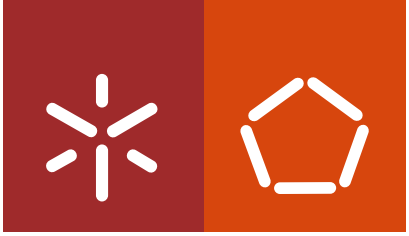

Universidade do Minho
Escola de Engenharia

Duarte Manuel Azevedo Fernandes

Power Saving Mechanisms for firefighters monitoring Wireless Body Networks

Philosophy Doctorate Thesis
Electronic and Computers Engineering

Work conducted under supervision of:
Professor Doctor José Araújo Mendes
Professor Doctor Jorge Miguel Nunes dos Santos Cabral

June, 2018

STATEMENT OF INTEGRITY

I hereby declare having conducted my thesis with integrity. I confirm that I have not used plagiarism or any form of falsification of results in the process of the thesis elaboration.

I further declare that I have fully acknowledged the Code of Ethical Conduct of the University of Minho.

University of Minho, 11th of June 2018

Full name: Duarte Manuel Azevedo Fernandes

Signature: Duarte Manuel Azevedo Fernandes

ACKNOWLEDGMENTS

I wish to express my sincere gratitude to my advisor, Professor Jorge Cabral, for his supervision, guidance throughout this study and for the freedom to explore new ideas. His invaluable suggestions, constructive criticism and contribute on the writing of this academic work enabled the author to present this thesis in this form. My sincere gratitude to my advisor, Professor José Mendes, for his support and encouragement.

I would like to also thank to all PROTACTICAL working group members, especially Professor Ana M. Rocha for the valuable scientific guidelines and financial support.

I would like to thank to my friends Filipe Lima and Reza Abrishambaf that were a great influence to me. Not only helped me revising some articles, but they have also shared their experience with me, showing me that all the constant uncertainties, doubts and failures during the course of this study are natural and should be seen as part of the recipe for success.

I wish to thank to two important persons in my life, my mother and my best-friend but also brother João Pedro, for all their unconditional love, support, encouraging and huge patient especially during the last four years.

I want to thank to my soulmate Mariana Lima for her patient, support and for believing in me more than I do. It was arguably the source of my motivation, making you proud of myself is the best reward I can receive.

Many thanks to my colleagues and friends André Ferreira, Shafagh Tohidi, Lila Maciel Pires and Paz for the incredible atmosphere that they have created at the laboratory for me. It has been a pleasant and gratifying experience to share this physical space with you over the past few years.

Finally, the last but not least my friends including but not limited to Lazaro Vidal, José Barbosa, Catarina Araújo and Sérgio Branco for their friendship and many joyful moments shared over the past years.

This work was supported by the Foundation for Science and Technology (FCT) of Portugal under Grant SFRH/BD/92082/2012.

ABSTRACT

Wireless radio channels are typically unstable medium for communications. However, due to the advent of nodes attached to the human body, the radio channel conditions experienced by the wearable nodes are quite unique in comparison to those experienced in traditional networks, such as Wireless Sensor Networks (WSNs). Wireless Body Area Networks (WBAN) are being deployed for an ever-increasing number of applications, however, the time-variant nature of the signal attenuation, phenomenon designated as fading, promotes data packet loss and hampers the WBANs of reaching their full potential.

The goals of this thesis are threefold: first, we explore emergent technologies in the field of sensing such as non-intrusive wireless-enabled nodes and electrodes embedded in textile structures (e-textiles) to develop a WBAN for long-term monitoring of the user. This network is integrated into a Cyber-Physical System (CPS) which combines sensing, actuating, communications, networking, computing and control technologies to provide a better awareness of the on-going firefighting mission and to improve the safety of all elements of an emergency response team.

Second, we aim to establish a better comprehension of the impact that WBAN operation scenarios have on intra-WBAN communications. Following a scenario-based radio channel characterization, it is proved that large-scale fading is the predominant effect in on-body communications. In addition, this effect varies according to the edge of the Network node location. For instance, when they are located at limbs (e.g. the user's wrist), the mobility of the nodes leads the on-body links to frequent commutations between line (LOS) and non-line of sight (NLOS), which results on fading magnitudes of around -18 dB for 2.45 GHz communications. The Edge of the Network node located at the user's wrist ensures both reliability and latency requirements for most of the scenarios, but with an inefficient use of the energy available. Furthermore, in-depth analysis of the on-body wave's propagation shows that fading signal component follows a regular pattern during periodic user's activities that matches with the user's gait cycle period.

Third, the challenges associated to intra-WBAN communications encouraged the investigation on strategies able to ensure reliability with minimum effect on other performance aspects. A Transmission Power Control (TPC) mechanism designated Proactive-TPC (P-TPC) that employs a hybrid operation principle and targets resource-constrained nodes is proposed. This solution relies on RSSI samples to approximate the fading signal during the user's gait cycle, while the instant within the on-going gait cycle is determined using an acceleration

signal. Then, the minimum radio output power, called transmission power level (TPL), needed to ensure a successful data packet delivery is estimated. The proposed P-TPC mechanism consumes nearly 35% less energy than communication systems transmitting at maximum TPL allowable on on-body communications (0 dBm). At same time, specific absorption rate (SAR) and probability of inter-network interference are improved. The P-TPC is suitable for emergency network traffic as the reliability requirement is ensured in an energy-efficient way and without sacrificing latency.

A novel packet scheduler mechanism called by Power Control and Packet Scheduler (PCPS) is proposed. The advantages of Neural Networks and Fuzzy Inference Systems for modelling nonlinear dynamical systems are explored. Therefore, a model that describes the on-body channel as a function of operating environment, the relative position of the user's arm, and the body posture is proposed. The PCPS mechanism improves the communication reliability (this approach assures around 10% less data packet loss than communications carried out at 0 dBm) at the expense of the latency, making this solution suitable for regular network traffic. Thus, this mechanism shows that unreliable links can be made reliable if data packets are transmitted at instants in which the radio channel quality is favourable for successful data packet delivery.

RESUMO

As *Wireless Body Area Networks* (WBAN) estão a ser desenvolvidas para um número cada vez maior de aplicações de monitorização, substituindo as tradicionais comunicações por fios por comunicações sem fios. Estes canais são geralmente meios de comunicação bastante instáveis, contudo, devido ao advento de dispositivos vestíveis, as condições a que os canais estão sujeitos são bastante singulares em comparação com as vivenciadas pelas redes sem fios tradicionais. A natureza variante no tempo das atenuações sofridas pelo sinal transmitido, fenómeno chamado de *fading*, é a principal razão para a baixa fiabilidade das comunicações quanto realizadas em redor do corpo humano. Este fenómeno promove a perda constante de pacotes de dados, o que impossibilita as WBANs de alcançarem todo o seu potencial.

O trabalho de investigação aqui apresentado tem três objetivos principais: primeiro, as tecnologias emergentes nas mais diversas áreas são exploradas de forma a implementar uma WBAN para a monitorização a longo prazo de bombeiros no teatro de operações. Esta rede é integrada num *Cyber-Physical System* (CPS), que implementa um sistema distribuído de monitorização de equipas de emergências através da combinação de diversas tecnologias para a deteção, atuação, comunicação, rede, computação e controlo do sistema proposto.

O segundo objetivo visa estabelecer uma melhor compreensão do impacto que as especificidades dos cenários de operação têm nas comunicações da WBAN. Uma abordagem de caraterização do sinal baseada em cenários é adotada. Este estudo demonstra que a componente *large-scale fading* do sinal (que provém das obstruções criada pelo corpo e sua mobilidade) é o efeito predominante nos sinais transmitidos (na banda *Industrial Sientific and Medical*) e que a sua magnitude vária com a localização dos nós. Para nós localizados em membros móveis do corpo humano, o canal de comunicação entre recetor e transmissor está em constante comutação entre a existência e a ausência de linha de visão, o que se traduz em *large-scale fading* próximas de -18 dB. Por exemplo, para o nó localizado no pulso, um dispositivo padrão é capaz de assegurar os níveis fiabilidade exigidos pelas aplicações e latências inferiores aos limites máximos impostos pelo grupo de trabalho IEEE 802.15.6 contudo, a fonte de energia disponível é utilizada de forma ineficiente.

Em terceiro lugar, os desafios encontrados pelas WBANs encorajaram os autores a investigar estratégias capazes de garantir comunicações fiáveis mas sem comprometer os outros requisitos de desempenho. Assim, um mecanismo do tipo *Transmission Power Control* (TPC), designado *Proactive-TPC* (P-TPC), é proposto. O P-TPC adota um princípio de operação hibrido e visa dispositivos com recursos limitados. Esta solução utiliza as amostras da força do

sinal recebido para aproximar a componente *fading* do sinal durante um ciclo de marcha, por sua vez, a aceleração sentida pelo nó é utilizada para identificar, em tempo real, o estado do ciclo de marcha. Assim, em qualquer instante, o sistema é capaz de determinar a qualidade atual do canal e estimar a potência de transmissão mínima necessária para garantir a entrega do pacote de dados no destinatário. A solução P-TPC consume menos 35% energia que os sistemas de comunicação que transmitem dados à potência de transmissão máxima permitida em WBANs (0 dBm). Ao mesmo tempo, minimiza a taxa de absorção específica (SAR) e a probabilidade do sistema interferir com redes coexistentes. Este algoritmo é adequado para trafego de dados de emergência, pois garante comunicações fiáveis com um consumo energético eficiente e sem sacrificar a latência das transmissões.

Finalmente, um mecanismo do tipo *Packet Scheduler*, chamado *Power Control and Packet Scheduler (*PCPS), é proposto. Este mecanismo explora as vantagens das redes neuronais e dos sistemas de inferência Fuzzy para descrever sistemas dinâmicos não lineares e criar um modelo capaz de descrever os canais radio das WBANs em função do ambiente de operação e da posição relativa do braço e postura do utilizador. A solução proposta aperfeiçoa a fiabilidade das ligações à custa da latência, o que faz desta solução adequada para canais radio aquando o trafego de dados normais. O PCPS assegura até menos 10% de pacotes de dados perdidos nas transmissões do que sistemas que transmitem à máxima potência permitida em WBANs. Esta solução demonstra que ligações não fiáveis tornam-se confiáveis se os pacotes de dados forem transmitidos apenas nos instantes em que a qualidade do canal de comunicação é favorável à entrega de pacotes bem-sucedidas.

INDEX

LIST OF FIGURES

LIST OF TABLES

LIST OF ABBREVIATIONS AND ACRONYMS

6LoWPAN	IPv6 over Low-Power Wireless Personal Area Networks	MEPF	Minimum Energy Packet Forwarding Protocol
AA-TPC	Accelerometer Assisted-TPC	MICS	Medical Implant Communication System
ACF	Autocorrelation Function	MSE	Mean Square Error
ACK	Acknowledge	NB	Narrowband
AFD	Average Fade Duration	NHS	National Health Service
AFME	Adaptive Fade Margin Estimator	NLOS	Non-Line-of-Sight
AIC	Akaike Information Criterion	NN	Neural Network
AMDF	Average Magnitude Difference Function	NTW	Network
ANFIS	Adaptive Neuro-Fuzzy Inference System	OP	Outage Probability
AP	Access Point	PAN	Personal Area Network
A-TPC	Two-step Adaptive TPC algorithm	PCPS	Power Control and Packet Scheduler
BCU	Body Control Unit	PCPS	Power Control
BI	Beacon Interval	PD	Personal Device
BLE	Bluetooth Low Energy	PER	Packet Error Rate
BPSK	Binary Phase Shift Keying	PH	Potential of Hydrogen
CAP	Contention Access Period	Physical	PHY
CDF	Cumulative Distribution Function	PPDU	Physical Protocol Data Unit
CF	Complementary Filtering	PPE	Personal Protective Equipment
CFP	Contention Free Period	PPP	Precise Point Positioning
CO	Carbon Monoxide	PRP	Packet Reception Rate
CO_2	Carbon Dioxide	PS	Power Scheduler
COTS	Commercial off-the-shelf	PSD	Personal Digital Assistance
CPS	Cyber-Physical System	PTF	Power Transfer Function
CSMA/CA	Carrier Sense Multiple Access with Collision Avoidance	P-TPC	Proactive-TPC
CU	Control Unit	QoS	Quality-of-Service
DTW	Dynamic Time Warping	Q-QPSK	Quadrature Phase-Shift Keying
ECG	Electrocardiogram	RF	Radio Frequency
E-H	Enhanced-and-Hold	RMSE	Root Mean Square Error
EM	Electromagnetic Waves	RO	Research Objective
EMG	Electromyography	RSSI	Received Signal Strength Indicator
EPP	Energy Per Packet	RWS	Reactive Without Scheduler
ETX	Expected Transmissions	SAR	Specific Absorption Rate
FCC	Federal Communications Commission	SF	Superframe
FDA	False Detected Accelerations	S-H	Sample-and-Hold
FIS	Fuzzy Inference System	SINR	Signal-to-Interference-plus-Noise Ratio
FL	Fuzzy Logic	SoC	System-on-Chip
GPS	Global Positioning System	SW-based	Software-based
G-TPC	Gait Cycle TPC	TbO	Time-between-Outages
GTS	Guaranteed Time Slot	TC	Coherence Time
HBC	Human Body Communication	TG6	IEEE 802.15.6 Task Group
HW-based	Hardware-based	TPC	Transmission Power Control
IMU	Inertial Measurement Unit	TPL	Transmission Power Level

IoT	Internet-of-Thing	TRD	Technical Requirement Document
ISM	Industrial Science and Medical	TRH	Target Range Upper Limit
LCR	Level Crossing Rate	TRL	Target Range Lower Limit
LM	Link Margin	UAR	Undetected Accelerations Rate
LOS	Line-of-Sight	UWB	Ultra-Wide Band
LQE	Link Quality Estimator	WBAN	Wireless Body Area Networks
LQGI	Linear Quadratic Gaussian Control with an Integrator	WLAN	Wireless Local Area Network
LQI	Link Quality Indicator	WMEWMA	Window Mean Exponential Weighted Moving Average
MAC	Media Acess Control	WMTS	Wireless Medical Telemetry Service
MAE	Mean Absolute Error	WSN	Wireless Sensor Network
MBAN	Medical Body Area Network	ZUPT	Zero-Velocity Update

CHAPTER 1

SCOPE OF THIS THESIS

Recent developments in wireless communication and miniaturization of sensor/actuator technologies have driven the advances in wearable nodes [1]. Over the last few years, the revenue worldwide from wearable device sales has significantly increased, passing from USD 2 billion in 2013 to more than USD 15 billion in 2017 [2]. By the end of 2018, USD 38.84 billion are forecast [3]. Moreover, the percentage of wearable technology ownership has suffer a strong increase, from 7% in 2014 to 15% nowadays and it is foreseen that it can reach 28% by the end of 2017[2].

This type of networks enabled a new domain of research leading to the development of suitable network architectures, generally designated as Wireless Body Area Network (WBAN) [4]. They are sometimes referred as one of the most promising technologies in a near future ([5], [6]) due to the great potential to provide high efficiency and convenience for non-invasive monitoring of the human body performance and vital signals. The WBAN features enable the application of this emergent network technology in wide variety areas. During the last decade, wearable systems have been a major topic of research and development, being firstly oriented towards the medical and well-being fields, such as, patient's health monitoring, elderly people surveillance and sleep quality evaluation [7], [8]. According to UK National Health Service (NHS), the use of innovative technologies to improve health-care to chronically ill with fewer hospital visits and admissions could save up to 7 million pounds per year [2].

Typically, WBANs comprise a set of wearable (and/or implantable nodes) nodes arranged around (and/or inside) the human body, communicating within a short range (5 m distance) with variable rates, according to measured parameters and application requirements [4], [9]. These nodes designated Edge of the Network nodes can gather specific information, such as vital signs, body posture and movements or environment parameters in real time, using wireless communication technologies, and deliver the information to a node, designated Coordinator node, to perform long-term and continuous monitoring [1], [10].

The applications of WBANs are tremendous and their requirements and specifications are dependent on the nature of each application. This thesis focuses on the application of WBANs to emergency response team monitoring, one of the most challenging environments for this type of networks, as analysed in the next section.

1.1 The Challenges of Wearable Nodes Application

The implementation of a WBAN to real-life applications has been under pressure to reach the end-user, but the sector still embraces a number of challenges that are hampering the wearable systems of reaching their full potential. Monitoring firefighters and emergency response teams during their activities is seen as one of the most difficult and challenging scenarios for WBANs. In this application, users are submitted to conditions which limit the performance of WBAN systems - harsh surrounding environment, intense movements and dynamics of operators. Such conditions, which cover wide operation areas and represents immediate life-threatening to the operators (e.g. toxic gases and high temperatures exposure, skin burns and risk of collapse) [11], [12] represent a tremendous challenge for WBANs to secure efficiency, efficacy and reliability in order to become an effective life-monitoring system used in the benefit of professionals and the society.

According to the IEEE 802.15.6 Task Group (TG6), the WBANs technology must be able to handle different requirements in terms of data rate due to the high diversity of sensors used. At the same time, a WBAN must ensure the follow requirements [13]:

- Packet error rate (PER) should be less than 10% for a 256 octet payload (i.e., 256×8 bits of data) even when the person is in motion. A reduction of the network capacity is acceptable, but the data should not be lost;
- The latency in data transmission, which refers to the time interval between the acquisition and processing (or visualization), must be lower than 125 ms in medical applications, whereas in non-medical applications a latency up to 250 ms is acceptable; Jitter, which is the transmission latency that varies over the time, should be less than 50 ms [13].

Although the TG6 group generalizes the maximum delay for all the applications in the medical area, this requirement is dependent not only on the application area, but also on the type of parameter measured. For instance, the acceptable latency may vary from 50 ms for Endoscope capsules [14], up to 150 ms for Electrocardiogram (ECG) monitoring [15]. Independent from the application, it is widely accepted that the quality of the WBAN systems depends on their capacity to provide the acquired signals with negligible latency (instantly in the user perception), that is, real-time communication [16].

On the other hand, energy efficiency in WBANs is also an important aspect in this field, since the amount of energy available is limited (as the Edge of the Network nodes are battery

powered and in many cases, battery replacement or recharging may not be feasible for quite long periods [17], [18]). In emergency response team applications, it is expected that batteries last for several hours or days as professionals normally work intensively for long periods with no breaks and in remote areas where access to the power grid is scarce. Thus, for such applications, WBAN nodes able to operate in an highly energy-efficient way are required [1], [5]. The technical requirements from the TG6 group do not specify the WBAN autonomy per application, since this parameter is application driven. However, they refer that power saving mechanisms should be incorporated to allow WBANs to ensure communication reliability in an energy-efficient manner, even when operating in power constrained environments [19].

WBANs are not autonomous systems, since the information generated within the network is not made remotely available (for professionals, such as healthcare personnel, fire command centre, etc.). The integration of communications, computation and control technologies is required, to enable target the decision to remote and more complex information systems. The goal of distributed intelligent systems, known as Cyber-Physical System (CPS), is to create a smart control loop to interconnect the WBANs nodes and the remote information systems though communication networks (as depicted in Figure 1.1). This approach allows the remote information system to gather the data acquired by the WBANs and to manage the physical actuators embedded in the Edge of the Network nodes [20], [21].

1.2 The Technological Problem to be Solved

The CPS approach has the potential to significantly contribute to the progress of Smart firefighting and simultaneously provide user comfort and safety. However, the advent of wearable and mobile nodes communicating through wireless links around the human body, turns the task of ensuring all the Quality-of-Service (QoS) features a very challenging research problem in WBANs. On-body communication (data exchange between wearable nodes) is the most challenging communication scenario in WBANs, since they are inherently unreliable due to the path-loss variability in inter-node distance within a short timeframe.

The human body plays an important role in the performance of communications in WBANs. The on-body links are highly dynamic due to the following reasons: (i) Electromagnetic Waves (EM) tend to penetrate the body tissue, dissipating the signal power as heat [22], [23]; (ii) signal energy attenuation due to the obstruction of human body, phenomenon designated as shadowing [24], [25]. The human body acts as an EM wave's propagation medium, where the emitted EM waves tend to be diffracted by the human body originating surface and creeping waves. These EMs may only represent a small percentage of all signal energy initially

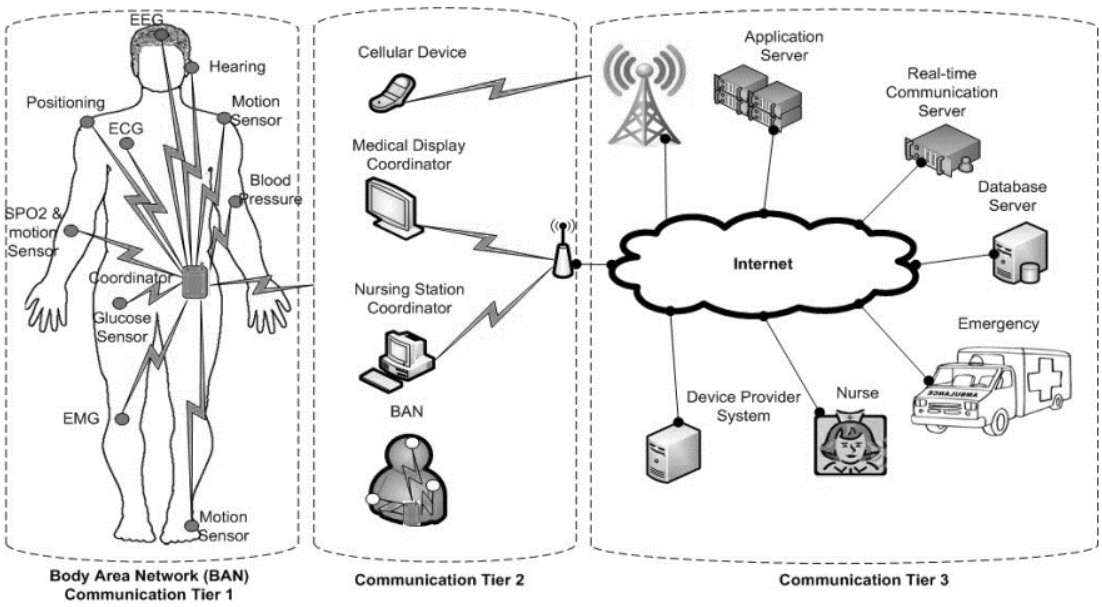

Figure 1.1. Cyber-Physical System architecture comprising a WBAN for the user's monitoring in hospitals, source [21].

transmitted [24], [26], [27], however, in the absence of direct waves, the surface and diffracted waves may be the main source of energy of the signal received by the Coordinator node [23], [27], [28]; (iii) large-scale fading (called slow fading signal component), which refers to slow signal fluctuations over small distances, but high in magnitude [24], [25]. This type of fading occurs due to the human movement that promotes the frequent commutation of the radio propagation conditions between Line-of-Sigh (LOS) and Non-Line-of-Sight (NLOS). This can cause a fluctuation in the signal attenuation that can reach 30 dB [26]; (iv) temporal variations in the wireless radio channels, which are a result of potential distortions on the antenna radiation pattern due to changes on antennas' direction; (v) the inherent body mobility may render WBAN radio channels prone to internetwork interference [18] due to the coexistence of other systems or devices, distorting the system performance in terms of reliability [10].

The unreliability of wireless transmissions around or along the human body have discouraged the application of Wireless Sensor Networks (WSN) developments in WBANs. Thus, WBAN-specific research and design issues with new lines approaches are required to optimize the performance of on-body communication in WBANs [29].

1.2.1 Scientific Challenges

In the last few years, to meet the QoS requirement of WBAN applications, research efforts have been mainly focused on the design of more energy-efficient hardware: through the integration of various subsystems into a very compact node [30]; through the transformation of energy harvested from different sources, such as, Potential of Hydrogen (pH) level [30], [31],

human body heat [31], [32] or Radio Frequency (RF) radiation [31], [33], into an electrical potential to power WBAN nodes; through antenna design and intelligent antenna selection according to the link conditions to improve the communication reliability [33]–[35]; through Media Access Control (MAC) [18], [36]–[38], and Routing protocols [39]–[42], Interference Mitigation schemes [43]–[45] and Transmission Power Control (TPC) mechanisms.

The research on the latter mechanisms (TPC) aims at increasing the energy efficiency of transmissions by adjusting the radio module output power (also known as Transmission Power Level (TPL)), at run-time and according to the radio channel conditions [46], to the lowest level possible that ensures the successful delivery of data packets, with the minimum effect on other performance aspects [4]. This type of mechanisms has drawn considerable attention, since in any wireless node, the radio-communication is the process that consumes the larger proportion of the available energy [47], being responsible for up nearly three quarters of the total power consumption [10]. In addition, the quality of the signal, link connectivity and interference level between nearby nodes are directly related with the adopted output power level, i.e. the TPL [4]. As a consequence, the performance of MAC protocols, routing mechanisms and interference mitigation schemes are significantly influenced by the output power controller [10]. Furthermore, the TPC mechanisms can be executed simultaneously with the previous approaches, as a complementary energy-saving strategy [48], as demonstrated by the protocol stack proposed for multi-hop WBANs [49]. According to research work [50], due to the nature of WBANs, the TPC mechanisms play an important role in future developments of WBAN technology, being an integral part of the network in several applications [50].

Although static and pre-defined TPL mechanisms are used on the majority of the WBAN projects, this approach may be inadequate [48], [51] due to the variability of the on-body link quality. Therefore, data packets transmission performed at high TPL values may assure reliable links, low latency and Specific Absorption Rate (SAR), but may also result in unnecessary energy consumption. On other hand, the data packets transmission carried out at low TPLs may ensure energy savings, but at the same time the reliability and latency may be sacrificed due to the increasing retransmissions.

A mechanism able to sense the radio channel quality and properly update the TPL might be able to minimize the power consumption, reduce the SAR (an average TPL of -15 dBm is used in [39]), improve the receiver nodes quality due to mitigation of RF interferences (PER improvements up to roughly one quarter is reported in [52]), as well as delays in transmissions

due to retransmissions of lost data packets (in [53] and [54] a delay reduction up to about 6% and 30% were reported, respectively).

The design of a TPC mechanism with a holistic view of the radio channel in WBANs links is crucial for the effectiveness and applicability of TPC mechanisms. However, this is a relative new research area, and, as a consequence, there are still some challenges and open issues:

- The majority of the TPC mechanisms addressed in the literature are only feasible for scenarios prone to stable channel quality, for instance, when user is standing still. Other solutions rely in the feedback (measured signal power) from the receiver node (usually the Coordinator node) to estimate the current radio channel quality and then update the TPL. However, this leads to a significant increase of the traffic overhead (additional packet transmissions required to exchange control information between nodes in order to estimate radio channel quality and update the TPL);
- Radio channel estimations must be computed fast and must have the sensitivity to detect changes in radio channel quality. However, agility and reliability of the TPC mechanisms are requirements that are in conflict [55]. For instance, the use of a single sample of the measured metric that translates the current radio channel quality might result in inaccurate estimates. Several samples increase the accuracy of estimations but reduce the TPC mechanism agility, since radio channel quality changes are expected, thus, by the time the radio channel is estimated and the power is adjusted, the radio channel could have changed;
- Developing TPCs for Edge of the Network nodes (which have strict constraints on processing and working memory) with low complexity is a challenging problem. Solutions proposed for WBANs must be kept simple and light enough to be successfully implemented in such resource-constrained nodes.

All the effects listed in section 1.2 turn the radio channel conditions experienced by wireless nodes attached to human body quite unique in comparison to those experienced in traditional networks. The analytical models, widely used in WSNs to describe the signal attenuation as a function of the distance, are not suitable to describe the behaviour of the wireless links in WBANs. In WBANs, the distance does not have the most predominant influence on the radio channel behaviour [26]. In fact, the signal propagation around the human body is not well-understood yet. However, reaching a good comprehension of the factors that affect the on-body communications is extremely important in the design of effective TPC mechanisms for WBANs.

Such scenario and technological background have led to the following research questions that were the basis of this thesis:

- Is it possible to implement a body area network where communications are wireless and at same time ensure the reliability desirable for the target application?
- How does the WBAN scenario operation affect the link quality metrics?
- Which strategies can be implemented to optimize the communications around the human body?

1.2.2 Research Objectives

This research project is committed to exploring the integration of several technologies to build a CPS approach to a smart Personal Protective Equipment (PPE) for improving the user's performance, resilience and safety in emergency response team application. A special care was placed on the design of a smart Personal Protective Equipment that gathers information related to the user. In this context, sensor and actuator technologies integration in the garment, as well, as data gathering and communication technologies at on-body level are required. Ensuring reliable on-body communications, which can be quantified through the Packet Reception Rate (PRR)/Packet Error Rate metric, in the proposed WBAN was vital to enhance the QoS requirement. Therefore, the metric PRR is considered the main performance metric to be improved. However, according to the network traffic (emergency or regular traffic), the WBAN privileges certain metrics to the detriment of others (Table 1.1 summarizes the privileged metrics, organized by degree of priority, for each type of network traffic), as follows [56]:

- Emergency traffic – this type of network traffic is initiated by Edge of the Network nodes when sensed physiological data exceeds a predefined threshold. The resultant data packets have higher priority than other types of data, since this transmission must be reliable and with very low latency. Thus, second critical performance metric is the latency, while energy consumption must be minimized whenever possible;
- Regular traffic – refers to the network traffic in normal conditions without the critical time request. In such traffic, the energy consumption metric is considered the second critical performance metric while the latency is the last one.

In this regard, one of the goals was to investigate potential strategies to improve the main core metrics of this research work, which must be robust and intelligent to deal with the necessary trade-off between performance metrics. In addition, solutions must be kept simple

Table 1.1. Types of network traffic and respective privileged metrics.

Network Traffic	**Main Metric**	**Second**	**Third**
Regular	Reliability	Energy Consumption	Latency
Emergency	Reliability	Latency	Energy Consumption

and light enough to be successfully implemented in resource-constrained nodes. In summary, the main research objectives (RO) of this project are as follow:

- RO 1 - *Development of a WBAN for Firefighter Personal monitoring*: Development of sensors and actuating nodes, distributed in the user body through attachment to user garment. Integration of nodes in a centralized network of the type WBAN to provide long term monitoring of users. This WBAN must permit its integration with other technologies, following a CPS approach;
- RO 2 - *Establish a better understand of the impact that WBAN operation scenarios have on intra-WBAN communications*: Understand the on-body radio propagation in each link built in the proposed WBAN and, according to the fading behaviour and link performance, discuss potential solutions to optimize the WBAN's link performance;
- RO 3 - *Mechanism to optimize the metrics of interest in the scope of this thesis in Emergency Traffic*: After achieving a better comprehension of on-body radio propagation in RO 2, this research work aims to enable the WBAN nodes with a computing/control technology capable of estimating the conditions of the radio channels and determine the minimum transmission power required to ensure their successful sending. This type of algorithm (TPC mechanisms) aim to ensure that the system meet the requirements of the application in WBAN's emergency traffic.
- RO 4 - *Mechanism to optimize the metrics of interest in the scope of this thesis in Regular Traffic*: Enable the WBAN nodes with a computing/control technology (often denominated packet scheduler) capable of sensing the radio channel and avoid data packets transmission in instants that radio channel is in outage. Such solution might be able to ensure the reliability required and reduce the energy consumption due to data packets retransmission. However, these metrics might be improved at the expense of the latency metric, making it suitable for the WBAN's regular traffic.

1.3 Project Approach

The research work started with the development of a CPS able to interconnect several elements required to make the collected information in a WBAN remotely available. The CPS addressed in this thesis comprises three main blocks, including: i) a Base Station, ii) Ad-Hoc Network, and iii) a WBAN for sensing user's garments and trigger alarms. Figure 1.2 depicts the overview of the project approach followed in this thesis.

In this type of systems, the data from the physical world is delivered to the Ad-Hoc network, – after being acquired, measured and processed in the WBAN , which has the responsibility of connecting the several WBANs with the Base Station (offers a holistic view of the theatre of operation).

As wireless communications are adopted, the wireless radio channels and in particular the on-body channels, are unreliable. For that reason, the main focus of this thesis is the intra-WBAN communications. The main source of unreliability on intra-WBAN communications is the fading, which promotes data packet loss, higher latencies on data packet transmission and higher energy consumption.

The challenges associated to intra-WBAN communications encouraged the investigation of strategies that can be implemented and incorporated as computing and control technologies in WBAN, aiming to achieve effective and reliable communications between wearable nodes in a way that can be used as life monitoring system, e.g. firefighting or patient monitoring.

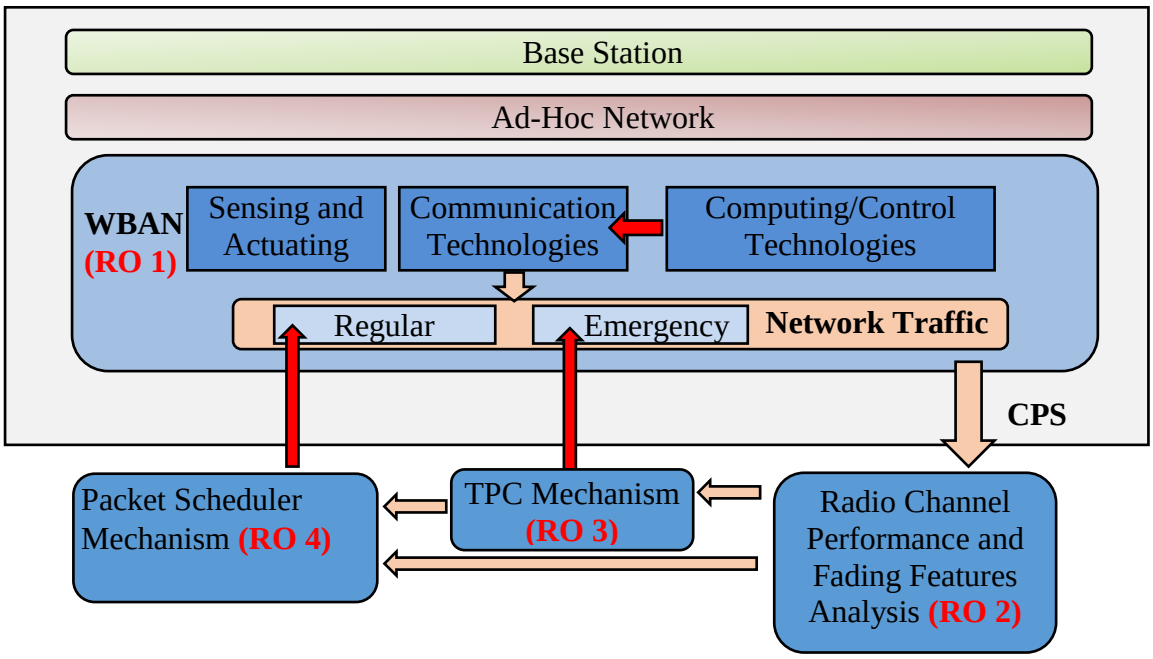

Figure 1.2. Overview Project Approach.

Every node from the WBAN and each operation scenario are characterized by their own particularities and combination of them. In the proposed approach, the research started with the attempt to understand why the communication between nodes that are able to communicate in a range of 20-30 meter (traditional networks), are not capable of achieving the same efficiency in WBANs with maximum distances of 10-40 cm (chapter 4). A scenario-based radio channel characterization was made in order to assess the communication performance for each pair of nodes. The outcome of this research allowed the identification of strategies for each communication link with potential to improve the performance. At the same time, a survey fed with state-of-art research was produced in order to fulfil the gap for a thorough analysis of solutions to improve communication in links with time-variation fading features, which is presented on chapter 2.

Two strategies were investigated to optimize the metrics performance of time variant quality links in emergency and regular traffic - The *TPC Mechanism* and *Packet Scheduler Mechanism* block, respectively. These two strategies are computing and control technologies integrated in the protocol stack, aiming to ensure the successful deliver of emergency or regular data packets, respectively. In the next section, the research methodology is described in detail.

1.4 Research Methodology

The research methodology has been defined and implemented to meet the requirements for successfully accomplish the objectives defined in section 1.2. To achieve the RO 1- *Development of a WBAN for Firefighter Personal monitoring*, the integration of emerging technologies in the field of sensing, such as non-intrusive wireless-enabled nodes design and electrodes material embedded in textile structures, as well as wireless technologies to provide long term monitoring of firefighters were explored. Several Edge of the Network nodes with different embedded sensors (to measure several different signals related to human body but also the environment such as quality of the air) and actuators (to trigger alarms) were implemented. These nodes, which are integrated into different pieces of the personal firefighter garment (a wired solution would be impracticable), transmit the measured parameters to the Coordinator node through the low-power ZigBee communication technology. The latter WBAN element not only manages the network, but also executes the role of gateway. A Wi-Fi card was incorporated into the Coordinator node to allow WBAN integration with other technologies within a CPS approach.

To investigate the radio channel performance and fading features in each wireless link of the WBAN developed (RO 2 - *Establish a better understand of the impact that WBAN operation*

scenarios have on intra-WBAN communications), the experimental characterisation of the on-body communications and performance evaluation in terms of the metric of interest in the scope of this thesis, namely reliability, energy-efficiency and latency were carried out. To understand the influence that factors such as user's movement and posture, node location and environment have in the received signal power, experimental work has been performed in different testbeds following a scenario-based approach. Users were invited to perform an activity (standing, walking, running and crawling) for a short period of time while nodes (different locations are considered namely indoors, such as house rooms and laboratories; and outdoors, such as urban open spaces) transmit data packets at a fixed interval period. This interval must be small enough to capture the variability of the radio channel behavior. For this reason, transmissions occur every 35 ms. To analyze the on-body signal magnitude, the received signals are considered as a combination of three components: path-loss, large- and small-scale fading (this differs from large-scale fading for presenting faster variations in short periods of time, but with less amplitude variations [24], [57], [58] and it is result of the multi-path components effect on the emitted signal [59]), in contrast with the approach often adopted in the literature (signal is considered a random variable). Moreover, several first-statistical models are tested against the empirical data and those that best fit in empirical data are proposed as the model that best describes the fading for a specific operation scenario.

To address the RO 3 – *Mechanism to optimize the metrics of interest in the scope of this thesis in Emergency Traffic*, a mechanism of reduced complexity able to ensure the requirements of the WBANs in emergency traffic was developed. Emergency data packets have higher priority than other type of data packets in WBANs, since the transmission of these data packets must be reliable and with very low latency. A novel TPC mechanism that takes advantage of the acceleration signals locally available in the Edge of the Network nodes, employing a hybrid operation principle (closed-loop control and inertial-sensor TPC) and targeting resource constrained nodes is proposed in chapter 6.

In regular traffic, communications do not have strict requirements in terms of delays in transmissions. Therefore, RO 4 – *Mechanism to optimize the metrics of interest in the scope of this thesis in Regular Traffic* consists in developing a strategy to improve the reliability and energy-efficiency of communications at the expenses of the latency. In this regard, the advantages of Neural Networks and Fuzzy Inference Systems in modelling nonlinear dynamical systems to build a model able to describe the radio channel conditions (Received Signal Strength Indicator (RSSI) variations and radio channel outage probability) were explored. This

model, which receives the user's arm posture (angles between different segments of the arm) and body posture and the operating environment as inputs is an important element to the *Packet Scheduler Mechanism* block. This delays data packets transmission to instants in which radio channel conditions are more prone to successful data packet delivery. The previous mechanism was implemented on the developed Edge of the Network nodes, tested experimentally and validated by comparing the results of its performance with those of other solutions addressed in the literature. Through simulations, the data packet scheduler was tested and his performance assessed by comparing with that of other solutions developed for the same purpose.

1.5 Key Assumptions and Considerations

In wireless communications, data packets are considered lost data packets if one of the following conditions is verified:

- Signal power, which is translated by the metric RSSI in this study, lower than the receiver sensitivity (it is transceiver-dependent and indicates the minimum signal power level with an acceptable bit error rate necessary to ensure an accurate received signal decode);
- Signal-to-Interference-plus-Noise ratio (SINR) lower than 6 dB [60].

The RSSI metric is the measure of the chip error rate of the first eight symbols of the incoming data packet, which estimates the quality of the error of a successfully received data packet. The SINR determines the probability of correctly decoding a symbol during the process of demodulation [47].The latter parameter is determined at each receiver as the ratio of the power of the signal of interest P_{signal} to the combined power of the additive white Gaussian noise (P_{noise}) and the interference caused by the other active transmissions in range ($P_{interference}$), as given in the following expression

$$SINR = \frac{P_{signal}}{P_{Interference} + P_{noise}} \quad \textbf{(1.1)}$$

Thus, the reliability of the WBAN communication system is influenced by the parameters P_{signal}, $P_{interference}$ and P_{noise}. The former parameter, considered in this thesis to determine the signal attenuation and to analyse the fading effects on the radio propagation, is translated through the metric RSSI. The $P_{interference}$ is not addressed in this thesis, while P_{noise} (depends on factors related to the thermal noise of the radio transceiver) influence on signal power is already present in the measured RSSI samples. The metric RSSI is a weak indicator of the radio channel conditions when radio transceivers are subjected to RF interference [4]. In

this thesis, it is assumed that there is no RF interference from external networks. Although simple solutions allow networks to avoid (e.g. radio channel hopping strategies) inter-network interference and the adoption of low TPLs in communications reduces the level of interference between WBANs, it will be hard to ensure in scenarios with high density of networks.

The present research has some limitations that must be highlighted. The set of scenarios considered in the experimental methods were limited to a unique physical layer as well as to a unique band, namely narrowband (NB) and Industrial Science and Medical (ISM) radio band, respectively. According to some research works that performed experiments in different physical layers and frequencies, such as [24], [61], [62], both parameters may have impact on path-loss and fading features. However, the narrowband physical layer and the ISM band are widely adopted and there is no perspective that this trend changes in a near future (c.f. section 2.1).

The experimental method adopted has also some disadvantages. The scenario-based experiments are performed for short intervals and for a specific activity that the user must repeat during that interval. This method offers poor repeatability and low accuracy. Consequently, the fluctuation rhythm and fading features may vary from experiment to experiment. In addition, the real measures require a significant number of resources, whether human or economic [26], [63]. The number of users considered in current research is short since the WBAN nodes are part of the PPE in contrast with the trend adopted in the literature (body worn-nodes). Although the followed approach allows us to capture the effect of the antenna-body electromagnetic interaction in the fading features, it reduces the number of different human bodies features covered in experiments.

1.6 Thesis Outline

This thesis is structured in eight chapters. The current chapter addresses the motivation for the research questions RAISED in this thesis. In addition, the research objectives, the followed approach and the research methodology are explained. The remaining of this document is structured as follows:

- Chapter 2 – A generic wearable system architecture typically adopted in the literature is described and the implementation of several projects proposed for emergency response team application are analysed.
- Chapter 3 – A generic structure of the TPC mechanisms process is provided and used to describe the different solutions addressed in the literature. A taxonomy to classify

the different TPC mechanisms developed and described in the literature is proposed and, finally, a comparative summary of the state-of-the-art TPCs for on-body channels in WBANs is provided. Parts of this research work have been published in [64].

- Chapter 4 – The CPS, in which the proposed WBAN is integrated, is described and system functionalities are addressed. A more detailed information about the platforms, sensors and actuators that compose the proposed WBAN is provided as well as the final node locations.
- Chapter 5 – The performance of the several links of the proposed WBAN is evaluated in terms of the metrics reliability and latency. Moreover, the fading is decomposed, and the several effects analysed as a static process. Later their time dependency is extracted from empirical data and analysed. Parts of this work have been published in [65].
- Chapter 6 – The fading oscillation while user is performing periodic movements is analysed and these features are explored to design a TPC mechanism able to ensure high reliability, low latency and consumption and to keep the SAR as low as possible. The scheme proposed is experimentally evaluated in different scenarios and performance results analysed. Parts of this work have been published in [66] and the initial ideas was published in [67].
- Chapter 7 – The impact of the movement of the user's arm with different angles orientation is analysed. Then, a model developed to describe the radio channel quality in function of the angles between different user's arm segments is presented. Finally, a Packet Scheduler mechanism is proposed, implemented and assessed, for several conditions, through simulations for several scenarios.
- Chapter 8 – This thesis concludes with a short review of the proposed WBAN and the mechanisms proposed to optimize the on-body communications. In addition, directions for future research are provided.

CHAPTER 2

BACKGROUND

The networks of the type WBAN comprise several independent nodes powered with communication capabilities [68]–[71]. According to Movassaghi et al., WBAN's nodes can be classified according to their functionality, implementation and role in the network [68]. Regarding the classification of the nodes based into their functionality, the categories are the following:

- *Body Gateway* – This node has the task of gathering all the data coming from Edge of the Network nodes and ensure the interaction of the WBAN network with the user or with external entities such as other WBANs, networks or information systems. The link between the WBAN and other entities is ensured through external gateways while the interaction of the WBAN with the user is assured through displays or LEDs on the Body Gateway node and/or actuators (e.g. vibrating motor) embedded on any Edge of the Network node. In some research works, the Body Gateway node is sometimes called Coordinator node, Personal Device (PD), Personal Digital Assistant (PDA) or Body Control Unit (BCU);
- *Edge of the Network*– these nodes can be categorized into Sensor or Actuator nodes. The former node comprises sensors to measure a very specific set of parameters. Several types of sensors can be found in WBANs. The sensors can be either physiological (e.g. ECG, temperature, blood pressure and glucose, etc.), biokinetic (gyroscope, magnetometer, accelerometer) or ambient (e.g. gases, temperature, humidity, etc.) sensors. In subsection 2.1.3, more detailed information on the most common sensors found and characteristics of the measured parameters in WBAN projects is provided. Besides measuring parameters, the sensor nodes may also process data and provide wireless response to information [18]. Finally, Actuator nodes comprise actuators to change attributes of a physical object aiming to notify the user (situations in which a sensed signal is above a pre-defined threshold or notifications sent from external nodes) through (for instance) RGB LED or vibration motors.

The classification of WBAN nodes based on the way that they are implemented within human body (classification method proposed by the IEEE 802.15.6 TG [13], [19]) is as follows:

- *Implant* – These nodes are implanted in the human body, either inside the body tissue or immediately underneath the skin;
- *Body surface* – Some existing nodes of this type are smart watches, smart glasses, smartphones, earphones or smart textiles attached to garments which enable the wireless monitoring of temperature, heart rate, physical activity, moisture, etc. (anytime and everywhere). Thus, body surface nodes are wireless nodes that are placed on the surface of the skin or in the proximity of the human body (up to 2 cm away of the body [18], [72]);
- *External* – These nodes are not in contact with the user body. Due to the range limitations of the communication technologies adopted in WBANs, these nodes are typically within a 3-10 m distance of the user body [18], [70], [73]–[75].

Three different classifications of the WBAN's nodes are based on the role that they take in the WBANs:

- *Coordinator Node* – The coordinator of a WBAN has the same role as the Body Gateway described above;
- *End Nodes* – These nodes are resource-constrained nodes programmed to perform their embedded application. These nodes are designated Edge of the Network node when classified based on their functionality;
- *Relay Node* – These nodes are also called intermediate nodes, and, as its name suggests relay the data packets from the network transmitter. The transmitter can be the Coordinator (in the case of downlink communications) or one of the End nodes (uplink communications). Sometimes, data packets transmitted by wireless nodes located in limbs (such as hands or feet) need to be relayed in order to reach the Coordinator. Relay nodes might be capable of sensing data and interacting with the user or other entities.

According to the IEEE 802.15.6 TG, there are four possible communication scenarios in WBANs [18], [42]:

- *On-Body* – Refers to the communications between Edge of the Network node implemented in WBANs as body surface nodes and the Coordinator node which is also on the user body;

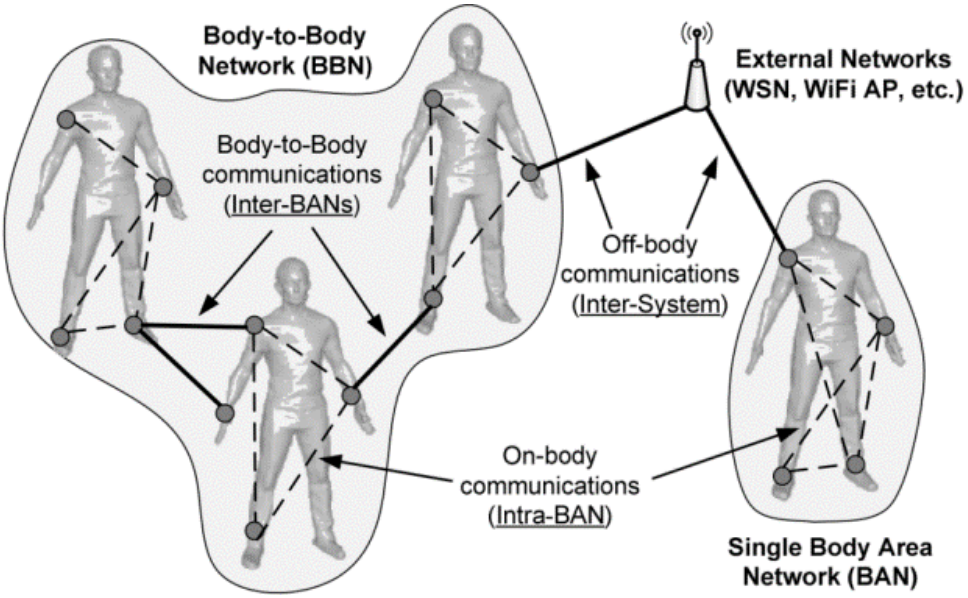

Figure 2.1. Communications scenarios in Wireless Body Area Networks, source [2].

- *Off-Body* – Communications between Body Surface/Implant nodes, usually Body Gateway and External nodes. The range of these communications depends on the technology adopted for this purpose;
- *In-Body* – Refers to the communications between Implant nodes and Implant/Body Surface nodes;
- *Body-to-Body* – Refers to the communications between Coordinator nodes of different WBANs.

From the set of communication scenarios depicted in Figure 2.1 (unique exception is in-Body communication), On-Body is the one that has attracted more interest of the research community [13], since, as analyzed in subsection 1.2.1, the obstruction of the human body to waves propagation lead to high path-loss and turns the radio channel time-variant which might promote data packet losses.

2.1 Wearable Systems

In this section, a generic WBAN communication architecture based in segments is described. This architecture is used (section 2.1.2) to describe and compare wearable systems approached in the literature for emergency response team application. Finally, in section 2.1.3, the most often used sensors in WBAN projects are listed and the characteristics of the parameters measured by such sensors are highlighted.

2.1.1 Communication Architecture

The literature often divides the communication architecture of the research works in wearable systems into communication tiers as depicted in Figure 1.1 [18], [21], [41], [73]. This generic communication architecture comprises three segments:

1. Intra-WBAN Communication (Tier-1), refers to the on-body communications;
2. Inter-WBAN Communication (Tier-2), covers the off-body communications between the Body Surface nodes or Implant nodes with External nodes;
3. Beyond-WBAN communication (Tier-3), refers to the communications that enable interactions with an eventual back-end system/information system.

Regarding the Tier-1, it refers to the interaction between WBANs nodes within a communication range lower than 2-10 m. The ZigBee and Bluetooth are the most adopted communication protocols (c.f. Table 2.1).

The second tier refers to the off-body communication between the WBANs and a components within the Tier-3 (e.g. smartphones, other WBANs or Ad-Hoc network/WSN relays). Several solutions have been used for this purposed, namely Personal Area Network (PAN); direct communications; infrastructures such as Wireless Local Area Network (WLAN); or the use of mesh architecture networks, such as Ah-Hoc networks or WSNs. Research projects that rely in PANs aim to process and display information in smart portable nodes operating close to the WBAN. In such cases, the Tier-3 is only implemented if the information is required in a large scale. The communication protocol Bluetooth and wireless networking technology Wi-Fi are the most adopted to perform off-body communications in wearable projects. In some cases, for instance the research projects [76]–[78], the Coordinator node is a smart node (smartphone in the pocket or an Internet-of-Things device) that is able to ensure the data transmission to a back-end server without requiring the implementation of the Tier-2, suggesting that wearable systems' communication architecture is application-specific.

The Tier-2's implementations, based in infrastructures such as Local Area Networks or WLANs, are the most adopted approach. They are suitable for systems that operate in places with a limited physical area, such as hospitals, offices or houses. The wireless networking technology Wi-Fi is the preferable communication technology to this segment, as it offers large bandwidths to data transmission and performs a centralized network. Other solutions use mesh networks, which are able to ensure a higher coverage area than the previously mentioned infrastructures, since routers can be introduced to extend the network coverage. Another advantage of this solution is the fast network setup, a fundamental feature in emergency

scenarios. Typically, the Coordinator node transmits the user data to an external gateway (an External node that is part of the infrastructure or mesh network, for instance static router nodes). In CodeBlue research project, an External Node called Access Points (AP) also operates as a database server [79].

The Tier-3 ensures the dissemination of the gathered information in Tiers-1/2 to the information systems. This segment when interlinked with the components and the technologies of the Tier-2 establish a large CPS that connects the WBANs to information systems (such as Smart Healthcare, Smart Cities, Smart Homes, Smart Manufacturing, etc.) to make this information Worldwide (W-W) available. These information systems share a common component, the back-end database, which performs the critical task of storing the acquired data. For instance, in Smart Healthcare system addressed in [80], this database allow systems to create a patient profile through the patient information gathered and the previously stored historic. This information can be made available to be remotely accessed by healthcare personnel such as doctors or nurses. The wireless mobile telecommunications technology 3G and 4G, and the wireless networking technology Wi-Fi often used in Tier-3.

2.1.2 Projects

Monitoring emergency response team is regarded as one of the most difficult and challenging scenarios, as the surrounding environment is harsh, highly dynamic, covers wide operative areas and represents immediate life-threatening to the users (e.g. exposure to toxic gases, high temperatures, skin burns, and the danger of collapse) [11], [12]. To address these problems, several Personal Protective Equipment's have been proposed in the literature, where different design approaches have been proposed to support user during an urban fire to meet the user requirements and the unique challenges faced by the emergency responders. There are several differences between the various Personal Protective Equipment's addressed in the literature, namely in the design choices in terms of monitored parameters, Edge of the Network nodes' location, and wireless communication protocols of the tier-1 and tier-2.

The number and type of physiological and environmental parameters monitored by the several proposed PPEs varies highly. PPE like WASP [81], iVital [82], WearIT@Work [11], [12] and PHASER [83] do not monitor environmental parameters, FIRE [76] does not monitor physiological parameters and PPL [84], GLANSER [85] and CoenoFire [86] do not monitor both kind of parameters. On the other side, the ProeTEX [12] and i-PROTECT [87] PPE offer a wide range of monitored parameters, the former is more focused on physiological parameters and the latter is more focus on the environmental parameters (environmental conditions and

toxic gases concentration/presence). Unlike most of the PPEs found on the literature, the FIRE relies on sensors preinstalled on the building for monitoring environmental parameters. The use of such sensors can give a better awareness of the conditions inside the building as well as an idea about the fire progression and expansion. But, if the PPE only relies on these sensors, like the FIRE PPE, with the progression of the fire these sensors can be destroyed and, therefore, the users and the fire command centre will not be aware about the conditions inside the building. To increase the comfort, reduce the size and weight of the sensors and, consequently, increase the user acceptance of the proposed solution, several techniques were proposed for the integration of smart textiles into the garment. The ProeTEX and iVital PPE rely on textile electrodes for the acquisition of the user's heart rate, and the former uses piezoelectric and piezo-resistive sensors, textile motion sensors and textile antennas for the acquisition of breathing rate, determine inactivity and the data reception/transmission, respectively. The i-PROTECT PPE, proposes the use of optical fibers integrated with technical textiles for the acquisition of breathing and heart rates and the user's temperature. Finally, the PPE proposed by Soukup *et al.* [88], aims to acquire the humidity and the nitrogen dioxide (NO_2) through the use of screen printed sensors, the same technique is employed for the development of antennas.

Another key feature in a PPE is the modularity of the proposed system. By combining a modular architecture with a distributed processing logic at the node level, it is possible to reduce the overall hardware complexity, the size of the Edge of the Network node and the amount of data to be sent (resulting in a transmission-power consumption reduction). Moreover, a modular architecture also makes the system more versatile, as new Edge of the Network nodes can be added without modifying the PPE architecture. The on-body communication (Tier-1) can be done through the use of wired [12] or wireless [82], [83], [88], [89] technologies. The use of wireless technologies makes the PPE more flexible and robust (i.e., it is possible to place an Edge of the Network node at any location, without the need of a physical connection, and the connections are not damage by use or washing, for example). Different wireless communications protocols, Bluetooth/Bluetooth Low Energy (BLE) [81]–[83], [90], ZigBee [89], MOTOTRBO [87] or other proprietary RF-based [88] were used for the on-body communication, or the communication within the WBAN. Projects like WASP and ProFiTex rely on wireless communications within the WBAN, they are based on all-in-one modules for the acquisition of the target parameters. The use of such modules makes the PPE more vulnerable to failure if the module is damaged during a mission, the fire command centre will not receive the updates about the user condition.

The bidirectional real-time off-body communication (Tier-2) is of utmost importance in a PPE system, since receiving the monitored parameters in real-time and transmitting alerts to the user at any moment are essential for decision making support and user's safety, respectively. Several design approaches have been proposed, each one has advantages and disadvantages. The iVital project relies on the building Wi-Fi network to send the data to the fire command centre. This approach in an urban fire scenario is very unreliable due to the low likelihood of the building network to be operational. A similar approach was adopted by the FIRE project, in this project a wireless sensor network (WSN) was preinstalled on the building, designated SmokeNet, and is used for the communication between the users and the fire command centre [76]. Projects like WASP, PHASER and CoenoFire rely on the mobile telecommunications technology 3G to send/receive data, which might not be available inside large buildings. Additionally, the WASP and the i-PROTECT projects, use the MOTORTRBO mobile radio communication system from Motorola to communicate with the fire command centre. Projects like WearIT@Work, [40] and [89] are based on the strategic deployment of ad-hoc networks. The WearIT@Work project proposes the LifeNet network, which has a system for the automatic distribution of beacons as the users are entering the building [11]. A similar approach was adopted in [88], however the beacon placement is done dynamically by the users. The ProeTEX project proposes the strategic deployment of a long-range communication system, based on Wi-Fi, at the intervention site for bidirectional communication [91]. The ProFiTex project follows a different approach, they developed the Smart Lifeline, which is a braided data and security rope carried by users. It is equipped with data transmission and energy supply capabilities. The communication between the users and the lifeline is wireless and based on ZigBee technology.

2.1.3 Sensors Features

Although WBANs comprise a limited number of sensors and are application-specific, they usually present a higher diversity of Edge of the Network nodes than traditional networks. There are various sensors that are often found in WBANs: Blood Glucose, Air Quality (CO, CO_2), Blood Oxygen, Heart Rate, Inertial sensors, Body Temperature, Blood Pressure, ECG, Electroencephalography (EEC), Electromyography (EMG) sensors and Endoscope Capsule. These sensors can be categorized according to the type of data collected (continuous or discrete time-varying signal), type and location (implant sensor, wearable sensor and external sensor), communication traffic (data rate) and maximum acceptable latency.

Table 2.1. Wearable System features in terms of parameters measured, communication protocols adopted for the three tiers that composes the communication architecture and hardware used.

Project	**Parameters measured**	**Tier-1**	**Tier-2**	**Tier-3**	**E-textile**	**Platform in Tier-1**
WearIT@Work [11]	Location, acceleration to detect arm movements and vibrations, body temperature and heart rate	Wired	Ad-Hoc (ultrasonic)	N.A	No	-
WASP [81]	Heart Rate, breathing rate, activity level and posture	Bluetooth	MOTOTRBO	N.A	No	Zephyr technology
ProeTEX [12]	Heart rate, breathing rate, body temperature, blood oxygen, fall detection, CO and CO_2 concentration, environmental temperature, heat	Wired (RS485) and ZigBee	Ad-Hoc (Wi-Fi)	N.A	ECG textile electrodes, piezoelectric and piezoresistive sensors	-
ProFITEX [92]	Breathing and heart rate, movement pattern and stance, skin temperature, activity level and environment temperature	ZigBee (IEEE 802.15.4)	Wired	N.As	No	Zephyr technology
i-PROTECT [87]	Breathing and heart rate, body temperature, environment parameters and toxic gases	MOTOTRBO	MOTORBO	N.A	Yes. Sensor heart and breathing rate and body temperature	-
iVital [82]	Heart rate, activity level, location and falls	Bluetooth	MOTORBO	N.A	Yes. ECG sensor is based on textile electrodes.	-
FIRE (SmokeNet) [76]	Location, temperature and air quality	Smartphone is the sensing platform	WSN	N.A	No	Telos Sky mote
LifeNet [93]	Temperature and air quality	Ultrasonic	Ad-Hoc (ultrasonic)	N.A	No	RELATE Bricks [94]
PHASER [83]	Hear Rate, ECG, respiratory rate, skin temperature, blood pressure/glucose and user activity (accelerations)	Bluetooth	3G or Wi-Fi	N.A	No	-
Ghosh et al. [89]	Heart rate, body temperature, toxic gases	ZigBee	Ad-Hoc network (ZigBee)	N.A	No	TelosB
CoenoFire [86]	Speed, activity level, location (GPS) and heart rate.	ANT radio	N.A	Cellular Network (4G)	No	-
Soukup et al. [88]	Heart rate, activity level, toxic gases, inner and outer temperature and humidity.	ZigBee	Ad-Hoc (Wi-Fi)	N.A.	Yes. E-textile wiring harness	-
PPL (2008) [84]	User location and tracking	N.A.	-	-	No	-
GLANSER [85]	User location	N.A.	Ad-Hoc (ZigBee)	N.A.	No	-

Table 2.2 lists the most common sensors found in WBAN applications and summarizes their features, showing that every sensor has his own requirements in terms of data rate and latency requirements. The sensors communication traffic is quantified high (thousands of bits are generated per second), low (few hundred bits generated per second) and very low (less than a hundred bits per second) level of communication traffic, whereas the latency requirements are categorized as low (few seconds or minutes), high (less than 250 ms) and very high (lower than 125 ms) according to the demand level.

2.2 WBAN Features

This section approaches the particularities of the WBANs. First, the set of requirements that WBAN networks must meet to ensure their applicability in a wide range of purposes is presented. After, the most widely adopted communication standards in WBAN networks developed for applications that aim to monitor the users that are part of an emergency response team are identified and compared.

2.2.1 WBAN Application Requirements

Several research groups started developments in Wireless Personal Area Networks (WPAN) in the 90s, aiming to interconnect the Body Surface nodes [18]. Several WPANs performance improvements resulted from these developments, namely lower power consumption, short range and low-cost wireless communication standards, such as Bluetooth and ZigBee (IEEE 802.15.4). Although these technologies are often adopted in WBAN projects, they do not offer enough flexibility to cover all the data rate and Quality of Service (QoS) requirements of the wide range of WBAN applications listed below. The limitations of these technologies do not enable the implementations of WBANs able to address the application's requirements [18], [42].

In November 2007, the IEEE Standards Association established a study group as IEEE 802.15 Task Group 6 (TG6) to specify physical and MAC layers to address the specific challenges encountered in WBANs [95]. The TG6 started in 2008 with an invitation of contributions for candidate wireless applications in or around a body, which require or might take advantage of the WBAN communication standard [96]. In September of 2008, the TG6 provided a technical requirement document (TRD) [97] gathering a set of technical aspects that proposals for the IEEE 802.15.6 WBAN standard must fulfill. The TG6 requirements covers several issues, such as performance, reliability, availability and maintenance-level, as follows:

- WBAN links should support bit rates in the range of 10 kb/s up to 10 Mb/s;

Table 2.2. Main features of sensors often present in WBANs, sources [14], [15], [17], [102], [142], [192], [193].

Sensor	**Parameter Measured**	**Placement**	**Signal type**	**Data Rate**	**Latency**
Blood Glucose	Measure the blood sugar level	Wearable	Discrete	Low (1.6 kbps)	Low (few minutes)
Air Quality	CO, CO2, etc.	External/Wearable	Discrete	Very low	Low
Blood Oxygen	Blood oxygen saturation	Wearable	Discrete	Very Low	Low (< 3s)
Heart Rate	Number of heart beats per minute	Wearable	Discrete	Very Low	Low (< 3s)
Magnetometer	Measure magnetic induction intensity	Wearable	Continuous	Low (35 kbps)	Low
Body Temperature	Temperature of human body	Wearable	Discrete	Very Low (120 bps)	Low
Accelerometer	Acceleration on each spatial axis of three-dimensional space	Wearable	Continuous	Low (35 kbps)	Low
Gyroscope	Angular velocity of rotating	Wearable	Continuous	Low (35 kbps)	Low
Blood Pressure	Peak of pressure of systolic and the minimum pressure of diastolic	Wearable	Discrete	Low	Low (<3s)
electroencephalogram	Measure the spontaneous brain activity	Wearable	Continuous	High (90 kbps)	High (latency < 150 ms)
ECG	Measure the heart electrical activity	Wearable	Continuous	High (71-288 kbps)	High (latency < 150 ms)
EMG	Measure the electric activity of skeletal muscles	Wearable	Continuous	High (320 kbps)	High (latency < 150 ms)
Endoscope Capsule	Used to record images of the digestive tract for use in medicine	Implant	Discrete	Low	Very High latency (< 50 ms)

- The PER should be less than 10% for a 256 octet payload (i.e. 256 x 8 bits of data) for the 95% best-performing links based on PER, i.e. at a given signal-to-noise ratio, those 5% of radio channels that PER performance should not be used to determine if reliable requirement is met;
- Edge of the Network nodes should be scalable up to a number of 256;
- Edge of the Network nodes and Body Gateway nodes should be capable of reliable communication even when the user is moving. Although it is acceptable for network capacity to be reduced, data should not be lost due to unstable radio channel conditions The considered applications include postural body movements relative to sitting, walking, twisting, turning, running, waving arms and dancing, among others, which result in the shadowing effect and radio channel fading. Nodes of different WBANs may move individually with respect to each other, promoting interference;
- Edge of the Network nodes should be capable to joint or be removed from the WBAN in less than 3 seconds;
- Latency (communication delay), jitter (variation of one-way transmission delay) and reliability must be supported for critical WBAN applications. The TG6 categorize the WBAN application in medical and non-medical, where the maximum acceptable

latency in the former applications is 125 ms while in non-medical applications is 250 ms. The jitter on communications should be less than 50 ms;

- On-body and in-body WBANs should be capable of coexist in and around the human body;
- Security and privacy are key concerns in medical applications, a multi-level security should be ensured, and the level that best suits is application-specific. Thus., security must be lightweight, scalable and energy efficient;
- The physical layer should support at least ten co-located WBANs randomly distributed in a volume of 6 m^3;
- All Body Surface and Implant nodes should be capable of transmitting at 0.1 mW (or -10 dBm) and the maximum radiated transmission power should be equal or less than 1 mW (or 0 dBm). This complies with Specific Absorption Rate (SAR) of the Federal Communications Commission's 1.6 W/kg in 1 g of body tissue[1] in US, which equates to a maximum transmitter radiated power of 1.6 mW; and EU SAR regulations: 2 W/kg in 10 g, which limits the radio-frequency transceiver output power in EU < 20 mW;
- WBANs should be capable of operating in a heterogeneous environment where networks of different standards cooperate amongst each other to receive information;
- Capability of providing a fast (<1 sec) and reliable (99.9999%) reaction when exposed to emergency situations and alarm messages. Higher priority must be provided to this type of messages;
- A transmission range of at least 2 meters shall be supported (while meeting link bit rates). However, in some applications the range can be extendable up to 5 meters;
- A WBAN can incorporate Ultra-Wide Band (UWB) technology with a narrowband transmission to cover different environments and support high data rates. For instance, some medical applications such as ECG monitoring might require a UWB-based WBAN to support higher data rates;
- Power saving mechanisms should be incorporated to allow WBANs to operate in power constrained environment.

In November 2008, the TG6 issued a Call for Proposals for development of the IEEE 802.15.6 standard [98], as a consequence of the high number of responses to the call of

[1] Http://www.fcc.f.ov/oet/rfsafety/sar.html

applications, confirming the industry's interest in WBANs. The TG6 call for proposals received 34 proposals which were assessed based in their capacity to fulfil the technical requirements above listed. The several proposals were merged into a single draft of the standard in April 2010, while the rectified version [19] was released in 2012. This standard defines the Physical (PHY) and MAC layers and has as main key feature the flexibility to support several (medical and non-medical) applications with its own of requirements in terms of data rate, energy efficiency, and reliability. This standard aims to give the manufacturers the flexibility to design their nodes in an application-specific way, since the applications requirements cannot be simultaneously maximized [99].

Although the technical requirements presented by the TG6 [97] were defined to assess potential standards, they provide valuable insight into the expected requirements of the target applications and serve as guidelines for developers to design appropriate networks for a wide range of applications [13]. Nowadays, the network performance are often qualified in terms of its main QoS parameters such as delay profile, delay jitter, and data packet loss rate [100].

2.2.2 Standard Solutions

The analyse of the wearable systems proposed for emergency response team monitoring application shows that the wireless communication standards ZigBee and Bluetooth Low Energy (BLE) are the most adopted on Tier-1 communication segment of communication architecture depicted in Figure 1.1.

Comparison of Wireless Communication Standards

There are several important factors to consider when choosing a wireless technology, namely QoS requirements (scalability, uninterrupted connectivity, promote information exchange, mitigation across the network and interconnect plug and play devices), power usage (fundamental to the design of energy-efficient WBANs) and SAR (according to the IEEE 802.15.6 TG, technologies must follow local or international regulations) [18]. Table 2.3 summarizes some of the characteristics of the most used communications standard in WBAN area and standards specially thought to handle the specific requirements of WBAN applications.

Table 2.3. Features of the most used wireless technologies in WBANs, source [18], [73].

Technology	**Frequency**	**Data Rate**	**Coverage Area**	**Modulation**	**Network Topology**
IEEE 802.15.4 (ZigBee)	2.4 GHz (ISM band)	20, 40, 250 kbps	10-100 m (on-body only)	O-QPSK, BPSK (+ASK)	Star, mesh and cluster-tree
IEEE 802.15.6 (UWB)	3.1-10.6 GHz	110-480 Mbps	5-10 m (on-body only)	OFDM, DS-UWB, BPSK, QPSK	Star
Bluetooth Low Energy	2.4 GHz (ISM band)	1 Mbps	10 m (on-body only)	GFSK	star

In terms of QoS requirements, the IEEE 802.15.6 standard is the most appropriate for supporting applications with different data rates, being suitable for short range applications (5-10 m) with high data rate [18]. However, to best of the author's knowledge there is not IEEE 802.15.6 transceiver commercial available able to enable a multiple layer operation mode. The TG6 defined three different physical layers, namely (1) Narrowband (NB), (2) Ultra Wide Band (UWB) and (3) Human Body Communication (HBC) for the IEEE 802.15.6 standard. Some UWB transceivers can be found in market, which have been mainly used in indoor localization systems, complementing GPS for WBAN tracking [101]. Although this band is the one with more potential to WBAN applications (band frequencies are Worldwide available; support of high data rates (110-480 Mbps) [18], [73]; short range communication (<10 m) [72], [102]); and signals are emitted over a large bandwidth, providing robustness to jamming with low probability of interception [17]. The industrial interest on this technology decreased due to the costs of the technology and the data rates of the first devices introduced, which presented lower values than the data rates theoretically estimated. Furthermore, the energy consumed by UWB transceivers is significantly higher than Narrowband transceivers in receiver mode [60].

Regarding the power consumption and SAR metric, the BLE is more adequate than the IEEE 802.15.4 standard. The BLE is the ultra-low power consumption configuration of the Bluetooth technology with the follow key features: robustness, low power consumption and low cost [103]. The BLE offers the following implementation's types: single-mode BLE, suitable for low energy nodes with small-factor and short-range communication (<10 m); and dual-mode that enable the nodes to operate in both high-power (in the case of a smartphone for audio streaming, for example) and low-power (to connect to a heart rate monitor, for example) modes. The BLE transceivers can consume 92 nJ/b and their cost is considered low [18]. Theoretically, the BLE node power consumption is comparable to that of IEEE 802.15.4, but the data rate is four times higher [104]. However, the reported BLE throughput was lower than 100 kbps [105], [106]. The communication standard BLE is the most convenient standard for short-term high data rate applications [18], since it is able to support applications with different

data rates (up to 1 Mbps) within a range of less than 10 m. This technology only supports star topology [73] and this limitation is seen as the main disadvantage of the BLE technology, since it limits the scalability of WBANs.

Although the IEEE 802.15.4 standard does not stand out in any of the factors summarized at the beginning of this section, this standard is the one that has received more attention from the scientific community so far. Several research projects were successfully built using the IEEE 802.15.4 standard (c.f. section 2.1). According to Yazdi et al., the IEEE 802.15.4 standard will remain a serious candidate for WBAN applications due to its maturity, availability and variety of low-cost commercially available transceivers [107]. The interest of the industry and from the research community dictated the emergence of solutions (such as ZigBee, IPv6 over Low-Power Wireless Personal Area Networks - 6LoWPAN -, and WirelessHART) that complement the standard with higher level protocol's layers, turning the IEEE 802.15.4 the most used standard in both WSNs and WBANs projects.

The IEEE 802.14.5 frequency bands and maximum achievable data rates shed light on the main disadvantages of this standard, namely: (1) high probability of being subjected to inter-WBAN interference and (2) standard not able to meet data rate requirements of all WBAN applications.

Wireless communication protocols such as ZigBee, Bluetooth, BLE and Wi-Fi share the same frequency spectrum [71]. Thus, the transmission range of WBANs and other types of network can overlap, causing interference that can degrade the WBAN QoS, leading to unnecessary energy consumption and performance degradation [75], [108]. The maximum data rate of the IEEE 802.15.4 standard is 250 kbps, which limits the target WBAN applications, since it is not enough to support the data rate requirements of some applications (c.f. Table 2.2). However, the IEEE 802.15.4 maximum data rate is higher than those required in most of the WBAN applications.

IEEE 802.15.4

Since the IEEE 802.15.4 is the most adopted standard in WBAN projects, it was chosen as the standard for the WBAN application addressed in chapter 4. A brief description of the PHY and MAC layer of the IEEE 802.15.4 is provided in this section.

The target of this standard is the low data rate and low power consumption applications with low requirements in terms of latency and performance [73].

The PHY layer of the IEEE 802.15.4 specifies 26 half-duplex radio channel across three different bands, which differ in the region availability, data rate and modulation technique

adopted. The 868 MHz ISM band (a single radio channel with a data rate up to 20 Kbps using Binary Phase Shift Keying modulation), the 915 MHz ISM band (ten radio channels with a data rate up to 40 Kbps using BPSK modulation) and the 2.4 GHz ISM band (divided into sixteen radio channels with a bandwidth of 2 MHz and maximum data rate of 250 Kbps using Q-QPSK modulation with a communication range up to 100 m) [109]. The 868 MHz and 915 MHz ISM bands are not worldwide available (only in Europe and United States) and offered bandwidth is short to the majority of the applications. The 2.45 GHz ISM band is the most popular and most adopted in WBAN projects, since it offers worldwide availability, short range communications, low power consumption operation, and acceptable on-body propagation characteristics (although higher than the 868 MHz and 915 MHz ISM bands [60]). At the same time, nodes transmitting in this band only require small and light antennas.

To reduce concurrent transmissions among Edge of the Network nodes, this standard specifies two access mechanisms, namely beacon- and non-beacon-enable [110]. For instance, in non-beacon-enable access, the Edge of the Network nodes have to sense the radio channel before transmitting data. The unslotted Carrier Sense Multiple Access with Collision Avoidance (CSMA/CA) protocol is used. Thus, Edge of the Network nodes only transmit data when the radio channel is free. Otherwise, the transmission is delayed by a random amount of time. In beacon-enable mode, the radio channel access is managed through a Superframe (SF). Beacon frames, which are transmitted periodically to Edge of the Network nodes, delimit SF boundaries, ensuring synchronization in the network. Beacon Intervals (BI) are used to define the time between two consecutive beacons. Thus, by receiving the beacons the Edge of the Network nodes get knowledge of the SF duration and the moment when they can transmit their data packets. The SF structure comprises two portions, the active and inactive portion. The former portion consists of 16 equally spaced slots, so-called SF time slots, corresponding to 15.6 ms each (assuming 250 Kbps in 2.45 GHz band). This portion is divided into two periods, the Contention Access Period (CAP) and Contention Free Period (CFP) as depicted in Figure 2.2. In the CAP period, the Edge of the Network nodes access to the medium exactly like in non-beacon mode, but within the SF time slots. The CFP period is divided in time slots named Guaranteed Time Slot (GTS), which are allocated by the Coordinator node to the Edge of the Network nodes (these nodes can only transmit data during his GTS in a contention free fashion).

2.3 Wireless Communication Basics

On-body communications are not well understood yet, being the number of research works addressing this subject very reduced when compared to those carried out in the WSNs

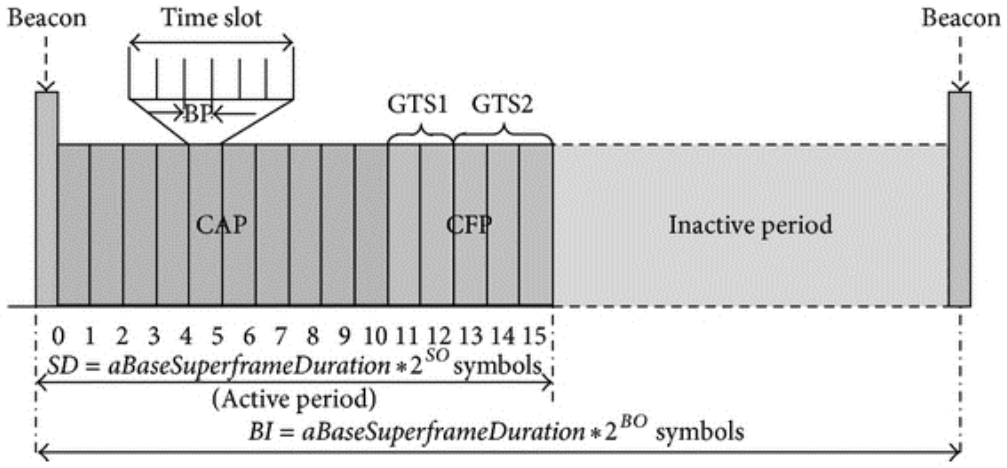

Figure 2.2. Superframe structure of the IEEE 802.15.4 standard [110].

communication field. On-body electromagnetic waves propagation have been typically modelled in two levels of abstraction, using path-loss and fading models.

2.3.1 Path-Loss Models

The path-loss models describe how the attenuation in power (density) of the electromagnetic waves decays logarithmically with the distance. Log-distance path-loss model was developed for traditional networks, but several research works (e.g. [27], [111]–[116]) have used it to model WBAN radio channels. This model is expressed as [111]:

$$P_{dB}(d) = P_{0,dB} + 10 * n * \log\left(\frac{d}{d_0}\right) = -|S_{21}| \quad (2.1)$$

where P_{dB} refers to the path-loss in dB at distance d in cm, which decays logarithmically at a rate n; $P_{0,dB}$ refers to the path-loss in dB at a reference distance d_0 [117]. The value of the coefficient n is environment-dependent, and authors extract it by adjusting the curve of the model to empirical measurements [117]. Although distance influences the on-body communication reliability, it is not the dominant factor as defended by several authors, e.g. research works [111], [112], [118]. For example, a weak and hardly noticeable relationship between distance and path-loss is reported in [111] (for a fixed distance between the Coordinator and End node, the model predicts always the same path-loss). A pair of nodes at the same distance but in located at different body limbs are subject to significantly different levels of attenuations [112]. Thus, the coefficients of expression (2.1) must present different values for each pair of nodes [26]. This suggests that the average signal power cannot be treated as a deterministic value and cannot be described using a simple power-distance equation. Due to the high diversity of radio channel conditions, an one-model-fits-all approach is not possible in WBANs.

Since the WBAN radio channels have different properties from other radio channels, the research community has started looking for alternative ways to model these radio channels, opting for the development of models for specific communication scenarios.

The TG6 proposed three radio channel models designated CM3A, CM3B and C3MC that describe the signal power on a per-link basis, discriminating the empirical data to be analysed in terms of location of the node, frequency of operation, and surrounding environment. This approach allows authors to reach a relation of cause-effect [119]. To take into consideration the variability of the path-loss, the TG6 has adopted the standard log-distance path-loss model and included a log-normal shadowing variable. For example, the CM3A model includes a normal distributed variable, which represents th*e* shadowing effects [119]:

$$P_{dB}\left(d_{[mm]}\right) = a * \log\left(d_{[mm]}\right) + b + N \tag{2.2}$$

where P_{dB} refers to the path-loss in dB at distance d in mm, a and b are coefficients of linear fitting, N is a normal distributed variable, with an average value zero and standard deviation σ, dB. CM3A channel models were fitted to empirical data, gathering from WBAN using the measurements performed for several static pairs of nodes (located at the user's left wrist, left upper arm, left ear, head, shoulder, chest, right rib, left waist, thigh, ankle and hip), covering different narrowband frequencies (400-450, 608-614, 950-956, 2400-2450 MHz) and environments (hospital rooms and anechoic chambers) while the user was standing. Table 2.4 summarizes the obtained results, i.e. values of (2.2) parameters. More detailed information about measurements set, derivation, and data analysis is provided by research work [14]. Other studies tested the CM3A model against empirical data [113], [120].

2.3.2 Fading Models

To overcome the difficulties in capturing and modelling the properties of the on-body channel due to its stochastic properties, WBAN radio channels are commonly modelled using statistical distributions, designated fading models, proposed for each configuration scenario. This approach was initially suggested by the IEEE 802.15.6 Task Group. In the CM3C channel model, the path loss model is complemented with a fading distribution. Fading models are typically divided into two sub-models: first- and second-order statistical model.

First-Order Models

The first-order statistical model aims to describe the signal amplitude assuming that it is a wide-sense stationary process [60]. The WBAN fading distributions are obtained through the determination of well-known distributions such as Normal, Log-normal, Nakagami-m, Gamma,

Weibull, Rice, Rayleigh, etc. that best fit the empirical data. These distributions abstract from any time dependency or temporal correlation in the signal.

Smith et al. analysed how often a particular distribution was found to best fit the radio channel and concluded that the distributions that are more consistent in terms of the relation between number of times that a distribution is considered and the rate of "approval" are Log-normal, Nakagami-m, Gamma and Weibull [13].

The log-normal distribution is the best-suited distribution for scenarios where the user is standing [113], [121] or when involuntary movements are performed [59], [122], [123].

The Nakagami-m distribution is suited for dynamic scenarios (severe fading scenarios, i.e. very dynamic time-variant nature of the signal attenuation) [122] and it should not be considered to statistical modelling fading in stationary scenarios [62], [124].

The Weibull and Gamma distribution are often suggested as suitable to describe radio channels subjected to severe levels of fading [111]. For example, for scenarios in which the user is walking or running and the selected band is 427 MHz, 800 MHz, 820 MHz, or 2.36 GHz ([62], [122], [125]); and when the user is standing up and standing down at several sub-GHz bands (444.5, 611, 953 MHz) [26]. According to D'Errico and Ouvry, the Weibull distribution can be used to describe the fading amplitude for several movements of the user [62]. This distribution and the Gamma distribution are known for their ability to model an agglomerate of data collected for long periods [62], [126]. For instance, Smith et al. collected data for 2 hours while the user (wearing several Edge of the Network nodes) performed daily activities, predominantly on indoor environments [99].

Second-Order Models

The path-loss and the first-order fading models do not take into consideration the temporal correlation of the radio channel. The fluctuation of the power of received signal over time can be described using several parameters such as fading rate, fading duration, fading magnitude, Doppler spread, outage and non-outage period, outage rate, and coherence time. This knowledge is important to the development of several strategies that aim to improve WBAN communications (e.g. design of protocols and error correcting codes [127], radio channel

Table 2.4. CM3A parameters values for different scenarios, source [14].

Frequency (MHz)	**Hospital Room (a; b; σ)**	**Anechoic Chamber (a; b; σ)**
400-450	3; 34.6; 4.63	22.6; -7.85; 5.60
608-614	16.7; -0.45; 5.99	-17.2; 1.61; 6.96
950-956	15.5; 5.38; 5.35	28.8; -23.5; 11.7
2400-2500	6.6; 36.1; 3.8	29.3; -16.8; 6.89

behaviour prediction [128], Transmission Power Control mechanisms [129], data packets retransmission strategies [26], packets schedulers [130], interleave size optimization, and data packets sizes scaling [59]). It can be also used to analyse the system throughput [121], to identify the Edge of the Network nodes locations more susceptive to have poor communication radio channel conditions (in terms of fading features) and the best location for potential relay nodes [25]. The second-order parameters are extracted from the received data packets by means of second-order techniques such as Level Crossing Rate (LCR), Average Fade Duration (AFD), and Autocorrelation Function (ACF).

The LCR technique is typically used to quantify the rate at which a signal strength crosses from above to below a given threshold level per second. This technique can be used to provide the fading rate parameter. The AFD technique enables the determination of the fading duration, i.e. the total time that a signal remains below the threshold over the number of crossings. The received signal is often normalized and the average value of the signal removed so that all signals have a 0 dB mean value [123]. Several thresholds have been considered, for instance, in the range -30 dB to 30 dBm with increments of 0.5 dB [59], -30 dB to 15 dB in steps of 0.5 dB [123], −20 to 10 dB in steps of 0.5 dB [121], and -30 to 10 dB in steps of 0.5 dB [25].

Both the AFD and LCR techniques are highly dependent on radio channel dynamics, for instance, Franco et al. reported a fading rate of 3Hz and 2.4 Hz (considering an assigned 10 dB threshold) while the user was running and walking in an indoor environment, respectively [25]. The same study showed that the surrounding environment has a significantly influence in the fading rate parameters, since authors reported lower values at outdoors environments. Regarding the fading duration, the same authors concluded that for the same threshold the signal remains under the threshold for the duration of a single data packet (10 ms) [25].

The technique ACF is used to identify repeating patterns in the fading signal based on the following assumption: "due to the often repetitive nature of human body movement caused by both physiological and biomechanical processes, it is anticipated and indeed expected that noticeable correlation may exist between current and previous observations of the received signal" [124]. The technique ACF is useful to determine the coherence time value, since the majority of the research studies determine and validate coherence time by verifying if the autocorrelation coefficients of the amplitude of two signals (in the time domain) is greater than 0.5 [131] or 0.7 [125], [132]. The parameter coherence time describes the time dispersive nature of the fading in the time domain, similar to the Doppler spread in the frequency domain (coherence time and Doppler spread are inversely proportional to each other [131] and practical approximation have been derived ($T_c = 9/16\pi f_m$) in [117]). The parameter coherence time is

an important measure for the WBAN field, since it specifies the amount of time over which the radio channel is assumed to be stable, i.e. the period in which is possible to perform a successful data packet transmission [125]. This metric is used to specify the data packet lengths and maximum symbol rates that can be achieved [13], [125], [131]. Several research works (e.g. [26], [62], [125], [131], [133], [134]) have studied this parameter in different scenarios, showing is values depends on node location and movements. D. Smith et al. obtained a TC mean (average of all pair of links) of 48 ms while the user was walking and 31 ms when the user was running for 20 s [125]; other type of user's movements have been considered in the literature, such as "standing up/sitting down" (coherence time value on the range of 85-310 ms) [26] and jogging (27 ms) [131]. In the research work carried out by Fu et al. relative to Doppler spread, the authors have reported coherence times (link user's left ankle-user's right hip) of 308 ms, 125 ms and 27 ms for movements standing, walking, and jogging, respectively [131].

2.4 Summary

This chapter provides background information about the field of study wearable systems, aiming introduce the main concepts that will be used on the following chapters. First, a generic wearable system architecture is presented, which is then adopted to review and compare several WBAN projects addressed in the literature for emergency response teams. An in-depth analysis of these projects' design choices for each architecture's tier in terms of communication protocols, monitored parameters and hardware platforms was also presented. This analysis showed that although the licensed free bands are more favourable for reliable communication as the amount of RF interference is reduced, the unlicensed frequency bands such as the 2.4 GHz ISM band is often the first choice for the majority of the WBAN projects analysed. In regard to the wireless communication standards, the ZigBee (IEEE 802.15.4) is the one most often adopted in on-body communications and will remain a serious candidate for WBAN applications due to its maturity and availability. Afterwards, the most adopted sensors, for emergency response applications, in WBANs were highlighted and their requirements in terms of data rate and latency were discussed. This analysis showed that the ZigBee protocol does not meet the data rate requirements of all type of sensors frequently required in WBANs.

Finally, a brief revision of the on-body fading characteristics was performed the WBAN radio channel models were discussed. This revision has shown that path-loss models are not suitable to describe the unique characteristics of wireless on-body signal propagation. Techniques adopted to extract the on-body signal propagation characteristics were also addressed.

CHAPTER 3

TPC MECHANISMS: THE STATE OF THE ART

The time-variant nature of the fading is a critical issue in WBANs. An inefficient use of the transmission output power might cause critical data packets to be lost and hence can be a threat to potential critical WBAN applications. In this regard, to meet the strict requirements of WBAN applications, a Transmission Power Control (TPC) mechanism able to adjust the radio-frequency (RF) transceiver output power accordingly to the unique changing conditions observed in WBAN radio channels is mandatory [135].

Several TPC mechanism have been explored to adjust the transmission output to minimize the energy consumption in WBANs with star [1], [4], [136]–[145], [5], [146], [9], [22], [39], [46], [48], [50], [135] and multi-hop topologies [49], [51]–[54], [147] and to mitigate inter-network interference in coexisting WBANs [10], [43], [153], [44], [45], [108], [148]–[152].

TPC mechanisms also have an important role in the task of mitigating the inter-network interference. The inherent body mobility may render WBAN radio channels to inter-network interference due to the coexistence of other systems or devices. Since WBAN nodes are wearable, people unpredictable movements may lead to nodes moving in and out of each other's range [18]. In WSNs, the inter-network interference problem has been mitigated by using a centralized coordinator, which controls the medium access and the RF transceivers output power of all surrounding WSNs [44]. However, this solution is not applicable in WBANs, since WBANs works independently in a distributed way and due to their inherent dynamics it is unfeasible to allocate a global coordinator [18]. Several strategies proposed to avoid inter-network interference also control the RF transceiver output power control to reduce the interference between coexisting networks and devices. Due to the mobility of WBANs, areas with a high density of WBANs are expected. Thus, strategies such as radio channel hopping or theory game might be inefficient due to the limited number of available radio channels. Thus, the TPC mechanisms developed to WBANs have an important role as a technique to avoid and reduce the RF interference between coexisting WBANs through the control of the Signal-to-Interference-plus-Noise ratio (SINR) in each of the coexisting networks, offering a better stability for all networks [43], [44], [108], [149]. The TPC mechanisms addressed in the

literature have shown to be able to reduce the RF interference and significantly decrease the power consumption [149].

The research community focused on implementing TPC mechanisms for the on-body radio channel in WBANs that use the narrowband propagation methods. This may be due to the fact that on the majority of the WBAN applications, the communication subsystem operates in narrowband frequencies, especially unlicensed ones such as Industrial Scientific and Medical radio bands (centred at 2.45 GHz) [36], [65] and [66]. Furthermore, first- and second-order statistics on data obtained from several research works[25], [26], [62], [113] proved that there are no major differences between frequency bands: 400 MHz (centred frequency of Medical Implant Communication System (MICS) band), 600 MHz (centred frequency of Wireless Medical Telemetry Service (WMTS) band), 900 MHz (ISM band), 2.395 GHz (centred frequency of Medical Body Area Network (MBAN) band), 2.45 GHz (ISM band) and 3-5 GHz (low UWB bands). This is another reason why TPC mechanisms should be further developed for 2.45 GHz band and used in other communication bands.

This thesis is focus on TPC mechanisms designed to be applied on star topology WBANs where mitigation of inter-network interference is not their main goal (however, reducing the output power may reduce the likelihood of this network to affect the performance of neighbourhood networks). Inter-network mitigation TPCs require cooperation between Coordinator nodes of different WBANs. This chapter will focus on the events within the WBAN itself. TPC mechanisms for multi-hop WBANs are thus not covered in the present section because typically WBANs have a very low density of Edge of the Network nodes which, in some cases, turns this type of TPCs impractical. However, TPC mechanisms addressed to multi-hop networks adopt some of the principles described in this chapter.

The following features are expected in TPC mechanisms designed for on-body communications: (R1) agility to react to changes in radio channel conditions; (R2) to estimate and also (R3) anticipate the run-time behaviour of on-body radio channels; (R4) fast in reaching the optimal transmission output power; (R5) low memory usage; (R6) low traffic overhead (imposed by control packets, data packets, beacons and acknowledges (ACK)), (R7) able to operate in dynamic scenarios (characterized for having user movement); (R8) able to detect possible incidental disconnections on wireless links, preventing unnecessary fluctuations in the transmission output power output; and (R9) low complexity. A generic architecture to describe the operation principle of the TPC mechanisms addressed in the literature is here proposed. Figure 3.1 depicts the overview of this architecture that comprises two main blocks:

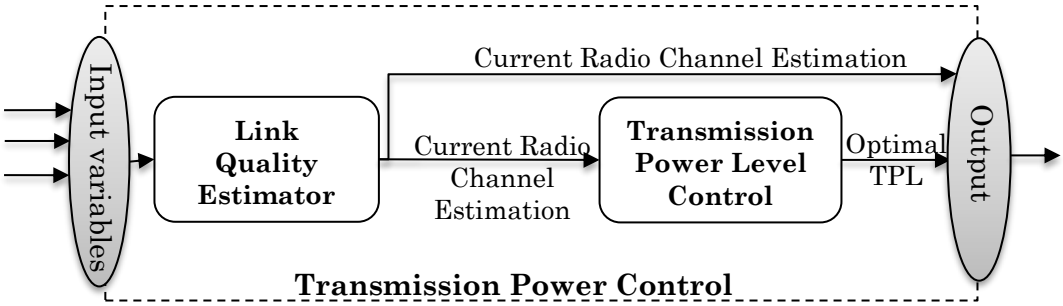

Figure 3.1. Generalized representation of the output power control process.

- Link Quality Estimator (LQE), responsible for quantifying (estimating or predicting) the current quality of the wireless links in order to modify the output power in an energy efficient way;
- TPL control module, responsible for selecting the most suitable transmission output power, according to the output of the LQE.

In this section a comprehensive analysis of the methods used in LQE and TPL Control blocks is carried out in sections 3.0 and 3.2, respectively. In section 3.3, a taxonomy to classify the different TPC mechanisms developed and addressed in the literature is proposed. In addition, a comparative summary of the state-of-the-art TPCs for on-body radio channels in WBANs, highlighting their similarities and differences in terms of design choices and fulfilment of the WBAN application' requirements, is provided in section 3.3. Finally, in section 3.4, the issues and challenges in the design of TPCs are highlighted.

3.1 Link Quality Estimator Module

To be able to analyse and assess the different methods used to estimate the current radio channel quality, a taxonomy, depicted in Figure 3.2, classifying the different LQEs, was proposed and used. The LQEs are categorized as Hardware-based (HW-based), Inertial Sensor-based and Software-based (SW-based) methods. As SW-based LQE methods rely in the Expected Transmissions (ETX), Packet Reception Rate (PRR) and SINR metrics to estimate/predict the radio channel quality, they are only adopted in TPC mechanisms though to multi-hop WBANs and to mitigate inter-network interference. For that reason, this section is only interested in HW-based and Inertial Sensor-based LQEs. For detailed information about the SW-based methods, please refers to literature [64].

3.1.1 Hardware-based LQE

Estimators based in HW-based solutions can be described as mechanisms that rely on physical layer metrics' readings. These metrics are provided by the RF transceiver, such as, the

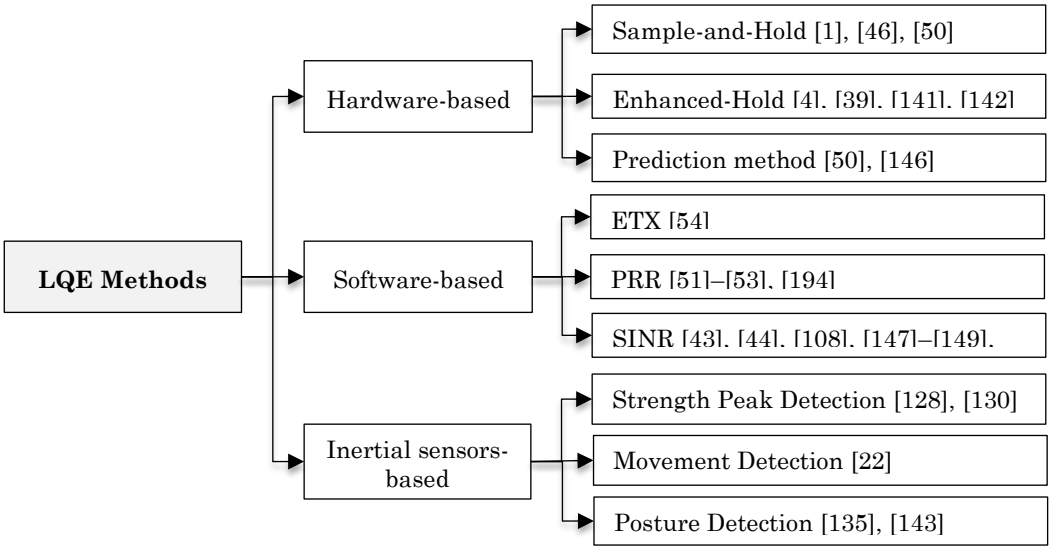

Figure 3.2. Taxonomy of the LQE methods for on-body channels in WBANs.

Received Signal Strength Indicator (RSSI) - computed internally by averaging the power signal over eight symbol periods of the incoming packet [47] – and the Link Quality Indicator (LQI) – the measure of the RF transceiver chip error rate of the first eight symbols of the incoming packet [47] which estimates the quality of the error of a successfully received packet. However, as these metrics can only be fetched on the data packet receivers (in the Coordinator node rather than in Edge of the Network nodes), extra data packets, often designated as control packets, such as beacons, acknowledges or other data packets are needed to convey these information back to the original data packet senders (Edge of the Network nodes). The LQEs that fit within this category are classified according to the method adopted as Sample-and-Hold (S-H), Enhanced-Hold (E-H), or Prediction method.

Sample-and-Hold Method

In the S-H method, the metric RSSI is often the estimated output, the result of the radio channel quality estimation process is the measured RSSI of the last data packet received. This method has been reported as a very reliable approach to estimate the radio channel conditions in stable-channel-static scenarios [1], [46], [50], which occur when the user remain static and in environments with a reduced number of reflecting objects.

Enhanced-Hold Method

Similar to the previous method, the majority of the proposed LQEs based on the E-H method adopt the RSSI metric to estimate the current radio channel condition. To provide a reliable LQE output, designated radio channel gain ($\bar{\bar{R}}$) and given by (3.1) [1], [142], both the power of the last measured sample (R_n) and the history of RSSIs received from the Edge of the

Network nodes are taken into consideration. This latter component of (3.1) is the weighted average of the lowest RSSI samples (α) [39], [141].

$$\bar{R} = \alpha\bar{R} + (1 - \alpha)R_n \tag{3.1}$$

The determination of the optimum value of α and the number of samples considered to estimate the radio channel gain are key issues. Parameter α manages the existing trade-off between the agility of the estimator to react to changes in radio channel and the reliability of estimations. Its optimum value depends on the sensor location and the surrounding environment. For instance, in slowly varying radio channels, higher values of α can be used, giving more weight to the current radio channel sample and making the LQE more agile to react faster to the changes in radio channel conditions. In radio channels that present high and fast quality variations, lower values of α can be used, which increases the weight of the radio channel history, making the estimator less agile, but with less fluctuations in estimations.

Researchers usually rely on experimental data to determine the most suitable values for the average weight parameter, proposing either static and pre-defined values or more than one value. Shah et al. proposed two different values according to the radio channel conditions, namely α_1 and α_2 – which are inversely proportional – for good and bad radio channel conditions, respectively [39], to increase the TPC mechanism performance in both conditions. Di Franco et al. proposed an adaptive α that is updated by increasing or decreasing, at run-time, the current value of α by a constant, according to the mean square error (MSE) of estimations [142]. The research work [4] proposed a LQE that combines estimation metric RSSI and LQI, designated RSSI/LQI estimator. Through experimental observation of the relation between LQI and PRR, they concluded that the metric LQI is not highly influenced by interferences, but it has a much higher variance than the RSSI (regardless of the user movement), thus requiring the use of the average LQI to estimate/predict the radio channel conditions. As this solution might impair the agility of a TPC to adapt the TPL, authors proposed a LQE that relies in the weighted average of LQI, given by (3.1) (parameter $\bar{R}$ and R refer to the weighted average LQI and last LQI samples, respectively), to identify if the radio channel is subjected to interferences (if the weighted average of metric LQI is higher than a threshold), whereas the weighted average RSSI, given by (3.1), is applied to estimate the signal attenuation when the radio channel is not subjected to interferences.

Prediction Method

The LQEs following the prediction method estimate the radio channel conditions (radio channel gain) by reducing the number of control packets exchanged between the Edge of the

Network nodes and the Coordinator node. Research works that fit in this category are scarcer. Predictor LQEs proposed in [50] are very simple. Either the sample-and-hold method or the enhanced-hold method are used to predict with 250 ms, 400 ms, 800 ms and 1 s ahead, for time intervals between received data packets ranging from 10 ms up to a maximum of 400 ms. These prediction mechanisms presume that there is an inherent long-term temporal stability of the radio channels, that can be quantified by the metric Coherence Time (TC). This metric specifies the time over which the radio channel is assumed to be stable [125]. Therefore, a prediction scheme requires the TCs higher than the prediction interval to ensure an acceptable reliability, otherwise the control power can be either unreliable (data packets can be lost) or energy inefficient (power higher than the minimum needed to ensure successful data packet deliver).

The Weighted alternate-least-squares technique proposed in [146] is more complex than the previously described. This LQE aims to predict the next T_{pr} RSSI samples ahead of the last sample received (maximum referred is up to 2s). A fraction of the measurement of RSSI samples (N_s) received by the Coordinator node is saved in its memory, taking the n_r last samples received to search over the previous N_s samples to find the closest match. The prediction signal portion (S_p) is estimated using an alternate least-squares formulation that is weighted by the last sample received. According to the authors, the number of n_r must depend on the superframe (SF) period (t_s).When comparing the performance of this LQE set up with a N_s of 4s and a n_r of 5 ($t_s = 10\ ms$), 4 ($t_s = 20\ ms$),3 ($20\ ms < t_s < 120\ ms$) and 2 ($t_s > 120\ ms$), with a sample-and-hold based LQE with transmissions performed at a pre-defined and static TPL (-10 dBm) and sampling periods varying from 10ms to 120 ms, the authors concluded that there are clear improvements in all predictions from 120 ms ahead to 2s ahead over the sample-and-hold and static TPL transmissions, showing good prediction accuracy up to 2s ahead, even in scenarios with the TC of 500 ms.

3.1.2 Inertial Sensor-based

As user's body posture and movement are considered to greatly influence radio channel behaviour [48], some LQEs rely on inertial sensors, such as accelerometers and gyroscopes, to estimate or predict the radio channel conditions. The methods relying on inertial sensors can be categorized in terms of the strategy adopted as, Strength Peak Detection, Movement Detection and Posture Detection.

Strength Peak Detection

This type of LQEs aims to explore the periodic fluctuation of the link quality to improve the transmission energy efficiency. The research work [130] has shown that there is a strong

correlation between the RSSI of emitted signals and the acceleration signal when the user is walking. Through the acceleration signal it is possible to determine the signal quality fluctuation period as well as the instants that the signal strength is expected to be high.

The LQEs addressed in [128], [130] rely in the accelerometer information to determine the peak of the RSSI metric, according to the correlation between radio channel quality and acceleration (positive or negative, acceleration peak or valley respectively) previously identified. However, the accelerometer data only indicates which time instant within the gait cycle the radio channel quality is expected to be maximum, thus, the estimation or prediction of the RSSI in order to provide it to the next TPC block, the TPL control block, is still required.

All approaches that follow this type of LQE opt for applying this in a receiver-side approach, since this solution is too complex to be executed in a typical (resource-constrained) Edge of the Network nodes due to the methods adopted to track the gait cycle offset. The transmitter after receiving information about the time interval between two adjacent gait cycles will opportunistically schedule the intra-BAN traffic so that packets are transmitted when the RSSI metric is expected to be high. The received signal strength indicator value of each data packet received at the receiver radio is used to estimate the radio channel quality following the same principle of the Enhanced-and-Hold LQE: the weighted average of the RSSI value is calculated. This solution minimizes the amount of the information collected at run-time, since data packets are set off to the instant that radio channel quality is expected to be maximum. The main disadvantage of this solution is related to the need of tracking the acceleration signal. Techniques to detect the user activity (such as motion or motionless user state) and to identify accelerations values on the user's stride are required. Experimental tests carried out show that some methods to predict the peak of the RSSI value are very efficient, but this LQE is limited to scenarios where the user performs periodic movements.

Movement Detection

The LQEs based on the movement detection method allow, through the modules of the acceleration vector, to recognize if the Edge of the Network node is moving (> 9.8 m/s2) or is static. When the user is static, the LQE estimates the relative position of the Edge of the Network node through the orientation of the acceleration vector. Then, using the empirical data – gathered during trial tests with several users and scenarios (positions and different TPLs) – the current state of a link is estimated. For example, between the node located on the user's waist (Coordinator node which is the receiver) and the node in the user's right arm (Edge of the

Network node which is the transmitter). This estimation results on the potential RSSI value of a data packet, if transmitted at a specific TPL in that orientation conditions [22].

Posture Detection

These type of LQEs identify posture based on the information obtained from inertial sensors. The radio channel characterization phase allows the identification of the expected radio channel quality for that specific scenario, which can involve more scenario configurations beyond posture. The author proposed a LQE to estimate radio channel quality in a well-defined application: monitoring infants during sleep is proposed in [144]. This LQE was employed in a WBAN comprising a node, designated Wearable IoT Device (several parameters were collected, such as, breathing rate, heart rate, temperature and infant's position) and a Coordinator node attached or close to the infant body (distance < 2 m). Assuming that the infant remains static for long periods while sleeping, the proposed LQE implements a two-step process: estimation of the radio channel gain by applying a LQE based on the sample-and-hold method and determination of the current user's position through an accelerometer, to estimate the current level of fading. Since some user positions are more prone to Non-line of sight (NLOS) effects (which result in fast variations on radio channel quality in a short period of time, peak-to-peak difference up to 15 dBm, due to body obstruction and multi-path components), this information can be very useful for the TPL control to adapt its behaviour in long-term.

However, the main goal of these posture detection LQEs is to overcome the main drawbacks pointed out to the receiver-side LQEs. These are related with the collection of huge information from transmitted data packets and extra packets at run-time, to inform the transmitter about the current state or the most suitable TPL (e.g. control packets, hello packets and beacons), thus incurring in extra overhead. The LQE solutions proposed in the literature following an inertial sensor-based method, can estimate or predict the current radio channel quality, but the algorithm is employed in a sender-side way.

The solution A-LQE, [135], [143] predicts on-body link quality variations, through RSSI metric and some constant parameters related to human body features and movement detection provided by a 3-axis accelerometer sensor. This LQE is based on Adaptive Neuro-Fuzzy Inference System (ANFIS), a multilayer feed-forward network consisting of nodes and directional links, which combines the main advantages of Artificial Neural Networks and Fuzzy logic, namely, learning capabilities and knowledge representation with inference capabilities. These are two important methods of artificial intelligence for modelling nonlinear problems.

The LQE proposed, for instance, to link between the Coordinator node located at the user's waist (receiver) and Edge of the Network node located at the user's right arm (transmitter), involves the interaction of several input parameters, such as the TPL, the body position, the circumference and the total body fat, to provide as output the predicted RSSI.

3.1.3 Summary and Insights

This subsection provides some synthesis of overall insights and conclusions learned from the individual LQE approaches addressed in this chapter.

The RSSI, PRR, ETX, SINR and LQI metrics are not exclusive to WBANs, they were first applied to estimate the radio channel quality of WSNs links (LQE) [55]. However, LQEs used in WSNs were not designed to handle the link quality variations observed on WBANs links. There are two main limitations of the WSN's LQEs that makes them unsuitable for WBANs. In WSNs the fast link quality variations is not a critical concern and WSNs' LQEs do not distinguish the different types of fading.

For example the PRR- and Window Mean Exponential Weighted Moving Average (WMEWMA)-based LQEs, which are widely adopted in WSNs [55], have very low performance in terms of reliability in estimations when applied in WBANs due to very low agility to track the very dynamic radio channel variations [51]. The Sample-and-Hold method, which is very agile and firstly adopted in WSNs, shows accurate estimation. However, as this LQE quantifies the fading as a stochastic process (without distinguishing large-scale from the small-scale fading), when integrated in a TPC mechanism and applied to WBANs it will lead to poor TPC's performance. In WBANs it is important to separate both types of fading. This is because the main influence on radio channel quality is the large-scale fading and the small-scale fading refers to fast variations in time but short variations on the magnitude of the signal around the small-scale fading. Quantifying the radio channel quality as the measure of only one measured sample can lead to precipitous TPL updates. Therefore, the number of samples considered to estimate or predict the radio channel quality, as well as the weight given to the radio channel history, allows to better manage the trade-off between agility and reliability in estimations. As stated before, in slowly varying radio channels, higher radio channel history's weight turns the LQE more agile to react faster to the changes in radio channel conditions, whereas low radio channel history's weight turns the estimator less agile, but with less fluctuations in estimations. Research studies that resulted in LQEs for WBANs analyses the radio channel behaviour and study the influence of these two parameters on the reliability of

estimations, since their optimal value is scenario-dependent indicating that these parameters can take different values during WBAN operation.

The LQEs designed to WBAN links are here classified in HW-, SW- and Inertial Sensor-based. The former method relies on physical layer metrics' readings, being the RSSI the most adopted in the literature. The HW-based LQEs have some limitations: first, their metrics can only be measured for successfully received packets (the link quality is overestimated when radio channel suffers excessive packet packet losses by not considering the information of lost data packets); second, the RSSI metric provides a quick and accurate estimate of the radio channel quality, but it is highly influenced by RF interferences, resulting in degradation on link quality, in terms of estimated RSSI, making it a weak indicator of the radio channel conditions. The experimental studies performed by Kim et al. regarding the relation between RSSI and PER showed that the smallest RSSI that ensures the WBAN requirements, in terms of reliability, increases significantly when subjected to interferences [4]. Therefore, the HW-based LQEs addressed in the literature are devised to WBANs configured with a star topology (lower amount of exchanged control packets than in multi-hop topology) if operating in environments not prone to RF interferences.

Even though the combination of metrics in one LQE has not been explored in the literature, metrics, such as LQI and SINR, might help the HW-based LQEs to validate the radio channel quality measures through the verification of the presence and level measure of the RF interferences that link is subjected. Due to the traffic overhead inherited from closed-loop control (c.f. subsection 3.3.2), the inertial sensor-based LQEs appears to overcome this limitation. However, the advances in this type of LQEs are still very limited. This type of LQEs have potential to replace the HW-based LQEs in WBANs, since the body is the main influence of the radio channel quality, but solutions are much more complex, their design are time-expensive and, until now, are restricted to static scenarios.

3.2 Transmission Power Level Control Module

The TPL Control block is responsible for updating the transmission power to reach the optimal value - the minimum TPL value able to ensure the successful delivery of data packets in destination [154]. This is an important feature from an energy saving and interference mitigation perspective. According to the performance behaviour, the TPL control mechanisms are classified as reactive-based or predictive-based.

3.2.1 Reactive-based TPL Control

The majority of the reactive-based TPL Control mechanisms addressed in this subsection, rely in margins, such as target RSSI range (R_{target}) and LQI range (L_{target}), or in a threshold (thus, radio channel quality must be always higher than the value set as threshold) [136]. The margin is used as a guideline to update the TPL parameter, so that future LQE estimations fit within RSSI target values range, resulting in a lower probability of losing data packets and higher signal stability. The TPL control mechanisms based on this approach only react to LQE estimations outside the RSSI range. As the goal of this module is to ensure that radio channel conditions are maintained between thresholds, the determination of the higher (TRH) and lower (TRL) limits of this target range are vital. If the lower limit is high, the probability of data packets' loss will be reduced, but at expenses of a higher power consumption; if it is low, the probability increases (due to the proximity of the $Rx_{sensitivity}$, in case a SW-based RSSI is used) and data packets' retransmission may outweigh any energy savings promoted by the TPLs [142]. The upper and lower values of the margin play an important role in the TPL update. A narrow target range can lead to a higher number of TPL updates due to the unstable behaviour of the radio channel, whereas a large one reduces the number of TPL updates, but may reduce the energy efficiency of the transmissions.

These parameters can be dynamically updated at run-time to meet the deployment scenario, since in every scenario (different environment, nodes location and user movements), the radio channel is subjected to different influences [123], [131], [155], which lead to different fading properties (such as fading rate, duration and magnitude) and outage events' probability. Most of the researches adopt a static and predefined target RSSI range, compromising either the energy efficiency or the communication reliability, leading to underestimated or overestimated TPLs, in high frequency. Moreover, as body posture is always changing, as well as the movements performed, the target RSSI range can be dynamically updated, at run-time, according to the type of activity performed by the user [154] or to the radio channel variation [39]. Sodhro et al. proposed a mechanism able to update at run-time the TRH. A very similar algorithm was also proposed by Kim et al. in their research [4], where the non-static parameter TRH is updated. To this a value is added, which represents the radio channel quality variation (standard variation of n RSSI samples). Afterwards, the TPL is updated in each interaction until the optimal TPL is reached - without previous knowledge of this value. The most representative TPL control approaches: Binary, Linear, Dynamic, and Hybrid.

Binary

This approach, described as aggressive in the literature, performs alterations in the TPL parameter, exponentially increasing or decreasing it. For instance, if the LQE output (used as input of TPL control) is higher than the target range (R_{target} or L_{target}), the algorithm updates the current TPL at a midpoint between the previous TPL and the minimum TPL – usually defined taking into consideration the lowest TPL available in the transceiver [156]. If the LQE output is lower than the target range, the binary algorithm changes the current TPL at the midpoint between the previous TPL and the maximum TPL (often 0 dBm). According to the results achieved by Lee et al, this reactive approach is more suitable to static scenarios, characterized by negligible levels of fading and high radio channel quality stability [46], and reaches the optimal TPL faster than other approaches, thus reducing the number of exchanged control packets, and, consequently, energy consumption [1], [46]. The principle of this algorithm was initially proposed and described in [156] and several TPC mechanisms adopted TPL control mechanisms based on a similar concept.

Dynamic

The dynamic algorithm is also considered an aggressive approach. It determines the optimal TPL on the basis of a straight-line equation. This TPL control, proposed in [9], assumes that there is a linear relationship between the RSSI and the TPL, which is considered valid when the user is standing. The equation is determined taking into consideration two previously measured RSSI values – transmitted at different TPLs, for instance at minimum and maximum [5]- and a specific slope. As radio channel conditions do not change, the algorithm is able to estimate the optimal TPL [9]. In static scenarios, this algorithm is faster at reaching the optimal TPL - as a consequence, more energy efficient than the Linear-based TPL controls [5], [46]. In a similar scenario, the dynamic-based TPL control consumes less energy than the binary algorithm, since the straight-line equation is determined taking into consideration two (previously) measured RSSI values, both out of the target RSSI range, whereas in the binary approach more than two control packets may be required to reach the optimal TPL. To detect changes in radio channel behaviour, researchers [5] proposed a dynamic algorithm, designated extended dynamic TPL control, based on the slope of the straight-line equation. A line equation with a negative slope is considered incorrect, triggering the transmission of new data packets to generate a correct one.

Linear

The Linear approach is also considered in the literature as an conservative algorithm and was mentioned for the first time in [157]. This approach updates the TPL step-by-step until the optimal TPL is reached, and can vary over time according to the operation scenario. According to Lee et al., this technique is not appropriated to radio channels presenting negligible levels of fading, because several iterations are required until the optimal TPL is achieved [46]. The algorithm is more efficient in dynamic scenarios. This kind of scenario are characterized by high levels of path-loss due to body obstructions and harsh fading. In Linear-based algorithms, the TPL is linearly changed (slightly increased or decreased) close to the target RSSI range, without causing abrupt variations in the radio channel (due to the output power adopted in transmissions), thus reducing the number of control packets exchanged [1]. Several TPC mechanisms adopted a Linear-based TPL control, actuating in a way that the TPL is increased or decreased by a constant unit or an adaptive unit, updated at run-time based on the radio channel conditions [39], [141]. Several TPC mechanisms adopted a Linear-based TPL control, actuating in a way that the TPL is increased or decreased by a constant unit or an adaptive unit, updated at run-time based on the radio channel conditions [39], [141].

Hybrid

The TPL control based on the Hybrid method selects the most appropriate control, conservative or aggressive, when a concrete scenario is identified. This method combines both linear and binary/dynamic approaches in an algorithm [46] to overcome the main drawbacks of the previously described approaches in terms of the radio channel quality behaviour. Therefore, the main challenge of such a TPC mechanism solution, is its capability to identify and differentiate, at run-time, a stable from an unstable radio channel. The schemes proposed in the literature to perform this task are analysed in subsection 3.3.2.

3.2.2 Predictive-based TPL Control

Predictive-based approach consult the LQE's prediction result before settling the TPL, i.e. the future radio channel state after transmissions are settled at a specific TPL. This solution uses models to select the most appropriate TPL at run-time, but from the developments proposed in the literature, this type of TPL control solutions seem to be applicable only in communications occurring in standing scenarios.

In [136] a TPL control based in a predictive behaviour is proposed, where the most suitable TPL is determined according to a RSSI model. This model (which needs the TPL level as input parameter) is derived from curve fitting of empirical data gathered in a radio channel

characterization (for different scenarios). The TPL control tests several TPLs until the best result in terms of RSSI is reached, i.e. the TPL that ensures a RSSI fitting within the target RSSI range, designated the optimal TPL to the current radio channel conditions. Vallejo et al. also proposed a TPL control based in a predictive approach, since it does not update the TPL until the optimal TPL is reached [135], [143]. This TPL control uses the A-LQE estimator, which is based in ANFIS, to predict the future radio channel behaviour of the radio channel for a specific TPL. After testing all possible TPLs, the TPL control block compares and selects the TPL that ensures the best radio channel conditions.

3.2.3 Summary and Insights

This subsection provides some synthesis of the individual LQE approaches analysed throughout this chapter.

Table 3.1 summarizes the features of each type of TPL control algorithm, highlighting their level of complexity, time required to compute the optimal TPL, capacity to operate well regardless of the subject and the node location, target scenarios, main advantages and disadvantages.

Although both approaches can operate in static scenarios with good performances, the predictive approach is the best suited. Since radio channel models from the literature show a good fitting to the empirical data collected during the characterization, and since radio channel quality can be well described in function of some variables such as TPL, only one iteration is required for determining the optimal TPL. These solutions are more complex and require more computational resources. However, the time required to execute these algorithms do not affect the performance of the TPC, since no significant changes are expected in fading magnitude (the Edge of the Network nodes may stay within the target RSSI margin for a long time for the same TPL [46]). Due to the excessive control overhead in terms of control packets from the Coordinator node to the Edge of the Network node, the application of the reactive approach in these scenarios leads to an inefficient use of the radio channel bandwidth, increases the probability of RF interference to other devices or networks and increases the energy consumption.

The reactive approach is suitable for dynamic scenarios. When a WBANs radio channel is classified as slow-channel fading, the measured RSSI allows the TPC to track the radio channel quality and update the TPL accordingly to the current radio channel quality. The predominant fading component, the large-scale fading, shows small variations between RSSI samples that are measured in intervals between 10 m and 35 ms, even when the user is running [25], [119],

Table 3.1. Comparison of the features of both Reactive and Predictive TPL Control Mechanisms.

	Reactive	**Predictive**
Complexity	Very Low	High
Convergence Speed	Low	High
Generic Capabilities	Yes	Yes
Scenarios	Static & Dynamic	Static
Main Advantages	-Do not require previous radio channel characterization	- No data packets exchanged; -Very fast convergence to the optimal TPL;
Main Disadvantages	-High network traffic; -Low convergence to optimal TPL; -On-body transmission configuration-dependent.	-Require algorithms to recognize body posture and nodes relative-position; -Require that subjects have been completely characterized with respect to the RSSI and PER metrics in all scenarios;

[155]. However, due to the small-scale fading, the RSSI values measured are in the proximity of the large scale fading with fast variations on time but short in magnitude (-5 up to 5 dBm) which makes the fading signals behaviour approach a stochastic process. Due to the small scale fading, the target RSSI ranges are important for TPCs that adopt a reactive based TPL control mechanism. More studies about the most suitable TPL's upper and lower values based on the Edge of the Network node location, user movement and surrounding environment are required since these factors clearly influence the magnitude of the small-scale fading and traffic overhead. Thus, pre-defined upper and lower values of the TPL margin might not be recommended in WBANs, since small scale fading has different features according to the deployment scenario.

Reactive approaches show very low complexity with execution times between 0.1 ms-10 ms, suggesting that during the time spent to estimate and update the TPL, the radio channel fading remains static. However, since the transmit primitive uses the MAC layer, this may introduce some latency before a data packet is transmitted (maximum 50 ms [130]), the authors decided to configure some CSMA protocols parameters of IEEE 802.15.4 MAC (for instance the Clear Channel Assessment backoffs to zero) to reduce the data packet transmission operation (≈2.56 ms), giving more control to the TPC mechanism during transmission time [130], [137], [145]. An alternative solution might be to execute the TPC algorithm after the Clear Channel Assessment in order to determine if the radio channel is free (in beaconless or beacon mode of IEEE 892.15.4), proceeding the transmission process and ensuring that there is no performance degradation and robustness due to outdated radio channels since by the time radio channel is estimated and the power is adjusted the radio channel will not change.

Soft computing techniques [135], [143] or analytical equations [136] are the key of predictive TPC approaches. These methods are being explored as a tool for modelling these ill-defined systems to forecast the radio channel quality, focusing on the influence of the TPL

in radio channel quality. However, due to the difficult in describing the on-body communication features, (to the best of the author knowledge) there is no predictive TPL proposed to scenarios where user is moving in the literature.

Cheffen et al. proposed a dynamic radio channel model for on-body wireless communication (user's wrist-user's hip link) while the subject is walking [158]. The angular variations of the transmitting and receiving antenna gains (due to angular variation of the corresponding body part during waking) is used to estimate the signal fading. However, this radio channel model has not been experimentally tested or applied in the context of a TPC algorithm.

3.3 TPC Mechanisms for On-body Communications

Several TPC mechanisms have been proposed over the years for on-body channels in WBANs, providing solutions with different schemes and strategies to improve the wireless on-body transmissions. In this section, a comprehensive survey of the state-of-the-art on the TPCs specifically designed to on-body channel transmissions in WBANs is presented and each TPC mechanism classified according to its design goal. Within each subsection, the strategy adopted is described. The TPCs description starts with the identification of methods adopted on the process of link quality estimation and TPL determination, followed by a brief description of the TPC specificities, concluding with a critical analysis of each TPC mechanism based on the WBANs application requirements. The different TPCs are analysed in chronological order to provide the reader a better insight into the evolution of the research focus on each topic.

3.3.1 Classification of the TPC Mechanisms for On-Body Communications

For the classification of the different TPC mechanisms, a taxonomy cantered on the main design choices, depicted in Figure 3.3, is proposed. The TPC mechanisms are categorized based on the following characteristics: 1. Link Quality Estimator, 2. TPL control, 3. Goals, 4. Topology (star or multi-hop), 5. Algorithm (centralized, decentralized and hybrid), 6. Scenarios (static or dynamic) and 7. Communication Standard adopted to the physical and MAC layer to data packets transmission.

The Goal attribute classifies the different TPCs according to the target priority requirements. Even though the TPC mechanisms are designed to ensure WBANs application requirements, they are application-specific. Thus, the technologies of the TPC mechanisms are projected to handle with different requirements in terms of reliability, data rates, latency and life-time. According to the intended goal, TPC mechanisms can be classified in terms of 1. Energy-efficiency, 2. Connectivity and 3. Interference-mitigation.

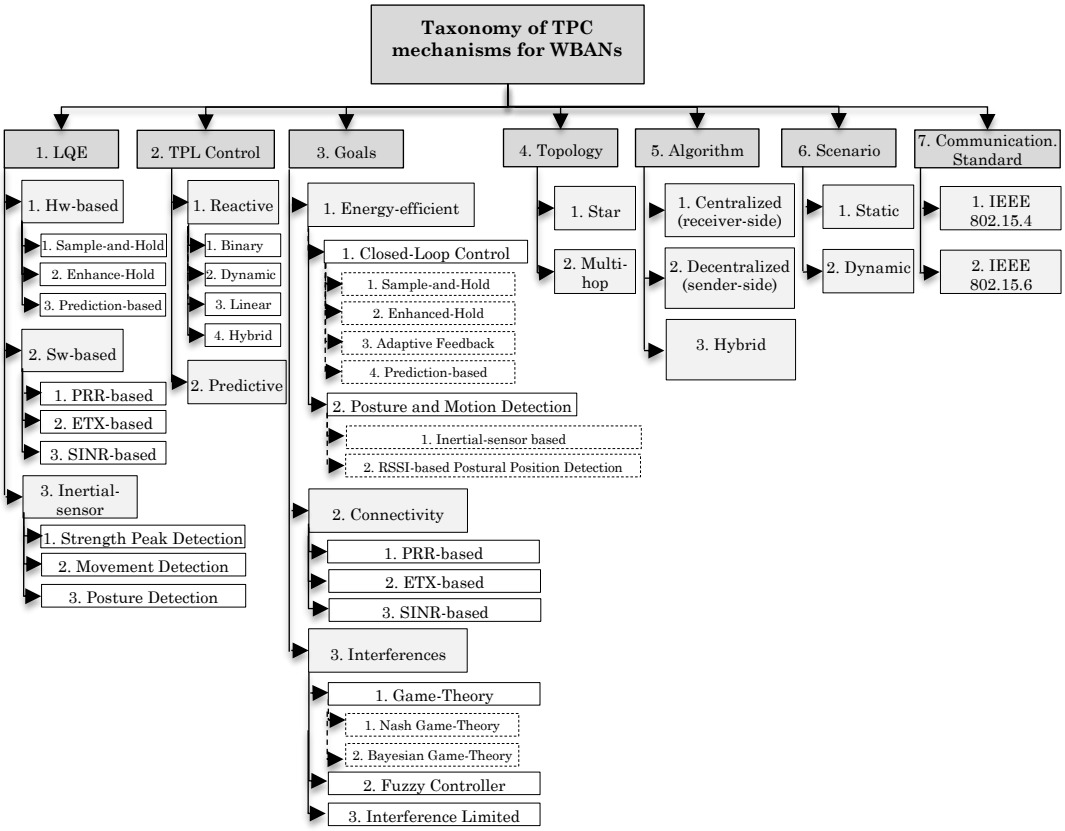

Figure 3.3. Taxonomy of TPC solutions for WBANs.

The Energy efficiency goal attribute refers to a TPC that follows a specific design choice to increase the life-time of a network. As a consequence, it may sacrifice other performance metrics, for instance the latency. These mechanisms are suitable for energy-sensitive applications, such as, when long periods of WBAN operation is required or when battery replacement or recharging is not feasible. One of the main problems of a WBAN transmission is related to the external interferences that may deteriorate the communication throughput, resulting in a higher PRR. Performance-sensitive applications tend to privilege the PRR increase in detriment of latency and/or energy metrics. The connectivity goal refers to the TPC mechanisms for latency-sensitive applications, requiring transmissions with lower end-to-end delay. The latter TPC solutions are thought to networks with a multi-hop topology. First, a parent node (Coordinator or relay node) is chosen and the optimal TPL to each hop is determined.

As previously discussed, this thesis is of particular interest in the TPC mechanisms developed for WBANs (configured with a star topology) designed for applications sensitive to data packet loss, but where the efficient use of available energy is crucial. Therefore, the current section only covers the developed TPC solutions for energy sensitive applications. The

remaining mechanisms that fit into other categories are not analysed here, but a detailed description and comparison analyse of such TPC solutions is provided in research work [64].

3.3.2 TPC Mechanisms for Energy-Sensitive WBAN Applications

As previously mentioned, the TPC mechanisms proposed for energy-sensitive applications can be classified in two groups: Closed-Loop Control or Posture and Motion Detection.

Closed-Loop Control based TPC Mechanism

The TPC mechanisms following a Closed-loop control strategy are usually suggested for star-topology WBANs with the objective of reducing energy consumption during data transmission. It is assumed that, unlike the sensor nodes, the Coordinator node is not energy-constrained. The basic operation principle is illustrated in Figure 3.4. The first data packets transmitted by each Edge of the Network node are sent at the maximum value allowable in on-body communications, so that the Coordinator node is able to apply an LQE estimator. This LQE is based in the HW-based RSSI metric of the last data packet (a sample-and-hold TPC mechanism), or in the average radio channel gain of a data packet set (enhanced-hold TPC mechanism). Therefore, the LQE and the TPL control blocks, in their traditional form, are applied in a receiver-side way (as it will be seen later in this paper, they can be applied in a sender-side approach). Then, the TPL control scheme is executed to determine, according to the LQE output, the most suitable TPL. The result of the TPL control operation is transmitted back to the Edge of the Network node (at the maximum TPL allowed), as a control packet or as an ACK. After reception of the control packet, the Edge of the Network node updates its TPL, ensuring that future data packets are transmitted at this newly updated TPL until another control packet from the Coordinator node is received. The TPC mechanisms that fit in this category are classified as (A) Sample-and-Hold mechanisms, (B) Enhanced-Hold mechanisms, (C) Adaptive Feedback Periodicity mechanisms and (D) Prediction-Based Power Controller mechanisms.

(A) Sample-and-Hold Mechanism

This type of mechanisms follows a reactive behaviour, as it adopts a sample-and-hold LQE that relies in the acquisition of the RSSI metric as estimation parameter. Solutions of this type proposed in the literature combine the sample-and-hold LQE with a TPL control (also applied in a receiver-side way) namely, Binary [1], [46], Linear [1], [46], [50], Dynamic [1], [5], [46] and Hybrid [46] TPL controls. Only the RSSI value of the last received packet is considered and the TPL control sets a target RSSI range to ensure a stable signal and power values higher than the lower limit. The results obtained from of the application of this type of TPCs

demonstrate that these solutions are agile and fast to converge to the optimum TPL in static scenarios. In this context, the signal is relatively stable (signal remains within the target RSSI range for a long time at the same TPL), the communication system consumes less - Smith et al. reported a reduction of 55% on energy consumption when comparing with a system transmitting at a the pre-defined and static TPL of 0 dBm [50] -, and the communication reliability is ensured, i.e. PER<10%. Nevertheless, they are not able to effectively handle with dynamically changing wireless body radio channel environments, as shown by Yi et al. through experimental tests [1]. The high variability of the radio channel, as consequence of body shadowing but, in particular, due to the small- and large-scale fading, suggest that changes in the TPL should be avoided to prevent unnecessary exchanges of control packets that significantly increase the energy consumption, as well as, the radio channel overhead, due to the high number of control packets needed.

Guan et al. proposed a TPC mechanism, designated PID-based power controller, comprising a Proportional-Integral-Derivative controller, a very common approach to control a certain variable in several areas, due to its satisfactory performance and simple structure [139]. This controller manages the output parameter, the TPL level, in relation to the tracking error, which is the difference between the reference RSSI value and the estimated RSSI resulting from the receiver-based, sample-and-hold LQE. Running in the Coordinator node, this controller uses as feedback signal the RSSI value estimated at each data packet transmitted, adopting the sample-and-hold method. The TPL control, applied in a sender-side way, follows a Linear-based approach, since after calculating the input function error, the output parameter of the controller is used to increment the TPL in the latest transmission. In comparison with the typical structure of a PID controller, some changes were proposed.

Authors added a Saturation and Quantizer block to generate the TPL boundaries, i.e. to define a finite set of discrete output power levels (-25 to 0 dBm). The first block limits the

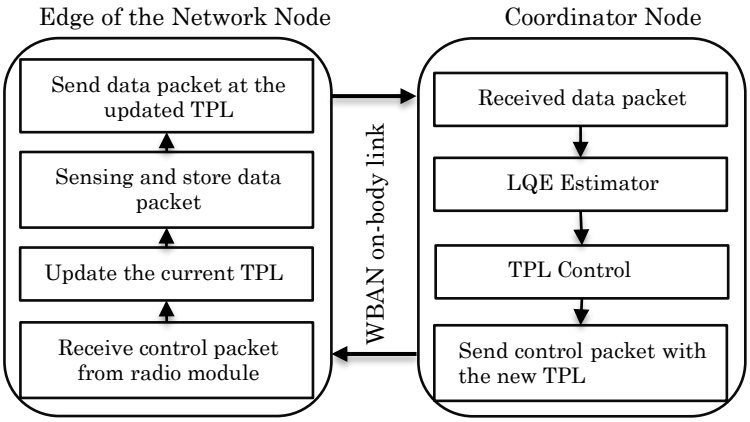

Figure 3.4. Closed-loop control architecture overview.

potential TPL values available to the TPL control, named bound of saturation [25 dBm, 0dBm], whereas the latter rounds up the updated TPL to the near discrete value. As this TPC follows a closed-loop architecture, the new updated TPL is then transmitted to the Edge of the Network node through a control packet. The analysis of the simulation results for two links, (1) user's right waist - user's chest and (2) user's right waist - user's right ankle, show that this is able to turn the communication subsystem more energy-efficient. According to the results, this solution saves energy by approximately 7% and 68% to link (1) and (2) when the user is walking, respectively. When the user is running, the system ensured energy savings of roughly one quarter for the link (2), whereas link (1) consumed more of 9% power than transmissions carried out at static TPL 0 dBm.

(B) Enhanced-and-Hold Mechanism

The most representative solutions of this type of mechanisms are from [4], [39], [140]–[142]. The LQE adopted consists in an enhanced-hold estimator, using the current estimation metric value and the historical one to estimate the current radio channel quality.

The TPC mechanism proposed by Kim et al., designated RL-TPC, combines the RSSI/LQI estimator - applied in receiver-side approach – with a Linear-based TPL control - applied in receiver-side approach - with an adaptive target RSSI range, which defines the upper limit as a static variable and updates the lower one according to the standard deviation of the RSSI of several samples [4]. Upon detection of the radio channel under interference, through the weighted average of the LQI values of 5 samples in a row, the TPC mechanism switches to another available radio channel. When the radio channel does not have high levels of interference, the TPL is gradually updated if the result is not within the target RSSI range margin, through (1). This solution was applied into link wrist-pocket and empirically evaluated in indoors to three different activities: (a) static, (b) walking slowly (2.5 km/h) and (c) walking a bit faster (5 km/h). This solution reduces the average TPL, being it -17 dBm, -14 dBm and -12 dB in activities (a), (b) and (c), respectively, and, as consequence, the consumed energy power is reduced by 40%, 35% and 30% respectively. The resultant average RSSI is close to -84 dBm, -82 dBm and -81 dB to activities (a), (b) and (c), respectively. In all scenarios considered during the experimental evaluation, the solution was able to ensure a PRR higher than 90%.

In [39], a TPC mechanism designated Energy-Efficient Adaptive Power Control (APC) was proposed, where the LQE and the TPL control are applied in a receiver-side and sender-side way, respectively. The data-driven LQE is based on an enhanced-hold mechanism. However, the authors propose the adoption of two possible values to the weighted parameter (α) to

provide flexibility to the TPC, by reacting differently to a perceived increase or decrease in radio channel quality, emphasizing energy savings or the PRR. These values are static and pre-defined and determined through Monte Carlo simulations in Matlab, using the gathered data. The authors classified the radio channel, namely the good and bad radio channel conditions, according to the PER – given by expression 1-PRR. The average weight values are randomly selected and the effect on the system performance is checked. The optimal values reported of α_1 and α_2 – 1 and 0.4, respectively –, were those that ensured the better balance between reliability and energy efficiency. If the radio channel presents good conditions, the LQE turns to a sample-and-hold HW-based RSSI estimator to be faster to converge to the optimal TPL. In bad radio channel conditions, the TPL is updated slowly to avoid under and overestimations of radio channel measurements, since it turns into a HW-based RSSI enhanced-hold method. The solution proposed by Shah et al. adopts a Hybrid-based TPL control, i.e. a binary approach for good radio channel conditions (α_1 is selected in the radio channel gain equation) and a Linear-based approach to bad radio channel conditions (in expression (3.1) the value of α_2 is considered). Moreover, the TPL control relies in an adaptive target RSSI range margin as guideline for the TPL updating, more specifically, the upper limit. As the TPL control is applied in a sender-side way, it means that the radio channel gain information, estimated at receiver-side, is transmitted to the Edge of the Network node using control packets. The LQE is responsible to determine if the radio channel is under good or bad conditions. To perform it, the radio channel gain is compared with the latest power sample measured. If $\bar{R} > R_{latest}$, the radio channel is considered in good state, if not, it is considered in a bad state. Through simulations, the performance of this solution, when applied to link user's right wrist-user's right hip, in environment indoor and while the user is walking was tested. The reported results show that this solution saves just under a half of the whole energy consumed when a static and 0 dBm TPL is adopted.

Although commercial-off-the-shell IEEE 802.15.6-compliant radio-frequency transceivers are not yet available, some TPC mechanisms have been designed to operate in conformity with IEEE 802.15.6 standard [140]–[142]. Gao et al. proposed a TPC mechanism for WBANs with a transceiver that adopts stacks in conformity with the MAC layer proposed by IEEE 802.15.6 standard, operating in beacon mode with SF boundaries [140]. This mechanism is based in a closed-loop control architecture and applies the HW-based enhanced-hold method (running in a receiver way and following a data-driven approach) and a Linear-based TPL control block that adds to the previous TPL values, the minimum TPL adaptation level value of the set. The determination of the TPL is performed by the Edge of the Network nodes, thus, the Coordinator

node includes the result of the estimation performed by the LQE in packet acknowledge. This must be transmitted back to the Edge of the Network node after reception of the data packet, within an interval always lower than the time defined as short interface space period, pSIFS (time that a Edge of the Network node, after transmitting its data packets in its allocated slot, waits, in the remaining SF, for an ACK, before going to sleep). Through simulations, the researchers have verified that the proposed solution ensure a Edge of the Network node lifetime by 12.4% (66% of the time transmissions are below -12 dBm) in comparison to the Edge of the Network node that transmits at 0 dBm TPL. According to Shah et al., to same conditions, the solution APC ensures more energy-efficient transmissions than the solution [140] (the link user's right wrist-user's right hip, while user is walking, consumes less 18% of energy power) [39].

A two-fold TPC mechanism, designated Two-step Adaptive TPC algorithm (ATPC), was proposed in project [141] and in [142], designed for WBANs that adopt the IEEE 802.15.6 MAC and operating in beacon mode with superframe boundaries. Although this mechanism does not follow the typical closed-loop control scheme, since the TPC is applied in a sender-side way, it is designed for WBANs with star topology and with the objective of reducing energy consumption without sacrificing other performance metrics. In the first step, the Hw-based, enhanced-hold LQE estimator is applied in a sender-side way, following a beacon-based approach. As beacons are mandatory for maintaining network synchronization and are transmitted periodically by the Coordinator node (authors tested at a sampling interval of 15 and 150 ms), they are used to measure the radio channel gain of each Edge of the Network node at the beginning of each SF. The period of an IEEE 802.15.6 SF is defined by beacons, thus the Edge of the Network nodes are awake to receive the first beacon that indicates the start of a SF and after go to sleep. They awake again at their allocated time slots to transmit the data packets, waiting for an ACK (emitted by the Coordinator node) during the interval pSIFS, before going to sleep.

In the second step, the optimal fade margin to be added to the LQE estimation is defined by a mechanism, designated Adaptive Fade Margin Estimator (AFME). This mechanism relies in prediction errors calculated through the difference between the radio channel gains obtained in step 1 and the current radio channel gain – this is the RSSI of an ACK received by the Edge of the Network node. The AFME sets a lower (2 dB) and an upper limit (4 dB) and an initial value of the fade margin (3 dB). This margin is then dynamically updated in the following way: the prediction error at every SF is compared with the lower and the upper limits. If the error is higher than the last one (previous SF), the margin is increased one unit until the maximum

upper threshold is reached. If the current error is lower than the last one, the fade margin is decreased one unit until the lower threshold is reached [141], [142]. When the last data packet is lost, the previous fade margin is increased in three units to reduce the probability of losing further data packets.

These two TPC mechanisms differ from each other on the TPL control method adopted. In the solution described in [141], the TPL is calculated (TRL is set as a static and predefined value and the standard deviation of n RSSI samples is summed to the TRL), whereas in the solution [142], the TPL control follows a simple Linear-based approach, applied in a sender-side way. Based on the reported results from both solutions, it is possible to conclude that the TPC reliability decreases when the SF period increases, since slot allocation, granted for each Edge of the Network node, does not start immediately after beacon reception. Moreover, the time interval between beacon reception and slot allocation is different for each Edge of the Network node. For instance, the TPC mechanism performs well for low delays (15 ms), but poorly for high delays, as in the case of 150 ms. To overcome the problem associated with higher delays of fast varying radio channels, authors suggested setting lower values of α in the enhanced-hold Hw-based RSSI LQE equation, increasing the weight of radio channel history [141], [142]. For links user's chest-user's waist and user's chest-user's arm the ATPC saves approximately one quarter of energy compared to the fixed TPL (-10 dBm).

(C) Adaptive Feedback Periodicity Mechanism

This type of TPC mechanism adapts, as suggested by its designation, the period between control packet transmissions, to accommodate the variation in radio channel quality in real-time. Solutions proposed in [138] and [1] are excellent examples of its application and potential. Both adopt the enhanced-hold LQE, running in the Coordinator node, whereas, regarding the TPL control, Moulton et al. implemented a Linear based one and Yi et al. implemented a Binary based one, following, in both cases, a receiver-side approach.

Moulton et al. solution aims at: i) reducing the control packets periodicity, when the radio channel gain falls outside the target RSSI margin, so that the TPL mechanism is agile enough to react to the changing radio channel conditions at run-time, and ii) increasing the control packets periodicity, when the radio channel gain is within the target RSSI range, (radio channel quality is stable), to promote savings on the overall energy consumption due to a reduction of control packets transmission [138]. As the TPC mechanisms must avoid long control packet transmission intervals – if interval is too long, when control packet is transmitted it does not reflect the changing radio channel conditions sufficiently fast –, Moulton et al. defined a

minimum and maximum interval, namely 2 and 64 control packets, respectively. According to the results reported, it is clear that when the user performs periodic movements (such as, walking), the period between control packet transmissions is high at the beginning (starts in 2 s and remains in 2-8 s within the first minute). After the TPL control reaches the optimum value, the control packets are emitted at a very low period (between 16-32 s), significantly reducing the average number of control packets exchanged. This solution achieved an energy saving up to 15% and 21% in comparison to a static TPL (0dBm) while the user is walking and standing, respectively (the researchers do not address the metric PRR).

In their research article, Yi et al. claim that when the radio channel is unstable, i.e. the RSSI value fall outside the target RSSI range repeatedly, there is a frequent deliver of control packets and the resultant energy consumption may exceed the TPC energy savings [1]. The solution proposed by Yi et al. does not update the TPL periodically, instead it controls when the TPL control is applied by varying the control packet transmission interval on the basis of the radio channel condition.

The first task of the TPC mechanism LQE is to determine whether the radio channels present a stable quality or not. When the radio channel is stable, i.e. the difference between the radio channel gain and the last RSSI sample is smaller than a certain limit, the TPL control is executed (applied in a receiver-side way); when the radio channel is unstable (radio channel estimations fluctuate), the TPL control is deferred and the control packet is not sent, waiting until the radio channel becomes stable to execute the TPL control. However, the reported results demonstrated that too short or too long periods between control packets transmission can have a negative impact on the energy efficiency of the WBAN. Short periods lead to high energy consumption due to the frequent transmissions of control packet transmission. Too long interval between control packets transmission turns the TPC less efficient - slow reactions to changes in radio channel conditions are expected which increase the energy consumed per data packet successfully transmitted [1].

Researchers experimentally tested this solution and compared to a TPC based on the Sample-and-Hold operation principle with different design choices in terms of the TPL control adopted. Results demonstrate that excessive control packet transmission may lower the energy efficiency of the system. The experimental test took up 360 s and was performed to links user’s chest-user’s stomach and user’s chest-user’s back in indoors. During this interval the user performed a sequence of user´s movements (standing, walking, standing, and running). According to results reported, the different mechanisms have equivalent performance in terms of PRR (<10%), but the transmitted control packet and the energy power consumption varies

considerably. The TPC that adjusts the control packet transmission interval reduces the number of transmitted control packets by 90% in comparison to a Sample-and-Hold approach configured with a binary-based TPL control, which has a maximum amount of control packets. In terms of energy consumption, the proposed solution saves achieves a 40% reduction on average.

(D) Prediction-based Power Control Mechanism

Another variant of TPC mechanisms identified in the literature and based on the operation principle of the closed-loop control architecture is designated Prediction-based Power Control. This type of mechanism aims to perform long predictions to reduce the number of iterations between the Edge of the Network nodes and the Coordinator nodes, i.e. increase the rate of control packets exchange. Several prediction-based TPC mechanism were introduced in the literature, such as [50], [136], [146].

Guo et al. proposed a TPC mechanism, designated Minimum Energy Packet Forwarding Protocol (MEPF). The LQE adopts the sample-and-hold method, applied in a receiver-side way, and the TPL control follows a predictive approach. This block, applied in a sender-side way, comprises a RSSI model built based on RSSI TPL shifting curves, to predict the RSSI and, in just one iteration, define the optimal TPL [136]. In addition, the MEPF adjusts the TPL of the Coordinator node ACK, since the TPC result is transmitted to the Edge of the Network node in Coordinator node acknowledgment after reception of each data packet. This TPC stores lost data packets in the buffer until the link is good enough to retransmit this information. As the Edge of the Network nodes are typically resource-constrained, this mechanism adopts a threshold to increase the probability of successful data packet retransmission, avoiding the buffer from being full [136].

When comparing the Closed-loop Control TPC mechanisms described and analysed in the previous paragraphs, namely (1) the TPC mechanism that uses a sample-and-hold method LQE [50], the (2) TPC mechanism that employs an enhanced-hold LQE [50] and the (3) TPC mechanism that predicts the estimator metric using the Weighted alternate-least-squares prediction technique [146], it is clear that both Prediction HW-based LQEs solutions are combined with a TPL control block that applies a target RSSI to allow the TPC to perform long term predictions. Therefore, solutions (2) and (3) are considered similar because they adopt a sender-side TPL control based on a Linear approach, differing only on the sender-side LQE selected, as mentioned before. These solutions were designed, developed and tested to ensure an efficient power allocation for long intervals - up to 250 ms, 400 ms, 800 ms and 1 s -, with

an time interval between received data packets, for a given link, varying from 10 ms to 400 ms. The reported results reveal that both TPCs have similar performance in terms of outage percentage (<10%). However, this performance parameter decreases with an increase in the of prediction interval. For instance, from 250 ms to 800 ms, the outage percentage increases up to 2.5% and power consumption up to 0.1 mW. Moreover, the interval between data packets transmission also influences the TPCs performance. According to the results reported, increasing the period, the outage percentage slightly increases in average 2%-4%, whereas the average circuit power transmission seems not be affected. Solution (3), revealed to be more complex than solutions (1) and (2) since it aims to ensure an efficient power allocation up to 2 s. The LQE adopted is the weighted alternate-least-squares predictor, applied in a sender-side way, and the Linear-based TPL control is applied in the Edge of the Network node. Therefore, the predicted signal portion S_p is transmitted in the control packets to the Edge of the Network node, as a vector of the RSSIs.

The performance of this TPC solution was compared with the performance of the solutions (1) and (2) in terms of energy consumption and outage probability. Solution (3) was set to predict and allocate an optimum TPL for 5 samples ahead, when a sampling interval of 10 ms is selected, and for 2 samples ahead, when the sampling interval is higher than 120 ms. In both cases, the number of samples corresponding to the last 4 s of the signal have been used. For a prediction of 1 s ahead and with the sampling interval adopted, the power consumption of each method is relatively constant. The TPCs (2) and (3) outstand in terms of this performing metric, reducing significantly the energy consumption, even when compared with low TPLs, such as -10 dBm, where reductions of 8% and 22% were reported for solutions (2) and (3), respectively. Regarding the outage probability, and considering a prediction of 400 ms ahead, the TPCs (1) and (3) ensured the best performance. However, it was noticeable that for any sampling interval, as well as, $Rx_{sensitivity}$, the TPC (3) provides lower outages probabilities than the TPC (2) - up to 0.5%-1% below. Both TPCs ensure outage probabilities lower than 10%, regarding the sampling interval. Researchers also evaluated the TPC (3) for predictive power control 250 ms, 400 ms, 1s and 2 s ahead, for a sampling interval of 50 ms. Considering -90 dBm as the Coordinator node $Rx_{sensitivity}$, the predictor algorithm seems to be able to ensure the reliability requirements of the IEEE 802.15.6 WBAN applications, since outage probabilities lower than 7% were reported. This demonstrates improvements (for all the prediction periods mentioned above) when compared with transmission, with same configuration, but at a static TPL of -10 dBm (13% of outage probability). Therefore, the

prediction period ahead has not revealed high influence in the performance of TPC (3) in what concerns outage probability. Moreover, authors concluded that this solution is able to ensure the reliability requirements for a prediction of 2 s ahead, even for a TC of 500 ms [146]. Although this TPC mechanism ensures a reduction of the number of control packets that convey this information back to the Edge of the Network node (several predicted samples), it is only applicable to periodic user's movements that are performed for long periods (as pre-defined movements performed in experimental tests). Thus, it is not reliable when the user performs daily activities.

Posture and Motion-based Mechanisms

The posture and movement of WBAN users have the most significant influence on the radio channel quality. Several researchers explored different techniques to recognize the user's posture and/or movement. The solutions from [22], [128], [130], [135], [143], [144] opted for estimators based on (a) inertial sensor-based methods, that through posture and/or movement, translate the current radio channel quality. Other solutions determine the current posture knowing in anticipation the current and previous radio channel estimations (RSSI samples) and are designated (b) RSSI-based Postural Position Detection TPCs

(A) Inertial Sensor-based TPC Mechanisms

Regarding solutions that rely in inertial sensor-based LQEs, the author proposed a TPC mechanism to monitor infants during sleep [144]. This mechanism is applied in a receiver-side approach. The closed-loop control method (c.f. Figure 3.4) is used to estimate the current radio channel quality (RSSI), by applying a sample-and-hold method. Moreover, in the TPL updating, the fading level information is considered. Since in NLOS transmissions the signal strength has high and fast variations and the RSSI hardware-based estimation is prone to inaccuracy, updating the TPL in an aggressive manner can drive the RSSI outside the RSSI range. To recognize the positions that are more susceptible to fading, authors conducted a radio channel characterization based in scenarios (different environments, TPLs, positions and distances). This TPC combines a RSSI hardware-based LQE and a TPL control, which uses the fading level information to update its strategy on the TPL selection. When data transmission occurs in LOS, it is expected that radio channel remains static. In this situation, the TPL control adopts an aggressive methodology, a Binary based TPL control to speed the convergence to reach the optimum TPL. In bad radio channel conditions, which can be translated in unstable radio channels, the TPL control switches to a conservative TPL updating, adopting a Linear-based TPL control. This avoids fluctuations in TPL selection (RSSI may go farther from

the target RSSI margin), and ensures that the RSSI remains within the target RSSI range for long periods, reducing the number of TPL updates (from 14 updates to 6, when compared with the aggressive approach). As a consequence, the level of overhead in the radio channel is reduced. Results reported show that the TPC mechanism is agile to react to radio channel changes and is able to maintain the RSSI level within the target RSSI range. This was not verified in a WBAN operation using a pre-defined and static TPL [144].

Solutions proposed in [22], [128], [130], [135], [137], [143], [145] aim to overcome the main limitations of the receiver-side LQEs, namely the one related with the run-time collection of huge information from transmitted data packets and extra packets (control packets), which is needed to inform the transmitter about the current state or the most suitable TPL (e.g. control packets, hello packets and beacons) and incurs in extra overhead. These solutions can exhibit a predictive behaviour [22], [135], [143] or an estimation behaviour [137], [145].

Vallejo et al. proposed a TPC mechanism based on a Fuzzy logic controller, designated Proactive-TPC [135], [143]. The main advantages of this type of controllers are their robustness, ease of design (due to the use of linguistic variables instead of mathematical expressions) and flexibility. According to Kazemi et al., fuzzy controllers have the great capability to map nonlinear and complex relationships between input and output spaces [108]. The Proactive TPC mechanism comprises the A-LQE, to predict the RSSI variations and the TPL control, responsible for adjusting the TPL to the minimum value required (experimentally determined) to ensure the successful data packet delivery. The TPC mechanism can follow either a conservative or an aggressive strategy, as the TPL is selected according to the current radio channel state and the prediction of the future state. The RSSI spectrum is divided in several zones and a threshold zone is defined (-80 dBm) to set this value as the minimum RSSI value. Taking into consideration the scenario, the TPL is defined to each zone. The number of zones depends on the number of TPLs available in the transceiver node, ensuring, in case of a large number of TPLs, a finer granularity in the output power. The researchers opted to define three zones, namely RSSI values higher than -75 dBm (Zone 1), values within range -75 dBm (Zone 2) and values lower than -80 dBm (zone 3). The TPC mechanism was assesses while the user was static in pre-defined positions. According to the results reported, despite the high oscillations in the TPL selection, due to the high variability of radio channel quality, this mechanism was able to maintain the RSSI value higher than the minimum threshold and promoted a reduction of more than 20% on the total energy consumption.

Solutions from [22], [137], [145] follow a similar approach. The LQE adopted relies in movement detection, based on a 3-axis accelerometer sensor to estimate/predict the radio

channel quality, while the user is performing periodic movements. The TPC mechanism proposed by Vallejo et al., which is applied in a sender-side way and designed as a reactive algorithm, relies in an extensive radio channel characterization for each subject and scenario, at different TPLs, adjusted through movement detection from an accelerometer. The RSSI is predicted when no movement is detected ($|\overrightarrow{g}| \approx 9.8m/s^2$). In this case, the TPC estimates the relative position of the user through acceleration orientation (only predefined static positions were considered, such as, seated with different orientations of arms and legs) and using the empirical data obtained in the radio channel characterization, the TPC control determines the optimum TPL. When the user is moving (user walking), the optimal TPL is estimated by the LQE through acceleration measurements. If $|\overrightarrow{g}| \gg 9.8m/s^2$, then the TPL control selects the maximum TPL allowed, 0 dBm, to avoid data packet losses. This may lead to a non-energy-efficient use of the radio transceiver and RF interference with other devices and networks.

The TPCs algorithms, designated Gait Cycle TPC (G-TPC) and Accelerometer Assisted-TPC (AA-TPC), addressed in the research works [137] and [145] to the link user's hip (receiver node)-user's ankle (sender node location), respectively, aim schedule the data packets transmissions at the point when the link is at his best quality in each gait cycle. These algorithms merge a strength peak detection-based LQE, proposed in [130], and a Linear-based TPC control mechanism following a receiver-side approach. These solutions assume that the receiver (Coordinator) node is not resource-constrained, for instance a smartphone, since the TPC algorithm is too complex and, thus, has to be executed in such nodes. This node is responsible for estimating and determining the most suitable TPL, but techniques to track the gait cycle offset and to estimate the on-going gait cycle period have to be executed. This process aim the determination of the period of time that the sender node must wait between data packet transmission. This information and the estimated optimal TPL are transmitted back to the emitter nodes as control packet. When this information is received, the emitter configure its output power to the new optimal TPL and calculate the time elapsed since the last data packet transmitted to determine the remaining time until transmission of the data packet according to the information proved by receiver. These solutions, sacrifice the latency (which is the higher than maximums allowed in medical and non-medical applications) of the transmissions to reduce the energy consumptions (26.4% and 25% in [145] and [137] respectively) and the data packet losses (reduce the data packet loses up to 65% [145] and 4% [137] in comparison with

a Enhance-and-Hold based-TPC mechanism). The two above cited TPC algorithms differ from each other on the techniques adopted to the gait cycle offset.

(B) RSSI-based Postural Position Detection TPCs

The solutions proposed by [9], [48] fit within the class of TPCs that predict the current postural position using the RSSI measurements (without relying in information from inertial sensors to estimate postural position) resulting from the closed-loop architecture. The proposed solutions adopt the sample-and-hold method (which belongs to the HW-based category of LQEs), applied in a receiver-side way and using the RSSI metric as estimation parameter. They also rely in a target RSSI margin to update the TPL in a way that ensures RSSI values stability and immunity to packet losses. Through a scenario-based radio channel characterization that aims to determine the RSSI-TPL relation, as well as, radio channel quality expected in very specific user postures (the users were invited to follow sequence of four right hand movements, representing four natural sitting postures), researchers identified the existence of a linear relation between these parameters for static scenarios. Both RSSI process and the body postural process are modelled as a linear, stochastic system. The current postural position is estimated through a Linear Quadratic Gaussian Control with an Integrator (LQGI) whereas the optimal TPL is determined through an analytical model that describes the RSSI in function of the TPL parameter. The newly TPL is transmitted to the Edge of the Network node as a control packet. This TPL control, which is part of the LQGI, has a control variable that updates the TPL control behaviour. For instance, for high values of the control variable, the TPL convergence will be faster (binary approach, resulting in less TPL updates), but may lead to a tracking error increase (difference between RSSI measured and RSSI predicted). For low values, a Linear-based TPL control is implicit, ensuring a slow convergence, higher control packets exchange, but also a tracking error decrease.

3.3.3 Comparative Analysis of Energy-Sensitive TPCs

This subsection summarizes and compares all the TPC solutions developed for energy-sensitive WBAN applications previously described.

Although the closed-loop control-based TPC mechanisms are not suitable to predict the run-time behaviour of the on-body radio channels, they are simple (algorithms with low complexity, but may demand high memory usage), effective (minimize energy consumption), able to detect incidental disconnections and ensures fast reactions to any changes in the radio channel. The several TPC mechanisms addressed in the literature are very different in terms of the LQE and TPL control mechanisms employed. The main disadvantages of these type of TPC

solutions are related to the traffic overhead resulting from the collection of huge information (from transmitted data packets and control packets) at run-time. This TPC operation principle might promote an extra overhead thus resulting on a weak network utility. Moreover, the metric RSSI, which has been the most adopted LQE metric, is largely influenced by interferences (high sampling transmissions also promote the increase of RF interferences) from coexisting WBANs or other systems. Therefore, these type of TPC approaches are more suitable for environments not subjected to a high RF interference.

The most devised approaches for static, dynamic, dynamic with fading presenting a periodic behaviour, and very dynamic (strict fading features that leads to frequent disconnections and lost data packets) scenarios are the Sample-and-Hold, Enhanced-and-Hold, Prediction-based Power Control TPCs and Adaptive Feedback Periodicity, respectively.

The sample-and-hold based mechanisms is the most agile and less complex, this makes this approach a good solution to static scenarios, since it requires a very low number of exchanged control packet to reach the optimal TPL. However, it is not suitable for dynamic fading scenarios due to the fast-change fading, in particular, the small-scale fading. As the radio channel quality can vary abruptly in short time periods [123] (Chaganti et al. reported an average fading variance of ± 10 dB [123]), this method will lead to unreliable estimations and impose a higher effort to the TPL control (higher fluctuation in TPL updating) to meet the WBAN application requirements. It also requires a higher amount of control packets when compared to the Enhanced-and-Hold based solutions, which ensures fewer fluctuations in estimations and in the TPL to update. However, the latter solutions are less agile even though this performance metric and, consequently, the TPL updating fluctuation can be optimised through the algorithm parameters configuration (such as weight given to the radio channel history and RSSI target range) according to the radio channel propagation conditions.

The solutions Adaptive Feedback Periodicity are devised to very dynamic scenarios since in such scenarios updating the TPL may not be recommended. These solutions, which are based on the principle of either the Sample-and-Hold or Enhanced-and-hold method to sense the radio channel quality, operate by controlling the period between control packets to accommodate the variation in the radio channel quality. The reported performance of these mechanisms demonstrates that too short or too long periods between transmissions of control packets can have a negative impact on the energy efficiency of the WBAN. Shorter periods lead to high energy consumption due to the frequent transmissions of control packets. A too long time interval among control packets transmissions turns the TPC less efficient. Slow reactions are expected, which increase the energy consumed per data packet successfully transmitted [1].

Although these solutions may lead to reduce energy consumption in transmission through a good run-time comprehension of the fading conditions, the PER and latency on communications may be significantly increased (due to the data packet losses, since solutions opt by not updating the TPL when signal in considered unstable).

The high amount of control packets exchanged has led the scientific community to propose Prediction-based Power Control TPCs solutions. These solutions assume that there is an inherent long-term temporal stability of the radio channels which makes this solution the most devised approach to radio channels showing periodic fading fluctuations. However, these solutions might not perform well in user's daily activities, since the coherence time averages reported in the literature are not higher than the maximum prediction period that research works aim to ensure (around 1 s). In [146], researchers performed a radio channel characterization for long periods while the user carried out his daily activities and coherence time values of 500 ms were reported. Usually, on-body characterizations are scenario-based and lower time values are reported, e.g. 308 ms when the user is walking [131], 125 ms [131] and 48 ms [125] when the user is running, 27 ms when the user is jogging [125], [131], and between 85ms and 310 ms [26] when the user is standing up/sitting down. Besides the fact that the radio channel remains stable only for periods of time inferior to the maximum predicted ahead (1 s), the stability of the radio channel also depends on other factors, such as, the type of movement, user posture, Edge of the Network node location (some positions, for instance, user's wrist or user's foot, are susceptive to larger movements), surrounding environment, as well as, body features or $Rx_{sensitivity}$. Therefore, this kind of solution does not seem suitable to improve the performance metrics of radio channels that experience variable fading effects. Performance results reported by research works, such as [50], are just satisfactory in static or dynamic scenarios where the fading magnitude follows a periodic behaviour over time.

The most suitable TPL control mechanism solution for the TPC mechanisms previously described is the scenario- and LQE-dependent. For instance, a binary approach is less efficient in dynamic fading scenarios, since in the presence of high radio channel quality variation the TPL control predicts the optimal TPL incorrectly. Owing to the big changes in the TPL value, the following LQE estimations are further away from the target RSSI range, resulting in data packet loss and unnecessary energy consumption. Therefore, this solution matches well with a Sample-and-Hold method, as both are recommended only to static fading scenarios. The dynamic-based TPL control has lower power consumption than the binary algorithm, since the straight-line equation is determined taking into consideration two (previously) measured RSSI values, both out of the target RSSI range, whereas in the binary approach more than two control

packets may be required to reach the optimal TPL [46]. Nevertheless, the operation principle of the dynamic-based TPL control is only suitable for scenarios where the radio channel is very stable. The suitability of this approach in dynamic scenarios is not clearly demonstrated, as the linear relation between the estimation metric and the TPL is not perceptible. However, even in scenarios where the user remains standing, the radio channel is susceptible to be time-varying due to body shape changes caused by the physiological process, such as breathing and slight-changes in posture, and changes in operation environment [26]. The linear approach was designed to cope with the dynamic scenarios since the TPL is linearly changed (slightly increased or decreased) close to the target RSSI range, without causing abrupt variations in the radio channel (due to the output power adopted in transmissions), thus reducing the number of control packets exchanged [1].

The Predictive-based TPL control has never been applied to TPC mechanisms based on a closed-loop control operation principle. The research work [46] empirically evaluated the performance of these TPL controls in an Enhanced-and-Hold operation principle TPC. The energy consumption and the PRR of the links user's chest-user's stomach and user's chest-user's back (these links do not typically experience severe large-scale fading) were analysed while user performed different activities, namely standing, walking and running in an indoor scenario. The linear-based TPC is those that consumes more energy in static fading conditions (more 23%, 14% and 23% than the binary, dynamic and hybrid, respectively), for instance in link user's chest-user's stomach while the user is standing or walking, but consumes less energy in dynamic fading scenarios (in link user's chest-user's stomach while the user is walking or to link user's chest-user's back to all the user activities). The binary scenario is better than the linear approach in static fading scenarios, since this approach reaches the optimal TPL faster. Moreover, this solution shows better results than the dynamic approach (this is the worst in dynamic scenarios) in all scenarios, achieving up to 5% average energy saving. The hybrid approach has better energy efficiency than the other ones in all scenarios tested. Regarding the PRR performance, all the TPC mechanisms meet the reliability requirements of WBAN applications.

As several research works showed through empirical radio channel characterization, the user0s body posture and movement are considered the main radio channel behaviour influence [48]. The Posture and Motion-based TPCs rely in different techniques to determine the current user posture and/or movement to ensure the WBANs requirements in terms of the network traffic application. In most of the applications data packets are required to be transmitted at diverse sampling periodicity since this is signal-specific (for instance, some parameters are only

sensed and transmitted at a frequency of 1 Hz such as environment-related parameters) or an event-based monitoring is required. The inertial-sensor based solutions addressed in the literature are typically more complex than closed-loop control based TPCs, but require low memory usage, low traffic overhead and are faster reaching the optimal TPL. However, the advances reached on this field are still limited. The research works that propose a solution of this type have to reach a great comprehension of the fading effects experienced by on-body signals. However, these signals are not well-understood, since the number of research works focused on the radio channel characterization and modelling is short when compared to the research works carried out on the traditional networks. These studies must take into consideration several factors that may affect the emitted signals such as the posture, movement, TPL and operation environment into the radio channel quality - it is impractical to conduct experimental experiments in all scenario configurations possible and one-model-fits-all approach to describe signal attenuation is not reliable [13], [26], [111], [159]. This fading effects analyse, which may drive to an analytical model, is used to determine the most suitable TPL according to the estimated radio channel conditions.

The inertial sensor-based TPC solutions rely on hardware to determine the posture and/or activity of the user to estimate the current radio channel quality or predict it in future instants. Different solutions have been addressed in the literature to either estimate [137], [145] or anticipate [22], [135], [143] the radio channel quality according to the user posture and movement. However, the proposed solutions to predict the radio channel quality are limited to static scenarios. For instance, the research works [22] only predict the RSSI when the user is static (this information is extracted from the accelerometer) through the acceleration orientation that permit estimate the relative position.

The research works that rely in models, such as ANFIS [135], [143], show great performance in static scenarios (but only in this one), as they cover a high variability of scenario configurations. Different TPL controls have been adopted, the majority of the research works rely on models that are obtained through the radio channel characterization in order to ensure that the optimal TPL value is reached faster, or opt by dividing the range of potential RSSI values into zones (to each one a TPL is assigned). The Posture and Motion-based TPCs that adopt Movement Detection based TPL control mechanism do not take into consideration all influencing factors of radio channel behaviour (such as, different environments, movement velocity and different postures) that make the instantaneous signal strength noisy. This solution uses the accelerometer to determine whether there is or no movement. When the user is moving the TPC is not executed. Therefore, this solution is not suitable for dynamic scenarios. The

RSSI-based Postural Position Detection TPCs do not rely on inertial sensors to estimate the current user posture.

The research works [9], [48] rely on the RSSI information (collected by following a closed-loop operation principle) to perform such task. Even though the results achieved are excellent in what concerns the lower error in RSSI estimation and the better energy performance, when compared with ordinary closed-loop architecture based TPLs, this TPL control is not suitable for dynamic scenarios. As the signals of a link have a dynamic and stochastic behaviour, it is impracticable to predict user posture or movement based on the RSSI, due to the numerous influences in the radio channel behaviour. All the Posture and Motion-based TPCs provide a great accuracy for static positions (if the user performs exactly the same postures that were considered during the radio channel characterization phase), but they do not take into consideration the underlying motion of the human body. This limitation is due to the LQEs based on the inertial sensor method, since none of them is able to cope with all changes in orientation of the human body, mobility of the subject and other spatiotemporal aspects (such as the room layout, people in the vicinity, etc.).

Since the user's body position and movement have a major impact on the radio channel behaviour, LQEs relying on 3-axis accelerometers may play an important role in future TPC mechanisms, as, besides velocity and displacement estimation, can also detect body-position and posture when used as inclinometer. These type of solutions are more complex than closed-loop control-based TPCs but are more energy-efficient when applied in scenarios in which there is no movement, since it does not require packets exchange and are faster reaching the optimal TPL. However, developments in this type of approaches do not have enough maturity to overcome the performance of the closed-loop control-based TPCs n dynamic scenarios.

As observed in this section, solutions that are only based on closed-loop control architecture or in inertial sensors are not able to ensure all features required in a TPC for WBAN communications. The research works [144] and [137], [145] have combined the closed-loop control operation principle and inertial-sensors information. Zang et al. proposed a TPC mechanism designed to WBANs subjected to changes in user posture but without motion [137], [145]. A previous radio channel characterization work allowed the researchers to understand which user postures lead the radio channel to experience high fading variability and to determine their design choices according to the fading effects nature in each posture. Unlike the research work [144] , the research work [137], [145] was designed to handle with the fading effects caused by human mobility. However, this solution only estimates the radio channel quality while the user performs periodic movements. The goal of this research in postponing

the data packets transmissions to the time instants where the radio channel quality is near a maximum within the user's gait cycle, which improves the system reliability since in such time instants there are fewer chances of data packets be lost. This solution sacrifices the latency metric (to levels much higher than the maximums allowed in WBANs) to improve the metric PRR and the energy consumption. These type of solutions show the advantages of merging both principles – can be executed in dynamic scenarios and can adapt their behaviour to the radio channel quality at run-time- even though the advances observed are still limited to very specific scenarios.

In Table 3.2, the design choices of the different TPC mechanisms are compared according to the taxonomy proposed, depicted in Figure 3.3, namely, LQE (1.), TPL Control (2.), Goals (3.), Topology (5.), Algorithm (5.), Scenario (6.) and Communication Standard (7.)

Table 3.3 presents a comparison between the TPC mechanisms in terms of compliance with the features required for WBANs, namely, agility to react to changes in radio channel conditions (R1), ability to estimate the run-time behaviour of on-body radio channels (R2), ability to anticipate future radio channel quality states (R3), ability to fast reaching the optimal TPL (R4), low memory usage (R5), low traffic overhead (R6), ability to operate in dynamic scenarios (R7), ability to detect incidental disconnections on wireless links (R8) and low complexity (R9).

Table 3.2. Comparison between the TPC mechanisms for energy-sensitive WBAN applications, highlighting the design choices of each TPC.

Reference	LQE	TPL Control	Goal Method	Topology	Algorithm	Scenario	Comm. Standard	Year
[48]	1.1.1	2.1.4	3.1.2.2	4.1	5.1	6.1	--	2009
[136]	1.1.1	2.2	3.1.2.2	4.1	5.1	6.1	--	2010
[9]	1.1.1	2.1.4	3.1.2.2	4.1	5.1	6.1	--	2010
[138]	1.1.2	2.1.1	3.1.1.3	4.1	5.1	6.1	--	2010
[50]	1.1.1/1.1.2	2.1.1	3.1.1.4	4.1	5.2	6.2	--	2011
[146]	1.1.3	2.1.1	3.1.1.4	4.1	5.2	6.2	--	2012
[5]	1.1.1	2.1.3	3.1.1.1	4.1	5.1	6.2	--	2013
[4]	1.1.2	2.1.1	3.1.1.2	4.1	5.1	6.2	--	2013
[22]	1.3.2	2.2	3.1.2	4.1	5.2	6.1	--	2013
[46]	1.1.1	2.1.4	3.1.1.1	4.1	5.1	6.2	--	2014
[1]	1.1.2	2.1.2	3.1.1.3	4.1	5.1	6.2	--	2014
[139]	1.1.1	2.1.1	3.1.1.1	4.1	5.3	6.2	--	2014
[140]	1.1.2	2.1.1	3.1.1.1	4.1	5.1	6.2	7.2	2014
[141]	1.1.2	2.1.1	3.1.1.2	4.1	5.2	6.2	7.2	2014
[135]	1.3.3	2.2	3.1.2.1	4.1	5.2	6.1	--	2014
[142]	1.1.2	2.1.1	3.1.1.2	4.1	5.2	6.2	7.2	2015
[143]	1.3.3	2.2	3.1.2.1	4.1	5.2	6.1	--	2015
[39]	1.1.1/1.1.2	2.1.1	3.1.1.2	4.1	5.3	6.2	--	2016
[144]	1.1.1	2.1.4	3.1.2.1	4.1	5.1	6.1	7.1	2016
[145]	1.1.2	2.1.3	1.2.1	4.1	5.2	6.2	--	2016
[137]	1.1.2	2.1.3	1.2.1	4.1	5.2	6.2	--	2017

3.4 Issues, Challenges, and Future Research Directions

In the following subsections, issues, challenges and future research directions in the design of TPCs for WBANs will be highlighted.

3.4.1 Issues and Challenges in TPCs for WBANs

Many studies have been carried out on mechanisms that aim the control of the TPL for miniaturizing energy consumption, RF interference and SAR in WBANs, but none of them are able of meeting all the TPC mechanisms requirements yet.

In part, the main reason for the failure is due to the wide number of factors that influence the radio channel conditions that turns the estimations and/or prediction of the radio channel quality a difficult task.

Holistic Link Quality Estimations

The design of a LQE able to offer a holistic view of the radio channel in WBANs links is crucial for the effectiveness and applicability of TPC mechanisms. However, this is a relative new research area, and, as a consequence, there still are some challenges and open issues.

Many works have analysed the capacity of several software- and hardware-based metrics in quantifying WBAN links properties. So far the TPCs addressed in the literature that take decisions based on estimations of a single LQE metric tend to fail in providing a holistic view

Table 3.3. Comparison between TPC mechanisms for energy-sensitive WBAN applications in terms of requirements

Reference	R1	R2	R3	R4	R5	R6	R7	R8	R9	Year
[48]	✓	✓	X	✓	✓	X	X	X	✓	2009
[136]	✓	✓	✓	X	✓	X	X	X	✓	2010
[9]	✓	✓	X	X	✓	X	X	X	✓	2010
[138]	X	✓	X	X	✓	X	✓	X	✓	2010
[50]	✓	✓	X	X	X	X	✓	X	✓	2011
[146]	✓	✓	✓	✓	X	✓	✓	X	X	2012
[5]	✓	✓	X	✓	✓	X	✓	X	✓	2013
[4]	X	✓	X	✓	✓	X	✓	X	✓	2013
[22]	✓	X	✓	✓	X	✓	X	X	✓	2013
[46]	✓	✓	X	X	✓	X	X	X	✓	2014
[1]	✓	✓	X	X	✓	X	X	X	✓	2014
[139]	✓	✓	X	✓	✓	X	X	X	X	2014
[140]	X	✓	X	X	✓	✓	✓	✓	✓	2014
[141]	X	✓	X	X	✓	✓	✓	✓	✓	2014
[135]	X	✓	✓	✓	X	✓	✓	X	X	2014
[142]	X	✓	X	X	✓	✓	✓	✓	✓	2015
[143]	✓	✓	✓	✓	X	✓	✓	X	X	2015
[39]	✓	✓	X	X	✓	X	✓	X	✓	2016
[144]	✓	✓	X	X	X	X	✓	X	✓	2016
[145]	X	✓	✓	X	X	✓	✓	✓	X	2016
[137]	X	✓	✓	X	X	✓	✓	✓	X	2017

of the radio channel. In this regard, the selection of representative link quality metrics and the design of a new approach for combining these metrics in a single LQE is a challenging problem. The research work [4] proposed one of the few LQE solutions that combine heterogeneous metrics, but the combination of other metrics should also be considered to investigation.

As stated by Baccour et al., the agility and reliability of LQEs (radio channel estimations must be computed fast and LQE must have sensitivity to detect changes in radio channel quality) impose a very challenging problem [55]. As the majority of the LQEs for WBANs addressed in the literature rely on several samples of a specific LQE metric to estimate the desired output parameter, it is necessary to find an optimal trade-off between the LQE stability and the ability to cope with radio channel quality dynamics.

Due to the lack of a holistic assessment methodology (to be used regardless of the nature and used metrics of the LQE under consideration) and the difficulty in providing a quantitative assessment of the LQE accuracy, the way how link quality estimator is validated and how LQE configuration parameters are dynamically tuned still remains an open issue within the WBAN field.

Low Complexity

One of the challenges faced during the developing of TPC mechanisms for WBAN Edge of the Network nodes is related with strict constraints on processing and memory space. Solutions proposed for WBANs must be kept simple and light enough to be successfully implemented in such resource-constrained Edge of the Network nodes.

Some very promising TPC mechanisms based on ANFIS models have been proposed and evaluated through simulations. However, the resultant neural network and number of fuzzy rules turn unfeasible this type of solution in WBAN networks. Inertial-sensor based TPCs that predict the RSSI peak value on periodic movements rely in complex techniques that need to process several amounts of accelerometers (memory space required is superior to the one available on a typicall sensor node SoC, the CC2420 [130]), which forced the authors to implement these solutions in a receiver-side way (increasing the dependency on control packets).

The assessment of the TPCs performance in terms of metrics able to quantify the TPC computational load and running time as well as how computation load of the algorithms affect the power consumption have been ignored. The way how TPCs can be assessed and compared to other solutions in terms of these metrics still remains an open issue.

Impact of Loss of Feedback radio channel in TPCs

Most of the research works in TPC field is reliant in feedbacks from the receiver in a form of either control packets, beacons or ACK, constructing a closed-loop control system to allow TCP mechanisms to accommodate dynamic changes in the environment adaptively. Generally, it is assumed that for each data packet transmitted, the transmitter has access to the output value of the LQE block or the optimal TPL transmitted as control packet by the receiver. The impact that control packets loss has on power control schemes (in terms of performance degradation and robustness) has been ignored, remaining as an open issue in the TPC field.

The TPC addressed in [49] proposes a strategy to identify incidental disconnections, to distinguish it from broken links and to proceed in such situations in a way that reacts reasonably fast and avoids fluctuating TPL. To the best of the author knowledge, this research work in the TPC field for WBANs is the only one that proposes a block to deal with incidental disconnections as part of the TPC architecture. The authors also analysed the effect of incidental disconnections on TPC performance, showing that the detection of incidental disconnections and the design of the appropriate approaches to react to it is a challenging problem.

Design of Appropriate Protocol Stacks to merge with TPCs

The LQE is a fundamental block for several protocols (e.g. MAC, routing, mobility management, radio channel interference mitigation, localization and self-organization) [52], [55], thus, the integration of TPC mechanisms with these protocol solutions already addressed and validated in the literature and/or the design of adequate protocols to support TPC procedures are important research challenges. Research works [151], [160] propose that through a tightly integration of TPC techniques with other mechanisms, higher gains can be achieved.

For instance, the research work [21] shows that appropriate routing protocols can use the TPL as a routing metric to achieve energy-efficient and low-latency end-to-end communications between the on-body sensors and the Coordinator node. Other routing protocols (e.g. [49], [52], [53]) use the metrics often adopted in this type of protocol (PRR, SINR or ETX) to choose the most reliable path. After this process, the TPC algorithm choose the optimal TPL to each Edge of the Network node that built the communication path. This scheme allows the extension of the per-link transmission power assignment schemes to the network topology level.

Regarding MAC protocols design, research works [49], [161] have focus on the design of more effective MAC control to work with TPC algorithm through either the adaptation of the most adopted standards in WBANs (e.g. IEEE 802.15.4 in [161]) or the design of new

approaches in order to facilitate the power control algorithm and analyse of the overall performance. The research works [49], [53], [140]–[142], have opted by developing TPC mechanism for WBANs with a transceiver that adopts stacks in conformity with the IEEE 802.15.4/IEEE 802.15.6 MAC layer.

The research work [49] addressed the design of a TPC built on top of two modified layers, namely the MAC and Network layer.

The design of suitable protocols is a very challenging problem, as evidenced by the limited number of solutions found in the literature. However, the implementation of these protocols to cooperate with TPC mechanisms is an important future research direction for ensuring the WBAN requirements in a wide range of applications [22], [44], [48], [108], [128], [149].

Researches in the TPC field for WBANs is relatively recent. The number of works is significantly reduced in comparison to the number of solutions addressed in the literature in other fields such as MAC, radio channel interference mitigation, routing protocols, etc. Therefore, how to build TPCs solutions on top of these protocols (that are already validated in the literature) to balance energy and reliability in an acceptable way but without leading to deep changes in such protocols (for instance by using their LQE metric as estimation metric of the TPC LQE block) is still an open issue.

TPCs to accommodate all Wireless Radio Channels Scenarios

Several challenges and issues arise due to the high heterogeneity found in wireless radio channel conditions and wide variety of WBAN applications with different demands.

TPC techniques are designed to unicast data packets, but they must also be extended to support broadcast and multicast data packets. This challenge has not been addressed in the literature so far.

The feedback approach in TPCs resumes to the ACK-, beacon- and data packet-driven approaches. However, unlike verified to WSNs, there was not been driven an comparative performance to determine the most appropriate approaches for each WBAN scenarios [162]. Therefore, it is still an open issue in the TPC field.

Another open issue is related to some assumptions taken in the TPC design approach. For instance, TPC mechanisms are evaluated through simulations/experimental tests assuming that all the Edge of the Network nodes produce the same data rate and have the same periodicity. However, this does not happen in real applications due to the diversity of the different sensors required by WBAN applications. Thus, the trade-off between data packet loss, latency and overhead as well as the impact of the sensor data periodicity needs to be addressed.

Research works focus in proposing an effective TPC for scenarios where user performs periodic movements should extend this scheme to other daily activities (like running and ascending/descending stairs, etc.). However, solutions have opted by evaluate solutions in experimental tests while user is walking, thus, the performance and effectiveness of such solutions in daily activities has not been addressed. Moreover, movements never are exactly periodic, thus, the key challenge is to develop mechanisms for capturing the locality of on-body node movements caused by human postural mobility.

As discussed in this document, TPC solutions are proposed for very specific wireless radio channel scenarios. Some approaches are feasible for scenarios prone to stable radio channel quality to single hop; others are suitable for scenarios with dynamic scenarios with severe irregularities in user movement or periodic movements; other solutions are effective in scenarios where multi-hop topology ensures a higher communication reliability and TPCs are required to ensure a good trade-off between reliability and power consumption; and other approaches performs well when scheduling the data packet transmission among multiple WBANs is a very challenging task. There is not a single and flexible TPC mechanism in the literature able to effectively operate in any circumstances.

3.4.2 Future Research Directions

Although, several research works have been surveyed in this study, there are still many aspects that need to be approached in order to increase the performance and usability of TPCs in WBANs. Key future research directions in TPCs for WBANs are provided in this subsection.

Off-Body Communications

As depicted in Figure 1.1, communications between the Coordinator node and an External node are required to turn the information gathered in WBAN available on internet. Off-body signal propagation is very similar to the verified in on-body communications, since radio channel conditions are dynamic. Emitted signals are shadowed by human body and are influenced by surrounding environment conditions. In addition, as the ZigBee (IEEE 802.15.4), Bluetooth and Wi-Fi (IEEE 802.11) are communication technologies in this communication segment, the nodes on this segment are subjected to RF interferences. The Coordinator node, which is also energy-constraint node, is located in a WBAN, thus, RF interference magnitude is non-deterministic due to the WBAN mobility, which might demand TPCs mechanism to reduce TPL of coexisting Coordinator nodes to improve the overall network utility. Therefore, seems reasonable claim that most of the advances reached to on-body communications have potential to improve off-body communications. Off-Body Communications have not received

so much attention from the research community, however, reliable off-body communications are also critical to implement suitable monitoring systems.

Low traffic Overhead TPCs for Dynamic Scenarios

Through data exchange between Edge of the Network nodes (e.g. TPCs for latency- and energy-sensitive applications) or between Coordinator nodes of different WBANs (e.g. TPCs for performance-sensitive applications), the several TPCs surveyed in this article show their ability to improve the communications reliability and minimize energy consumption. The cooperation between nodes (Edge of the Network or Coordinator nodes) leads to a significant and undesired communication traffic. The use of inertial-sensors data as a LQE metric is a relative new research area, thus, several research challenges still remain to be addressed.

As human body is the predominant influence on the radio channel behaviour, further research on Posture and Motion-based mechanisms is required as a way to reduce cooperation between nodes. User movement and relative position of the Edge of the Network node in relation to the Coordinator node constitutes extremely useful information that allows the Edge of the Network nodes to take decisions without requiring exchange data [143]. By itself, modelling the radio channel quality based on the body posture, the movement and the relative position of the Edge of the Network nodes (information process through inertial sensor data) is a promising research topic. The inertial sensors are already embedded in the Edge of the Network nodes of a large number of the WBAN implementations and sampling inertial sensors data does not have a significant impact on the energy consumption when compared to sending and receiving control packets [130], [135]. Therefore, a data fusion algorithm should be adequately integrated with a Kinematic radio channel model (e.g. [158]) together with a radio channel model that describes the radio channel in function of the posture, the movement and the Edge of the Network nodes' relative position.

So far the TPC solutions addressed in the literature accommodate different behaviours in order to adjust the power control algorithm to the radio channel quality conditions, but future research could also make use of the actual battery level (in the algorithm) as part of the TPC behaviour decision making. This would allow nodes with different power sources and power requirements to be addressed in the energy balancing process [163], especially in TPCs though to mitigate RF interferences between nodes or networks.

Integration of the WBANs in a Cyber-Physical System

The development of a WBANs integrated in a CPS as depicted in Figure 1.1, which enables the collection of information from many others WBANs, offering several advantages to TPCs, namely: 1) increasing of the situational awareness of Coordinator nodes position, physiological and environmental conditions [101]; 2) refinement of LQE and TPL control parameters (according to the small-scale fading changes that is widely influenced for the environment) such as radio channel history weight (α) in equation (3.1); and TRH and TRL; 3) reduction of the cooperation between WBANs, since CPS systems might be able to interpret the WBANs location and adjust the TPL value according to overlapping communications ranges, as explored in the interference-mitigation scheme addressed in research work [151]; 4) reduction of the computational effort in the Edge of the Network nodes and Coordinator nodes through the distribution of the workload; and 5) system capable of interpreting and adjusting to the dynamic changes of the environment in real time [101].

In spite of the advantages of the integration of WBANs in a CPS, only the research work [149] proposed a TPC that takes advantage of the intrinsic CPS characteristics.

CHAPTER 4

PROTACTICAL PROJECT

In this chapter, a fully integrated Cyber-Physical System approach to a smart Personal Protective Equipment (PPE) is discussed, implemented and assessed.

4.1 Introduction

PROTACTICAL was a successfully R&D Project. PROTACTICAL is based on a Personal Protective Equipment is composed of a shirt, a coat, pants and boots. A WBAN is deployed in the PPE and critical data is gathered through electroactive substrates (e-textiles) with sensors and electronic circuits embedded into the textile structure for physiological signals monitoring, together with off-the-shelf sensors unobtrusively integrated onto the textile substrates. The monitored parameters, consistent with urban fire requirements, are heart rate, breathing rate, sweat detection, inner and environmental temperatures, heat flux across the coat, carbon monoxide and dioxide concentrations, user's activity and posture, absolute and relative position.

The array of real-time sensors data also ensures situational awareness during emergency events. However, as firefighting involves several actors, the PROTACTICAL CPS explores wireless communication technologies to ensure a multi-dimensional system at individual user (or PPE), emergency response team and fire command centre levels. Regarding to computation and control components, the real-time data transmitted is perceived as actionable information for computational technologies in order to provide data to powerful decision making tools.

The integration of each subsystem into a unique system ensures a close interplay between the "cyber" and "physical" worlds, i.e. a change in a world must be reflected in the other world. This allows, not only the real-time monitoring of various external (environmental) and internal (microclimate of the equipment and the user) parameters, which provides situation awareness, but also control and actuation at three distinct levels (PPE, emergency response team and fire command centre).

4.2 PROTACTICAL CPS Architecture

The architecture of PROTACTICAL CPS is depicted in Figure 4.1. The components of the system are defined across spatial levels, while the interactions between components and their

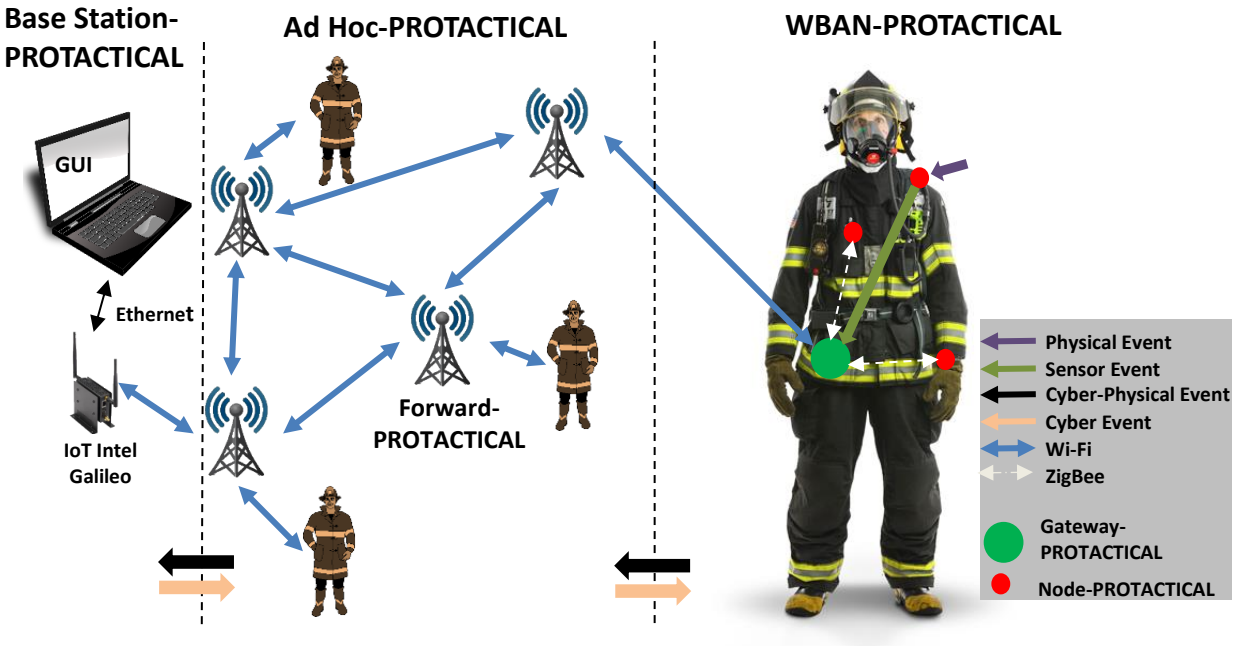

Figure 4.1. Architecture of the CPS-PROTACTICAL.

tasks are defined across temporal and spatial levels. The tasks performed for every component are described by an "Event-Action" relation. The target application defines the changes required in the physical world - which can be a change in an attribute, temporal or spatial status of a physical phenomenon or object or a combination of these different types of information and are designated as events, which have a predefined action after the respective event is triggered. These events can be generated from several nodes and the same event has a different level of abstraction in each PROTACTICAL CPS component, accordingly to the spatial level. For instance, considering the following event "Inner temperature of user garment is 40 ºC", the Node-PROTACICAL and the Coordinator node (here designed Gateway-PROTACTICAL) illustrated in Figure 4.1, have different levels of abstraction. In the node, the event is interpreted as the level of temperature in inner coat, while in the latter coordinator it can be interpreted as critical since it causes skin burns.

The spatial-temporal event model presented in [164] is adopted to capture close interactions between cyber and physical worlds. This model integrates different events over space and time while the information of the original physical event remains intact. Concepts such as Events Condition (combination of attributes, temporal, and spatial information, which are used to trigger changes in physical world), Events Instance (events required) and Actions (predefined actions triggered after the detection of an Event Instance), as well as, Observers components (nodes with capacity to collect data, assess it based on the event condition, and generate an Event Instance when conditions are respected) are introduced in the proposed architecture.

The components of the PROTATICAL CPS are categorized according to the spatial level (Cyber-, Physical-World or CPS Network), as depicted in Figure 4.1. There are five elements operating at the Physical-World:

- Sensors – interface between the physical and cyber worlds, resulting in physical events. The physical phenomenon measured is converted to information, containing attributes, time and/or space information;
- Actuators – capable of changing attributes of a physical object;
- Node-PROTACTICAL – it is a wearable Edge of the Network node composed by a microcontroller, designated computing component; a transceiver, communication component; a power source (small battery); sensors and/or actuators. The physical observations of sensors are exploited by Nodes-PROTACTICAL to generate a Node Event Instance based on Event Conditions of the Node-PROTACTICAL and respective sensor. This component represents the first level of Observers in CPS event model (Observer entity), being responsible for transforming real-time sensor data into actionable information;
- Gateway-PROTACTICAL – it is a Body Gateway node that has the task of gathering the real-time sensor data received from Nodes-PROTACTICAL and for managing the WBAN-PROTACTICAL. It also serves as second level of Observers in the CPS event model. In this context, this component is called event-driven control unit, since it can also collect the node Event Instance from the Nodes-PROTACTICAL, as input observations and generate cyber-physical Event Instance, or in other words, additional actionable information;
- Wireless Body Sensor Network (WBAN)-PROTACTICAL – a distributed network comprising several Nodes-PROTACTICAL and the Coordinator node of the network, the Gateway-PROTACTICAL. The wireless communication technology adopted in this network is the ZigBee. A detailed description of this network can be found in section 4.4.

The elements of the cyber world of the proposed CPS system, illustrated in Figure 4.1, are as follows:

- Fire command centre – in the context of PROTACTICAL CPS is called Base Station-PROTACTICAL or CPS Control Unit (CU), serving as the highest level of Observers in the CPS event model. This Observer entity is connected to the Ad Hoc-PROTACTICAL, receives cyber-physical Instance Events from

Gateway-PROTACTICAL, processes them according to certain rules and generates Cyber-Events. Moreover, at this level, Cyber actions are associated with determined Cyber-Events; these actions can be performed in CU or can be a command for WBAN-PROTACTICAL;

- Database Server – distributed data logging service. Events Instance that circulate inside the CPS network are automatically transferred to the database server after a defined time for later retrieval.

The CPS network is called Ad Hoc-PROTACTICAL and consists in an ad-hoc network with the responsibility of connecting the WBANs-PROTACTICAL with the Base Station-PROTACTICAL and Database Server. A continuous, reliable and efficient connection is ensured by the Ad Hoc Network, using Forward-PROTACTICAL nodes. The cyber-physical events emitted by any Gateway-PROTACTICAL are transported by the Forwards-PROTACTICAL to the CU. The CU, after processing the cyber-physical events emits an associated cyber action to the respective Gateway-PROTACTICAL through the CPS network created by the Forward-PROTACTICAL nodes. The wireless communication technology selected for this network was Wi-Fi.

4.3 Sensors, Actuators and Instrumentation Electronics

Recent advances in wearable, wireless communications, computer and electronic technologies have considerably reduced the size, cost, and power requirements of embedded/wearable systems. Low-power and low-cost nodes are now equipped with sufficient storage and data processing capabilities, making wireless sensing a reality in a wide range of applications.

The monitored parameters (physical events) of the PROTACTICAL Personal Protective Equipment are acquired through wearable multipurpose Edge of the Network nodes, Nodes-PROTACTICAL, with wireless (ZigBee), data processing and sensing capabilities, that send the processed data to the Gateway-PROTACTICAL (sensor event) at a predefined sampling rate. This sampling rate can be automatically updated if the Gateway-PROTACTICAL detects/identifies a critical situation (cyber event), i.e. the processing logic is distributed at Node-PROTACTICAL level.

In Table 4.1, the different modules (Nodes-, Gateway- and Router-PROTACTICAL) of the current version of the smart PPE are listed, where it is highlighted the embedded sensors in each module, parameters measured and the interface used to link module to the Coordinator node of the network: Gateway-PROTACTICAL. The architecture proposed for each Node and

Table 4.1. Nodes and monitored parameters in the WBAN-PROTACTICAL.

Module	**Garment**	**Sensors & Actuators**	**Monitored Parameters**	**Interface**
1	Shirt	Textile Electrodes Sensor	Heart Rate and Battery Level	ZigBee
2	Shirt	Textile Moisture and Temperature Sensors	Sweat Detection, Inner Temperature and Battery Level	ZigBee
3	Shirt	Piezo-Resistive Sensor	Breathing Rate and Battery Level	ZigBee
4	Coat	Heat Flux, Temperature and Inertial Sensors	Heat Flux across the coat, Inner Temperature, Inactivity, Posture, Fall and Battery Level	ZigBee
5	Coat	CO and CO_2 Sensors	CO and CO_2 Concentrations, Environmental Temperature, Relative Humidity and Battery Level	ZigBee
6	Boot	Inertial Sensors	Inactivity/Position and Battery Level	ZigBee
7	Coat	Buttons, RGB LED, Inertial Sensors and Vibration Motor	Inactivity/Posture, Panic Event, User Feedback and Battery Level	ZigBee
8	Pants	Inertial Sensors	Inactivity/Posture and Battery Level	ZigBee
Gateway-PROTACTICAL	Coat	GPS Module, UWB Transceiver, Barometer and Temperature Sensors	Absolute Position, Indoor Location, Altitude, Environmental Temperature and Battery Level	SPI
Router-PROTACTICAL	Coat	-	Battery Level	ZigBee

selection of components took into account the flexibility and unobtrusiveness of the solution, energy efficiency and autonomy and reliability of the measurements under harsh conditions. The Nodes-PROTACTICAL are composed for the following four blocks:

- Sensing and actuating block - several sensors and actuators may be embedded in nodes. Every node comprise a different combination of sensors and actuators;
- Energy block - nodes are self-powered through small batteries, with the capacity to continuously monitor the Edge of the Network node-specific parameters during the user's intervention;
- Processing/Transceiver block – it refers to the microprocessor and radio module (radio-frequency transceiver) adopted for each Node-PROTACTICAL. A low-power system-on-chip (SoC) was chosen to implement these two blocks: the CC2531 from Texas Instruments. This SoC includes a ZigBee-compliant transceiver and a MCS-51 compliant microcontroller on the same integrated circuit.
- Inertial Sensor – every Node-PROTACTICAL is also equipped with a LSM330DLC STMicroelectronics MEMS accelerometer.

The modular architecture of nodes allows reducing the amount of data to be sent, thus the energy consumption due to wireless communications, and enables customizing the PPE according to the user's needs (i.e. adding or removing Nodes-PROTACTICAL according to the intervention scenario). In addition, the proposed architecture allows adding new Nodes-PROTACTICAL to the PPE, to monitor other parameters, without modifying the other Nodes-PROTACTICAL.

Figure 4.2 illustrates the Node-PROTACTICAL 4 through a 3D representation of the developed hardware and, through a block diagram, the several components that compose this node.

4.3.1 Shirt

From the electronics point-of-view, the shirt was designed for the acquisition of physiological parameters that need direct contact or proximity with the skin and integrates knitted textile-based sensors, as well as, connections paths, embedded in the structure. The parameters monitored by the Nodes-PROTACTICAL placed in the shirt are heart rate, breathing rate, sweat detection, and inner temperature.

For the acquisition of the heart rate, textile electrodes with a voluminous structure to increase contact to skin were developed [165] and a two electrode configuration was selected. This configuration allows reducing the number and size of the connections paths, making the system more robust and less vulnerable to common-mode interference. The heart rate measurement is obtained by the front-end AD8232, from Analog Devices and the heart rate value is computed as described in [166].

The breathing rate measurement is carried out using a textile extension sensor [167]. The quantification of extension is based on the relationship between elongation and impedance.

Sweat detection is obtained from a textile moisture sensor, made of two conductive bars embedded on the shirt lower back, near the lumbar curvature, which is the location where most of the human's eccrine sweat accumulates [166]. The detection of sweat is based on a threshold value, defined by an electrical resistance and when the electrical resistance between the two conductive bars drops below the defined value, the system identifies the presence of sweat. This threshold value is defined based on the amount of sweat needed to cause skin burns, due the presence of humidity and high inner temperature (above 40 ºC).

The inner temperature is measured using a commercial off-the-shelf (COTS) digital sensor (ADT7320 from Analog Devices), placed in the same node-PROTATICAL of the textile moisture sensor (node-PROTACTICAL 2).

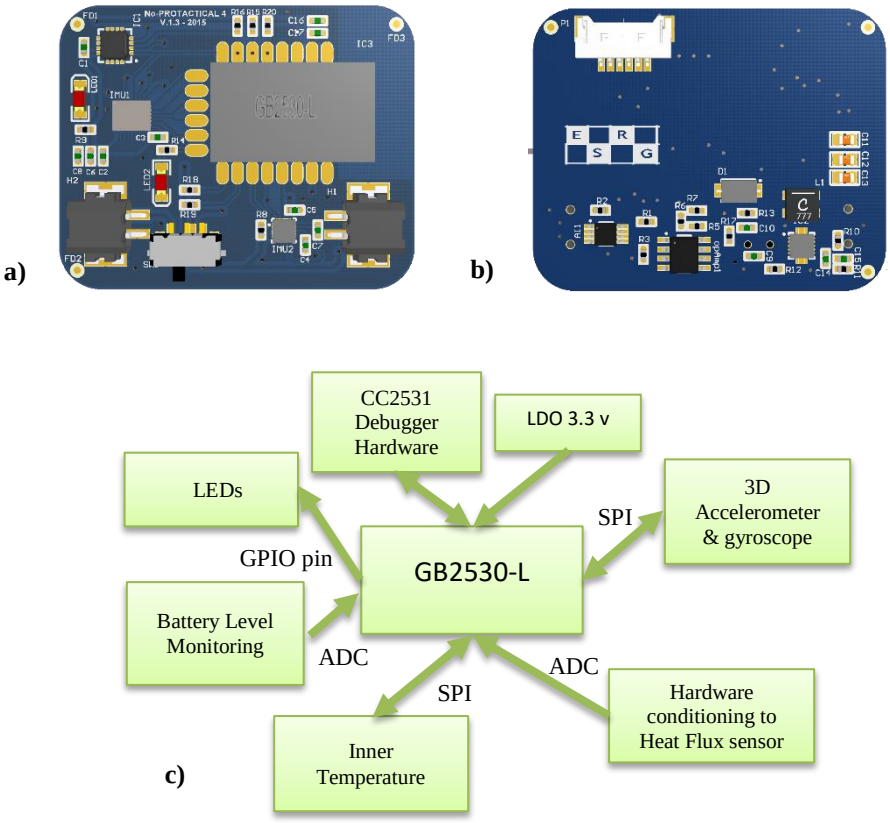

Figure 4.2. Node-PROTACTICAL 4: 3D representation of the hardware developed through Altium software – a) front and b) back view – and c) block diagram.

4.3.2 Coat

The coat's electronics are designed to monitor the environmental parameters and assess the user activity state. The nodes-PROTACTICAL incorporated in the coat measure various parameters, namely heat flux across the coat, inactivity, user's posture, fall detection, carbon monoxide (CO) and carbon dioxide (CO_2) concentrations, inner and environmental temperature, relative humidity, indoor location and absolute position. An alarm module is also included in the coat, responsible for notifying the user of an emergency situation. The coat also includes the module designated Gateway-PROTACTICAL for data transmission. This node will send the acquired information to the fire command centre using the ad hoc-PROTACTICAL network.

The heat flux across the coat is measured using a heat flux sensor from CAPTEC. This sensor provides information on the heat exchanges between the user and the environment. When heat flow passes through the surface of the sensor, it supplies a voltage proportional to the heat flux. The output voltage can be either positive or negative, depending on the heat flux direction (respectively, outwards and inwards). This sensor is integrated in the inner layer of the upper front of the coat (node-PROTACTICAL 4). This node also integrates a sensor for the

acquisition of the inner temperature of the coat (user's chest), using hardware COTS identical to node-PROTACTICAL 2.

To assess the user activity state during a fire intervention, two inertial sensor modules are used: one integrated in the coat sleeve (node-PROTACTICAL 7) and the other at the upper front of the coat (node-PROTACTICAL 4). These modules integrate one 3-axis accelerometer and one 3-axis gyroscope to detect long periods of immobility, falls, and user posture.

The monitoring of toxic gases, namely CO and CO_2, is carried out by node-PROTACTICAL 5. This node is integrated on the collar in the outer layer of the coat, close to the user's mouth and nose. The selected COTS sensors for monitoring the CO and CO_2 concentrations are the TGS2442 and the COZIR, respectively. The COZIR sensor also acquires the relative humidity and the environmental temperature.

For the acquisition of the environmental temperature, a type T thermocouple is used. This thermocouple was selected as it combines a wide temperature range (from -270 to 370 degrees Celsius), good accuracy (+/- 1 degree Celsius) and long term stability. The sensor is positioned in the coat outer layer, connected to Gateway-PROTACTICAL, close to the user's waist region.

The absolute position of the user is determined through a high precision Global Positioning System (GPS) module from U-Blox (Neo-6P). This module is based on an active antenna and relies on the Precise Point Positioning (PPP) technology to provide an accurate absolute position estimation of the user in outdoor environments. Although the performance of the sensor deteriorates in the presence of high obstacles and in indoor environments, this information is still extremely useful for the fire command centre for firefighting operation coordination. The GPS module is connected to the Gateway-PROTACTICAL, which is integrated in a front pocket of the coat.

For the indoor localization, a UWB transceiver from Decawave (DWM1000) is used to obtain ranging measurements. Based on the ranging measurements acquired, a trilateration algorithm is used to compute the position of the user. The estimated position is then refined based on the user's posture and the relative position estimated from the readings of the Node-PROTACTICAL 6. The UWB transceiver is connected to the Gateway-PROTACTICAL.

The alarm module (Node-PROTACTICAL 7) was designed to notify the user of emergency scenarios or to send an alarm to the fire command centre in case of panic. A RGB LED and a vibration motor are used to alert the user that an alarm was received/detected. The RGB LED is able to encode, using colours, up to seven different alarms (e.g. the combination of high inner temperature and moisture on the shirt, evacuation order, quality of the air or connection loss

with the Ad Hoc-PROTACTICAL network). The vibration motor (307-100 from Precision Microdrives), which is positioned in the inner layer of the cuff, has a normalized vibration amplitude of 6 g's and the vibration amplitude is driven by a microcontroller through a PWM signal. To notify the fire command centre that a panic scenario occurred, a two button configuration was selected. The buttons are placed on diametrically opposite sides in the node-PROTACTICAL 7 to avoid the generation of false alarms due to involuntary contact and must be pressed simultaneously.

4.3.3 Pants

The pants incorporate Node-PROTACTICAL 8 in the outer layer of the user's thigh area. Inertial sensors (3-axis accelerometer and 3-axis gyroscope) are integrated in this node for the evaluation of the user's posture and to detected inactivity. Similar to the node integrated on the coat sleeve, Node-PROTACTICAL 7, it aims to enhance inactivity detection, as it can independently detect legs' movement.

4.3.4 Boots

The Node-PROTACTICAL 6 is integrated in the boots. This node is dedicated to the estimation of user's relative position during intervention in the emergency site. Inherently it is also possible to detect long periods of inactivity. This node is equipped with a 3-axis accelerometer and a 3-axis gyroscope and a 3-axis magnetometer sensor. The accelerometer and gyroscope are used to estimate the distance and direction of the movement, respectively. The magnetometer, besides the information about changes in direction, provides the initial orientation of the user. For the continuous relative position estimation, methods such as the ones used in pedestrian dead reckoning are implemented. Figure 4.3 shows some examples of nodes, aiming to demonstrate its final appearance.

4.4 Wireless Communications and Networking

The value of the sensor data or actionable information depends not only in its features, such as accuracy and completeness, but also in its real-time accessibility, i.e. real-time transmission of parameters. Wireless technology communications were explored to integrate the PPE subsystems and the Base-Station PROTACTICAL. The networking technologies adopted and the distributed networks developed are described in the following sections.

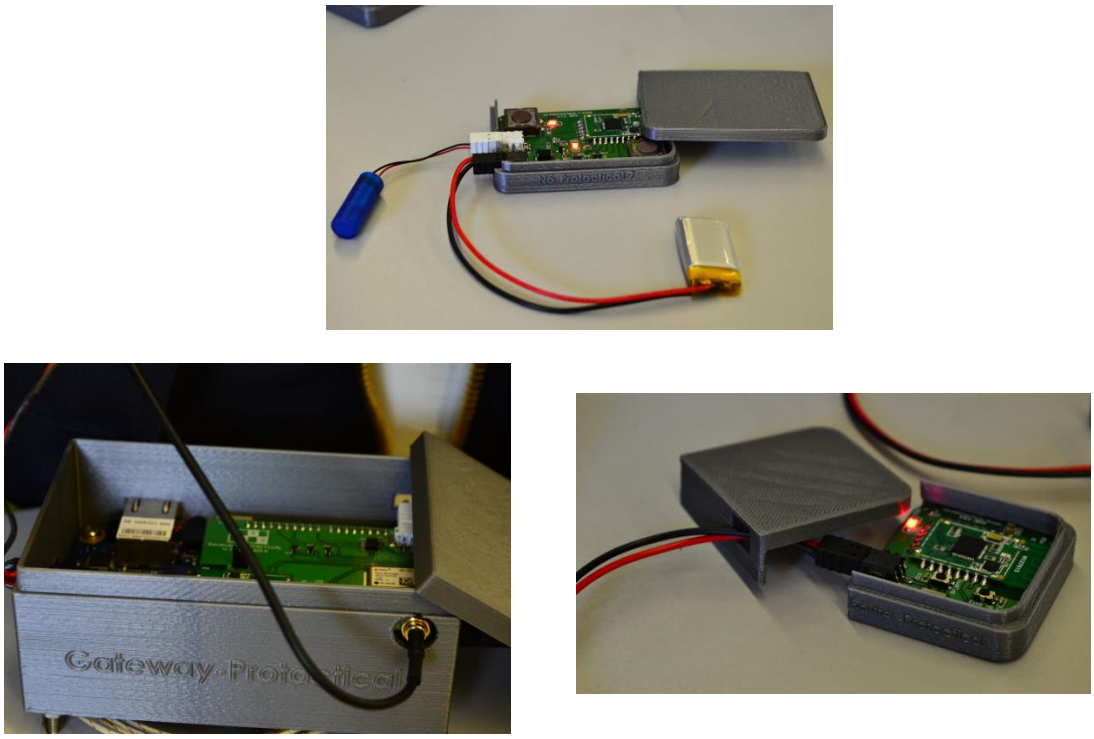

Figure 4.3. Examples of constituent elements of the implemented PROTACTICAL interactive system: a) Node- PROTACTICAL 7 (PAPS), b) Gateway-PROTACTICAL and c) Router-PROTACTICAL

4.4.1 WBAN-PROTACTICAL

The WBAN-PROTACTICAL comprises a set of wearable nodes, described in section 4.3, integrated into/onto the textile platform of the PPE, as depicted in Figure 4.4. Low-power wireless technology ZigBee was selected for the transmissions inside the WBAN range. As the WBAN-PROTACTICAL is subjected to different physical movements, path-loss and fading (effect of the presence of reflector objects in surrounding environment) [26], [111] may occur and, due to the coexistence of nodes from other PPEs PROTACTICAL or other systems, RF interferences are likely to happen. Therefore, to ensure the requirements of user's monitoring in critical applications and to comply with the requirements of standard IEEE 802.15.6 for networks operating close to the human body [19], a third element, designated Router-PROTACTICAL, was included in the WBAN-PROTATICAL.

An preliminary experimental performance evaluation of the several links in different environments (indoor and outdoor) were performed and results analysed in [66]. The version of the WBAN used in these tests is illustrated in Figure 4.5, corresponding to a Mock-up of the WBAN-PROTACTICAL. These tests correspond to a PER test, where results show that the Node-PROTATICAL lost several data packets transmitted to the Gateway-PROTACTICAL. The Node-PROTACTICAL 7 was not also able to successfully delivery all the transmitted data packets. This is especially evident when non-line-of-sight exists between nodes. The average PER value varies according to the movement performed. Lost data packets led to an increase

Figure 4.4. PPE prototype with several Edge of the Network nodes integrated into/onto the textile subsystem.

in latency of the data packets delivery, as well as, in waste of energy due the retransmission attempt and degradation of system reliability are expected to occur.

We included the Router-PROTACTICAL in the proposed solution to, in the future, analyse if multi-hop communication can be exploited as a solution to ensure alternative paths when there is no direct communication between Nodes-PROTACTICAL and Gateway-PROTCTICAL.

4.4.2 Ad Hoc-PROACTICAL

The CPS network connecting the Gateways-PROTACTICAL to the Base Station-PROTACTICAL is an ad-hoc network, designated Ad Hoc-PROTACTICAL, and it is implemented by nodes, designated Forward-PROTACTICAL, distributed at the incident scenario. These nodes are responsible for ensuring a path to transmission of data between Gateways and Base Station-PROTACTICAL, increasing the range of the network when required. The Forward-PROTACTICAL are composed by an Intel Galileo Gen 1 and a Wi-Fi card Intel Centrino Wireless-N135.

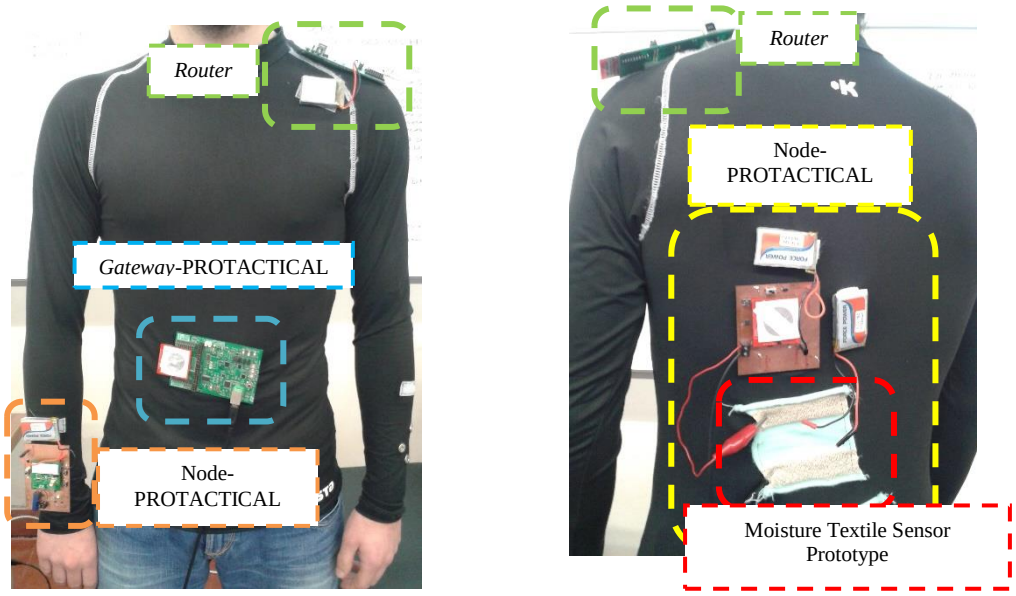

Figure 4.5. Mock-up of the WBAN-PROTACTICAL.

4.4.3 Data Driven Decision Making

Supporting decisions and subsequent decisions in real-time is paramount to ensure user safety, making data-driven decision making an important tool. In this regard, the challenges encountered in PROTACTICAL project are heterogeneity of data sets and uncertainty in modelling real-world phenomena. Regarding heterogeneity of data sets, the data coming from different observation points have different meanings with different levels of spatial and temporal abstractions, as analysed before. Moreover, PROTACTICAL CPS will deal, for the same physical event, with different events triggered over time and space (Sensor Event, Cyber-Physical Event and Cyber Event) and, consequently, different predefined actions are initiated. Therefore, the system must support random and periodic spatial-temporal events. This is ensured through the CPS event model adopted, which allows capturing heterogeneous characteristics of CPS for formal temporal and spatial analysis addressing random and periodic events, as well as, the temporal relationship between them. In addition, as parameters measured from sensors close to human body have complex interrelations, logical operators are used in event model to combine different types of events to capture composite events. Thus, the hierarchical architecture of PROTATICAL CPS (c.f. Figure 4.1) associated to the inclusion of logical operators, allows detection of complex critical events to the emergency response team safety.

In the proposed architecture for PROTACTICAL CPS, different levels of data-driven decision making were implemented. The Gateway-PROTACTICAL was designed to be an event-driven control unit, meaning that, when the CPS network cannot ensure a successful transmission of information between WBAN-PROTACTICAL and Base

Station-PROTACTICAL, the Gateway-PROTACTICAL is able to detect critical situations, support decisions and subsequent command actions, to reduce the time needed to detection, warning and response, thus ensuring the user's safety. The PPE user is notified of an occurrence of a critical event through Node-PROTACTICAL 7.

4.5 Summary

The PROTACTICAL solution concept currently implemented has the potential to significantly contribute to the progress of Smart firefighting and simultaneously provide user comfort and safety. The CPS can improve the decision making at several firefighting operation stages (user, team and fire command centre levels). All this combined makes the PROTACTICAL CPS a unique solution among the state-of-the-art smart PPEs. It adopts the ZigBee and Wi-Fi communication technology for communication Tier-1 and Tier-2, respectively. The communication Tier-3 is not yet implemented.

Taking advantage of the proposed CPS approach, other tools can be developed for a better awareness of the firefighting challenges, as well as, to improve user safety. Examples of such tools are generation of escape routes detection, detection of flashover events, and generation and analysis of biometric parameters.

However, the current implementation have shown some limitations. In the proposed WBAN, only wireless communication is performed while most of the projects proposed for user monitoring applications opt for wires. The preliminary study have shown that the IEEE 802.15.4 compliance nodes application in this regard lost several data packets. Although these nodes operate well in scenarios without any obstruction for several meters, when attached to human body they are not able to meet the Quality-of-Service requirements. Suggesting, that more investigation must be carried out in on-body communications to understand the causes of the data packets loss and how reliability, energy-efficiency, and latency in this communication scenario can be optimized.

CHAPTER 5

ON-BODY CHANNEL CHARACTERIZATION AND MODELLING

Several questions are addressed in this chapter, namely *How does the user activity affect the path-loss and fading on a millisecond-scale? Are the fading and path-loss affected by changing the node position and operation scenario? Are the links (with transmissions at the maximum power allowed) able to ensure the application requirements? Which approaches can be advised to each link in order to optimize communications?*

To answer these questions, a characterization of dynamic narrowband on-body propagation and a wireless communication reliability assessment was carried out. The emitted on-body signals were divided in several terms, which enables the assessment of the effect of several scenarios configuration aspects.

On the next section, an experimental method, the experimental method used to perform a radio channel measurement experiments (section 5.1) is described. The first- (section 5.2) and second-order (section 5.3) statistical results are analysed; a detailed description of radio channel performance analysis in terms of percentage of successful data packet delivered and a link margin evaluation (section 5.4) is made, having as reference the Quality-of-Service requirements imposed by IEEE 802.15.6 TG; and finally, some conclusion and remarks are presented, including general observations inferred from results from previous sections (section 5.5).

5.1 On-Body Time-variant Measurement

The on-body propagation was researched based on the combination of different parameters that enabled to analyse how the different communication operation scenarios affect the radio channel quality in order to ensure reliable transmissions. The configuration used in the time domain was set as following:

- **Wearable Node Configuration:** the WBAN-PROTACTICAL nodes are equipped with the IEEE 802.15.4-compliant CC2531 SoC, which has a maximum receiver sensitivity of -97 dBm, and the application uses a Texas Instruments ZigBee compliant protocol called Z-stack, in order to implement an IEEE 802.15.4 WBAN. Nodes transmit data packets at a maximum transmission power level allowed by on-body communications (0 dBm) to automatically meet the SAR guideline of the

Federal Communications Commission (FCC) [13]. In our case, the selected TPL was -0.5 dBm, since it correspond to the TPL available on the SoC's radio transceiver, close to the maximum allowed;

- **On-Body Nodes Location**: the study was performed in a 28 years old male, 1.69 m high and a weight of 74 kg. The user wore a garment with several Edge of the Network nodes distributed by several body locations. The version of the WBAN-PROTACTICAL used was only composed by two types of nodes, namely 1) the Gateway-PROTACTICAL, taking the role as the data packets receiver, located at the user's waist, and 2) the remaining nodes (Edge of the Network nodes), configured as transmitters, which were distributed across different parts of the garment. Three transmitters were used as an example of each group, in order to categorize the Edge of the Network nodes of the WABN-PROTACTICAL. This approach aims to eliminate redundant information, caused by Edge of the Network nodes from the same group, i.e. Edge of the Network nodes presenting the same type of obstacles to radio channel propagation. As such, the Edge of the Network nodes considered are Node-PROTACTICAL 2 (located at the user's back), Node-PROTATICAL 4 (located at the user's chest), and Node-PROTACTICAL 7 (located at the user's wrist);
- **Network Architecture:** the network architecture was developed in two phases. First, only star-topology were considered in order to identify links that do not satisfy the Quality-of-Service requirement of WBAN applications. However, a relay node was introduces (c.f. Table 4.1) in the WBAN-PROTACTICAL. Therefore, the WBAN can resort to multi-hop topology whenever required in order to ensure communication reliability;
- **Scenarios:** the experimental test bench follows a scenario-based approach, taking into consideration the huge variability of environments that a PPE might operate and the dynamism in terms of movements performed by the user. Thus, measurements were performed in both indoor (a laboratory with an area of 14mx7m filled with office furniture, two large textile industrial machines and with Wi-Fi) and an ordinary room (7mx6m composed by typical furniture); and outdoor urban environment (a street surrounded by buildings). The measurements were performed in controllable environments, in order to ensure that RF external interference did not affect the gathered RSSI sample. Radio channel measurements were performed on four different conditions regarding user's movement and position, namely

standing position (with no movement but the breathing movements, where every radio channel measure were carried out at a different location, e.g. close or far from walls), walking movement (where the user walks on random directions at an average speed of 0.75 m/s), running (randomly, taking many directions at average speed of 1.2 m/s), and crawling (following a straight direction at 0.30 m/s);

- **MAC Configuration:** as the configuration should ensure that the received signal translates the influence of the human body movements, the non-beacon-enabled mode of IEEE 802.15.4 MAC protocol was used. This mode represents the classical CSMA protocol [130], and gives the maximum control over the transmission time, allowing the next higher stack layer to control the transmission time quite accurately (typically on the order of 10 ms). The number of retransmissions and the CCA backoff were configured to zero, to reduce the data packet transmit operation from 10 ms to ≈2.6 ms plus a few milliseconds of CPU processing and processing jitter;
- **Transmission Scheduler:** each experiment for the different scenarios were repeated in three distinct occasions. Each experiment lasted for approximately 12 minutes, corresponding to the transmission of 350 data packets with an interval between transmissions of 35 ms (30 data packets measured per second seems enough to capture the variability of the radio channel behaviour) with a centre frequency at 2.45 GHz. A total of 37800 samples were gathered to evaluate the radio channel features of the Edge of the Network nodes of interest in several scenarios configuration.

5.2 First-Order Statistical Modelling of Received Signal Amplitude

The received signals can be modelled by either considering them as a random variable or decomposing them in several terms. Although the former approach is the most adopted method, the latter one is more useful for time-variant on-body radio channels in order to reach a better understanding of the factors responsible for affecting the radio channel. The Power Transfer Function (PTF), which allows the decomposition of the received signal in three components [25], [119], is expressed as:

$$P(t_n) = G_0 * S(t_n) * F(t_n) \tag{5.1}$$

where G_0 refers to the mean path gain, so-called radio channel gain; $S(t_n)$ refers to the effect of the human body on radio channel, namely the shadowing effect, resulting into large-scale fading, so-called slow fading signal component; and $F(t_n)$ represents the contribution of multi-

path components on received signal, namely the small-scale fading, so-called fast fading signal component.

5.2.1 Mean Radio channel Gain Model for Different Scenarios

The radio channel gain is computed as the mean of the received power signal that results for each scenario, i.e. nodes locations, activity, and environment of operation. From the results, the log-normal distribution was the one that describes G_0 in a more appropriate way. Therefore, the radio channel gain expressed in dB (negative values indicate the power path loss of the transmitted signal) can be represented by a Gaussian random variable:

$$G_0 \sim N(\mu_s,\ \sigma_s) \tag{5.2}$$

where mean value (μ_s) and standard deviation (σ_s) are scenario-dependent. The statistical analysis was performed on the radio channel gain of different scenarios. The results obtained for different operation environments, node locations, and user activities (Table 5.1), enabled the following observations:

- The path-loss (μ_s) is higher and its dispersion ($_{\sigma_{0_s}}$) is larger in outdoor environments, regardless of the activity and node location. This is due to the fact that the electromagnetic waves propagation occurs mainly by creeping waves[2], Line of Sight (LOS), and small reflections from ground, whereas when at indoor environments lower path-loss are verified;
- Indoor communications are more prone to multi-path components, which have an additional energy contribution [119]. This is particularly perceived when the communication radio channel is in shadowing, e.g. Node-PROTACTICAL 2, for which there is not line of sight between this node and the Gateway-PROTACTICAL. Gains are near of 10 dB for indoor environments;
- Although path-loss (μ_{0_s}) was expected to be higher inside of the room than in the laboratory environment as previously observed (lab environment is more prone to the presence of multi-path components), the hypothesis could not be verified in all test scenarios. The radio channel gain was always lower in laboratory if the user was

[2] EM waves, which are copies of the original EM wave resulting of the diffraction phenomenon, propagating along or around the user's body

standing, regardless of the Node-PROTACTICAL. However, when the user is walking or running, the radio channel gain was be lower for the room scenario;

- Activities that generically lead to worsts path-loss and dispersion are when the user is running and walking, with small differences between them when performed in indoor environments. The lowest path-loss is verified when the user is in a standing position (high multi-path component contribution) and when the user is crawling. In outdoor environments the standing activity presented the worst results in terms of radio channel gains, when compared to user walking and running, since the

Table 5.1. The 95% confidence interval of the mean ($\boldsymbol{\mu_{0_S}}$) and standard deviation ($\boldsymbol{\sigma_{0_S}}$) of the radio channel gain, and the standard deviation of the large-scale fading ($\boldsymbol{\sigma_{s_S}}$).

Movement	**Node**	$\boldsymbol{\mu_{0_S}(dB)}$	$\boldsymbol{\sigma_{0_S}(dB)}$	$\boldsymbol{\sigma_{s_S}(dB)}$
Laboratory				
Standing	2	[-73.4;-75.3]	[0.3;1.8]	[0.2;1.4]
	4	[-52.0;-52.6]	[0.4;2.2]	[0.3;1.8]
	7	[-65.1;-73.1]	[1.3;8.1]	[1.1;7.6]
Walking	2	[-81.8;-82.9]	[2.5;15.8]	[0.5;3.3]
	4	[-52.2;-54.8]	[0.7;4.3]	[0.4;2.7]
	7	[-75.2;-76.6]	[4.7;29.4]	[2.7;17]
Running	2	[-80.9;-81.4]	[3.1;19.4]	[0.8;5.1]
	4	[-55.4;-56.2]	[0.7;2.2]	[0.2;1.1]
	7	[-74.8;-78.3]	[4.73;29.86]	[1.8;11.2]
Crawling	2	[-78.3;-79.7]	[3.75;23.63]	[1.9;11]
	4	[-47.7;-51.2]	[2.7;17.1]	[1.1;6.7]
	7	[-62.2;-64.4]	[3.84;24.24]	[1.8;11.6]
Room				
Standing	2	[-75.7;-78.6]	[0.3;1.6]	[0.2;1.1]
	4	[-53.9;-58.1]	[0.1;0.5]	[0.1;0.5]
	7	[-67.6;-69.5]	[0.3;1.9]	[0.23;1.5]
Walking	2	[-83.5;-84.3]	[1.8;11.3]	[0.4;2.5]
	4	[-49.8;-50.7]	[0.2;1.4]	[0.1;0.81]
	7	[-72.0;-72.5]	[3.6;22.5]	[1.1;7]
Running	2	[-82.6;-84.4]	[2.2;14.1]	[0.4;2.8]
	4	[-50.39;-50.98]	[2.5;16.1]	[0.2;1.1]
	7	[-72.8;-73.1]	[4.3;27.1]	[1.1;6]
Crawling	2	[-82.1;-82.8]	[2.71;17.10]	[1;6.3]
	4	[-48.8;-53.5]	[4.4;27.5]	[3.0;19]
	7	[-64.1;-66.3]	[3.2;20.3]	[1.7;10.8]
Outdoor				
Standing	2	[-88.7;-89.2]	[0.41;2.6]	[0.5;2.5]
	4	[-55.9;-56.3]	[0.04;0.3]	[0.02;0.1]
	7	[-81.3;-83.8]	[0.8;5.3]	[0.8;5]
Walking	2	[-86.9;-88.3]	[1.4;8.8]	[0.3;2.1]
	4	[-55.6;-57.1]	[0.64;4.1]	[0.4;2.6]
	7	[-78.0;-80.1]	[5.3;33.3]	[3;18]
Running	2	[-85.1;-88.9]	[1.6;10.3]	[0.3;2]
	4	[-55.9;-57.9]	[1.2;7.6]	[0.2;1.2]
	7	[-75.4;-77.3]	[6.7;42.0]	[2.6;16]
Crawling	2	[-83.6;-84.6]	[1.3;8.4]	[0.5;3.1]
	4	[-52.3;-54.5]	[4.0;25.2]	[1.9;12]
	7	[-60.5-65.5]	[3.7;23.4]	[2.4;15]

multi-path components contribution is lower, thus increasing the resultant path-loss in case of NLOS. The crawling activity presents the best radio channel gain values, since reflections from the ground are the main energy contribution for the signal received by the Gateway-PROTACTICAL (it is not applied to Node-PROTACTICAL 2, since it is located at the user's back). This was observed for all type of scenarios;

- The dispersion (σ_{0_S}) in Node-PROTACTICAL 4 and in Node-PROTACTICAL 2 is very low when the user is in a standing position. Since in both cases the main propagation component contribution comes from creeping waves (low energy contribution). However, when dynamic activities are considered, the dispersion of the Node-PROTACTICAL 2 is very high whereas the Node-PROTACTICAL 4 always has very low dispersions. This is an indication that the node at the user's chest is less susceptive to path-loss variations then the Node-PROTATICAL 2 for dynamic scenarios. This fact can be justified because when the user is standing, contributions (both creeping and multi-path waves) to radio channel of Node-PROTACTICAL 2 are consistent, whereas if user movements are considered, his limbs are continuously obstructing the wave's path;
- The Node-PROTACTICAL 4 is the one that has the lowest path-loss for all activities and environments, being consistent for all cases since radio channel gain is always near to -50 dB. This can be justified by the fact that propagation occurs mainly due to creeping waves and "on-air" propagation also occurs with small distance between nodes, being less susceptive to changes in path-loss due to the dynamic activities, since there is no obstructions imposed by limbs to the wave's path. In such cases, the body shape and the body features (dielectric and permeability properties of the body tissue) may have a predominant influence on the signal attenuation [127], [133];
- The Node-PROTACTICAL 2 presents the worst path-loss for all the scenarios because it is always in NLOS and, thus, propagation occurs mainly by creeping waves. The situation is worst when the user performs movements due to obstruction created by the user's limbs, introducing dynamic shadowing. Dispersion of link Node-PROTACTICAL 2 is considerably higher at indoor environments than when at outdoors, indicating that at outdoor scenarios the presence of multi-path components due to environment influence might be negligible;

- The path-lost confidence interval range of Node-PROTACTICAL 7 is higher when the user is standing, since propagation occurs mainly by creeping and multi-path waves. However, this range is lower when user movement is taken into consideration. This is due to the fact that during most of the time there is line of sight between the Node-PROTACTICAL 7 and the Gateway-PROTACTICAL.

5.2.2 Slow Fading Model for Several Scenarios

In order to statistically analyse the slow fading signal component, a low pass filter that calculates the average of the received signal was applied in order to extract the slow component from the empirical measurements. Therefore, the sliding temporal window length was determined so as the variations were smoothed out while the variations on the received signal are still present due to user movement. The window size was selected to be 350 ms, corresponding to a number of samples, w, of 10:

$$S(t_n) \approx \frac{1}{w} * \sum_{n-w/2}^{n+w/2} \frac{P(t_n)}{G_0} \tag{5.3}$$

Figure 5.1 depicts the power transfer function of a received signal (raw data) and the same signal but without the influence of the surrounding environment (small-scale fading), i.e. the $G_0 * S(t_n)$ components of the power transfer function of equation (5.1). It allows the identification of the influence of both types of fading. The slow component in the measured signal results from the shadowing phenomenon created by user movements. It is noticeable that in the absence of movement the slow component is moderated, as shadowing conditions still exists but remain constant. Moreover, its magnitude strictly depends on the way that the user moves and its path trajectory (LOS or NLOS), for instance the slow component in Node-PROTACTICAL 7 is larger when the user is walking or running.

This subsection aims to determine the most reliable statistical model in order to analyse the received signal amplitude distribution over the different scenarios. To reach this goal, six distributions were considered to fit the received signal power, which are the distributions often considered during radio channel characterization and modelling, namely Normal, Log-normal, Gamma, Rayleigh, Nakagami-m, and Weibull distribution [13].

First, all the measurements were normalized and the statistical analyses on the slow component was carried out. All distribution parameters for each scenario were obtained using the maximum likelihood estimation (MLE).

The best fitting distribution was selected based on the Akaike Information Criterion (AIC), a widely adopted technique to determine the best fitting distribution in both narrowband and wideband communications [13]. The distribution that is the best fit model for each scenario, according to the AIC, is given in Table 5.2, where column ΔAIC_c reflects the difference between the AIC of the best fitting distribution and the AIC of the Log-normal distribution, and can be used to determine if this distribution is a good alternative distribution. As claimed in [62], a ΔAIC_c lower than 10 indicates the existence of a better suited alternate distribution.

The statistical analysis on the slow component of expression (5.1) show that the majority of the scenarios are well modelled by the log-normal distribution. This is due to the fact that there is a large number of effects contributing to the attenuation of the signal transmitted, which are multiplicative, or equivalently additive in the log domain. According to the central limit theorem a large number of random multiplicative effects will converge to a normal distribution in the log domain [62].

The distributions Weibull and Normal are good candidates since, accordingly to the research works [13], [62], [123], the Weibull distribution often provides a reasonable fit for scenarios where radio channel is subject to high levels of fading due to the human body, while

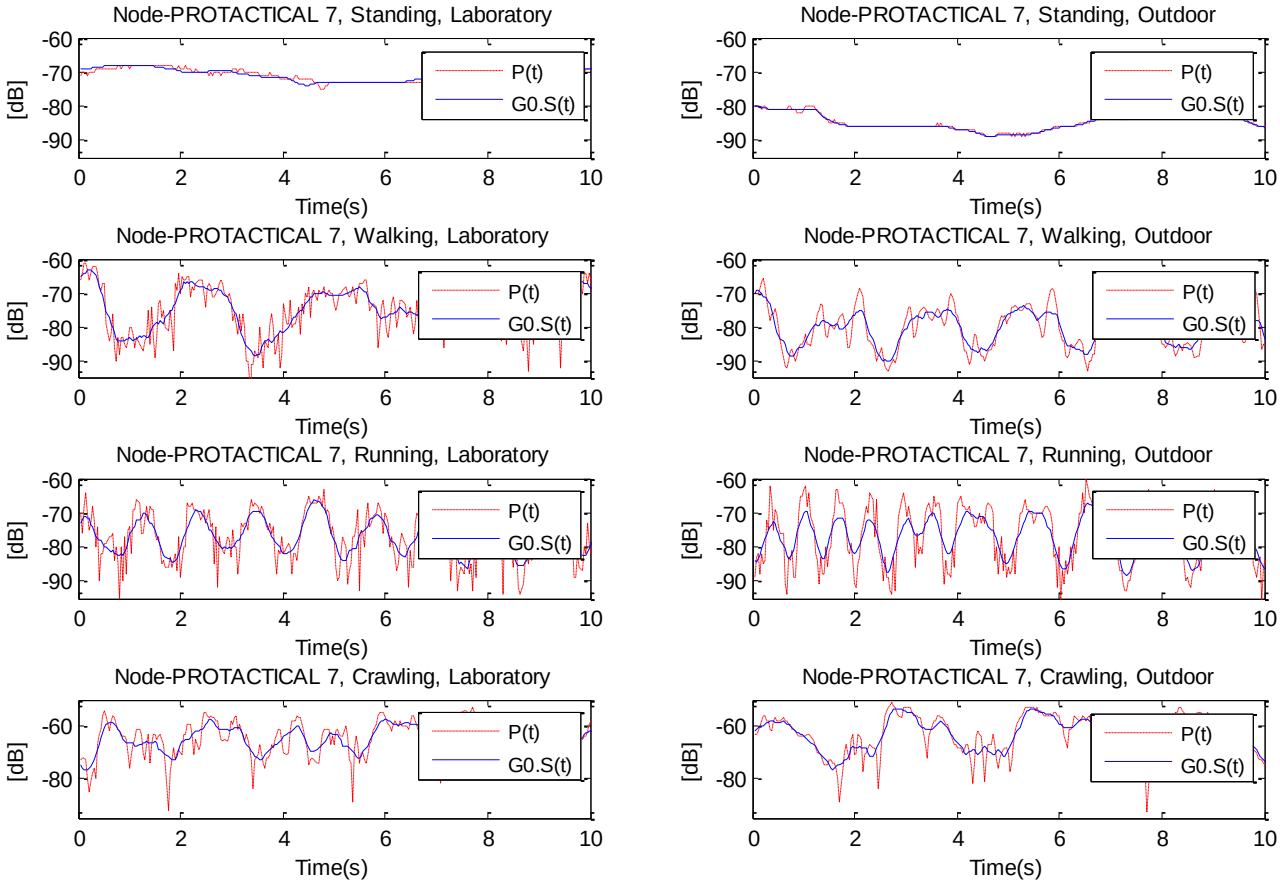

Figure 5.1. Time-variant power transfer function and shadowing component in indoor (laboratory) and outdoor environment for Node-PROTACTICAL 7.

Table 5.2. Best-fitting models for slow fading signal component in several scenarios.

Movement	Node	Best Distribution	ΔAIC_C
Laboratory			
Standing	2	Normal (σ=1.436; μ=-0.0532)	3.6
	4	Log-normal	--
	7	Log-normal	--
Walking	2	Normal (σ=2.011; μ=-0.0429)	6.5
	4	Log-normal	--
	7	Log-normal	--
Running	2	Normal (σ=2.672; μ=-0.0072)	2.4
	4	Normal (σ=1.257; μ=-0.057)	1.8
	7	Log-normal	--
Crawling	2	Weibull (α=25.739;β=83.25)	85.3
	4	Log-normal	--
	7	Gamma (α=283.65;β=3.709)	1.12
Room			
Standing	2	Log-normal	--
	4	Log-normal	--
	7	Weibull (α=64.11;β=70.076)	20.4
Walking	2	Log-normal	--
	4	Weibull (α=64.644;β=50.49)	30.28
	7	Weibull (α=24.25;β=73.975)	9.7
Running	2	Log-normal	--
	4	Normal(σ=1.28; μ=-0.0067)	5.6
	7	Log-normal	--
Crawling	2	Weibull (α=26.486;β=84.47)	9.2
	4	Normal (σ=6.1718; μ=-0.051)	9.7
	7	Log-normal	--
Outdoor			
Standing	2	Log-normal	--
	4	Log-normal	--
	7	Log-normal	--
Walking	2	Log-normal	--
	4	Weibull (α=63.2;β=89.096)	65
	7	Log-normal	--
Running	2	Log-normal	--
	4	Weibull (α=46.23;β=86.7)	37
	7	Log-normal	--
Crawling	2	Log-normal	--
	4	Normal (σ=2.28; μ=0.055)	5.7
	7	Log-normal	--

the Normal distribution seems a suitable statistical distribution to model shadowing effect on on-body communications in scenarios where the user is standing.

Summarizing, the slow fading signal component can be well described as a Gaussian random variable:

$$S(t_n) \sim N(0,\ \sigma_{s_s}) \tag{5.4}$$

where the standard deviation σ_{s_s} refers to the slow variations of the PDF due to the shadowing from human body, in a specific scenario. The σ_{s_s} resultant of empirical experiments in each scenario considered are shown in Table 5.1 and lead to the following observations:

- Larges dispersions occur when user is performing dynamic activities, being larger if the user is walking, indicating that user movement is responsible for the shadowing effect on the radio channel. Although the running activity is the most dynamic activity, the oscillations of the arms are more limited than the case when the user is walking because arms tend to be close to the body, whereas when user is stationary, the presence of a slow component in the received signal is the result of involuntary movements.
- The standard deviation is larger when at outdoor environments due to the almost nonexistence of multi-path components.
- Node-PROTACTICAL 2 has a larger variance when comparing with Node-PROTACTICAL 4 due to the obstruction of the LOS, especially in room and outdoor environments where multi-path propagation is limited. The Node-PROTACTICAL 7 is the one that presents the larger variance due to its location, since it is located at an extremely dynamic part of the user body, leading the electromagnetic waves propagation conditions to continuously commuting the radio channel communication conditions between LOS and NLOS.

According to D'Errico and Ouvry, the radio channel gain has a slow variation around the mean value (μ_{0_S}) that can be described by the total variance: ${\sigma_{T_S}}^2 = {\sigma_{0_S}}^2 + {\sigma_{s_S}}^2$ [119].

5.2.3 Fast Fading signal component Model for Different Scenarios

The fast fading signal component, which is depicted in Figure 5.1 and Figure 5.2, refers to the fast signal variations in a short period of time, but with lower amplitude variation than the slow fading signal component. However, as will be demonstrate on the next section, the influence of the fast fading signal component in data packets transmission must not be ignored. The measurements of the fast fading signal component, which are computed as the signal fluctuation around the slow fading signal component, show that the fast fading signal component can last for significant periods of times (i.e. average time below the slow fading signal component) and can reach relative high amplitudes. In particular, for Node-PROTACTICAL 7 when tested at the laboratory while the user is walking, the radio channel measurements of the fast fading signal component has a maximum amplitude of -13 dB, an average amplitude of -3.3 dB, and an average fast fading signal component duration of 71 ms (period of time required to transmit two data packets). As expected, due to the presence of a LOS wave and multi-path components [25], [119], the Rice distribution is the best fit to the fast fading signal component measurement data.

Table 5.3 shows the values of the Rice K-factor of the Rice distribution for different scenarios. This parameter is defined as the ratio between the power in LOS component and the power in multi-path components [25]. Therefore, a high K-factor values indicate a high ratio of the LOS wave component over the multi-path component [119]. The K-factor values in Table 5.3 led to the same observations presented in [119]. As expected, reported K-factor are generally higher when the user is standing, as the small-scale fading is lower. In contrast, radio channels are more unstable (a larger fading is expected) when the user performs movements, as the body obstructs the wave path the propagation occurs manly by creeping waves and reflections on the surrounding environment. In fact, the highest K-factors generally occur when the user is running due to the increasing of the energy diffracted or scattered from the user's body. Moreover, regardless of the Node-PROTACTICAL/location, the K-factor is slightly lower at indoor environments, since the energy contribution of the multi-path components increases and, in some cases, results in a more important contribution than the LOS waves. The Node-PROTACTICAL 2 is the one that presents the lowest K-factor, indicating the absence of LOS wave components. The Node-PROTACTICAL 7 is the node with higher dynamics, thus the resulting K-factor values show how its communication link is affected by the fast fading signal component. The Node-PROTACTIAL 4, due to the high K-factor values obtained, is

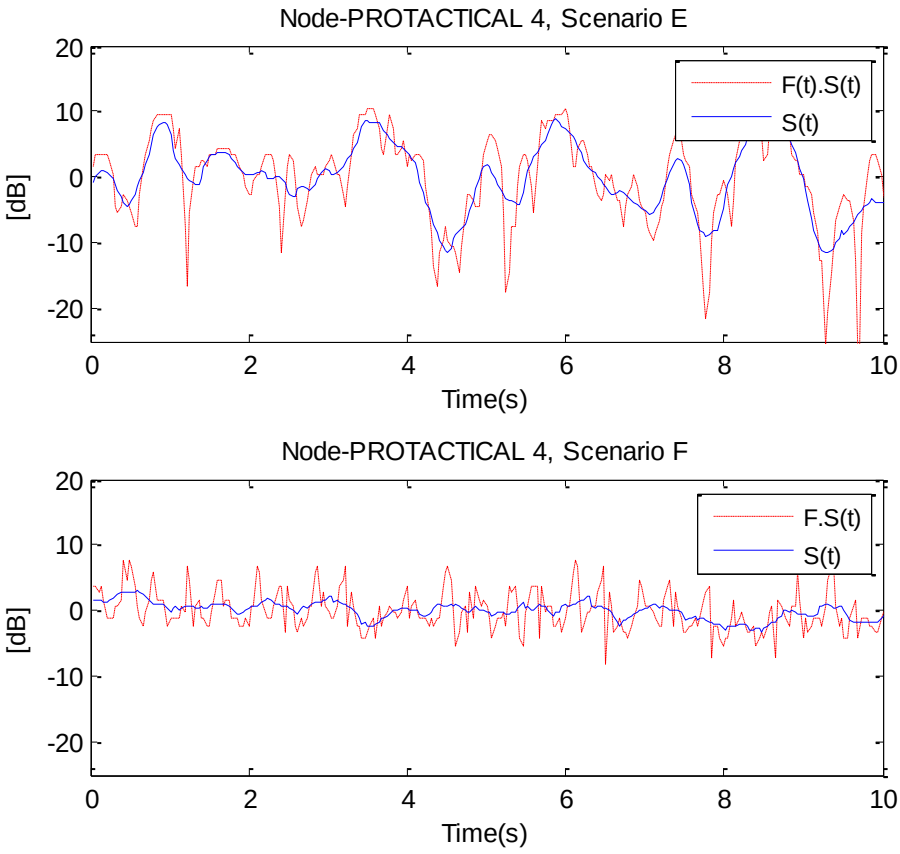

Figure 5.2. Temporal variations in the normalized signal emitted by Node-PROTACTICAL 4.

subjected to a strong LOS wave's energy contribution, which results in a stable radio channel, i.e. radio channel experiments a small fast fading signal component.

5.3 Dynamic Narrowband On-Body Radio channel: Time-Dependent Characteristics

The second order statistics, a statistical analysis of the time dependencies fading features and Doppler spread of the radio channel, are presented in this section. The comprehension of how the signal behaves with time is an essential tool not only to determine the best node location (as previously stated some locations are prone to poor radio channel conditions), the required topology in order to meet the QoS requirements (identification of the optimal location for potential relays) [25] and to evaluate the mobile radio system performance, but also on assisting the development of transmission mechanisms aiming to improve the radio channel throughput. Some example are the design of error correcting codes [127], radio channel behaviour prediction algorithms [128], TPC mechanisms [129], data packets retransmission strategies [26], data packets scheduler mechanism [130], interleaving algorithm, error-protection coding scheme, scaling the size of data packets to be emitted and radio channel modelling [59].

In this section a statistical analysis of the dynamic properties of the propagation radio channels of Node-PROTACTICAL 2, 4, and 7 is described. Only dynamic scenarios at the laboratory were considered in this analysis and they are identified by the letters A, B, and C, corresponding to the activities walking, crawling, and running, respectively; and outdoor scenarios D, E and F, correspond to the activities walking, crawling and running. To all the empirical measures gathered during the experimental test bench, the respective radio channel gains were removed (as exemplified in Figure 5.2). This approach allowed to analyse the dynamic properties of the radio channels, i.e. fading, without ignoring the influence of the small-scale fading contribution on the received power signal.

Table 5.3. Fast fading signal component statistics (K-factor) at several scenarios.

Movement	**Node**	**Laboratory**	**Room**	**Outdoor**
Standing	2	13.3	14.2	21.2
	4	102.2	105.9	114.1
	7	45.0	48	51.4
Walking	2	2.8	3.1	3.4
	4	45.1	45.3	48.1
	7	3.8	5.6	7.4
Running	2	1.2	2.0	2.7
	4	36.1	38.8	42.2
	7	2.1	2.5	4.7
Crawling	2	3.8	4.1	6.2
	4	9.3	10.5	17.7
	7	4.6	5.2	6.7

Several statistical parameters have been adopted to describe the fluctuation of the received signal over time, such as: Fading Rate, Fading Duration, Fading Magnitude, Doppler spread, and TC. Second-order techniques, such as Level Crossing Rate and Average Fade Duration, are used to extract the mentioned second-order parameters from the data gathered in the experimental test bench.

5.3.1 Fading Rate and Coherence Time

The Level Crossing Rate (LCR) is the frequency at which the signal crosses into fade, i.e. crosses a reference threshold relatively to the mean value (goes below the threshold). The average LCR of each Edge of the Network node for each scenario is graphically illustrated in Figure 5.3. The maximum LCR for all cases is always near of the mean value, a few dBs below 0 dB. Moreover, the measured values, when the mean value is considered as the threshold value, are lower but very similar to the maximum LCR observed. Furthermore, all radio channels, regardless of the scenario, are subjected to almost the same LCR value. This is only not the case when larger link margins are considered.

The fading rate, when considered the mean value as the threshold, can be used to estimate the Doppler spread, as proposed in [62]. Thus, a value between 2 and 4 Hz to average the Doppler spread was adopted for all nodes on the majority of the scenarios. The unique exception

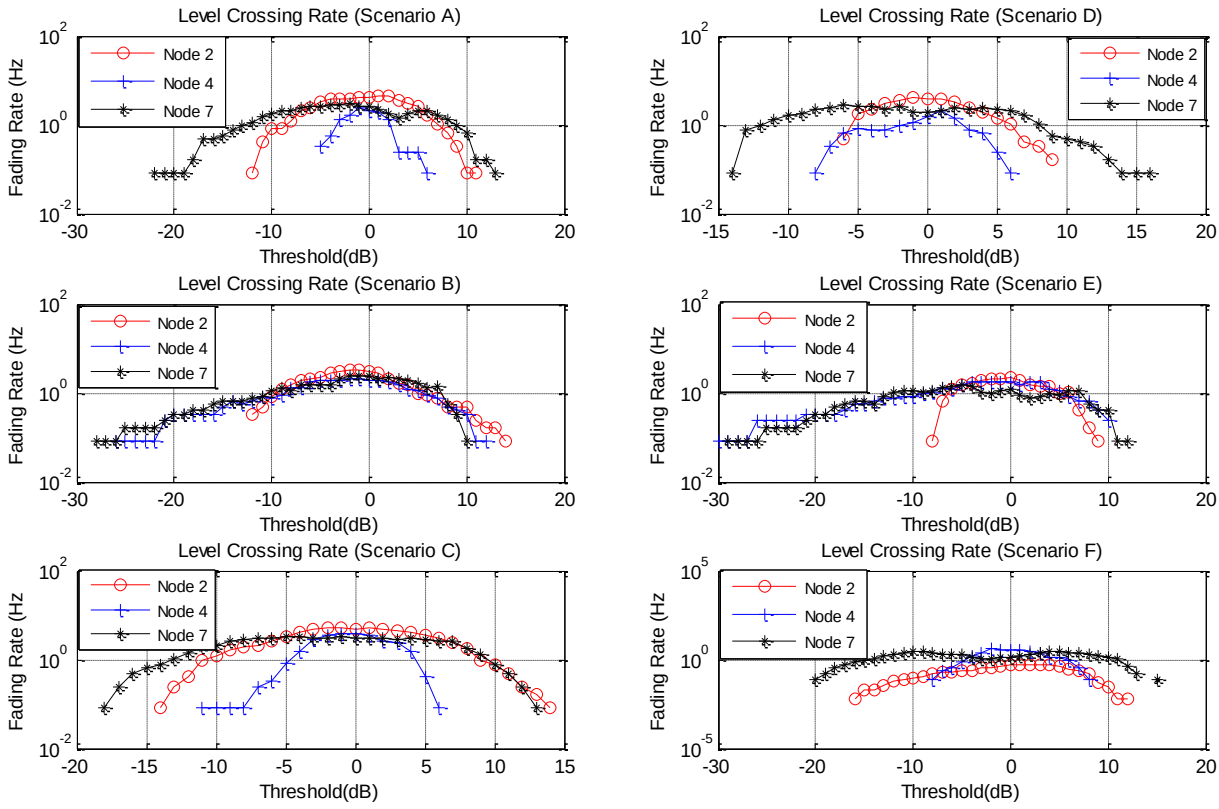

Figure 5.3. LCR of links Node-PROTACTICAL 2, 4, and 7 in different scenarios

might happen when the user is running in an outdoor scenario, since the influence of the multi-path is negligible due to the lack of reflecting objects. In this case, the worst LCR (<1 Hz) belongs to Node-PROTACTICAL 2 which is not so influenced for multi-path waves reflected from the ground as Nodes-PROTACTICAL 4 and 7. The LCR results shows that there is a strong correlation between the movement and the LCR values. As observed before, the fading amplitude seems to be higher when the user is running, leading to signal fading for higher link margins, for example, the average LCR of Node-PROTACTICAL 7 in scenario D at threshold -18 dB is 0 Hz (only after -14 dB the signal crosses into fade) whereas in scenario E a LCR near 0.5 Hz is observed. Adopting the approach usually embraced in the literature, a threshold of -10 dB is selected to deduce the fading depth of radio channels on the several scenarios [62], [119].

The average fading rate values by scenario are summarized in Table 5.4. As expected, the Node-PROTACTICAL 7 presents higher fading rates in all scenarios, whereas the Node-PROTACTICAL 2 has higher fading rates than the remaining motionless nodes, in activities performed at indoor environments since the received signal path is always obstructed, resulting into contribution of several phenomenon, namely creeping and multi-path waves. However, when at outdoor environments the radio channel Node-PROTACTICAL 4 presents a higher LCR value than Node-PROTACTICAL 2, this can be explained by the fact that this node is more affected by the movement, which leads to changes in distance and orientation between nodes. The LCR values are below 2 Hz for all scenarios (sometimes equal to zero), whereas Node-PROTACTICAL 7 has always fading rates lower than 3 Hz.

According to the coherence time values shown in Table 5.4, it is clear that the radio channels operating at outdoors remain stable for longer periods. The coherence time is the time duration over which the received signal strength is essentially invariant. Coherence times for the Node-PROTACTICAL 2 from 35 ms to 57 ms at indoors and from 41 ms to 78 ms at outdoors were reported. The radio channel of the Node-PROTACTICAL 4 stays constant up to a maximum of 96 ms and 121 ms at indoors and at outdoors, respectively. Coherence time values from 60 ms to 75 ms and from 96 ms to 145 ms were reported for the Node-PROTACTICAL 7 at indoors and outdoors, respectively.

5.3.2 Fading Period and Percentage of Poor Radio channel Quality Period

Fade duration is the time interval that a received signal remains in fading (below a reference threshold, usually -10 dB), whereas the Average Fade Duration (AFD) is described as the ratio between the total of duration that a received signal drops below a reference threshold and the

number of fading events. This parameter is used to determine the likely number of bits that might be lost due to the fading phenomenon, i.e. the average fading period. The radio channel is considered poor when fading is below a reference threshold. In Table 5.4 the values for maximum fading duration, minimum fading duration, AFD and standard deviation (to evaluate the dispersions of this statistical parameter) are presented for a threshold of -10 dB.

As expected the Node-PROTACTICAL 7 presents the highest AFD values in all scenarios analysed. The highest AFDs values occur for outdoors's scenarios, such is the cases of scenarios D, E, and F. In running activity, scenario F, the radio channel Node-PROTACTICAL 7 is subjected to the highest maximum fading duration, 385 ms, whereas the highest average AFD was obtained on scenario E, 155 ms. Therefore, for periodic actions, regardless of the environment, it is expected that radio channel Node-PROTACTICAL 7 will be subject to AFDs higher than 56 ms, The remaining Edge of the Network nodes presented lower AFDs values and fading durations, as expected.

Figure 5.4 depicts the cumulative distribution function (CDF) of the fading duration behaviour in radio channel Node-PROTACTICAL 7. It is observable that the fading duration, or poor radio channel quality (CDF of 0.9), is below 175 ms for scenarios A, B, and F. The fading duration does not exceed 450 ms. For scenario C the duration is less than 90 ms and does not exceed 140 ms. The fading duration is below 80 ms on scenario D without exceeding 175

Table 5.4. Fading features and Coherence Time for links Node-PROTACTICAL 2, 4 and 7 in several scenarios. Results obtained for a threshold of -10 dB.

Scenario	**Node**	**LCR (Hz)**	**AFD (s)**	**Max. Fade Duration (s)**	**Min. Fade Duration (s)**	**STD**	**Percent. of Poor Channel Period (%)**	**Average Fade Depth (dB)**	**TC (ms)**
A	2	1.22	0.035	0.035	0.035	0	4.2	-12.96	43.1
	4	0	0	0	0	0	0	0	84.5
	7	2.15	0.078	0.315	0.035	0.168	7.1	-14.4	69.9
B	2	1.47	0.047	0.105	0.035	0.012	6.8	-12.6	57.6
	4	1.31	0.057	0.14	0.035	0.030	7.4	-10.2	95.2
	7	1.146	0.105	0.455	0.035	0.035	12	-26.03	74.6
C	2	1.88	0.043	0.105	0.035	0.04	8	-13.2	35.8
	4	0.081	0.035	0.035	0.035	0	6.8	-11.2	47.6
	7	2.78	0.056	0.14	0.035	0.030	15	-18.3	59.6
D	2	0	0	0	0	0	0	0	47.11
	4	0	0	0	0	0	0	0	121.8
	7	2.29	0.056	0.175	0.035	0.033	12.8	-19.8	95.2
E	2	0.081	0.035	0.035	0.035	0	0.3	-10.3	78.1
	4	1.07	0.108	0.245	0.035	0.137	11.4	-20	104.7
	7	1.146	0.155	0.042	0.035	0.419	17.7	-25.6	145.6
F	2	0.90	0.040	0.105	0.035	0.012	3.7	-10.5	40.5
	4	0	0	0	0	0	0	0	49.7
	7	2.54	0.092	0.385	0.035	0.177	23	-20.2	137.7

ms. For scenario E the value of the fading duration is less than 320 ms the fading duration value never exceeds 420 ms. The standard deviations remains zero (or very close to zero) for motionless Edge of the Network nodes, i.e., Nodes-PROTACTICAL 2 and 4, whereas the radio channel of Node-PROTACTICAL 7 presents the highest fading duration dispersion for outdoor environments. These fading duration values shows demonstrate that there is correlation between the fading duration and the type of user's movement activity, speed and the environment at which the activity is executed.

Table 5.4 includes information about the parameter percentage of poor radio channel quality period given in percentage. This parameter is defined as the percentage of time that the received radio signal remains below a reference threshold (in such situation the radio channel conditions are considered poor). Once again, the value -10 dB is set as reference threshold. The worst results obtained occurred at outdoor environments, where the presence of the large-scale fading is high. Non-surprisingly, the worst results, in terms of percentage of poor radio channel quality period, where obtained during the running activity with poor radio quality periods of 15% and 25% at laboratory and outdoor scenarios, respectively.

5.3.3 Fading Magnitude

Fading magnitude refers to the maximum fade depth, with respect to the mean value, verified during the period of any fade. Table 5.4 shows the parameter maximum fading period for each scenario investigated for a threshold of -10 dB. The Node-PROTACTICAL 7 is the radio channel that is subjected to the maximum fading depth values and, as expected, it is worst when the user is performing activities at outdoor environments due to the shadowing effect mitigation due to presence of several electromagnetic waves propagation (differences in range of -2 dB up to -5 dB). In fact, the results shows a trend to the radio channel

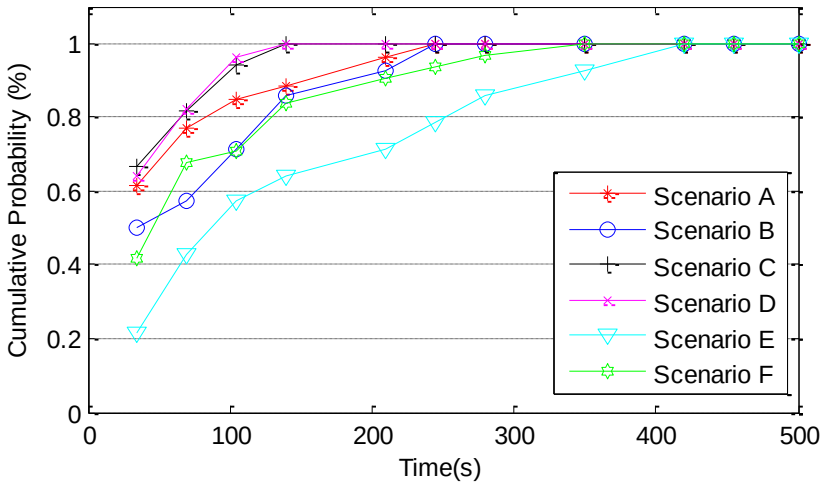

Figure 5.4. CDF for fading period in Node-PROTATICAL 7.

Node-PROTACTICAL 7 in all activities and all environments shows high average fading magnitudes, always higher than -18 dB. The majority of the fading magnitude (90% of the occurrences of fading) occurred in radio channel Node-PROTACTICAL 7 with a threshold value of -10 dB. For this Node, values of -22.3 dB, -28.46 dB, -18.5 dB, -14.7 dB, -29.18 dB and -18 dB were obtained for scenarios A to F, respectively.

Motionless nodes also presents some deep fading magnitudes, however, this values must be relativized, since in the majority of the cases the fading only occurs rarely (a couple of times), as indicated by parameter LCR, indicating that the majority of the time this radio channels cannot be considered poor radio channels in terms of propagation conditions, and when in fading (which is very unlikely for all activities in all environments, with the unique exception of crawling) the fading magnitude is only a bit lower than the reference threshold. Summarising, these statistical parameters provide a valuable information about the temporal characteristics of the Node's radio channels for the several scenarios.

5.4 Performance Analysis based on Radio channel Dynamics

This section aims to evaluate the performance of the current system in terms of the Quality-of-Service (QoS) requirements such as reliability and latency values.

5.4.1 Packet Error Rate Analysis

The PER metric indicates the percentage of data packets that were not successfully deliver to the Coordinator node, the Gateway-PROTACTICAL.

Figure 5.5 illustrates the radio channel performance in terms of PER values for all the scenarios, showing that radio channels Node-PROTATICAL 4 and 7 are able to ensure that requirements imposed by IEEE 802.15.6 TG in terms of reliability (PER<10%), regardless of the scenario conditions. Maximum PER values obtained have occurred for scenario F (6%) and scenario B (1%) on Nodes-PROTACTICAL 7 and 4, respectively. These radio channels are also able to ensure the latency requirements, since, as shown in Figure 5.5, the radio channel is in outage for periods lower than 125 ms and 250 ms (the maximums latencies to medical and non-medical applications).

The node with the worst results is Node-PROTACTICAL 2, the worst values are obtained for scenarios D and F, with PERs values higher than 10%. This downside on operation of this radio channels is due to the lack of the multi-path waves and due to their location, due to obstructions created by human body, blocking the electromagnetic waves propagation. The Node-PROTACTICAL 2 is not able to ensure the WBAN application requirements in terms of reliability. Thus, it is suggested the use of a multi-hop topology to overcome the limitations

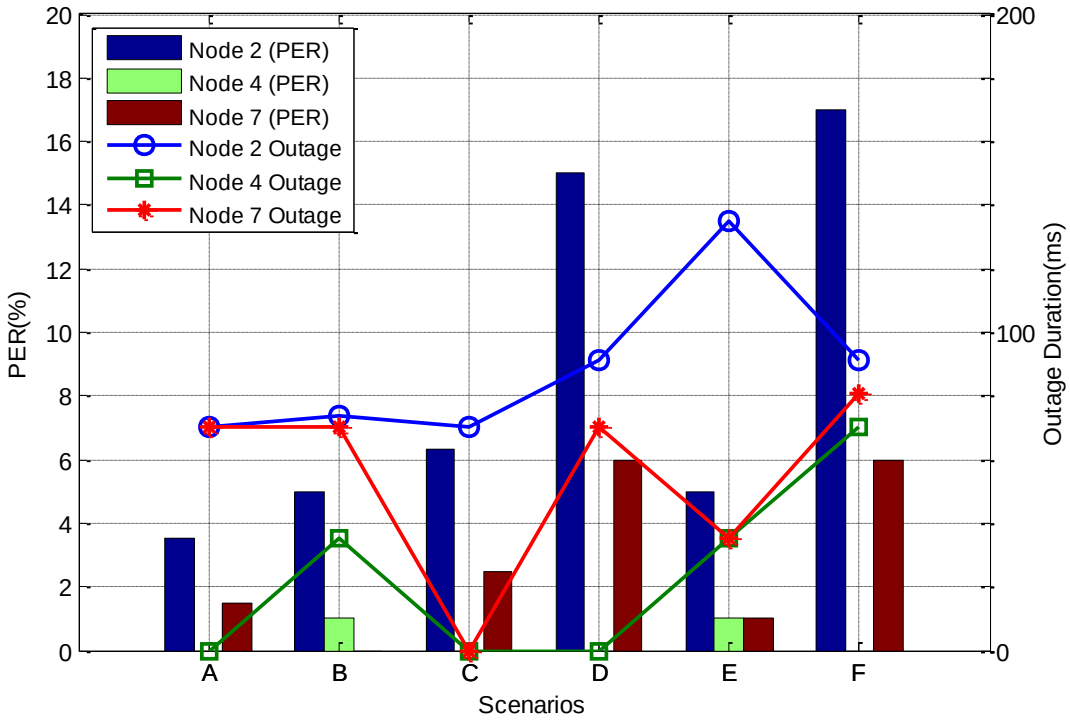

Figure 5.5. Percentage of the number of data packets transmitted that do not reached the Gateway-PROTACTICAL and average outage duration.

obtained for a star topology, being the WBAN responsible for commuting between multi-hop and star topology depending on radio channel conditions. However, Node-PROTACTICAL 2 achives satisfactory results in terms of latency, as the latency requirements of non-medical applications are respected for all the scenarios tested. Only in scenario E the Node-PROTACICAL 2 presents an average outage period higher than the maximum required for medical applications (135 ms as depicted in Figure 5.5).

5.4.2 Link Margin Analysis

In the previous subsection the radio channel is evaluated assuming that either the radio transceiver sensitivity or the TPL (Transmission Power Level) are static. Although this is verified in the measurement test bench described in the previous section, it is clear that another system may have different radio transceiver sensitivities and/or output transmission power. In fact, these parameters can be updated to reach an optimal radio channel performance in terms of both PER and latency values. It is especially relevant when applied protocols such as TPC (Transmission Power Control), which aims to maximize the energy efficiency of transmissions by adjusting the TPL at run-time and accordingly to the radio channel conditions [46]. The TPL is adjusted to the lowest level that ensure the successful delivery of the data packets, with minimum side effects on other aspects of the performance [4], such as latency and reliability. Thus, in this subsection a radio channel performance assessment with respect to a Link Margin

(LM) gain is proposed. It is based on the research work presented by Smith et al. in [155], but with significant differences. The Link Margin at t_n is here quantified in dBs and is given by following expression:

$$LM(t_n) = TPL_{Gain}(t_n) + Sys_{Loss}(t_n) - Rx_{sensitivity} \quad (5.5)$$

where $TPL_{Gain}(t_n)$ represents the gain (in dB) achieved, at round t_n when a different TPL is used. This gain is relatively to transmissions at the maximum allowed TPL, i.e. difference of radio channel gain of new transmission at updated TPL and radio channel gain reference (TPL equal to -0.5 dBm), c.f. Table 5.1. Higher and lower TPL transmissions result in lower and higher radio channel gain values [48]. In the proposed test bench the TPL adopted for radio channel operation is a static and pre-defined value (-0.5 dBm), thus $TPL_{Gain}(t_n)$ is zero. The $Sys_{Loss}(t_n)$ refers to the system losses, or in other words, the power transfer function $P(t_n)$, whereas $Rx_{Sensitivity}$ is the nominal radio transceiver sensitivity, which is typically measured in dBm. It indicates that the parameter Link Margin gain, given by expression (5.5), is dynamic and can be calculated taking in consideration the choices in terms of both TPL and radio sensitivity values.

In equation (5.5), the radio channel gain must be updated in order to translate the difference between the new radio channel gain verified and the radio channel gain used as reference (presented in Table 5.1). When a different radio transceiver sensitivity is used, the $Rx_{Sensitivity}$ parameter must represent this new sensitivity value. Thus, the wireless radio channel can be evaluated relative to a Link Margin gain at each round in order to evaluate if a radio channel is in outage using the following expression:

$$LM(t_n) < 0 \rightarrow outage \quad (5.6)$$

The remaining of this section aims to assess whether the nodes that have met the reliability requirements, namely the Node-PROTACTICAL 4 and 7, can meet the latency requirements imposed by the Task Group TG6 for different scenarios.

The statistical parameters introduced in section 1.1 (fading probability, fade duration, non-fade duration, and LCR) describe the dynamic nature of the fading signal component but do not enable the assessment of the radio channel performance in terms of latency on the communications. In this regard, other parameters are introduced, namely Outage duration, Outage probability, Non-Outage duration and Time-between-Outages. These parameters are illustrated in Figure 5.6.

Outage Duration

The outage duration of an outage state is quantified as the amount of time that a signal remains in the outage state, as illustrated in Figure 5.6 where the signal, which corresponds to the temporal behaviour between second 2 up to 5 of the signal transmitted by Node-PROTACTICAL 7 in scenario D, remains in outage for ≈0.5 seconds (N). This analysis enable to understand which link margins are required to ensure the latency requirements of WBAN applications, for either medical or non-medical applications. Figure 5.7 depicts the outage durations of radio channel Node-PROTACTICAL 7 in scenario A. As the percentage of outage durations that will last less than the period of time given by x-axis to a specific Link Margin gain, identified in the y-axis. For instance, considering a LM gain of 10 dB, if an outage occurs, three quarters of these outages will last less than 70 ms, following the same logic, 90% and 100% of the outages will last less than 105 ms and 280 ms, respectively. Therefore, in order to meet the latency requirements imposed by WBAN applications to medical and non-medical applications, to a 100% of outages, a LM of 17 dB and 11 dB are required, since for these margins the outage durations will last less than 125 ms and 250 ms.

Table 5.5 shows the results of the performance evaluation of radio channels in several scenarios in terms of several outage parameters at Link Margin identified as required to ensure the requirement latency of WBAN applications, given by column Link Margin gain (dB). As expected, Node-PROTACTICAL 4 demands lower Link Margin gain values, since this radio channel, as verified in fading characteristic analyses, is subject to short fading periods and low fading magnitudes were reported. Thus, a Link Margin gain value of 5 dB seems be enough to ensure the most challenging latency requirement, 125 ms, regardless of the scenario, whereas to non-medical applications Link Margin gain values lower than 5 dB seems to be able to ensure its latency requirements. Regarding Node-PROTACTICAL 7, the most demanding scenario in terms of Link Margin gain values is scenario A, requiring a Link Margin gain of 17 dB, since,

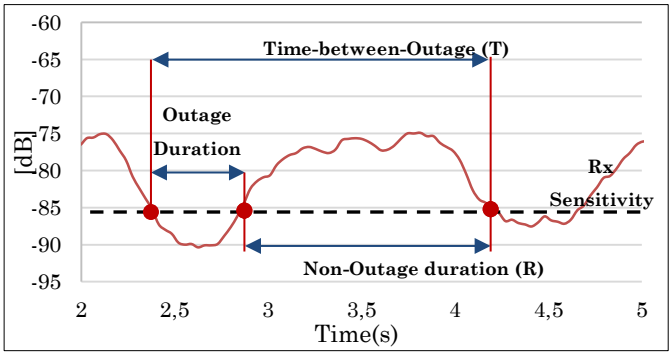

Figure 5.6. Illustration of the concepts Outage, Non-Outage duration, and Time-between-Outages.

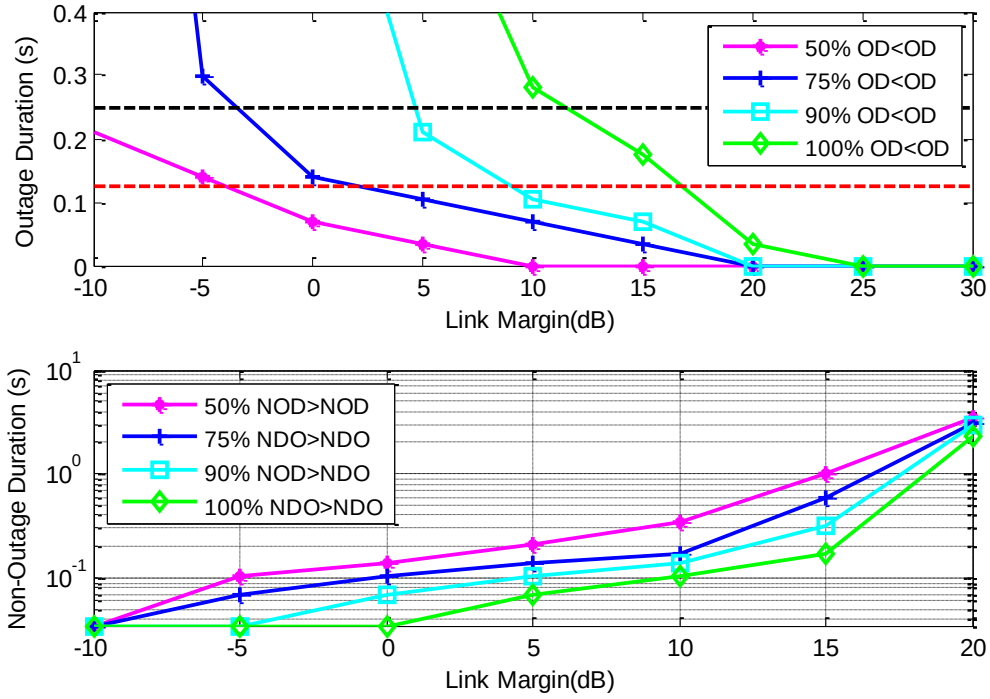

Figure 5.7. Period of the time that signal emitted by Node-PROTACTICAL 7 remains below (in Outage) and above (in Non-Outage) a link margin value (X axis) in scenario A.

as observed in fading duration analysis, this scenario leads to the highest fading durations (≈315 ms).

Outage Probability

Although the Link Margin gain values above defined as requirements are enough to ensure the latency requirements, the same conclusion cannot be made for other aspects of network performance. Thus, this subsection aims to analyse the probability of an outage occurring, considering the LM values identified in the previous subsection for each node accordingly to each test bench scenario. To the Link Margin gain values of 17 dB and 11 dB, required to radio channel Node-PROTATICAL 7 in scenario A, an outage probability of 4% and 13% are obtained, as depicted in Figure 5.8. Although in this scenario such outage probabilities give the impression of being acceptable, one quarter of the outages registered in scenario C, to the Link Margin gain value of 5 dB, are too high, indicating that this Link Margin gain value must be increased in order to reduce the outage probability and, consequently, rise the probability of both requirements, latency and reliability, being ensured for all scenarios. Relative to Node-PROTACTICAL 4, low outage probabilities (<2%) are obtained in Figure 5.8, indicating that such LM values are suitable to ensure both latency and reliability requirements.

Non-Outage Duration

The performance measure non-outage duration, concept illustrated in Figure 5.6 and analogous to the second-order parameter non-fade duration, consists in the total interval of time

Table 5.5. Radio channels result of Link Margin Analysis at several scenarios.

Scenario	Node	Link Margin gain (dB)		Non-Outage (ms)		Outage Probability (%)		Time-between-Outages(ms)	
		125 ms	250 ms	125 ms	250 ms	125 ms	250 ms	125 ms	250ms
A	4	5	4	105	70	1.4	8	70	105
	7	17	11	195	110	4	13	630	200
B	4	10	5	105	70	4.8	14.3	315	70
	7	15	10	175	105	3	8	175	150
C	4	5	3	210	175	1.7	10.2	210	70
	7	10	5	105	70	10	25	70	35
D	4	5	4	140	105	7.4	11.8	140	70
	7	12	10	105	70	3	10	70	35
E	4	15	10	350	105	2.8	8	140	70
	7	15	10	175	70	3	13	210	175
F	4	5	4	105	70	3.4	12.5	105	70
	7	13	9	385	105	15	21	245	35

that a received radio signal is not in outage state (i.e. received signal strength lower than the radio transceiver sensitivity). The top graph of Figure 5.7 illustrates the Node-PROTACTICAL 7 empirical non-outage durations at several LM values in scenario A. Taking into consideration the reference LM values previously identified, namely 17 and 11 dB, there is 100% of confidence that a period of non-outage will last more than 500 ms and 175 ms, respectively. These results have direct implication on the data packet length to consider, indicating that to radio channels low non-outage durations, small data packet sizes must be consider in order to ensure a successful transmission, whereas large data packet sizes require longer non-outage durations. The radio channel Node-PROTACTICAL 4 has 100% of confidence that for all cases the period of non-outage will last more than 105 ms, as shown in Table 5.5. This shows that the LM values considered to Node-PROTACTICAL 4 do not offer high confidence in terms of non-outage durations, limiting the data rate. Thus, higher LM values might be required.

Time between Outages

Another performance measurement proposed is the Time-between-Outages (TbO), which is analogous to LCR, and specifies how often outages occurs. The TbO metric is the period of time between the moments that the received signal crosses into consecutive outages, as depicted in Figure 5.6. The TbO should be as low as possible since it is desired small rates between outages. The TbO observed in radio channel Node-PROTACTICAL 7 in scenario A for a given LM value are illustrated in Figure 5.9, and can be interpreted in a similar way to previous graphs depicting other outage performance parameters. Considering the LM values required to this node in the scenario of interest, 17 and 11 dB, there is 100% confidence of TbO being greater than 385 ms (it indicates that a outage occurs every and 385 ms) and 175 ms, respectively.

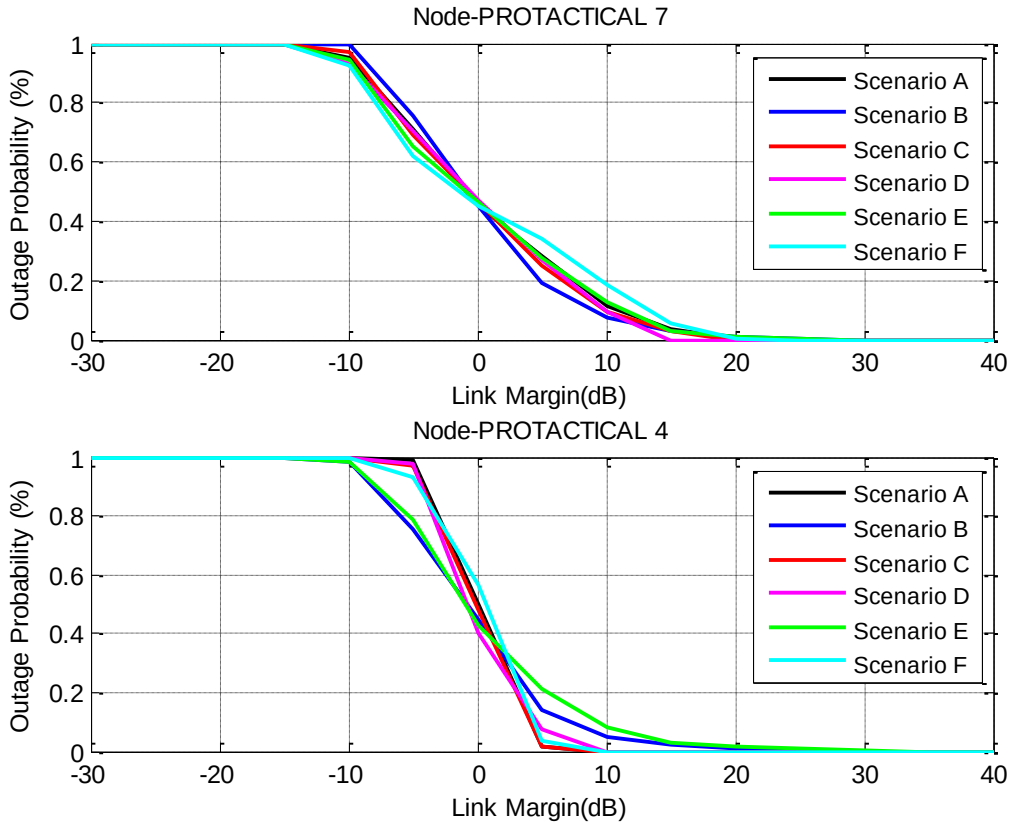

Figure 5.8. Probability of received signal power being lower than the transceiver Rx sensitivity in terms of link margin for both Node-PROTACTICAL 7 (top graph) and 4 (bottom graph).

Table 5.5 shows the TbO for each radio channel in every scenario of interest, revealing that the LM values initially considered as reasonable to Node-PROTACTICAL 4 lead the radio channels to shorter TbO (from 35ms up to 70 ms), which is not desirable, indicating once again that these LM values must be updated in order to ensure a better performance in terms of all the outage metrics.

5.5 Summary

In this section, the questions presented at beginning of this chapter were addressed.

How does the user activity affect the path-loss and fading on a millisecond-scale?

First- and second-order statistical analysis have shown that the user activity (that causes shadowing) is the predominant effect to the time-variation of on-body radio channels. As a consequence, the radio channel is a slow fading radio channel, as stated in other research works such as [24], [62], [111], [168]. The fading features and radio channel gain strongly depend on the considered user activity, therefore, the influence of human activity on the radio channel varies according to the location of the node, since some locations are more susceptible to movement than others. According to research works [63] and [158], body parts movements strongly affect the signal fading due to angular variations of the transmitter and receiver antenna

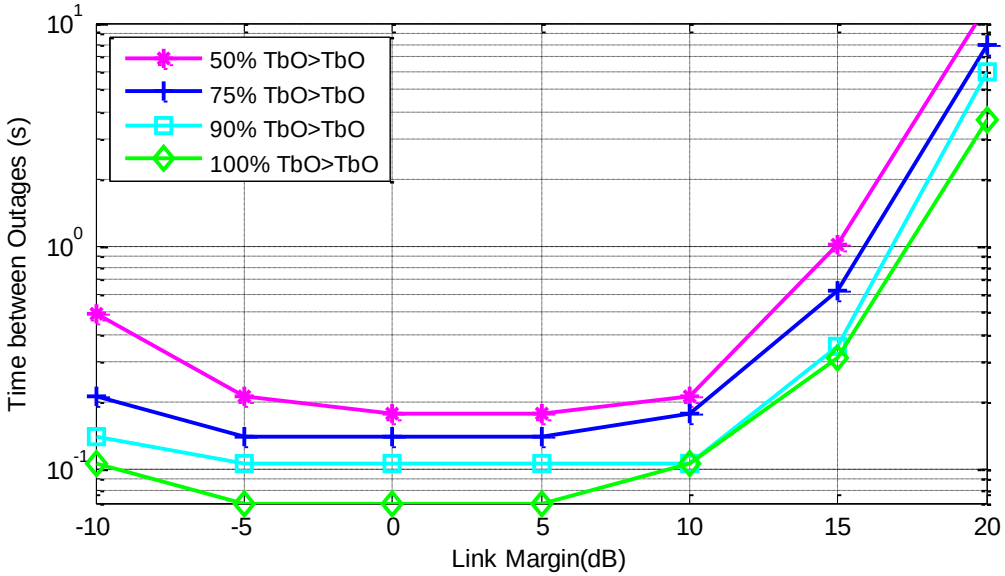

Figure 5.9. Percentage of time-between-outages, in terms of Link Margin, of Node-PROTACTICAL 7 in scenario A.

gains, as well as, a reduction in the antenna gains due to the angular variation of the corresponding body part during the walking activity. The antenna gain depends on the radiation pattern of the antennas.

Are the fading and path-loss affected by changing the node location and operation scenario?

The transmitter node located at the user's chest (Node-PROTACTICAL 4) presents a very stable radio channel, with consistent path-loss values (near to -50 dB) and with no occurrence of fading. Since this node is not located at a user's limb, its radio channel is not subjected to variable path-loss and fading features, and thus transmissions at the lowest TPL (-22 dBm) are enough to ensure the reliability requirement (with path-loss values near to -81 dBm). The Node-PROTACTICAL 7 is the most mobile of all the nodes. As a consequence of the frequent commutations between LOS (Line-Of-Sight) and NLOS propagation conditions, a wide range of radio channel gain values and fading magnitudes of -18 dB are observed (for all scenarios). The observed fading depths values of the Node-PROTACTICAL 2 are lower than -10 dB, but with high fading rates than the other nodes. According to the results obtained in this test bench, this node has the lowest radio channel gain values.

This test bench study has shown that the energy contribution of the multi-path components have a significant effect on on-body channels, leading to a radio channel gain increase of 10 dB. At the same time, surrounding environment also affects the fading features, turning the on-body channel more dynamic (higher fading rates).

Regardless of the scenario, the radio channel state remains unchanged during each data packet transmission period. It was also observed that there are only small differences on measured fading amplitudes of two to three consecutive data packets (35 ms is the period that separates each data packet transmission).

Are the links (with transmissions at the maximum power allowed) able to ensure the application requirements?

Empirical PER results revealed that the Node-PROTACTICAL 2 does not meet the QoS requirements defined by IEEE 802.15.6 TG in terms of reliability, since PER values higher than 10% were obtained. The remaining nodes assessed in the test bench were able to ensure the requirements of both reliability and latency, but with an inefficient use of the energy.

Which approaches can be advised to each link in order to optimize communications?

Regarding Node-PROTACTICAL 2, a multi-hop topology should be explored for scenarios where the star topology is not adequate.

Regarding the Node-PROTACTICAL 4, low LM values (within the range 4 up to 6 dB for all scenarios) are required and high stability was observed (maximums fading magnitudes of -10 dB, low fading durations, and low path loss). Therefore, the utilization of a TPL lower than 0 dBm (can be also static and pre-defined before WBAN operation) seems able to ensure the communication QoS requirements and, at same time, making the transmissions more energy efficient.

The radio channel performance assessment with respect to a LM gain value shows that the Node-PROTACTICAL 7 is the link that requires the highest LM gain values, for all scenarios. In some cases, a higher LM value than the suggested in Table 5.5 is required. Although the latency requirements are respected, a PER value above 10% is likely to occur for the LM gain values of Table 5.5 (due to the reported outage probability values). The reported periodic fluctuations (dynamic movements promote significant differences between the maximum and minimum fading depths in each period) reinforce the need for a TPC mechanism. It is the author's conviction that such solutions are able to increase the radio channel reliability and reduce the energy consumption in on-body communications.

TPC mechanisms seem to be a suitable and feasible solution to optimize QoS requirements in on-body communications. The on-body channel of Node-PROTACTICAL 7 is slow fading and both reported coherence time and non-outage values last in the order of the at least one hundred of milliseconds (value might increase with the optimization of the considered LM value). In addition, outages last in the order of milliseconds.

These features suggest that successful data packets transmission across of multiple communication data packets might be possible, and that estimations about the state of the link will likely hold true in the near future (for the next 30 ms - 145 ms). In other words, agile TPC mechanisms might be able to estimate and adjust the radio module power while the radio channel state remains unchanged.

CHAPTER 6

TRANSMISSION POWER CONTROL FOR ON-BODY COMMUNICATIONS

In this chapter a transmission power control (TPC) mechanism denominated Proactive-TPC (P-TPC), which explores the natural periodic movements of the human body, is proposed. This mechanism overcomes some of the main drawbacks of the TPC mechanism analysed in chapter 3. The proposed mechanism relies mainly on the acceleration samples from an inertial sensor to monitor the user's gait cycle when updating the WBAN's TPL parameter. The proposed solution employees a hybrid operation principle that will be further explained in the following subsections. Unlike other solutions proposed to execute in non-energy constrained nodes, e.g. smartphone that might take the role of Coordinator node, the Proactive-TPC targets energy constrained nodes (Edge of the Network nodes). Therefore, it was engineered to be simple and with minimal processing requirements.

There are several questions addressed in this chapter: *How does walking activity affects the fading signal pattern and is this influenced by the human body properties? How can accelerations in the user's stride be tracked and how to reduce the complexity of mechanisms (addressed in the literature) to be implemented at the sensor nodes? Can traffic overhead be reduced and can TPC still be employed effectively to dynamic scenarios? How can the proposed TPC mechanism be integrated into the protocol stack as a performance improvement strategy? Is the proposed TPC approach fast and agile enough to estimate the radio channel and adjust power before the radio channel quality changes? Can energy efficiency and reliability of communications be optimized without sacrificing latency?*

6.1 Fading Characterization

In the following section the experimental setup used for fading signal characterization is described. The fading properties and Link-Margin gain (LM) values expected in real scenarios are reported.

6.1.1 Experimental Testbed Configuration

Although nodes are located in several parts of the PPE, only signal propagation from the Node-PROTACTICAL 7 (which is attached to jacket with a body-surface-to-antenna separation that can vary from 2-4 cm) to the Coordinator node are characterized. This node was

selected from a set of eight Edge of the Network nodes, since the communications to the Coordinator node are more susceptible to alternate between LOS and NLOS due to user's changes on posture and movement as described in chapter 5. Furthermore, the limitations of the TPC mechanisms addressed in the literature is on handling transmissions in dynamic scenarios without increasing the traffic overhead due to extra control frames.

A scenario-based approach was used for signal characterization. Thus, empirical samples of the RSSI value were gathered in scenarios where users were walking on different environments (indoor, normal room and outdoor, urban area). Several users and different transmission power levels (TPL) were used on the test bench to gather the data.

The Edge of the Network nodes transmit data packets to the Coordinator node at a frequency of 30 Hz and at a TPL lower than the maximum allowed on communications in and around the human body (0 dBm) in order to automatically meet the specific absorption rate restrictions [13]. Moreover, the Node-PROTACTICAL 7 periodically measures its 3-axial accelerometer with a sampling frequency of 30 Hz. Two male (subject 1: 29 years old, 1.69 cm, 73 Kg; and subject 2: 20 years old, 1.75 cm, and 76 Kg) and one female user (26 years old, 1.61 cm, and 55 Kg) performed every scenario experiment on three different occasions. Each experiment takes around 60 seconds. Approximately half million RSSI values and 1800 acceleration values were collected during these experiments.

The transmission frequency is 2.45 GHz, which is part of the ISM band. Taking into consideration that this band is shared by several wireless technologies, experimental measures were conducted at controllable environments so as to reduce the influence of external RF interferences on transmissions. As a precaution, during each experimental test a spectrum analyser was used to ensure that the test bench spectrum band was not being used.

6.1.2 Fading Features

Figure 6.1 shows 15 seconds of the RSSI signal (bottom graph) received by the Coordinator node and transmitted by the Node-PROTACTICAL 7 during the experiment performed by user (subject 1) at the outdoor scenario. This figure also depicts the collected y-axis acceleration during the same experiment. The acceleration signal allows the identification of the subject 1 periodic movement, the gait cycle period, calculation of the acceleration of the user's stride, and also allows to determine that the fading follows a periodic behaviour with a period that matches with the gait cycle period, regardless of the test bench environments.

Therefore, considering the nature of the acceleration when the subject is walking, two higher and lower acceleration peaks occur during the interval of a gait cycle. The RSSI value

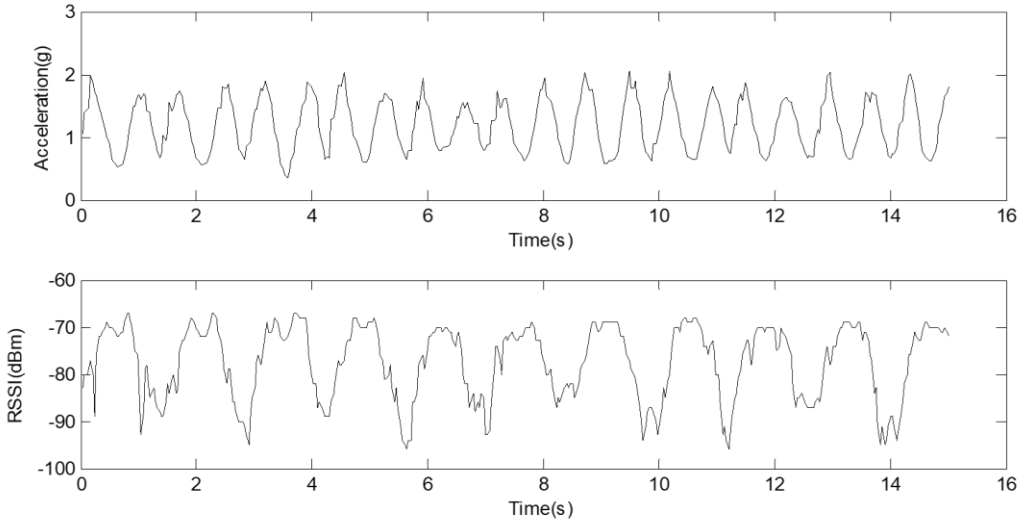

Figure 6.1. Fifteen seconds of the acceleration (top) and RSSI signal (bottom) regarding link created between the Node-PROTACTICAL 7 and the Coordinator node while subject 1 was walking outdoors.

shown in Figure 6.1 has a peak-to-peak magnitude between 20 to 25 dB. The higher peak value corresponds to the relative-position between nodes that allows LOS communication, Node-PROTACTICAL 7 positioned at the front of the user's torso, whereas lower peak values occur when the link is in NLOS, i.e. Node-PROTACTICAL 7 positioned at the user's back.

The RSSI value is higher and less noisy in LOS than in NLOS, since LOS wave propagation has a strong energy contribution on signal power, whereas in NLOS the signal power is mainly due to the contribution of multi-path waves resulting from body obstruction and reflections from ground and surrounding objects.

Figure 6.2 shows the fading during the first 15 seconds of an experiment performed by subject 1 (indoor). The RSSI signal (i.e. RSSI values over time) at indoor and at outdoor scenarios has different features, suggesting that the environment strongly affects the fading. The bottom signal of Figure 6.2 is noisier than the RSSI signal at the outdoor scenario regardless of the relative positions of Node-PROTACTICAL 7 and the Coordinator node. The fast-fading, which refers to fast RSSI value variations, in short periods of time due to energy contribution of multi-path components generated by objects on surrounding environment, also affects the

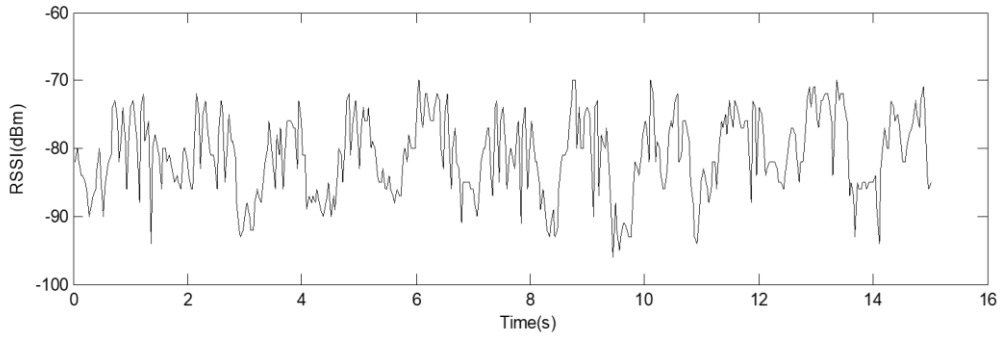

Figure 6.2. Fifteen seconds of the RSSI signal (bottom) regarding link created between the Node-PROTACTICAL 7 and the Coordinator node while subject 1 was walking indoors.

peak magnitude of the RSSI value.

Figure 6.3 summarizes the collected RSSI values, regarding the data packets transmitted during the two experiments performed by each subject (indoor) using boxplots. The box of the graph holds exactly half of the collected data. Both peaks, higher RSSI and lower RSSI values in the subject's gait cycle are affected in different ways. When subject 1 went from the indoor scenario to the outdoor scenario the value of the higher edge box increased 6 dB. This is due to the fact that multi-path components mitigate the effect of the relative-position (c.f. chapter 5). Regarding the lower edge of the box, it drops to values closer to the receiver sensitivity, because at outdoors the energy contribution of multi-path components is lower. Even though lower box edge at indoor scenario is higher, this illustration describes the signal as being static over time. The temporal evolution of the signal depicted in Figure 6.2 reveals that both lower and higher RSSI peak values are less deterministic at indoors, since they took values within a larger range when compared to the ones obtained at outdoor scenarios.

Finally, aspects related to the amplitude of the stride movement and velocity, as well as, user's body features, such as the user's arm length, user's wrist circumference, user's Body Fat Mass, etc. [143], also affect the signal behaviour along the time and the fading magnitudes. The Magnitude Gains are the difference between higher RSSI value peak and average RSSI value of the respective gait cycle. Magnitude Gains between ranges of 10-15 dB, 6-12 dB, and 3-10 dB were reported at outdoor scenario for subjects 1, 2 and 3, respectively.

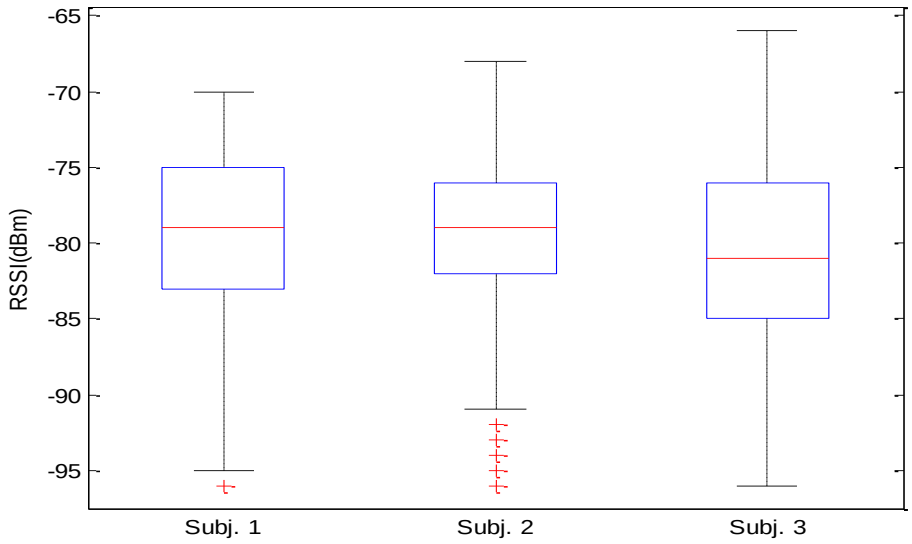

Figure 6.3. Variability of the RSSI values relative to transmissions from the Node-PROTACTICAL 7 to the Coordinator node (TPL=-0.5 dBm) when users were walking indoor for one minute.

6.1.3 Link-Margin Gain

A metric called Link-Margin gain is adopted in order to give an indication of the potential reduction of the RSSI value that might be achieved. Link-Margin is the difference between the RSSI value and the receiver sensitivity. Figure 6.4 and Figure 6.5 show the Link-Margin gains registered if transmissions occur within an interval ±35 ms and ±350 ms, with the center at the time of the higher and lower RSSI peak values, respectively.

This analysis approach (instead of verifying the Link-Margin at the exactly moment that the peak value occurs) was selected due to the fact that it is very unlikely that the system is able to accurately detect or predict the upcoming RSSI peak value due to an acceleration and the time required to process the information from 3-axis accelerometer, as suggested in [130]. In addition, data packets transmission might not be precisely controlled due to the latency introduced on the MAC layer and the airtime of an IEEE 802.15.4 data packet transmission (receiver-to-transmitter turnaround time of Coordinator node and acknowledgment – ACK – reception from the Node-PROTACTICAL 7).

Potential LM gain values shown in Figure 6.4 and Figure 6.5 were computed in relation to the smoothed fading signals with moving average window size of 70 ms and 350 ms. High Link-Margin gains were observed when transmissions were performed at intervals of time when the higher RSSI peak values occurred. Gains between 20 dB and 27 dB were obtained on experiments made with subject 3, whereas the Link-Margin gains of the remaining subjects are

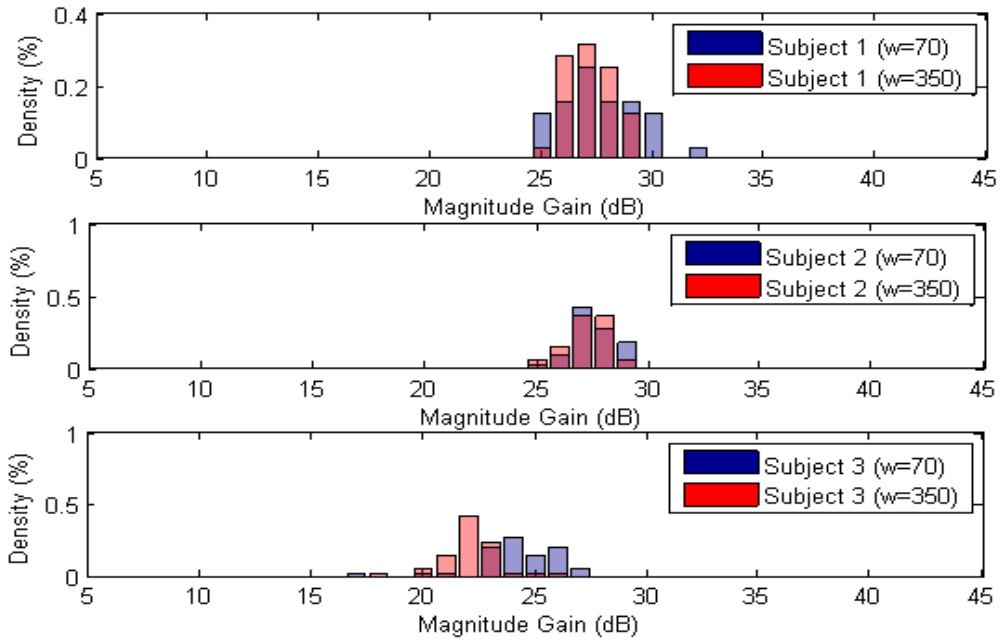

Figure 6.4. Normalized histogram of the reported Link-Margin Gains (at outdoors) for transmissions performed within interval ±35 ms and ±350 ms centred at the time of the higher RSSI peak

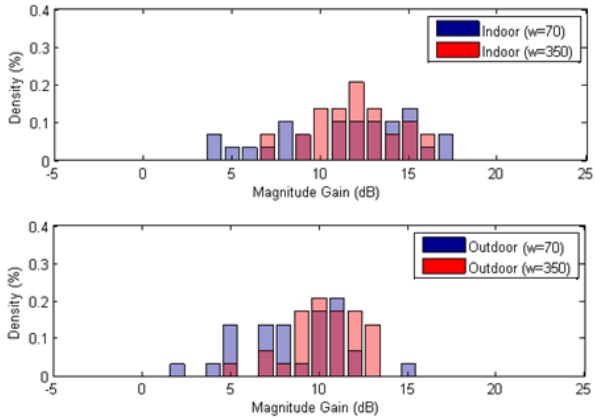

Figure 6.5. Normalized histogram of Link-Margin Gain if a data packet is sent within ±35 ms and ±350 ms of the lower RSSI peak (subject 1).

within the range of 25 dB to 30dB. Regarding the Link-Margin gains shown in Figure 6.5, the gains are substantial lower than the results of Figure 6.4, dropping to values between 5 dB and 15 dB. The analysis of the influence of the transmission interval in the Link-Margin gains shows that shorter intervals do not lead to substantial increasing on the Link-Margin gains. However, this conclusion should not be generalised to transmissions performed at the points of time between the higher and lower RSSI peak values, since during this interval the fading magnitude has a fast decay due to the user's limb movement, the communication channel quickly commutes between LOS and NLOS.

6.2 Proactive-Transmission Power Control

In the present section the design of the LQE and the TPL control block of the P-TPC mechanism is addressed and the influence of the several configuration parameters on their performance is assessed and analysed. Detailed information about the P-TPC mechanism operation principle is given and the algorithms used in each state of the P-TPC mechanism state machine to assure accurate radio channels prediction and TPL selection are described and evaluated in real scenarios. The P-TPC mechanism proposed was implemented as small software components in order to simplify the integration with standard communication protocols. Finally, details about the implementation of the P-TPC mechanism are given and the integration of the P-TPC mechanism with the IEEE 802.15.4 standard protocol stack was evaluated through experimental tests.

6.2.1 Link Quality Estimator (LQE)

The main goal of the proposed LQE is the reduction of the number of control packets exchanged between the Coordinator node and the Edge of the Network node. This can be achieved by exploring the regular pattern of the RSSI peak values with a period that matches

the user's gait cycle. Hauer et al. proposed an algorithm to predict future RSSI peak values, taking as assumption that the RSSI signal is periodic and that the period and the phase offset of the RSSI peak value relative to the beginning of the gait cycle is static [130]. However, as the user's walking speed is not constant, the LQE uses the accelerometer signal to track the acceleration of the user's stride in order to detect the beginning of a gait cycle, update the gait cycle's period and measure the phase offset of the higher and lower RSSI peak values relative to the beginning of the gait cycle.

To approximate the fading signal a linear interpolation was used, the proposed solution starts by mapping the measured RSSI samples into the gait cycle as depicted in Figure 6.6. This fading approximation function is used to predict the current radio channel quality (RSSI). The on-going gait cycle instant (in percentage) is provided as the LQE's input and the predicted RSSI value at that instant is the LQE's output. For example, to predict the future lower RSSI peak value the proposed LQE algorithm adds the latest gait cycle period to the last-known lower RSSI peak value.

The several graphs shown in Figure 6.6 result from the execution of an algorithm that assesses the influence of the number of samples (N) on the final fading approximation function. The data gathered during radio channel characterization was used to extract the RSSI samples at 1 Hz sampling frequency, during consecutive gait cycles. To determine the LQE's input, the acceleration signal was used to obtain the user's stride acceleration and thus to identify the

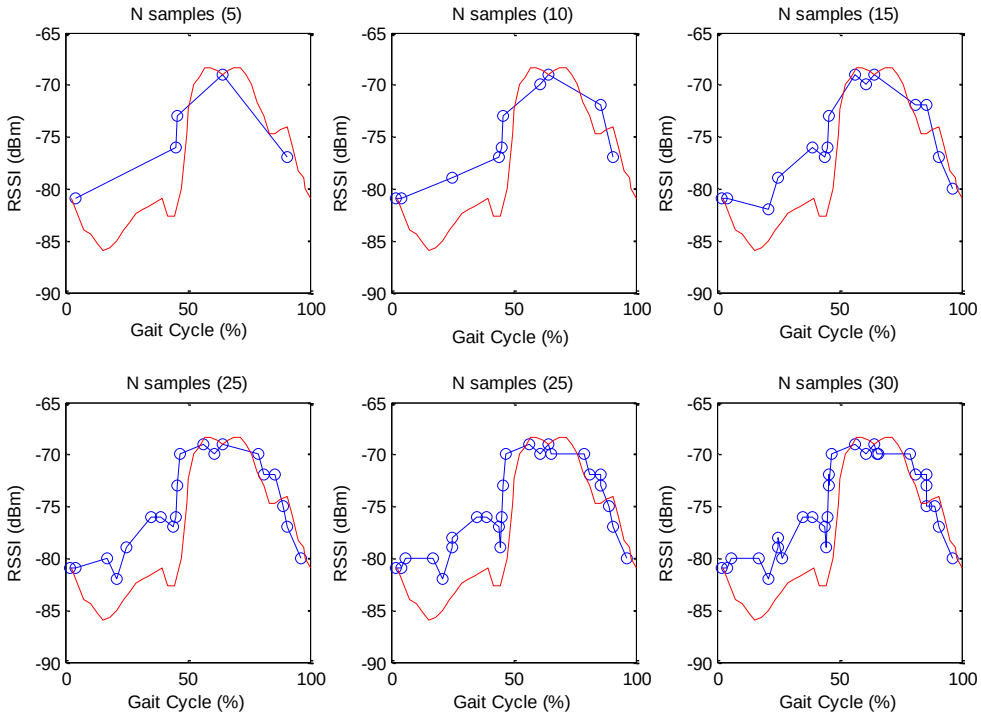

Figure 6.6. Approximated fading signal (red line) while human is walking (outdoor) by mapping N RSSI samples (blue line) measured in the Node-PROTACTICAL 7 onto the gait cycle period interval.

different gait cycles and calculate the gait cycle's period (during each gait cycle two acceleration peaks are expected). Therefore, the first acceleration peak detected is considered to be the beginning of the gait cycle and the time required to achieve two more acceleration peaks is considered the gait cycle duration.

The instant, at which a RSSI sample is extracted from the collected data, is mapped in relation to the gait cycle. Each instant is calculated by subtracting the current time from the on-going gait cycle to the time when the gait cycle started. After finishing the approximation to the fading signal, the higher and lower RSSI peak values can be extracted, as well as, their corresponding gait cycle instants. The approximated shape of the fading signal, visible in Figure 6.6, is used to predict the RSSI peak value for future gait cycles.

Figure 6.7 depicts the Mean Estimation Error, in dB, which is calculated as the difference between the empirical RSSI peak value and the predicted RSSI peak values. As expected, the approximation to the fading signal becomes better as the number of samples becomes larger. For N=3, the error obtained on the higher RSSI peak value estimation is larger than 5 dB for all subjects, and between -10 dB up to -15 dB when the algorithm estimates the lower RSSI peak value. The optimal number of RSSI samples is seven (N=7) regardless of the RSSI peak value of interest, since the mean error on the estimation of the higher RSSI peak value drops to 1.21 dB, 1.98 dB and 3.2 dB for subjects 1, 2 and 3, respectively. The higher RSSI peak value occurs at 64.58% of the gait cycle time. When the algorithm estimates the lower RSSI peak value (23.54% of the gait cycle) the average error was -3.65 dB, -5.19 dB and -4.64 dB for subjects 1, 2 and 3, respectively. However, when the experiment was carried at indoors, the lowest

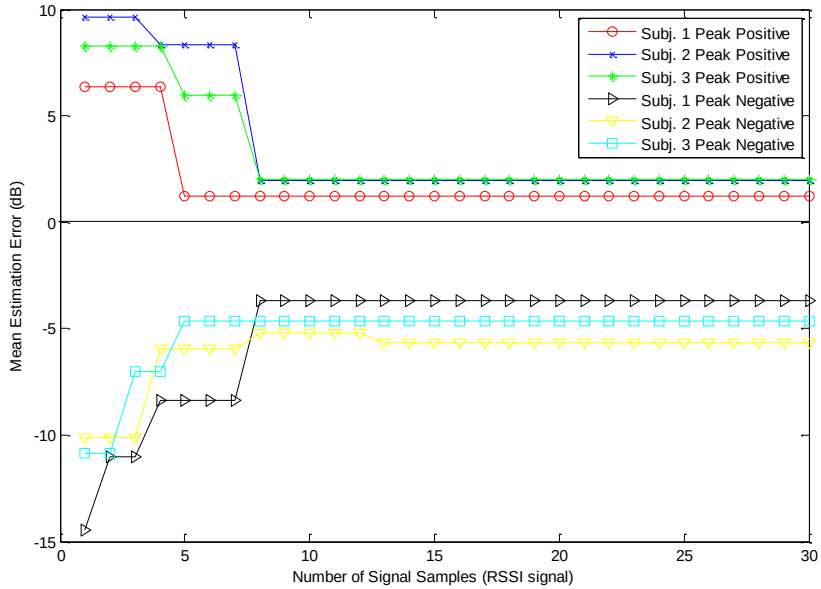

Figure 6.7. The influence of the number of RSSI samples on the prediction of the higher and lower RSSI peaks for outdoor experiments.

estimation error was obtained for N larger than 8. Fifteen RSSI samples were found to be the number that offers the best compromise between the LQE's performance at both environments. The instant when the RSSI peak values occur in the gait cycle is algorithm configuration-dependent, since it depends on the definition of the beginning of the gait cycle period.

Figure 6.8 shows the performance of the LQE algorithm (mean error and standard deviation) when estimating the higher RSSI peak value through the interpolation of 15 RSSI samples. As expected, the algorithm has better results during the outdoors experiments, since the emitted signals at outdoor scenarios are less prone to fast-scale fading influence, ensuring more stable signals. The minimum mean error is observed on subject 1 with a variance of 1.83 dB, and the worst results were obtained for subject 3 with a mean estimation error of 2.011 dB and a variance of 1.7 dB. These errors can be justified by the fact that two consecutive gait cycles were not perfectly matched as a result of small changes in the limb amplitude during the gait cycle and also due to the accelerations in the user's stride.

The LQE performance degrades for indoors scenarios due to the variability of the RSSI signal as a result of the fast fading component on the communication signal which translates into non-identical RSSI signal patterns. The mean estimation error is practically the same for all subjects, between 2.75 dB and 3.13 dB, whereas the highest variance registered occurred on subject 3 experiment: 2.42 dB. As the fast-fading negatively affects the performance of the LQE, the estimation of the lower RSSI peak value presents higher residuals, with a mean estimation error from -4.64 dB to -7.78 dB and average variance of 6 dB.

As a significant result, the fading signal shows that its peaks are regular within the gait cycles, which allows to estimate the current radio channel quality based on the on-going gait

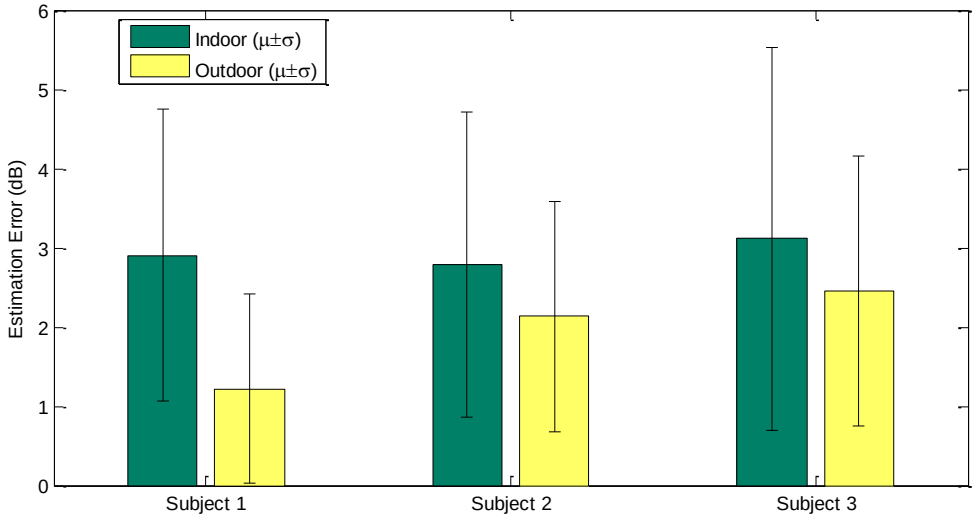

Figure 6.8. Proposed LQE's ability to predict the higher RSSI peak in indoor and outdoor environments through the fading approximation function comprising N= 15 RSSI samples.

cycle instant (0-99%). Furthermore, the information about the last gait cycle period and the user's stride acceleration enables to anticipate future instants in the on-going or the next gait cycles. These results are very significant, especially because the LQE algorithm aims to estimate gait cycle instants that will happen when communications are performed in LOS (regardless of the environment). Results show that at least 15 RSSI samples are required before the LQE algorithm can start estimating the radio channel quality. However, the mean error and the variance obtained indicates that residuals are expected and must be taken into consideration at the moment that an update to the transmission output power (TPL) is required. However, as shown in Figure 6.9, the potential Link-Margin gains are still significant.

6.2.2 Transmission Power Level Control

The TPC mechanism requires a TPL control block that receives the RSSI value estimated by the LQE as input and aims to determine the optimal TPL as output. Quwaider et al. observed a linear relationship between the TPL adopted on transmissions and the RSSI value measured at the receiver when the user was standing [9].

During the experimental radio channel characterization, tests were performed with different TPL values, ranging from -0.5 dBm up to -22 dBm, which allowed to determine if a linear relationship between the TPL and RSSI values exist. Figure 6.10 depicts the effect that the TPL value has on the higher RSSI peak value, showing that a linear relationship between these two parameters exists. The RSSI value, which can be described through the expression:

$$RSSI_i(a) = B_0(a).TPL_i + B_1(a) + \varepsilon(a) \quad (6.1)$$

where $RSSI_i$ is the RSSI value at the receiver for a transmission power TPL_i -0.5, -1.5, -3, -4, -6, -8,…, -22 dBm for subject a (i=1, 2, 3). The parameters B_0 and B_1 are the slope and the

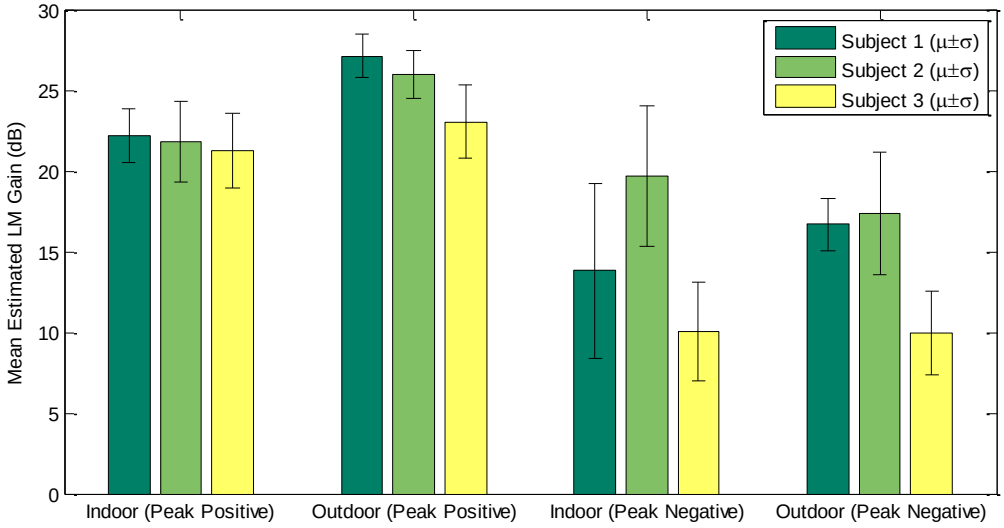

Figure 6.9. Difference between the predicted Link-Margin gains (difference between the predicted higher and lower RSSI peaks and the receiver sensitivity – and the empirical Link-Margin gains.

intercept of the fit model verified for transmissions at the maximum TPL allowed in on-body communications. Finally, the parameter ε is the error term that is obtained by finding the statistical distribution that better describes the model residuals (difference between observed values and values that model predicts). The error term is well described by means of a normal distribution and, consequently, by the parameters residuals mean and variation, namely ≈0 dB and 1.67 dB respectively.

In order to obtain the optimal TPL as fast as possible, a solution based on reactive-based approach (the dynamic one) is chosen. The slop parameter of expression (1) is used to determine the expected influence that the TPL metric has on the fading signal: $B_0(1)$=0.8441, $B_0(2)$=0.8812, $B_0(3)$=0.8109.

6.3 P-TPC Implementation

The hybrid TPC mechanism is implemented using the state machine depicted in Figure 6.11. It is composed by five main states: *Acceleration Acquisition; Periodic Mobility Detection; Fading Approximation; Gait Cycle Period Update and Phase Offset Tracking* and *TPC Mechanism.* The first two states, which are described on the next subsection (designated Acceleration Acquisition and Periodic Mobility Detection), aim to detect the periodic movement and to obtain the first gait cycle period (i.e. the time from initial contact of one foot to the following initial contact of the same foot). Once the periodic movement is detected the mechanism enters the *Fading Approximation* state on which the fading signal is captured by the gathered RSSI samples and a function able to approximate it is derived, please see subsubsection 6.3.2. The mechanism leaves the *Fading Approximation* state after obtaining the

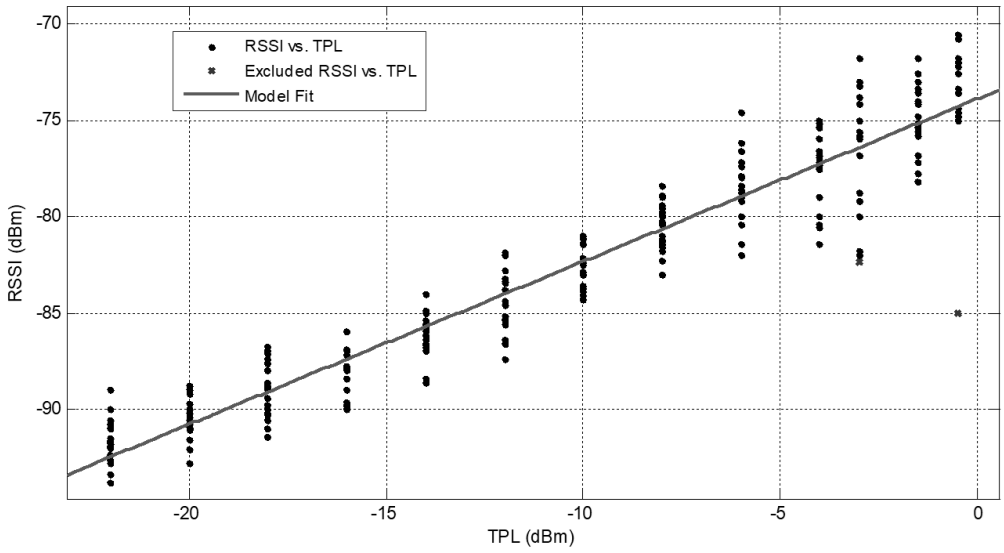

Figure 6.10. Mean Estimation error and variance, in dB, of Link-Margin gains estimated at higher and lower RSSI peaks by a number (N) of RSSI samples obtained for outdoor experiments performed by subjects 1, 2 and 3.

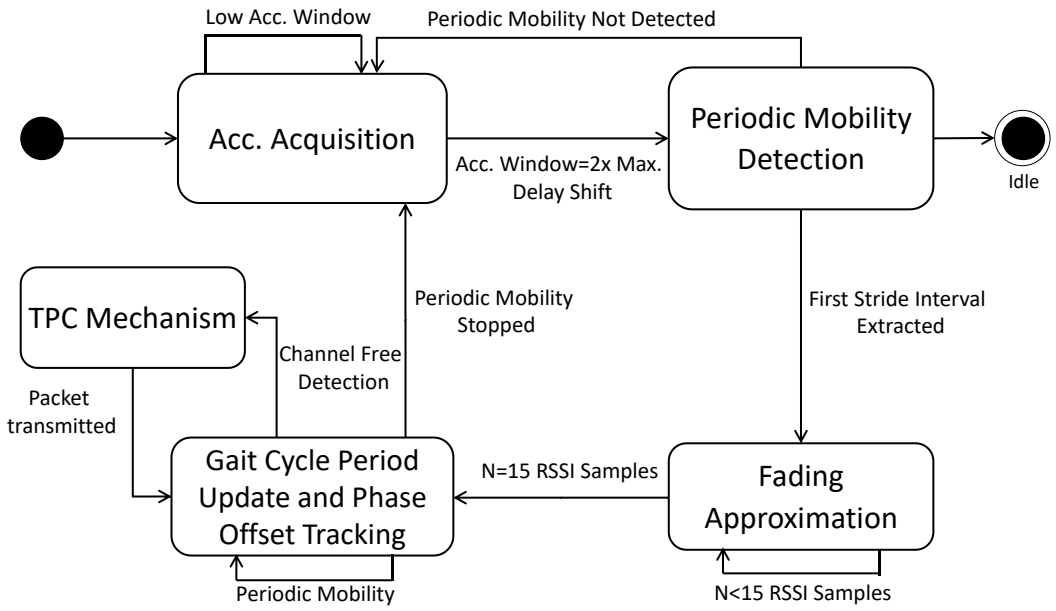

Figure 6.11. State machine of the proposed algorithm, being composed by five main stages.

fading approximation function and starts the *Gait Cycle Period Update and Phase Offset Tracking* state. This state goal is to compute the periods of each of the user's gait cycle and track the acceleration on the user's stride. The output of this state (period of the last gait cycle and estimation of the period of the on-going gait cycle) is crucial to ensure that the TPC mechanism operates efficiently, since the tasks of obtaining the on-going gait cycle instant (in percentage) and the radio channel quality estimation, which are carried out in the *TPC Mechanism* state, rely on the output of the *Gait Cycle Period and Update and Phase Offset Tracking* state.

The *TPC Mechanism* state (c.f. subsubsection 6.3.4) starts every time a data packet is ready to be transmitted. In this state, the TPC mechanism, which has the architecture depicted in Figure 3.1, is executed. The LQE block estimates the RSSI value through the fading approximation function and its output is used by the TPL Control block to compute the optimal TPL for the data packet to be transmitted. After the transmission of the data packet the mechanism leaves this state and returns to *Gait Cycle Update and Phase Offset Tracking* state in order to keep updating the gait cycle period.

6.3.1 Acceleration Acquisition and Periodic Mobility Detection

In the *Acceleration Acquisition* state, the acceleration samples, required for the *Periodic Mobility Detection* state to determine the first gait cycle period, are acquired at a sampling rate of 30 Hz. Samples are measured for an interval corresponding to the detectable gait cycle period, i.e. (2x2.1 s).

The mobility detection algorithm used in [130] is adopted in the *Periodic Mobility Detection* state for detecting the periodic mobility and to extract the first user's gait cycle period through the user's stride acceleration signal. It is called Average Magnitude Difference Function (AMDF) and it is a variation of the Autocorrelation Function (ACF) with lower computational complexity, since no multiplications are required. The AMDF algorithm, which enables the determination of the periodicity of a signal, is defined by the follow relation:

$$AMDF(\tau) = \frac{1}{L}\sum_{i=1}^{L}|s_i - s_{i-\tau}| \tag{6.2}$$

where L is the length of the frame of the sampled acceleration signal, s_i is the sample of the acceleration signal and $s_{i-\tau}$ is the delayed version of the acceleration signal sample, with τ representing the time lag in terms of samples. The value of τ that ensures a lower output value of the AMDF is considered the period of the signal. Thus the $AMDF(\tau)$ is computed by delaying the input s signal, subtracting the delayed waveform from the original, and summing the magnitude of the differences between sample values. The difference signal is always zero at delay 0 s, and is particularly small at delays corresponding to the signal period of a signal having a quasi-periodic structure.

The range of values of τ must be chosen for which the minimum and maximum values represent the minimum and maximum detectable gait cycle period. The delay shift of 700 ms and 2100 ms were selected as τ_{min} and τ_{max}, respectively. The period of the signal shown in Figure 6.12 is 1.23 s which is considered the first gait cycle period.

Algorithm 6.1 is responsible for mobility detection and extraction of the first gait cycle period. . In this algorithm, three criteria have to be verified to conclude the existence of periodic

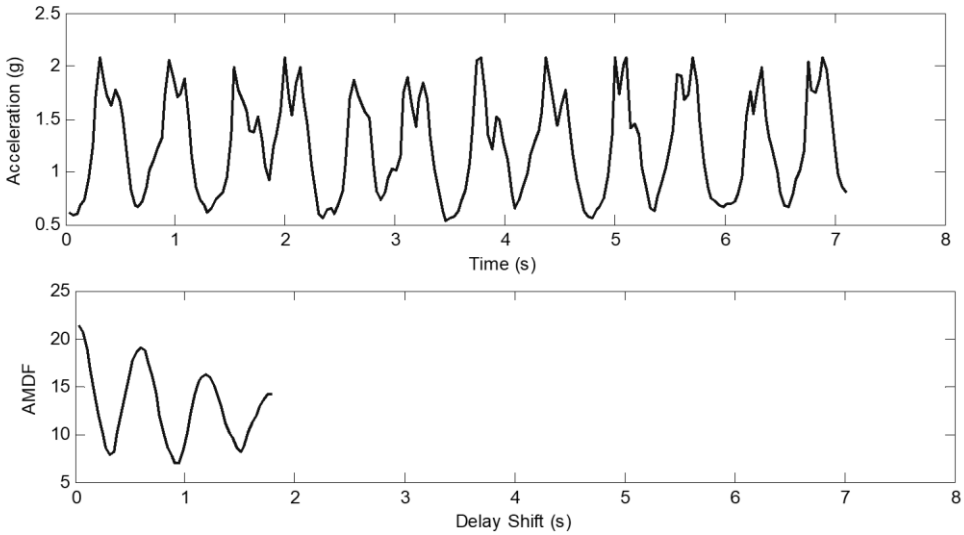

Figure 6.12. Acceleration Signal while subject 1 is walking outdoor and respective AMDF values to delay shifts from 0 to 2100 ms.

mobility: *i*) the time series of the acceleration signal must be at least equal to the maximum detectable gait cycle period; *ii*) on the *Periodic Mobility Detection* state the acceleration window size is divided into two parts and the results of the computed AMDF algorithm for each of the accelerations windows must not have a gait cycle period difference higher than the detectable minimum gait cycle period (700 ms); *iii*) finally, the minimum AMDF algorithm output value must be at least 50% less than the maximum valued outputted by the AMDF algorithm. These criteria's were obtained via trial-and-error in the performed experiences for the several users.

6.3.2 Fading Approximation

In the *Fading Approximation* state fifteen RSSI samples are required to ensure a suitable approximation of the fading signal. As the number of samples is low, a similar approach to the one chosen on closed-loop control TPC was adopted. The Node-PROTACTICAL 7 transmits the data packets at a frequency given by N (number of samples) divided by the first gait cycle period obtained from the *Periodic Mobility Detection* state. This allows to measure the RSSI value of the ACK received from the Coordinator node (transmitted at TPL -0.5 dBm). However, before applying an interpolation function to approximate the fading signal the collected RSSI samples must be aligned with the gait cycle. Thus, the gait cycle period and the phase offset must be determined.

The Dynamic Time Warping (DTW) algorithm is a well-known technique to find an optimal alignment between two time-dependent signal sequences (usually used to pitch detection [169]), assuming that the signal speed can vary. As mentioned, this algorithm is used to align two similar acceleration signals, $GaitCycle_{i-1}$ and $GaitCycle_i$ which are the acceleration signal for one full gait cycle and the acceleration signal of the consecutive gait cycle, so that both on-going gait cycle period (interval of $GaitCycle_i$) and the phase offset can be obtained. Therefore, giving two signals $GaitCycle_{i-1}$ and $GaitCycle_i$ of length n and m (67 and 58 samples respectively) the DTW algorithm constructs a matrix n-by-m (67 lines and 58 columns), from the signals on Figure 6.13, resulting in the matrix depicted in Figure 6.14, in

Algorithm 6.1. Mobility detection and extraction of the first gait cycle period.

Require: The accelerometer samples collection for 4.2 s, starting after occurrence of a valley (local minimum)
Input:
1: *Min_DelayShift:* minimum time lag
2: *Max_DelayShift:* maximum time lag
3: *Acc_signal:* vector of acceleration samples of the nearest 4.2 s
4: *Lenght:* the length of the acceleration samples vector
5: *win_size:* size of the moving average window
Output:
6: *Periodic_Motion:* Boolean variable indicating the occurrence of periodic motion
7: *GC_Period:* period of the last gait cycle
Begin
8: *Acc_signal* ⟵ moving average filter (*Acc_signal*, *win_size*)
9: *Acc_firstGaitCycle* ⟵ *Acc_signal* (0*: Length*/2)
10: *Acc_secondGaitCycle* ⟵ *Acc_signal* ((*Length*/2)+1*: Lenght*)
11: *AMDF_FirstGaitCycle* ⟵ AMDF(*Acc_firstGaitCycle, Min_DelayShift, Max_DelayShift*)
12: *AMDF_SecondGaitCycle* ⟵ AMDF(*Acc_secondGaitCycle, Min_DelayShift, Max_DelayShift*)
13: **If** (argmaxi{ *AMDF_FirstGaitCycle*}/2)> argmini{ *AMDF_FirstGaitCycle*} **then**
14: **If** (argmaxi{ *AMDF_SecondGaitCycle*}/2)>argmini{ *AMDF_SecondGaitCycle*} **then**
15: *FirstGaitCycle_Period* ⟵ Get_GaitCyclePeriod_Function(*AMDF_FirstGaitCycle*)
16: *SecondGaitCycle_Perio* Get_GaitCyclePeriod_Function(*AMDF_SecondGaitCycle*)
17: **If** ‖ *FirstGaitCycle_Period-SecondGaitCycle_Period* ‖≤*Min_DelayShift* **then**
18: *GC_Period* ⟵ *SecondGaitCycle_Period*
19: *Periodic_Motion* ⟵ True
20: **else**
21: *Periodic_Motion* ⟵ False
22: **end If**
23: **end If**
24: **end If**
End

which every element of the matrix (x, y) is an Euclidean distance, i.e. the difference between points $GaitCycle_{i-1}(x)$ and $GaitCycle_i(y)$.

The red line on graph of Figure 6.14 represents the warping path which is achieved under certain restrictions (please refer to [169]) and consists of a set of elements from the n-by-m matrix, p=($p_2, p_2, \dots, p_{L,}$), that defines an alignment on time between $GaitCycle_{i-1}$ and $GaitCycle_i$, for any sample in $GaitCycle_i$ the warping path represents a mapping into the reference sequence: $GaitCycle_{i-1}$, as illustrated on the bottom image of Figure 6.13. The warping path is a sequence of elements from a n-by-m matrix, thus it must be selected from a set of possible warping paths w= ($w_1, w_2, \dots, w_{k,}$). The warping path with lowest cost is selected, using the expression:

$$DTW(GaitCycle_{i-1}, GaitCycle_i) = min\left\{\sqrt{\sum_{k=1}^{k}\frac{w_k}{k}}\right. \tag{6.3}$$

The DTW algorithm leads to a computational complexity that is exponential in the sequence lengths n and m and requires enough space to save the n-by-m elements which is not possible on the majority of resource restrained Edge of the Network nodes, as was concluded by research work [137]. The DTW complexity is *O(MN)=O(7680)*, where *M* (the length of the sliding

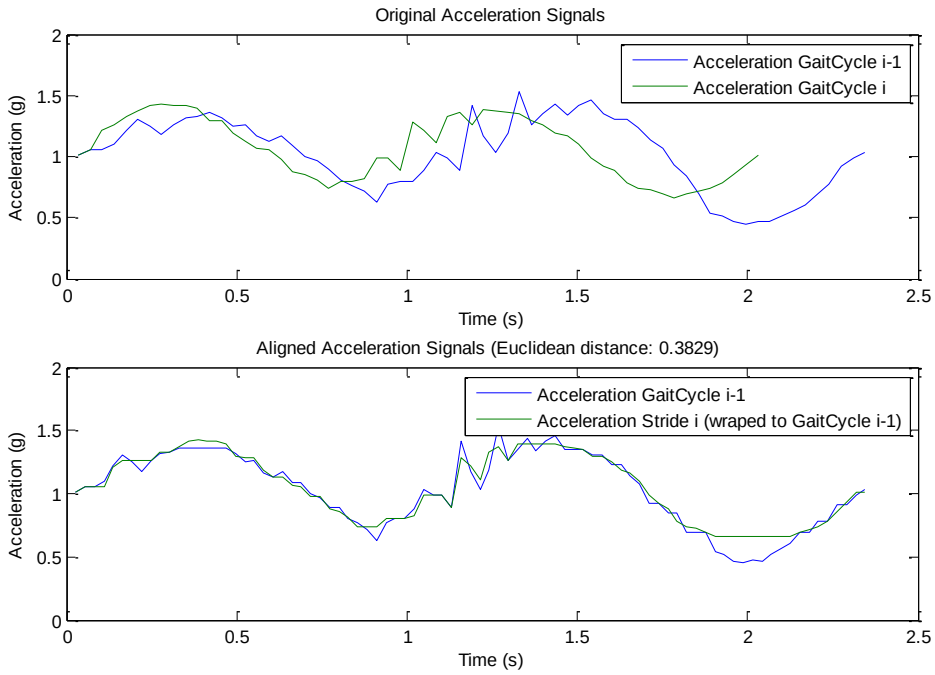

Figure 6.13. Two acceleration signals of two consecutive gait cycles (top graph) and signal as result of the DTW algorithm, i.e. aligned acceleration signals (bottom graph).

window) is set as 96 and N (the length of the acceleration template) as 80. Due to this complexity, the gait cycle tracking was implemented by the Coordinator node since it has more computing resources and more energy. The complexity can be reduced by avoiding computing the whole matrix through the selection of points, designed as anchors, in the reference sequence ($GaitCycle_{i-1}$) at an associated time $t_1, t_2, \dots, t_n$ [130]. For each anchor in the reference sequence, the acceleration data of $GaitCycle_i$ around an interval of time centred on anchor time t_i is extracted.

The Euclidean distance for each point on the extracted $Stride_i$ acceleration data in relation to $GaitCycle_{i-1}$ acceleration value in the respective anchor is calculated. From the resultant vector of distances the minimum values are then extracted and, as sampling rate is known, it is possible to obtain the phase offset and the time that the gait cycles period increases or decreases in relation to the previous gait cycle. If the minimum value is on the center of the vector it means that there was no acceleration whereas vector indexes higher than the center index indicates negative accelerations and lower indexes suggest positive accelerations, which can be converted to seconds by multiplying the difference between the index of the minimum Euclidean distance and centred vector index by the acceleration sampling interval.

Figure 6.15 shows an example of this approach in which three anchors were considered, corresponding to the extremes of the acceleration signal (set at the instant points 0.95 s, 1.47 s and 1.995 s of the $GaitCycle_{i-1}$ acceleration signal featured in Figure 6.15) during a gait cycle (in the case of the reference sequence acceleration values used as example and illustrated in

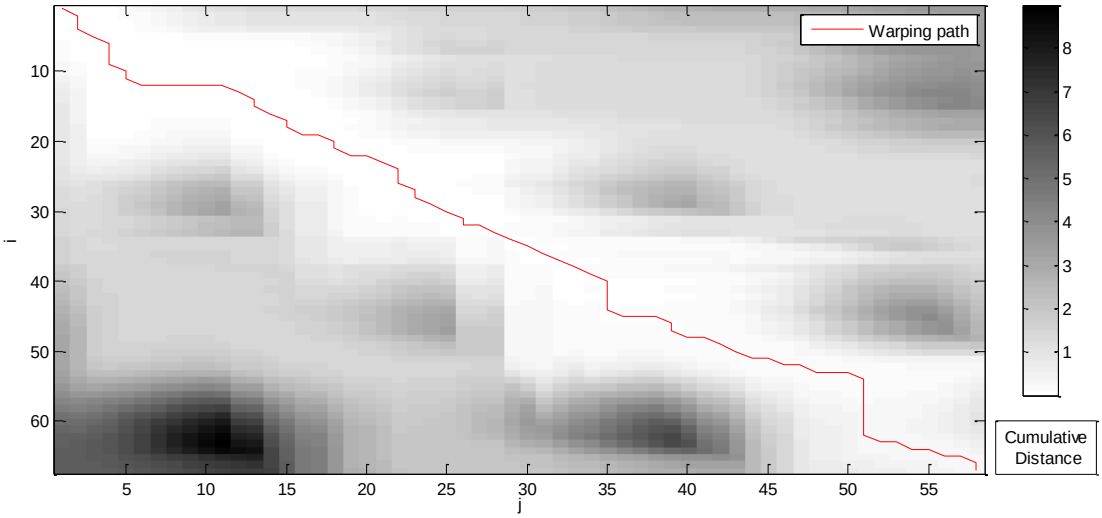

Figure 6.14. Distance matrix and warping matrix identified by red line for two acceleration signals as result of two consecutive gait cycles.

Figure 6.13), whereas the window size, which defines the interval around the anchors, is ±350 ms. The result is graphically represented on the bottom image of Figure 6.15 and corresponds to the Euclidean distances calculated by using a sequence of acceleration samples of the original acceleration measurements, whereas the top graph is the result when a filtered version of the acceleration signal is considered. It is observable that the minimum calculated Euclidean distances for anchor 2 occurs at -0.28 s and -0.245 s as shown in the bottom and top image of the Figure 6.15 respectively. Therefore, the Euclidean distances featured on the bottom and top image of the Figure 6.15 are slightly different. This observations shows that when the acceleration signal is filtered the calculated Euclidean distances are more accurate.

The window size is also relevant since it defines the maximum and minimum changes detectable on a gait cycle period. In Algorithm 6.2 the final algorithm to track the gait cycle is presented. A window size of ±140 ms and two anchors were selected for each gait cycle, corresponding to the high extremes of the acceleration signal. The first anchor is selected in $GaitCycle_{i-1}$ as the high value of the signal and this is considered to be the beginning of the gait cycle (even if it is not the case), and then the second anchor is predicted in next gait cycle by adding the gait cycle period to the reference acceleration signal. The Euclidean distance is then calculated in an interval of ±140 ms around the predicted anchor and the minimum value of this distance indicates an acceleration peak value. This instant is then added to the reference sequence gait cycle period resulting on the period of the on-going gait cycle.

The task of computing the gait cycle's period and tracking accelerations on the user's stride starts at the *Fading Approximation* state in order to allow the P-TPC mechanism to map the fading signal to the gait cycle.

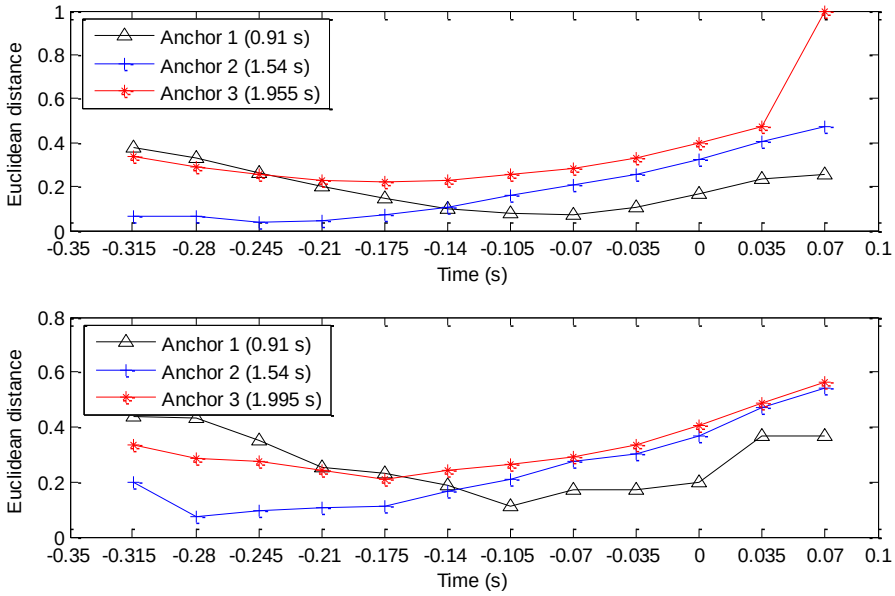

Figure 6.15. Euclidean distances between anchors (at time 0.95 s, 1.47 s and 1.995 s of the reference gait cycle shown in Figure 6.13) and acceleration samples of $\boldsymbol{GaitCycle_{i-1}}$ in an interval ±350ms centred in the respective anchor time.

6.3.3 Gait Cycle Period and Phase Offset Tracking

The modified DTW algorithm (c.f. Algorithm 6.2) previously proposed and described above is also executed during the *Gait Cycle Period Update and Phase Offset Tracking* state. As long as the user performs periodic movements, this state remains in execution, providing the user's gait cycle period of the on-going gait cycle. Updated values of the previous gait cycle and detection of the acceleration in the user's stride enable the P-TPC mechanism to determine the on-going gait cycle instant. This is achieved by counting the time elapsed since the beginning of the gait cycle and dividing it by the on-going gait cycle period (updated two times during a gait cycle period, since two anchors are used). This process is restarted on the beginning of the next gait cycle and repeated for the subsequent gait cycles. Thus, the last gait cycle acceleration signal is set as the reference $GaitCycle_{i-1}$, whereas the actual acceleration signal is considered the signal $GaitCycle_i$ on the DTW algorithm. To keep tracking the gait cycle period and the phase offset, the next sequences of gait cycle periods must be sampled in order to map the current time in the current gait cycle.

In order to reduce the energy consumption during the acceleration signal acquisition, a sampling frequency of 30 Hz was selected and a moving average filter with a window size of 70 ms was applied. Furthermore, only the y-axis acceleration data is read during an interval of 280ms centred on the predicted anchor time. This corresponds to 40% of the gait cycle period for an average gait cycle period of 1.3 s, and thus sixteen acceleration samples per gait cycle period are acquired.

The False Detected Accelerations (FDA) and the Undetected Accelerations Rate (UAR) error measurement criteria were used to assess the accuracy of the gait cycle tracking procedure summarized in Algorithm 6.2. The FDA, given in percentage, is computed as the total number of false accelerations (accelerations wrongly identified or calculated by the algorithm) detected from the total number of anchors:

$$FDA = \frac{\sum de/acelerations\ wrongly\ detected/calculated}{\sum anchors} * 100 \quad (6.4)$$

The UAR is calculated as the ratio of the total number accelerations not detected by the algorithm by the total number of anchors used during the algorithm execution:

$$UAR = \frac{\sum undetected\ de/aclerations}{\sum anchors} * 100 \quad (6.5)$$

Although the error measurement FDA is relatively significant to all subjects (superior to 6%), these values are due to Euclidean distances computation that led to wrong values, since all accelerations were correctly identified. Therefore, this algorithm seems to be reliable since

Algorithm 6.2. Gait Cycle Tracking.

Input:
1: *PreviousGC_Anchor:* acceleration sample of an anchor (first or second one)
2: *win_size:* size of the acceleration samples vector
3: *win_acc:* slide window for holding the acceleration samples
4: *GC_Period:* period of the last gait cycle
5: T_s: time interval of acceleration samples
6: T_{DTW}: the time poi not of performing the DTW
7: T_{Anchor}: the time point of the last detected anchor (first or second one)
8: $T_{current}$: the time of the current time point
9: *Euclidean_distance*: vector of Euclidean distances with a size *win_size*
10: *Index:* Index of a minimum point
Output:
11: *Current_GC_Period:* the current gait cyle period
Begin
14: $T_{DTW} \leftarrow (GC\_Period - (T_{current} - T_{Anchor}) - (win\_size * T_s)/2)$
15: **If** $T_{current} == T_{DTW}$ **then**
16: **do**
17: *win_acc* ⟵{*newAccsample, win_acc*(1:end)}
18: *num_samples++*
19: **while** receive an acceleration sample & *num_samples*< *win_size*
20: *PreviousGC_Anchor* ⟵1
21: Normalize_DataFunction(*win_acc*)
21: Euclidean_distanceFunction (*win_acc, Euclidean_distance*)
22: *Index* ⟵ argmin_i(*Euclidean_distance* (1,:))
23: *PreviousGC_Anchor* ⟵ *win_acc*(*Index*)
24: $T_{Anchor} \leftarrow T_{current}$-(*win_size-Index*)*$T_s$
25: **If** *Index+1*≤ ((*win_size*/2)-1) **then**
26: *Current_GC_Period* ⟵*Current_GC_Period* - (*Index** T_s)
27: **else If** *Index+1*≥ ((*win_size*/2)+1) **then**
28: *Current_GC_Period* ⟵*Current_GC_Period* + (*Index** T_s)
29: **else**
30: *Current_GC_Period* ⟵*GC_Period*
31: **end If**
32: **end If**
End

the almost all user's stride accelerations are detected by the proposed algorithm (maximum UAR value is 2.9%), but the accuracy of the calculated phase offset might require some improvements.

The results of the evaluation of the Algorithm 6.2 in different subjects are summarized in Table 6.1. This algorithm was executed during 120 s when the subjects were walking (gait cycles periods between 1.1-1.3 s) half of the time and at faster pace (gait cycle periods between 0.8-1.0 s) the remaining time.

6.3.4 TPC Mechanism

The IEEE 802.15.4 MAC layer was configured to beaconless mode, with the CSMA/CA backoff parameters set to zero, namely the CSMA/CA backoff exponent, backoff delays and number of backoff attempts. This configuration will further reduce latency on the transmissions and thus providing a higher control of the transmission time to the P-TPC mechanism. According to Akbar et al., the CSMA/CA configuration proposed achieves an end-to-end delay of 4.4 ms using a transmission bit rate of 250 kbps and a data packet with the maximum payload length of 127 bytes. This delay includes data packet handling and CPU processing time. However, it leads to a decrease in terms of network performance, since there is a higher probability of collisions [110]. The performance of the P-TPC mechanism following the configuration described above is discussed in section 6.4.

In summary, the P-TPC mechanism has two main components, the LQE and the TPL Control blocks and has the objective to minimize the energy consumption on WBAN's communications by dynamically adjusting the Transmission Power Level (TPL) at every data packet transmission. Therefore, the LQE and TPL Control blocks must be part of the communication protocol stack, at the MAC and at the PHY layer, respectively. Both blocks of the proposed P-TPC mechanism are included as part of IEEE 802.15.4.

A TPC mechanism able to minimize energy consumption during communications without sacrificing the latency is desired. With minimal latency the data packets are not delayed to periods when the fading signal reaches the higher RSSI peak value, since this might compromise the transmissions reliability but it will lead to latencies that can reach the gait cycle period [130].

By including the LQE in the MAC layer, the P-TPC mechanism is able to operate in any MAC protocol and it is capable to deal with the latency imposed by MAC protocols, since the LQE block is only performed after the detection that the radio channel is free (e.g. in the case of a slotted or no beacon based CSMA), as depicted in Figure 6.16.

Table 6.1. Error Measurement results of the Gait Cycle Tracking algorithm.

	FDA (%)	**UAR (%)**
Subject 1	8.9	1.3
Subject 2	6.3	2.9
Subject 3	6.8	0.9

The LQE block is implemented using a very simple process. This process only determines the time elapsed from the beginning of the on-going gait cycle (identified through the anchors of the proposed DTW algorithm) and divides it by the estimated on-going gait cycle period, as shown in Algorithm 6.3. This information (i.e. gait cycle instant in percentage) is then used to obtain the estimated RSSI value from the approximation function of the fading signal. The time interval required to execute the LQE process and get a radio channel quality prediction is 0.078 ms, which is lower than the time duration of each active superframe portion slot of IEEE 802.15.4 beacon mode (every time slot corresponds to 0.96 ms, assuming 250 kbps in 2.45 GHz band).

Finally, the TPL Control block (PHY layer) determines and configures the transmission output power of the transceiver to an optimal TPL, having as restriction the maximum TPL of -0.5 dBm. The linear model previously described allows the TPL Control block to interpret the influence that the power level has on the fading signal, as the fading signal approximation refers to the fading signal if the transmissions are made at the maximum TPL. This approach allowed to avoid the typical operation principle of a TPC mechanism in which a close loop between the

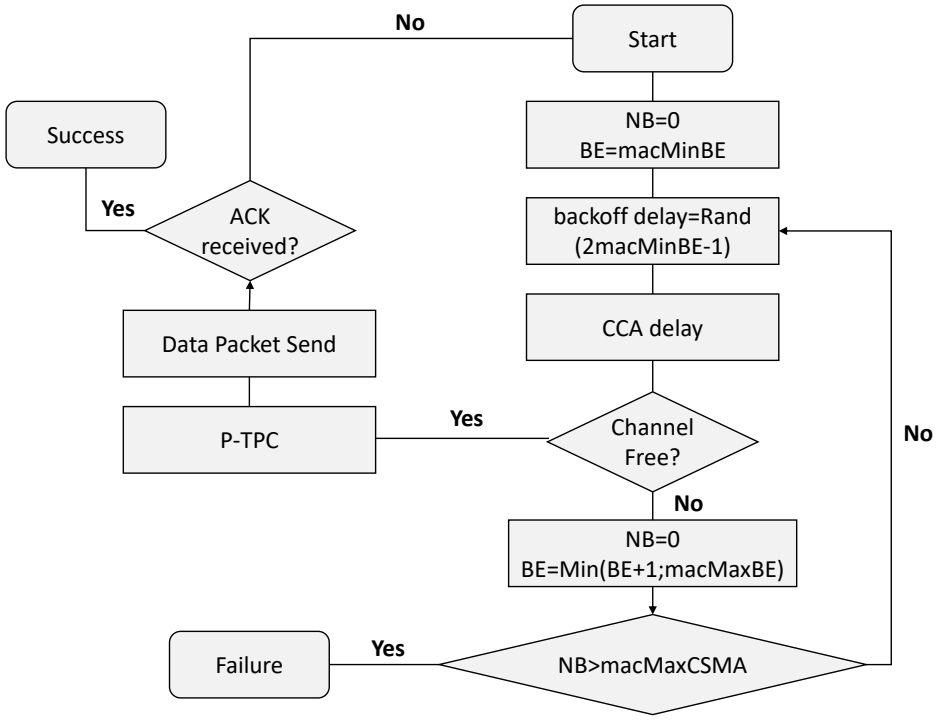

Figure 6.16. Data transmission flowchart as a result of the P-TPC mechanism inclusion in the beaconless mode of IEEE 802.15.4.

Algorithm 6.3. Radio channel Quality Prediction.

Input:

1: *Fading_Signal*: vector of RSSI samples corresponding to fading approximation
2: *N:* size of the fading approximation vector
3: *GC_InstantsFading:* vector, with size *N*, of gait cycle instants of each index of *Fading_Signal*
4: $T_{current}$: the time of the current time point
5: $T_{FirstAnchor}$: the time point of the last detected anchor (first one)
6: *GC_Instant*: the current gait cycle instant
7: *Current_GC_Period:* the current gait cycle period
8: *Index*: index of the current gait cyle in the *GC_Instant*

Output:

9: *Current_RSSI:* the current fading magnitude

Begin

10: $GC\_Instant \leftarrow ((T_{current} - T_{FirstAnchor})/ Current\_GC\_Period)*100$
11: **for** k=1,2,…, *N* **do**
12: **If** *GC_InstantsFading* (k-1)< *GC_Instant*≤ *GC_InstantsFading*(k) **then**
13: *Current_RSSI* ← *Fading_Signal* (k)
14: **end if**
15: **end for**

End

LQE and TPL blocks is required in order to reach an optimal TPL. A TPL Control solution based on the reactive-based approach (dynamic one) was chosen to obtain the optimal TPL as fast as possible. This solution required fewer control interactions, between the LQE and the TPL clocks, in order to reach the optimal TPL. Considering, as an example, the situation in which there is a high difference between the estimated RSSI value and the receiver sensitivity, the transmission power can be configured with a lower TPL. As shown in Algorithm 6.4, the TPL control updates the output power to the TPL that is in the middle of the TPLs range, which is defined by the two bounds: minimum TPL available in the radio transceiver and the current TPL. Several LQE-TPL control interactions might be required to reach the optimal value. As depicted in Figure 6.10, there were some residuals from the estimation operation and from the TPL influence on the fading magnitude as a consequence of the fast-scale fading. Therefore a threshold (variable *R* in Algorithm 6.4) higher than the receiver sensitivity must be used in order to avoid that during a gait cycle period the absolute RSSI values do not drop to values lower than the sensitivity threshold of the radio due to the high variability of the communication signal.

As shown in Table 6.2 and Figure 6.17, the optimal TPL is typically reached within 0.093 ms (maximum observed was 0.13 ms to an experimental testbed performed during one gait cycle of 1.7 s). The fast execution of the several P-TPC mechanism components offers the system a high control of the transmission time.

The memory footprint of the main components of the P-TPC mechanism are shown in Table 6.2. The AMDF is the component that requires more RAM resources, since several acceleration

Algorithm 6.4. TPL Control block based on reactive-based approach

```
Input:
 1: Current_RSSI: the current fading magnitude
 2: Slope_fitModel: slope of the TPL fit model
 3: TPLs_vector: set of TPLs available on radio transceiver
 4: High_IndexTPL: index of the highest TPL in TPLs_vector
 5: Low_IndexTPL: index of the lowest TPL in TPLs_vector
 6: OptimalTPL_found: Boolean variable to indicate that optimal TPL is found
Output:
 7: Optimal_TPL: estimated optimal TPL
Begin
 8: currentIndex ⟵ High_IndexTPL
 9: do
 10:   currentIndex ⟵ currentIndex+Int((Low_IndexTPL- High_IndexTPL)/2)
 11:  If (Current_RSSI + (TPLs_vector(currentIndex) * Slope_fitModel)) > R then
 12:     High_IndexTPL ⟵currentIndex
 13:  else
 14:    Low_IndexTPL ⟵currentIndex
 15:    currentIndex ⟵High_IndexTPL
 16:  end If
 17:  If Int((Low_IndexTPL - High_IndexTPL)/2)==0 then
 18: OptimalTPL_found ⟵True
 19:  end If
 20: while OptimalTPL_found==False
 21: Optimal_TPL ⟵TPLs_vector(currentIndex)
End
```

samples have to be kept in memory in order to detect the periodic movement and the extraction of the first gait cycle period.

The adoption of the DTW method and the computation of the whole distance matrix would consume 90% of the PROTACTICAL Nodes' memory resources (RAM), whereas the proposed solution (based on calculation of the Euclidean distance relative to anchors) only requires approximately 50 bytes.

6.4 Performance Evaluation

The performance of the P-TPC mechanism was evaluated using three different metrics: Packet Reception Rate (PRR), latency time, and the power consumption for each successfully transmitted data packet (obtained by dividing the total power consumed for all transmissions by the number of successfully delivered data packets).

The performance assessment was made by comparing the P-TPC mechanism with other TPC mechanisms. Due to the lack of TPC solutions that are designed to operate while the user is performing any dynamic activity, the Sample-Hold and Enhanced-Hold TPC mechanisms and the AA-TPC/G-TPC were selected and used to compare and assess the performance results. Three different configurations were used as TPL control solutions: linear, binary, and dynamic.

The TPC mechanisms were executed for a period of time equivalent to 20 gait cycles (slow and fast walking with gait cycle periods varying from 0.96 s up to 1.4 s), at both indoor and outdoor environments. The test was repeated three times for each scenario. Regarding the

Table 6.2. Memory footprint of the main P-TPC mechanism components as well as their execution time.

TPC	Flash (B)	xData/RAM (B)	Execution Time (ms)
AMDF	4288	1448	493.141
Accelerations tracking with gait cycle period updating	1296	144	0.103
Gait Cycle Period Update	1116	134	0.016
TPL Control	1620	320	0.0933
LQE	4396	655	0.078
Acceleration Sampling and Filtering	1299	48	0.127

AA-TPC/G-TPC experimental testbed, the RSSI value of -81 dBm and -86 dBm were set as the higher (TRH) and lower (TRL) limits of the RSSI target range (c.f. subsection 3.2).

The P-TPC mechanism updates the output power to the minimum TPL level that might ensure a RSSI sample lower than a threshold (similar to the lower RSSI value target range boundary). This threshold parameter is then updated at run-time and can take up to four different values. The threshold parameter is scenario and on-body propagation condition dependent (LOS or NLOS) thus, threshold values of -93 dBm (LOS) and -85 dBm (NLOS) were used for outdoor transmissions. During indoor transmissions the threshold values were set to -91 dBm (LOS) and -82 dBm (NLOS). The performance results obtained in terms of PRR, average TPL, energy per data packet (EPP), traffic overhead and average latency time are summarized in Table 6.3.

Only the experiments performed by subject 1 were included, since results from the two other subjects were found to be similar.

6.4.1 Reliability

The results summarized in Table 6.3 reveal that TPC mechanisms performance in terms of PRR follows a pattern. Since, the PRR values are slightly better at outdoors scenarios due to the nature of the signal, when compared to the values obtained for indoors scenarios.

The Sample-and-hold TPC mechanisms are able to ensure a PRR near to 100%, whereas Enhanced-hold solutions achieved a lower PRR percentage (above 95%), regardless of the scenario. For all the scenarios and operation environments, transmissions performed with TPLs updated at run-time lead to PRRs values lower than transmissions performed with a static and pre-defined TPL (-0.5 dBm).

PRR results verified at the indoor scenarios decrease between 1.6% and 3% relative to the results obtained at outdoor scenarios. Only the enhanced-hold dynamic-based TPC achieves better results in an indoor scenario. These results match with the conclusions reported in [46], where authors concluded that conservative solutions are more suitable to more dynamic radio

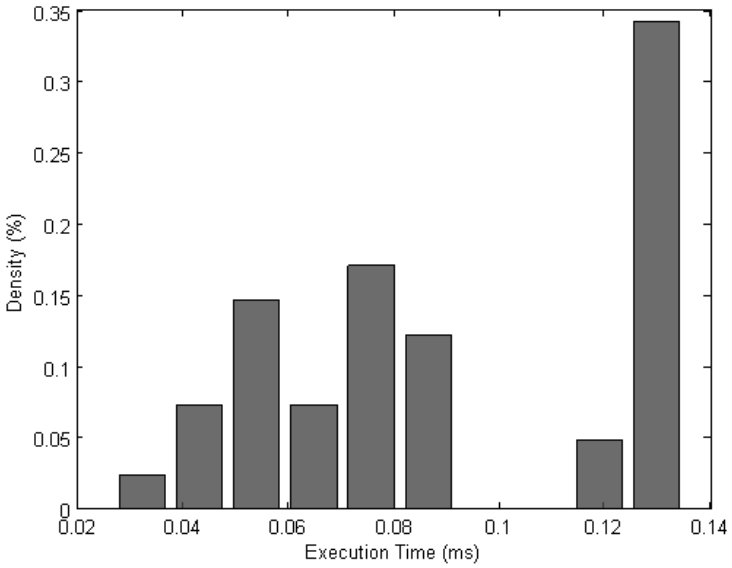

Figure 6.17. Execution time of the TPL Control algorithm performed on a cc2531 during a gait cycle of 1.7 s.

channels (indoor environments), whereas aggressive approaches are advisable for stable radio channels (outdoor environments).

Although closed-loop control based TPC results meet the reliability requirements of WBAN applications, the results are worse than those obtained with a static TPL -0.5 dBm (there is almost no losses of data packets). The AA-TPC and G-TPC solutions ensure that 100% of the data packets are successfully deliver to the Coordinator node. The P-TPC mechanism achieves a PRR very close to the maximum value. Although some data packets have been lost during transmissions, the PRR results obtained show that the number of data packets lost during transmissions is indeed very low. Therefore, the reliability requirement imposed by IEEE 802.15.6 TG is meet by the proposed P-TPC mechanism, with a performance equivalent to static transmissions at a fixed -0.5 dBm TPL.

6.4.2 Latency

The latency is interpreted as the time corresponding to the number of data packets that need to be retransmitted until the data packet is successfully delivered to the receptor. Transmitted data packets have a sequence number, allowing the receptor to identify data packets that were not received.

The average latency time presented in Table 6.3 suggests that it is very unlikely that, when an outage occurs (i.e. RSSI value lower than receiver sensitivity or data packet not received), its period be larger than the maximum latency time allowed for WBAN applications. Even though, the maximum average latency time at outdoors scenarios occurs when an E-H TPC solution was employed, whereas S-H TPC solutions lead to worst latency time results for indoors experiments.

Table 6.3. TPC mechanism performance results

TPC	PRR (μ±σ %)	Average TPL (dBm)	EPP (mJ/data packet)	Traffic Overhead (%)	Average Latency (ms)
Indoor					
Static TPL	98.9±0.8	-0.5	1.57	0	35
P-TPC	98.7±0.9	-11.7	1.03	3	37
S-H L	95.2±2.9	-12.7	1.10	41	46
S-H B	97.9±1.1	-10.3	1.06	30	48
S-H D	97.2±1.2	-9.7	1.19	33	46
E-H L	95.9±1.1	-12.5	1.09	37	37
E-H B	96.1±1.9	-10.21	1.08	33	43
E-H D	98.1±0.4	-10	1.06	33	35
AA-TPC	100	-16.7	0.92	31	948
Outdoor					
Static TPL	99.1±0.2	-0.5	1.57	0	35
P-TPC	98.9±0.2	-17.1	0.93	3	35
S-H L	98.2±0.7	-7.6	1.18	32	35
S-H B	99.8±0.1	-11.6	1.04	30	35
S-H D	99.1±0.5	-9.9	1.16	29	38
E-H L	97.5±1.2	-8.7	1.19	36	41
E-H B	98.4±1.5	-9.7	1.17	28	38
E-H D	97.2±1.4	-9.5	1.18	28	53
AA-TPC	100	-18.4	0.92	31	721

The proposed P-TPC mechanism ensures an average latency of 35 ms, being equivalent to the period between data packets transmissions in the experimental testbed (no loss of two consecutive data packets). A lower latency time is expected since the P-TPC mechanism ensures a high level of reliability, indicating that few (or even none) data packets are lost. Since the AA-TPC and G-TPC mechanisms only transmits when the link is at his best quality within each gait cycle, these solutions lead to latencies higher than the maximum allowed for WBAN applications, namely 948 and 721 ms. The performance of these solutions in terms of latency is gait cycle dependent and data packets transmission frequency-dependent.

6.4.3 Energy Consumption

Since the TPC mechanisms that employ the closed-loop control introduce a number of control messages, the power consumption analysis must include the cost of data packets and control packets transmissions. The energy consumed by the proposed P-TPC mechanism must translate the energy effort on the following tasks: data packets transmission, control packets transmission at the *Fading Approximation* stage (15 control packets), acquisition of the acceleration samples at *TPC mechanism* stage (in order to track the gait cycle period and phase offset) and finally power consumption due to the acceleration readings from the inertial sensor at the *Acceleration Acquisition* stage. The accelerometer (MEMS inertial sensor) used consumes 0.25 mW when active and 0.001 mW when in power-down mode. The P-TPC

mechanism starts by acquiring the acceleration samples for an interval of 4.2 s. After the AMFD algorithm is executed and the existence of periodic movements is verified. Thus, the energy consumption on *Acceleration Acquisition* stage is equivalent to the energy consumption of the transmission of a maximum-sized IEEE 802.15.4 DATA frame (133-byte Physical Protocol Data Unit) without ACK, at -0.5 dBm. In order to reduce the energy consumption in this task (gait cycle period and phase offset tracking), the accelerometer readings have a duty cycle of 40% of the gait cycle interval (1.3 s is taken as reference), reducing the energy consumption by gait cycle to the equivalent of a transmission of a control packet.

To determine the transmission cost per data packet, the model proposed in [9] was adopted, where packet energy cost is given by

$$E = \frac{(V.I.L)}{C} \tag{6.6}$$

where *V*, *I*, *L*, and *C* represent the supply voltage, the current drawn, the data packet size, and the radio channel capacity, respectively. For the results reported in this article, the following values were used: *V*=3.2 v, *C*=19.2 Kb/s, *L*=67 bytes (data packets) and *L*=3 bytes (control packets). The current drawn during transmission is TPL-dependent and can be consulted in [170]. The control packets are transmitted at the maximum allowed TPL.

The results summarized in Table 6.3 show that the closed-loop control TPC mechanisms require a high number of control packets at the indoor scenarios, when compared to the number obtained at outdoor scenarios, in order to keep RSSI value within the RSSI value target range. The TPC mechanism that relies in linear-based TPL Control solutions transmits a high number of control packets (an average 50 control packets) than the TPCs configured with binary or dynamic based TPL Control solutions. Although TPCs at the indoor scenarios transmit a higher number of control packets than at outdoors scenarios (≈30 on average), energy consumption per data packet is relatively similar for both environments, since at outdoors there is a negligible energy contribution from multi-path components. Consequently, fading magnitudes drop to values near the receiver sensitivity when in NLOS situations. Therefore, the average TPL is higher at outdoor than at indoor scenarios. The TPC mechanisms based on closed-loop control operation principle were able to reduce the overall energy consumption when compared to a system that transmits at the maximum TPL. An energy consumption reduction between 24% and 34% was achieved for outdoor scenarios, whereas for indoors scenarios the overall energy consumption reduction was between 24% and 32%, when compared to static TPLs transmissions. It is also interesting to note that the closed-loop control TPC mechanisms that achieved the lower energy consumption per data packet at outdoor scenarios are those that

adopted an aggressive TPL Control. For indoor scenarios, all TPC mechanisms achieved similar performance in terms of energy consumption per data packet.

The proposed P-TPC mechanism achieved an energy consumption of 1.03 mJ per data packet at indoor scenarios and 0.93 mJ per data packet at outdoor scenarios, including the acceleration sampling (AMDF and DTW algorithms). This corresponds to an overall energy reduction between 34.7% and 41.7%, for transmissions at indoor and outdoor scenarios, respectively. The P-TPC mechanism achieves similar energy saving performance to the AA-TPC/G-TPC at outdoors. However, for indoor scenarios, these mechanisms minimize the energy consumptions by 7% when compared to the P-TPC mechanism, since in such scenarios transmissions at any time within the gait cycle require the use of higher TPLs. Furthermore, as shown in Table 6.3, the P-TPC mechanism offers the most significant improvements in terms of energy-efficiency transmission, from all the mechanisms assessed. The P-TPC mechanism adds an extra traffic overhead of only 3%. It is an insignificant number when compared to the number of control packets transmitted by other TPC mechanisms assessed. Furthermore the proposed P-TPC mechanism reduces the bandwidth utilization. Closed-loop control based TPCs introduce high traffic overheads (near to 40%) to ensure an efficient control of the TPL adopted in data packet transmissions. Moreover, the average TPL during experimental tests of the P-TPC mechanism are, on average, between 9.5 and 5.5 dBm lower than the closed-loop control based TPC mechanisms. This result might reduce the RF interference level with coexisting nodes and networks.

6.5 Summary

This chapter described a novel TPC mechanism for on-body communications suited to scenarios where the user is performing periodic movements, such as walking or running. The fact that the user is performing periodic movements could limit the applicability of the proposed solution, however, as suggested in [145], the TPC mechanism can adopt a closed-loop control based scheme, for instance the E-H approach, in instants during which the user is not performing a periodic movement (reliability and latency requirements are still ensured but the average TPL, energy consumption and traffic overhead increases).

How does walking affect the fading signal pattern and is this influenced by the human body properties?

The fading signal (after extracting the small-scale fading component) has a period that matches with the user's gait cycle period. High Link-Margins (LM) gains were verified during the user's gait cycle. Accordingly to the reported LM gains and radio channel gains, the on-body

channel is able to ensure the Quality-of-Service (QoS) requirements, but, as a consequence of the high LM gains, the communication system presents an inefficient use of the energy available. A peak-to-peak magnitude between 20 to 25 dB and maximum LM gains between 25 and 30 dB are observed at outdoors. When in NLOS propagation scenarios, the LM gains are lower at outdoor scenarios (as a consequence of the absence of LOS wave's energy contribution as concluded in chapter 5). Although the measured RSSI values are close to the radio module sensitivity when outdoors, occurrences of lost data packets are practically inexistent for all the tests made.

How can accelerations in the user's stride be tracked and how to reduce the complexity of mechanisms (addressed in the literature) to be implemented at the Edge of the Network nodes?

The P-TPC mechanism continuously tracks the gait cycle periods and phase offset to determine the current instant within the on-going gait cycle in order to estimate the current radio channel quality. The first task of the P-TPC mechanism is to detect periodic movements through the AMDF algorithm. The TPC is ready to control the TPL after just 4.2 s, which is the time required to acquire and process the acceleration data required to evaluate the existence of periodic movements and extract the first gait cycle period. To track and determine the acceleration on the gait cycle, a modified DTW algorithm, which relies on acceleration signals that are locally collected, was proposed, discussed and implemented.

Can traffic overhead be reduced and TPC can still be employed effectively to dynamic scenarios?

The LQE relies in a fading approximation function, which follows a closed-loop control during a time interval equivalent to the first gait cycle period. This function is used to estimate the radio channel quality in function of the on-going gait cycle instant. This approach enabled to reduce the traffic overhead in comparison to the traditional closed-loop control based TPC solutions. The user's gait cycle varies accordingly to the speed of the movement, but fading features such as fading magnitude or LM gains remain unchanged at higher and lower RSSI values peaks. This demonstrates that there is a strong correlation between relative Edge of the Network node locations (in relation to the Coordinator node) and the fading magnitude.

How can the proposed TPC mechanism be integrated into the protocol stack as a performance improvement strategy?

Some TPC solutions addressed in the literature have a very low agility, since these solutions are complex and require the exchange of a large quantity of packages. To ensure that the P-TPC

mechanism has enough ability to accommodate time-variant changes in the radio channel quality, the proposed LQE algorithm was designed to be integrated into the MAC layer of the protocol stack. This approach turns this solution feasible for any MAC protocol, since the MAC schemes introduce some latency in data packet transmissions. The LQE is a very simple process (0.078 ms is the time required to estimate the current radio channel conditions) and it is only performed after detection of a free radio channel. Thus, by the time that radio channel is estimated, the TPL updated, and the data packet transmitted and the new output power is received by the Coordinator node, the radio channel has not suffered significant changes.

Is the proposed TPC approach fast and agile enough to estimate the radio channel and adjust power before suffering changes in the radio channel quality?

The Link Quality Estimator (LQE) relies in a fading approximation function. It was demonstrated that there exists a linear relationship between the TPL adopted on transmissions and the consequent RSSI value measured at the receiver, even for dynamic scenarios (Quwaider et al. have observed this relation for static scenarios [48], but for the best of authors knowledge, it has never been assessed for dynamic scenarios). A linear model that describes the RSSI value in function of the TPL was proposed (section 6.2.2).

The several implemented mechanisms, which are executed at different stages of the proposed P-TPC mechanism state machine, have a very low complexity, allowing their implementation in Edge of the Network nodes. Moreover, the dependency of the proposed solution in terms of exchanged control packets, between the node and the coordinator) is very low.

Can energy efficiency and reliability of communications be optimized without sacrificing latency?

The extensive experimental evaluation carried out showed that the proposed P-TPC mechanism is able to reduce the energy per data packet between 24 and 34%, when compared with a system that transmits data packets at the maximum allowed TPL, without sacrificing latency and reliability. The P-TPC mechanism achieves better performance results than state-of-the art TPCs mechanisms that follow a closed-loop control operation principle. Furthermore, the number of exchanged control packets is ten times lower than other existing closed-loop control based TPC mechanisms. The extra traffic overhead of the proposed solution is only 3% (promoting an efficient use of the bandwidth). Finally, the proposed P-TPC mechanism requires an average TPL lower than the other TPC mechanisms to ensure a reliable communication link, which reduces the RF interference and keeps SAR low.

CHAPTER 7

PACKET SCHEDULER FOR ON-BODY COMMUNICATIONS IN WBANS

The body movement has a significant effect on the first- and second-order statistics of the communication signal, as analysed in Chapter 5. According to Cheffena et al., the body movements can be used to estimate the fading signal, since the angular variations of the antenna gains promote time/varying channel conditions [158]. Therefore, in this chapter, the possibility of describing the on-body canal (Node-PROTACTICAL 7) according to the body posture, the operation environment and the Node-PROTACTICAL 7 relative position is discussed and analysed.

Since communications around and along the human body are too complex, turning impractical the development of an exact analytical formula to predict the radio channel conditions, the main research question addressed in this chapter is: *Can the on-body radio channel quality (RSSI and Outage occurrences) be anticipated through a model?* To answer this question, Neural Networks and Fuzzy Inference Systems were explored to model the nonlinear dynamical system (on-body channel quality). In section 7.1, a generic description of some of the most popular soft computing techniques is provided, while, in section 7.2, a detailed description of the hybrid soft computing ANFIS (Adaptive Network based Fuzzy Inference System) is provided.

The second research question addressed in this chapter is: If obtained, *how can such a model be used to reduce the PER and minimize the energy consumption in on-body communications?* To answer this question, in section 7.3, a novel approach that aims the increase of the system reliability, reduction of the SAR in wireless communications at expenses of latency is proposed. This approach explores the advantages of two different mechanisms, namely packet schedulers and mechanisms TPC, by merging them into a new hybrid approach. Detailed information about the proposed solution is provided in section 7.4. Furthermore, the performance of the proposed solution in different scenarios is also analysed in section 7.4 and performance results are compared to that of other solutions addressed in the literature.

Unlike the majority of the packet schedulers addressed in the literature (that are only suitable for scenarios where users perform periodic movements [128], [130], [137], [145]), the goal is to develop a mechanism that is applicable to either periodic or non-periodic movements.

The nuclear elements of this mechanism are the two ANFIS models built to describe the on-body channel (first research question).

7.1 Soft Computing Techniques

The soft computing techniques are a popular methodology for system identification to the purpose of modelling linear or nonlinear dynamical systems. Unlike the conventional hard computing techniques, the soft computing ones do not rely in mathematical models to identify and control dynamical systems. The soft computing techniques accommodate the imprecision of the real world through the exploration of the tolerance for imprecision, uncertainty and partial truth to achieve robustness, low solution costs and tractability. One of the most powerful soft computing techniques is called Adaptive Network based Fuzzy Inference System and it is categorized as a hybrid intelligent technique [171]. This chapter focus on using this soft computing as a tool for modelling an ill-defined system (on-body communications applied to many scenarios) in order to forecast the radio channel conditions in terms of the radio channel quality (RSSI and PER). As the ANFIS technique is a hybrid approach (two soft computing techniques are combined), the current section aims to introduce and describe the ANFIS technique, as well as, providing a brief overview of the techniques combined in ANFIS, namely the Neural Network (NN) and Fuzzy Logic (FL).

7.1.1 Neural Network-based Algorithms

The NNs resulted from the researchers' effort in modelling the human brain. Their main motivation is the fact that human brain is able to process incomplete information thanks to the biological properties of the nervous systems and the brain[171]. Developments in this scientific field drove to neural networks that model the human brain as a continuous time nonlinear dynamic system. The NNs follow an architecture in layers in which processing units (neurons) are interconnected by weights. Through the adjustment process of the interconnections between layers, the neural networks are able to learn and adapt from data. According to Buragohain, the most important features of this soft computing technique are [171]:

- Presence of a large number of simple processing units;
- Presence of a large number of parallel processing units;
- Presence of strongly connected processing units;
- Robustness against the failure of single processing units;
- Learning from data.

The architecture of a neural network is composed by layers that can be divided into three groups, as illustrated in Figure 7.1. These layers are as follows:

- Input layer, it is composed by all the input processing units together;
- Hidden layer, it is any layer that is between the input and output layer (intermediate layer). In any neural architecture might more than one hidden layer is found;
- Output layer, all the output processing units constitute this layer.

The neural network architecture offers a methodology for identification, learning and adaptation. This conceptual principle has been enhanced along the time, resulting in a set of popular neural network architectures, namely the Neuro-Fuzzy Network [143], Radial Basis Function Network (RBFN) and the Multi-Layer Perception (MLP) network [172].

7.1.2 Fuzzy Logic-based Algorithms

Fuzzy logic has two different meanings, in a narrow sense, FL is a logical system an extension of multivalued logic. In a wider sense, FL is a synonymous with the theory of fuzzy sets. This relates classes of objects with unshaped boundaries (i.e. the boundaries between qualitatively things exist but it is difficult to exactly defined them) in which membership (MF) is a matter of degree where the possibility of partial membership in it is admitted. The following example help us to understand the FL. In a two-valued logic (where either something is in or is out), Fridays are totally excluded of the group of weekends days. However, the human experience might suggest that Fridays are too part of the weekend (for instance, after finishing the working scheduler), thus, the multivalued logic (where the truth of any statement becomes a matter of degree) permits the inclusion of Fridays in both groups: week days and weekend days. The human intuition allows us to interpret and process imprecise and incomplete information received from the perceptive organs. The FL mimics the human brain through a methodology that computes with words to deal with impression and granularity. In this

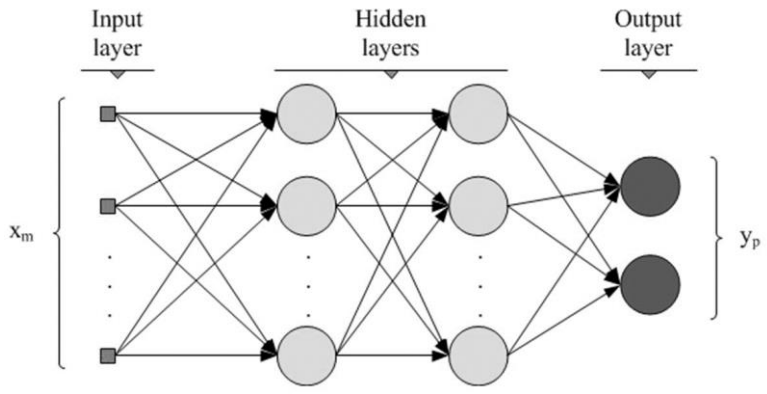

Figure 7.1. Types of layers that compose a NN [195].

systematic approach, the linguistic variables (whose values are words rather than numbers) is a basic concept.

The FL theory has been targeted to applications where the tolerance for impression can be explored to decrease the solution's cost. The Fuzzy Logic was introduced by Zadeh [173], [174] and since then it has been employed in a wide variability of applications thanks to the research and implementation of Fuzzy Inference Systems (FIS). Their applications range goes from consumer products (such as cameras, camcorders, washing machines, and microwave ovens) up to industrial process control (such as robotics, automatic control), medical instrumentation, decision-support systems (such as pattern classification, data classification), and portfolio selection (such as expert systems, decision making). The process of Fuzzy inference refers to the formulating the mapping from a given input to an output based on the concepts of fuzzy set theory, fuzzy if-then rules and fuzzy reasoning. The linguistic variables are expressed as fuzzy sets and defined in terms of degree of their associated membership functions. The fuzzy rules are composed by an antecedent and a consequent and have usually the following format:

Rule 1: **IF** *x* is *A* and *y* is *B* **THEN** *z* is *f*

where *x* and *y* are the input variables, the *A* and *B* are the fuzzy sets (on previous example, the day of the week is the input and weekend and week are the fuzzy set). These two, when merged with logic operators, form the fuzzy rule's antecedent. The $z=f$ in the consequent can be a constant, a fuzzy set or a crisp function. The fuzzy rules implement an efficient mechanism to deal with fuzzy consequences and antecedents. Finally, the fuzzy reasoning is a mechanism for performing inference with respect to the rules in order to reach to a reasonable output or conclusion [171]. Thus, a FIS is composed by three main components, namely a rule base comprising of the fuzzy rules, a database defining the fuzzy rules' membership functions and the reasoning mechanism. The most important features of the FIS are as follows:

- Conceptually easy to understand;
- FL is based on natural language, i.e. the inputs and outputs are described through qualitative description used in everyday language;
- It is flexible;
- Tolerant of imprecise data;
- FL can model nonlinear functions of arbitrary complexity through the match of input-output data;
- The expert experience can influence the final FIS in contrast to the neural networks where impenetrable models are created through the tanning data;

- The FL does not necessarily replace the conventional control methods, in many cases it aims to simplify and enhance their implementation.

Five steps must be carried out to reach a FIS from which decisions can be make, namely Fuzzification, Aggregation, Activation, Accumulation and Defuzzification. These steps might vary according to the type of Fuzzy system adopted. Although the steps of any FIS type are the same, they might have some differences. Therefore, the Mandami Fuzzy System type is selected in order to describe the set of steps required to reach a FIS.

- **Fuzzification**, in this step the inputs are taken to calculate the degree of belongingness to each of the fuzzy sets via the associated membership function. Usually, the inputs are a crisp numerical value limited to the universe of the discourse (the range of all possible values for an input to a fuzzy system) of the input variable and the output is the degree of membership in the fuzzy set (result is always between 0 and 1);
- **Aggregation**, after knowing the degree to which each part of the antecedent for each rule they are combine by logical operators, such as AND and OR. If the antecedent of a given rule is composed for more than one membership value from fuzzified input variables, one value that represent the antecedent result is obtained through the application of a fuzzy operator, since the output is always a truth value. Two AND methods are usually provided, the Min operator and Product operator to classification and approximation tasks, respectively. Two OR methods are usually implemented, namely the Max and the Probor (probabilistic method, which Is calculated according to the formula: $probor(a,b) = a + b - ab$) operator are used to classification and approximation tasks, respectively;
- **Activation**, the weight of each rule (value between 0 and 1, usually this value is one in order to do not affect the implication process) is calculated and applied to the value given by the antecedent of the given rule. Then the implication process is carried out to each rule, it receives as input a single number given by the antecedent of the given rule and provides as output a fuzzy set (represented by a membership function) which is reshaped using a function associated with the antecedent (a single number).
- **Accumulation**, in this step all the fuzzy sets given as outputs of each rule on the activation step are combined into a single fuzzy set to a decision be make.
- **Defuzzification**, in this step the fuzzy set built in previous step is received as input and a single value is provided as output. This crisp value can be obtained through different

methods, such as the centre of gravity, bisector of area, mean of maximum, smallest of maximum and largest maximum.

There are several different types of Fuzzy systems, which differ in terms of the Defuzzification method adopted. The three main ones and the mostly used Fuzzy systems are as follows:

- Mandami Fuzzy System, it is also known as the linguistic fuzzy system. This process is not computationally efficient, since a method (at defuzzification step) must be performed in order to the crisp value be reached;
- Singleton Fuzzy system, no fuzzy sets integration is necessary, since the rules' output are restricted to a singleton membership function. This type of Fuzzy system is considered a special case of the Mandami Fuzzy System and is widely employed in industry [171], as the complexity of the Defuzzification is simplified as well as the computational demand.
- Takaga-Sugeno Fuzzy System, this technique is considered an extension of the Singleton Fuzzy System. The output of each rule, *f* of the rule above identified as Rule 1, is a crisp function. This is represented by *f(x,y)* and usually is a polynomial for the input variables *x* and *y*.

7.1.3 Neuro Fuzzy-based Algorithm

The hybrid intelligent tools refers to techniques that combine the advantages of two or more soft computing techniques. The combination of the complementary techniques neural network and fuzzy logic led to hybrid system called neuro-fuzzy hybrid system, which is one of the most popular hybrid intelligent approach. In this regard, the main advantages of each soft computing technique are explored in this hybrid tool, namely the learning capabilities of neural networks to recognize patterns and adapt themselves to react to changes in the environment; and the knowledge representation and inference capabilities of fuzzy logic [135]. These approaches have been targeted to a high variety of complex and ill-defined systems where mathematical models are difficult to build. The neuro-fuzzy models can be obtained easier and are able to reflect properly the uncertainty of systems under consideration [171]. An effective method developed by Roger Jang for this purpose is called Adaptive Neuro-Fuzzy Inference System [175]. The ANFIS models can take the function of prediction system behaviour and/or system control [176]. To construct a neuro fuzzy model, the same steps required to build a FIS which are above describe must be carried out. These steps are performed in sequentially arranged

layers of the neural networks. The parameters of the extracted rules (for instance the membership functions) are then adjusted through the neuro network architecture. The neuro-fuzzy soft computing technique has the following features [171], [176]:

- This approach is inspired on biological neurons and is concerned with model extraction from numerical data (unlike symbolic artificial intelligence) which represents the dynamic behaviour of a system;
- It is a learning technique that uses fuzzy logic to transform given inputs into a output through highly interconnected neural networks processing elements and information connections;
- The human expertise – in the form of conventional knowledge – can used to build the set of rules that map an input space to an output space the rules;
- In the absence of system models or human expertise, the FIS models can be constructed through available sampled data;
- Soft computing is targeted to real world applications where conventional approaches are not suitable. Conventional techniques require either detailed description of the problems or precise mathematical model, which in most cases is impracticable;
- It relies more in intensive computing than in precise background knowledge to build the rules list;
- It enables accurate learning through the refinement of the fuzzy ID-THEN rules. In this regard, the interconnected neurons and information connections are weighted to map the numerical inputs into an output. The weights are tuned to optimize the model;
- Both linguistic and numerical knowledge are easily incorporated;
- Fault tolerance against broken neurons or rules are automatically ensured by the parallel and redundant architecture of the derived models. However, the model performance degrades gradually;

7.2 Adaptive Network based Fuzzy Inference System

A hybrid soft computing ANFIS was originally presented in 1993 by Jang [177]. ANFIS has been explored in the literature to describe and represent Mandami, Singleton or Takagi-Sugeno Fuzzy Systems by an ANFIS architecture. The process of building an Fuzzy model follows four steps: gathering data related to the system to be modelled, derivation of an initial FIS model from the input-output data, selection of the input variables of the FIS model, and updating the initial FIS model (fine tune the rules). A network structure like that of NN is

used to interpret the input/output map and to optimize the performance of the FIS. In this structure, inputs are mapped through input MFs and associated parameters, so-called premise parameters, and then through output MFs and associated parameters, so-called consequent parameters, to outputs. These parameters will keep changing during the learning process, since the weights of each neuron is updated. The current section describes the typical structure of ANFIS models as well as all the steps above mentioned.

7.2.1 ANFIS Structure

In order to describe this architecture, two IF-THEN rules based on a first order Takagi-Sugeno model with two inputs and one output are considered, also called type-3 FIS. In this model each rule's output is a linear combination of the input variables added by a constant term. The rules of this FIS might be stated as:

Rule 1: **IF** x is A_1 and y is B_1 **THEN** $f_1 = p_1 x + q_1 y + r_1$

Rule 2: **IF** x is A_2 and y is B_2 **THEN** $f_2 = p_2 x + q_2 y + r_2$

where x and y are the inputs of the model under consideration; A_i and B_i are the fuzzy sets; f_i are the outputs within the fuzzy region specified by the fuzzy rule; and, finally, p_i, q_i, and r_i are the design parameters that are determined during the learning process. The final output of the present example is the weighted average of each rules's output. Figure 7.2 depicts the ANFIS architecture that describes the reasoning mechanism of a Takagi-Sugeno model, where circles represent the fixed nodes and squares indicates the adaptive nodes. Each layer of the five-layer architecture of the ANFIS model that represent the two rules are explained in detail below.

- **Layer 1 (Fuzzification)**. All nodes in this layer are adaptive and receives the inputs variable of the model and have as output the fuzzy membership grade of the inputs. The output, also called node function, is given by:

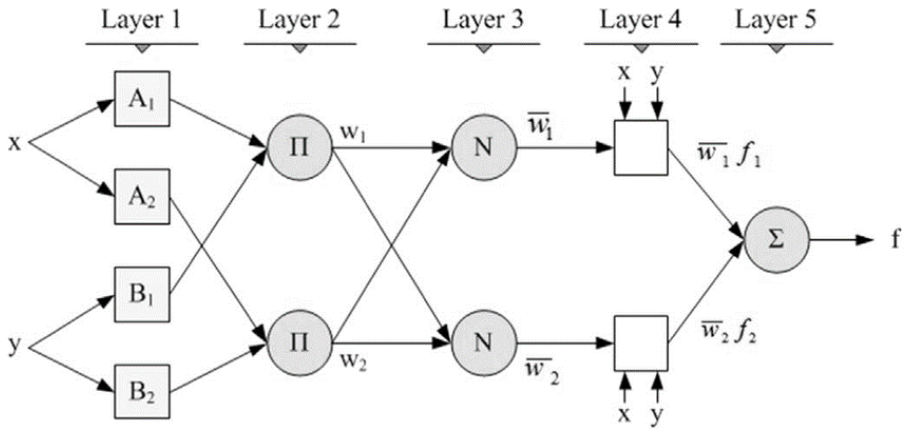

Figure 7.2. Architecture in layers of a Takagi-Sugeno ANFIS model.

$$O_{1,i} = \mu_{Ai}(x), i = 1, 2, \quad (7.1)$$

$$O_{1,i} = \mu_{Bi}(y), i = 1, 2, \quad (7.2)$$

where x and y are the inputs variables to node *i*, and A_i and B_i are the linguistic variable associated to their node function and $\mu_{Ai}(x)$ and $\mu_{Bi}(y)$ are the membership function of A_i and B_i, respectively. Different fuzzy membership functions can be adopted. Table 7.1 summarizes the most applied membership functions in ANFIS applications, where a_i, b_i, c_i and d_i are the premise parameter of the membership functions.

From the set of MFs above described, the bell shaped, and Gaussian membership function are the most predominant, since they overcome some drawbacks found on remaining MFs. For instance, a drawback pointed out to some MFs (such as triangular and trapezoidal) is related to the amount of information that is lost during the process of fuzzification. In regions of the triangular and trapezoidal MFs where the slope is zero, the MFs are not differentiable [171]. As a consequence, these MFs might have problems of learning from data.

- **Layer 2 (Inference or rule layer):** All the nodes are fixed and are responsible for calculating the firing strength w_i of each rule. Fuzzy logic operators are involver on this layer. The operator **AND** is applied in order to fuzzify the inputs. This operator is illustrated by symbol $\prod$, indicating that it is a simple multiplication. Therefore, the output of each node is then the product of all the incoming signs and can be represent as

$$O_{2,i} = w_i = \mu_{Ai}(x) * \mu_{Bi}(y), i = 1, 2, \quad (7.3)$$

- **Layer 3 (Implication layer):** All the nodes are fixed and each one calculates the ratio of the firing strength of a given rule to the sum of all the firing strengths of all rules. The output of this layer is the normalized (nodes are labelled by N) firing strength, which is given by

Table 7.1. Fuzzy Logic Membership Functions.

Membership Function	**Equation**	**Parameters description**
Bell-Shaped MF	$\mu_{Ai}(x) = \frac{1}{1 + \left[\left(\frac{x - c_i}{a_i}\right)^2\right]^{b_i}}, i = 1,2$	*c* determines the centre of the MF, *a* (is the half width) and b control the slopes at the crossover points {*c*-*a*, *c*+*a*}
Gaussian	$\mu_{Ai}(x) = exp\left[-\left(\frac{x - c_i}{a_i}\right)^2\right], i = 1, 2$	c represents the MF centre and a determines the MF width
Triangular-shaped membership function	$\mu_{Ai}(x) = \max\left(\min\left(\frac{x - a_i}{b_i - a_i}, \frac{c_i - x}{c_i - b_i}\right), 0\right)$	*a*, *b* and *c* (*a*<*b*<*c*) determine the x-axis coordinates of the three corners of the underlying triangular
Trapezoidal-shaped membership function	$\mu_{Ai}(x) = \max\left(\min\left(\frac{x - a_i}{b_i - a_i}, 1, \frac{d_i - x}{d_i - c_i}\right), 0\right)$	*a*, *b*, *c* and *d* (*a*<*b*<=*c*<*d*) determine the x-axis coordinates of the four corners of the underlying trapezoidal
Sigmoid curve	$\mu_{Ai}(x) = \frac{1}{1 + \exp[-a(x - c_i)]}, i = 1, 2$	a control the slope at the crossover point *x*=*c*; de sign of a specifies if the sigmoid is open right or left

$$O_{3,i} = \overline{w_i} = \frac{w_i}{w_1 + w_2}, i = 1, 2, \tag{7.4}$$

➢ **Layer 4:** In this layer, the nodes are adaptive. The output of each node is the product between the normalized firing strength of the rule under consideration and a first order polynomial. The output of this layer is given by

$$O_{4,i} = \overline{w_i} f_i = \overline{w_i}(p_i x + q_i y + r_i), i = 1, 2, \tag{7.5}$$

where $\overline{w_i}$ is the output of the layer 3 and the set of parameters $\{p_i, q_i, r_i\}$ is the consequence parameter set.

➢ **Layer 5 (Defuzzification):** This layer comprises just one node (fixed one) that is labelled with $\sum$, indicating that this node performs the summation of all the incoming signals. The output is given by

$$O_{5,i} = overall\ output = \sum_i \overline{w_i} f_i = \frac{\sum_i w_i f_i}{\sum_i w_i}, i = 1,2, \tag{7.6}$$

7.2.2 Initial ANFIS Model

The initial FIS model derivation process, also called training methodology [177], establishes the initial number of inputs, the linguistic variables, the type of membership functions, and the number of rules. The initial model determines the number of input variables that are considered during the next step: input variable selection. Then, learning techniques are employed to tune the parameters of the initial model to reach the optimal ANFIS model. The first step of the training methodology is to gather the input-output pairs, which are obtained from the system that is to be modelled. This data set is called training data set and consists of a set of input and output vector that are used to find rules and the premise parameters of the MFs. In this regard, techniques, such as grid partition and subtractive clustering, have been used. Different initial ANFIS models can be obtained according to the technique adopted [178].

Grid Partition Technique

This technique divide the input space into rectangular subspaces, i.e. a number of fuzzy regions based on a pre-defined number of MFs and their types to form the antecedents, through axis-paralleled partitions of each region [171]. Figure 7.3 depicts the grid partitioned fuzzy subspaces for a Takagi-Sugeno ANFIS with two input variables (which input has three MFs). This technique requires high computational resources, since the number of rules increase exponentially with the number of variable inputs [178]. For example, the number of inputs of the system above is two and the partitioned fuzzy subset for each input is three, then the number

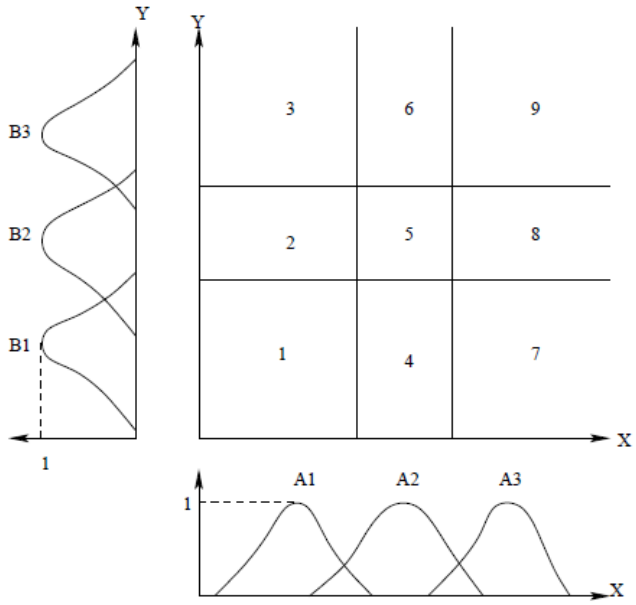

Figure 7.3. Application of the Grid Partition method in a problem with two inputs. The resultant Fuzzy subspaces are nine (as each input has three MFs) and are identified by a number from 1-9.

of possible fuzzy rules is 3^2. Consequently, this is only suitable for systems with a small amount of input variables. According to Jang, the number of input variables should be lesser than 6 [179].

Subtractive Clustering Technique

This technique distributes the data space into fuzzy clusters. It is applied to the input output pairs to for finding similarities and grouping similar information [180]. These groups, designated cluster of information points, are represented by cluster centres. In this technique every information point is considered with potential to be a cluster centre. It is expected different similarities between different groups of data points represented by cluster centres. The data point's potential is quantified as function of the Euclidean distances of all information points. The data points with a potential above a certain value as clusters centres. This technique collects *n* information points in an *M* dimensional space and each point x_i is setting as a potential cluster. Then, the potential (P_i) of each point is calculated through the expression

$$P_i = \sum_{j=1}^{n} e^{-\alpha \|x_i - x_j\|^2} \tag{7.7}$$

where $\|.\|$ denotes the Euclidean distance and the parameter α is given by:

$$\alpha = \frac{4}{r_a^2} \tag{7.8}$$

where r_a is the cluster radius that defines the neighbourhood, i.e. this parameter determines a sphere of data points with relevant influence on the potential cluster under consideration.

Information points that within the sphere with centre on the data point considered as potential cluster centre are accepted as neighbours. The constant value of the radius centre must be chosen in a way that an adequate quantity of clusters are inserted. A high cluster radius leads to generation of a small number of clusters, which turns the model too generalized; low r_a implies an excessive generation of clusters. Therefore, the radius selection is dependent of the desired model complexity and generalization capacity. After potential of every data point has been calculated, the point with the highest potential is selected and settled as the first cluster centre. The potential of each data point is then re-evaluated through the expression:

$$P_i = P_i - {P_1}^* e^{-\beta \|x_i - {x_1}^*\|^2} \tag{7.9}$$

where ${P_1}^*$ is the potential of the data point ${x_1}^*$, which is the first cluster centre. The parameter β is given by:

$$\beta = \frac{4}{{r_b}^2} \tag{7.10}$$

where r_b is a positive value (the value $r_b = 1.25 r_a$ is typically chosen [171]). This parameter is the radius that defines the data point that will have significant potential reduction. After revising all the potentials, the point with the highest potential among the remaining points is selected as the second cluster centre. After the kth cluster centre has been selected, the potential of each data point is re-evaluated using the expression:

$$P_i = P_i - {P_k}^* e^{-\beta \|x_i - {x_k}^*\|^2} \tag{7.11}$$

where ${P_k}^*$ and ${x_k}^*$ are the potential of the Kth cluster centre potential and the centre location, respectively. The process of re-evaluating the potential ends when the criteria ${P_k}^* < 0.15\, P_1^*$ is satisfied. Each vector ${x_i}^*$ is decomposed into two vectors, being represented as ${x_i}^*$ =[${y_i}^*$; ${z_i}^*$], where ${y_i}^*$ holds the cluster centre location on the input space and ${z_i}^*$ the cluster centre in output space. The number of linguistic variables and rules are indicated by the number of cluster centres, since each cluster centre is considered as a fuzzy rule that describe the system behaviour on the following was: "if input is near ${y_i}^*$ then output is near ${z_i}^*$". The degree to each rule of a given input vector y is defined as

$$\mu_i = e^{-\alpha \|y_i - {y_i}^*\|^2} \tag{7.12}$$

where α is given by (7.8) and y is an input vector used as example. The output of this system is given by

$$z = \frac{\sum_{i=1}^{c} \mu_i z_i^*}{\sum_{i=1}^{c} \mu_i} \tag{7.13}$$

In analogy to the inference system with if-then rules, each rule would have the following form:

IF Y_1 is A_{i1} and Y_2 is A_{i2} and … **THEN** Z_1 is B_{i1} and Z_2 is $B_{i2...}$

where Y_j and Z_j are the j^{th} input variable and output variable, respectively; A_{ij} is an exponential MF in the i^{th} rule with j^{th} input and B^{ij} is a singleton in the i^{th} rule associated with the j^{th} output [171]. Thus, the parameters A_{ij} and B_{ij} of the i^{th} rule, which is represented by cluster centre x_i^*, are given by

$$A_{ij}(Y_j) = e^{-0.5\left(\frac{Y_j - y_{ij}^*}{\sigma_j}\right)^2} \tag{7.14}$$

and

$$B_{ij} = Z_{ij}^* \tag{7.15}$$

where y_{ij}^* is the jth element of the cluster centre y_i^* and z_{ij}^* is the jth element of z_i^* and $\sigma_{ij}^2 = \frac{1}{2\alpha}$ [171], [181].

7.2.3 Input Variables Selection

Input selection is critical in a soft computing approach, as an excessive number of inputs will increase the computation time required for building a model using ANFIS architecture [177]. Therefore, it is advisable to keep only the inputs that are important to the system behaviour description to develop a reliable model that is too concise, practical, simpler and transparent. Jang et al. states that noise/irrelevant inputs, as well as inputs that are dependent on other ones must be removed. This will reduce the time required for model construction. The methods presented in [182] and [183] are widely adopted and they use the ANFIS architecture for determining the most relevant inputs. Both methods take as assumption that ANFIS models with the smallest Root Mean Square Error (RMSE) after a small number of epochs have a great potential of achieving a lower RMSE when more epochs are considered in the ANFIS training.

In the former method, all antecedent classes associated with a input variable from the rules are removed and the model is evaluated. If the RMSE decreases relative to the original initial ANFIS model, the input variable is removed, and the process is repeated to another input variable. If the RMSE increases, the input variable is not removed from the ANFIS model. This process is repeated until the RMSE can no longer be reduced. The ANFIS model for which the RMSE is the minimum is defined as the initial ANFIS. This method has the advantage of no new models generation is needed.

The method proposed in [183] builds several models which are then assessed. For instance, 35 (C_4^7) ANFIS models have to be generated if the system under consideration has a total of seven inputs and an ANFIS model with four inputs is desired [177]. The several combinations of inputs are evaluated. The ANFIS model with the lowest RMSE is chosen as initial ANFIS model.

7.2.4 Hybrid Learning Algorithm

This learning algorithm, which is composed of a forward pass and a backward pass, is extremely efficient in ANFIS systems [175]. For example, considering the example illustrated in Figure 7.2, the overall output of the ANFIS model can be expressed as a linear combination of the consequent parameters as follows

$$O_{5,i} = f = \frac{w_1}{w_1 + w_2} f_1 + \frac{w_2}{w_1 + w_2} f_2 \tag{7.16}$$

$$O_{5,i} = (\overline{w_1}x)p_1 + (\overline{w_1}y)q_1 + (\overline{w_1})r_1 + (\overline{w_2}x)p_2 + (\overline{w_2}y)q_2 + (\overline{w_2})r_2 \tag{7.17}$$

During the forward pass, the least squares method is applied to optimize the consequent parameters of the rules, i.e. nodes outputs go forward until the Layer 4 and the consequent parameters (p_i, q_i, and r_i) are updated using the least squares. The premise parameters are optimised by the gradient descent method that is applied during the backward pass. The ANFIS output is calculated by employing the consequent parameters found in the forward pass. The output error propagates backward from the output layer to the input layer.

7.3 ANFIS-Packet Scheduler

The radio channel characterization carried out and the radio channel temporal fading features, discussed in chapter 5, show that the relative position of the nodes are a prominent influence of both radio channel gain and fading magnitudes features. The Node-PROTACTICAL 7 is subject to changes in its relative position, which leads the radio channel to switch between LOS and NLOS. Some of its relative-positions in relation to Coordinator node might make it impossible to successfully deliver data packets, even for transmissions at maximum TPL. Empowering a mechanism with the capacity to sense when the radio channel is in outage might allow the communication system to avoid data packets loss and energy consumption due to data packet retransmission. Such an approach might lead to a significant increasing on PER at expenses of latency. Although latency increasing is seen as a disadvantage, in some applications or network traffic modes (for instance regular traffic),

latencies on communication a bit higher than the maximum suggested by the TG6 seems reasonable.

In this chapter, a mechanism, depicted in Figure 7.4, designated Power Control and Packet Scheduler (PCPS) is proposed. This mechanism aims to control the transmission power at each data packet transmission but also the *time to transmission* (interval of time between the instant that a data packet is ready to be transmitted and the instant that it is effectively transmitted by the radio module). Thus, this mechanism can delay the data packets transmission to some later period if required. The structure of the PCPS mechanism is made of three blocks:

- RSSI-prediction LQE - forecast the RSSI value in the on-body channel under consideration;
- TPL Control - adjusts the TPL to the minimum TPL required to ensure successful data packets delivery (according to the current radio channel conditions). The TPL Control algorithm proposed and validated on chapter 6 is selected to perform as TPL Control block in the PCPS mechanism;
- PER-prediction LQE - this block predicts the outage probability of the radio channel to a given scenario configuration.

A set of variables, which describes the relative position of the Node-PROTACTICAL 7, are given as inputs to the RSSI-prediction LQE. The LQE output is the predicted radio channel quality (RSSI) to the current scenario conditions (operation environment, body posture and arm relative position).

For each data packet transmission, the PCPS mechanism first set -0.5 dBm as default TPL of the RSSI-prediction LQE block. If the outputted value of this block is lower than the *RSSI Threshold* (can be the radio module sensitivity or a higher value), the PCPS mechanism immediately cancel/postpone the data packet transmission. However, if RSSI-prediction LQE's output is higher than the *RSSI Threshold* value, the TPL Control block is executed to quest for

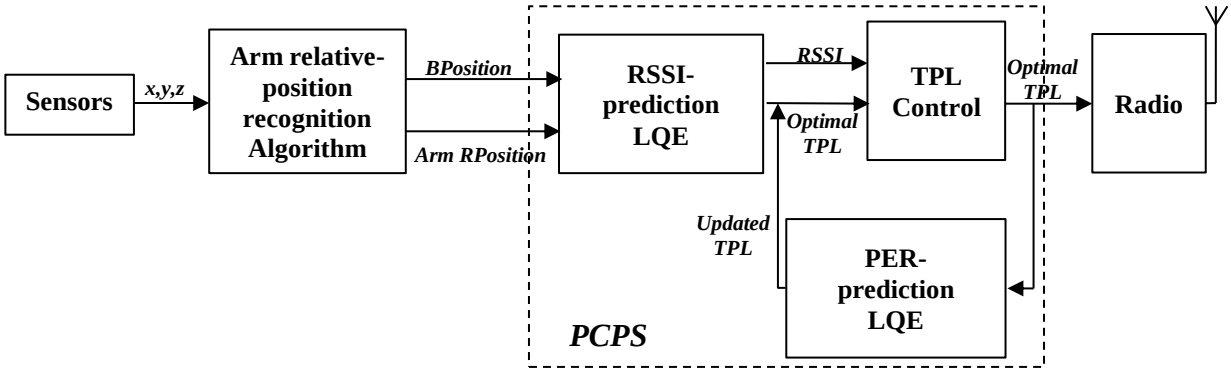

Figure 7.4. Diagram block representation of the proposed packet scheduler mechanism called PCPS.

the optimal TPL, implementing a dynamic-based approach and relying on the linear relation between RSSI and TPL analysed in section 6.2. This block outputs the minimum TPL that ensures the following criteria: (i) estimated RSSI (outcome of the execution of the dynamic based TPL Control block that) > *RSSI Threshold*. Typically, the TPC mechanisms addressed in the literature after finding out the minimum TPL – as result of the operation above described – enables the radio module to transmit the data packet. However, before the PCPS mechanism proceeds with the data packet transmission, the criteria (ii) PER-prediction LQE's output < *OP* (Outage probability) has to be met.

For the set of movements under consideration in this chapter (c.f. subsection 7.3.2), the RSSI alone is not a reliable indicator of the radio channel quality, since data packets loss is quite likely to happen (c.f. subsection 7.3.2) and the RSSI value is only computed for data packets successfully delivered. Therefore, the PCPS mechanism only allows the radio module to transmit the data packet if both (i) and (ii) are met. If this is not the case, transmission of the data packet is inadvisable and then deferred to a future point where radio channel conditions are more favourable to successful transmissions.

The outputted value (TPL) of the TPL Control block ensures the criteria (i), while the PER prediction LQE block has the task of checking if the inputted TPL also meets the criteria (ii). If this is the case, then this TPL value is set as optimal TPL for the radio module. Otherwise, the task of the PER prediction LQE block consists in the quest for the minimum TPL (a value higher than the one provided as input by the TPL Control block) that ensures the criteria (ii). When this TPL value is found, this is inputted into the TPL control block which will only update the estimated RSSI for this radio channel condition (relative arm position, posture, environment and new optimal TPL) without changing the TPL provided by the PER prediction LQE that is set as the optimal TPL value. Finally, the PCPS mechanism allows the radio module to transmit the data packet with the ideal TPL value.

This mechanism must represent a small protocol layer located between the MAC layer and the next layer protocol, the Network (NTW) layer. The protocol stack location is due to the need to intercept data packets from NWK to MAC layers, since this location allows the mechanism to queue and to delay the data packets transmission.

7.3.1 ANFIS Models Methodology

The research goal is to develop two different Link Quality Estimators aiming to predict the radio channel quality in terms of signal strength variability and outage probability on the communication link between the Node-PROTACTICAL 7 and Gateway-PROTATICAL, the

RSSI- and PER-prediction models. To achieve models that can describe the fading features, the ANFIS soft computing technique was adopted, involving the interaction of several input variables. In this subsection, the approach followed to find out meaningful and reliable models is described, these models were afterward integrated in the PCPS mechanism. To build reasonable models, the next four steps were followed.

- **Experimental Trial:** several experiments were carried out to collect RSSI samples that describe the time-variant fading signal. Moreover, the number of lost data packets on the different scenarios was also determined;
- **Input variables selection**: to remove redundancy and, therefore, to build less complex models, different combinations of inputs were tested;
- **Selection of a RSSI- and PER-prediction model**: different ANFIS models for each output parameter considered were developed. From the set of different types of Fuzzy systems the Takaga-Sugeno was selected, since it is considered more compact and efficient, leading to proper representations of the system behaviour with a minimum number of rules [135]. Since different models can be obtained according to the training technique adopted at the initial FIS model derivation process, the derivation of the initial FIS model through the grid partition and subtractive clustering initial generation method was tested. Moreover, model inputs with different number and type of MFs, such as Gaussian curve, Triangular-shaped and Generalised bell-shape were assessed. A linear MF was chosen as the output variable. To optimize the several initial FIS models, the method that combines the least-squares and the back-propagation gradient descendent method was adopted. As part of the process of input selection, models for the various combinations of input variables were built. To ensure that a minimum error tolerance was achieved, a training error tolerance of 0.0001(0.01%) was selected. Only two epochs were considered to the ANFIS training process to reduce the time for building the model. The capacity of the model to describe the output variable (linear MF) under consideration is translated through the computation of the RMSE that first needs to determine the residuals (difference between the actual and the desired output). Therefore, the network performance with lower RMSE were selected as the FIS models that better perform the role of LQE. Those models were created and evaluated using the MATLAB Fuzzy Logic Toolbox;
- **ANFIS models validation process:** the ANFIS models are validated against two datasets, namely the checking and testing one. The criteria used for evaluating the two models (one

for each output) are the RMSE, Mean Absolute Error (MAE), and Absolute Fraction of Variance (R^2) models.

The training and testing methodology adopted to build, analyse and select the most efficient and reliable ANFIS models is depicted in Figure 7.5. At the first step of this methodology, after collecting the empirical samples (of fading) in the experimental trial, the training and checking data, and the number, type and shape of the initial MFs are specified. According to Vallejo et al. the generalization capability of ANFIS models is ensured by the proper selection of a large training dataset [143], thus, suitable training datasets to train the ANFIS models must include as many system's situations as possible. The input/output vectors are randomly chosen from the vectors of input data, collected during the experimental characterization. The two desired models, namely the RSSI- and PER-prediction ANFIS, have different input data lengths, since the RSSI-prediction ANFIS model has at least one input variable less (the TPL is not used as input variable to this model, as a linear relation between the TPL and the RSSI signal has been proved in chapter 5).

In step (2) of adopted methodology, the initial FIS models were generated. The command provided by MATLAB to generate the initial single-output Sugeno FIS model is *genfis*, which requires three inputs, namely the *input* (an *N*-columns array, where *N* is the number of FIS inputs) and *output data* (an *M*-column array, where *M* is the number of FIS outputs) in matrix form, and *options* (where information about the learning technique, type and shape of MFs is provided). Both *input data* and *output data* must have the same number of rows, as each row represents a system situation.

The third step of the training methodology is to tune the initial single-output Sugeno FIS by using the input/output training data. All the training data passes through the NN by using the combination of the least-squares and backpropagation gradient descent methods to adjust the weights of the several nodes, finding the relationship between inputs and outputs variables which minimizes the error. The MATLAB provides the command *anfis* to train the FIS model. The training data was provided as input, the initial FIS model to be tuned and some training options, such as the maximum number of training epochs or the training error goal. These two training process configuration parameters are extremely important to the optimization of the FIS. The training tolerance error is a threshold value for the error between the actual and the desired and it is used to create an additional training stopping criterion stopping. The least-squares method determines the consequent parameters and the error is computed. If this error

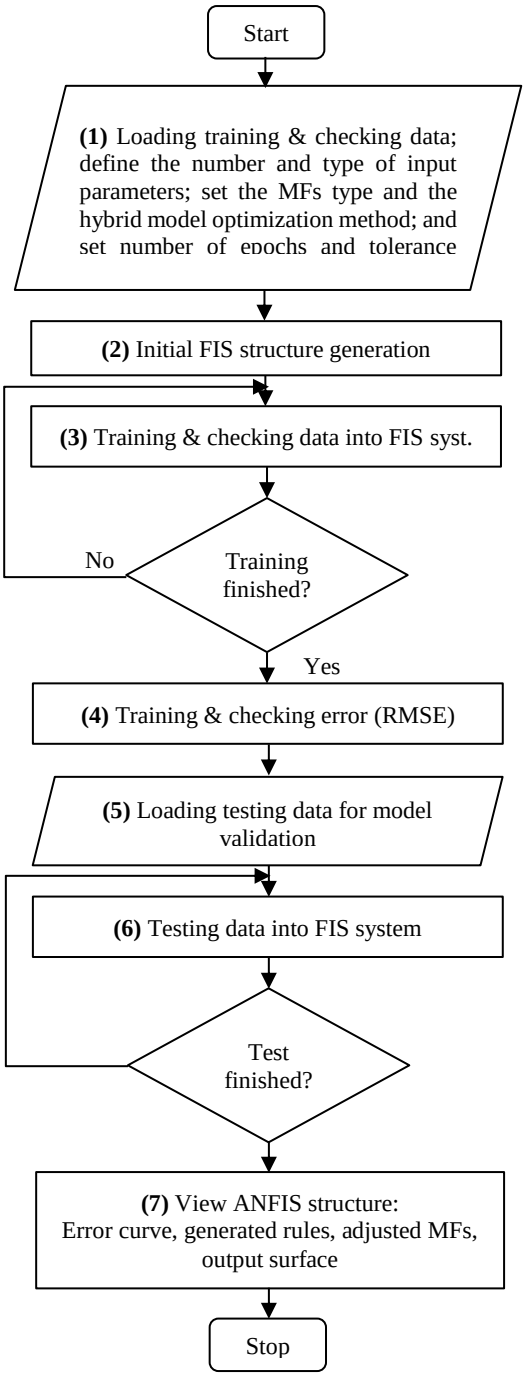

Figure 7.5. ANFIS training and testing methodology.

is larger than the training tolerance error, then the gradient decent method is applied to update the premise parameters.

The combination of the forward and backward propagation to optimize the consequent and the parameters associated with the MFs respectively is one epoch. The training process stops when the calculated error is lower than the tolerance error or when the number of epochs has been reached. When the training process is finished, the final MFs and the training error (RMSE) are provided as the *anfis* command output. Then, the checking data is used to verify the accuracy and effectiveness of the trained FIS model. This approach helps to handle with the

overfitting problem to increase the effectiveness of the model thanks to a better understanding of the system performance under new situations. The problem of overfitting is very common on machine learning. It occurs when training data is overtraining during the ANFIS training process, leading to output predictions over its accuracy [177], i.e. the error on training data is driven to a very small value. However, when FIS is evaluated against new data, it performs very poorly, suggesting that the FIS is not able to generalize new situations.

In steps (5) and (6), a performance evaluation of the model generated in the first step is carried out. The main goal of this step is to evaluate and control the potential of the model to over fit the data. The MATLAB command *evalfis* is used to study and evaluate the performance of the FIS models to analyse if satisfactory results are generated. The testing data, in the form of M-by-N matrix (where M is … and where N is number of input variables matrix form), and the trained FIS model are given as input. The output testing vector is not provided as input of the *evalfis* command. This function takes each row of the input testing data and returns the M-by-L matrix (L is the number of output variables) as output variable. Each output row is the system response to the input variables values provided in the same row number at matrix given as input to *evalfis* command (input and output matrix have the same number of rows). The *evalfis* output is then used to measure the model error, as the difference between FIS output and the desired response.

The checking and testing of residuals is used to evaluate the performance of the system, three different measurements, namely the criterion error RMSE, Mean Absolute Error (MAE) and the coefficient of determination (R^2) can be used to obtain the accuracy of the derivate models. RMSE, which is the standard deviation of the residuals (difference between the forecasted and the actual collected data) and used to monitor the training error, is given by

$$RMSE = \sqrt{\frac{1}{N}\sum_{j=1}^{N}(y_j - \hat{y}_j)} \tag{7.18}$$

where N is the number total of rows of the input training vector, y_j is the collected values given as part of output vector in training methodology and and $\hat{y}_j$ is the ANFIS outcome (model predictions). MAE indicates the average of all absolute errors, it is the difference between the predicted and the actual value, and is given by

$$MAE = \frac{1}{N}\sum_{j=1}^{N}|y_j - \hat{y}_j| \tag{7.19}$$

The coefficient of determination is a measure of how much the variance in the output collected data is explained by the model outcome and is frequently interpreted as how well a model explains and predicts future outcomes. The computed values must be within the range [0 1] and the higher the computed value, the better the fit. This parameter is given by:

$$R^2 = 1 - \frac{\sum_{j=1}^{N}\left(y_j - \hat{y}_j\right)^2}{\sum_{j=1}^{N}\left(y_j - \bar{y}\right)^2} \tag{7.20}$$

Where $\bar{y}$ is the average value of the collected samples, y_j is the collected values given as part of output vector in training methodology and and $\hat{y}_j$ is the ANFIS outcome.

Finally, in the step identified by (7) in Figure 7.5, additional information about the features of the final FIS models are obtained to study, analyse and better understand these models. The *gensurf* MATLAB command generates the output surface for the FIS provided as input to plot the FIS output variable against two selected variables from the set of FIS input variables. The rules resultant of the training methodology can be analysed using the *showrule* command. Another useful command is the *plotfis* that displays the high level diagram of an FIS. The fuzzy sets, the number of fuzzy sets of each input variable and the shape of MFs can be graphically visualized through the MATLAB command *plotmf*.

To find the best-fit models, ANFIS method are investigated through the combination of use of number of data sets, membership functions, and types of membership functions. Twelve and five ANFIS models were constructed using combinations of inputs, sample training data, membership function numbers, and membership function types for RSSI-and PER-prediction LQE, respectively. After trained, the models performance was assessed, and results were compared based on their performance in training and checking data sets. The two selected models to perform the task of RSSI- and PER-prediction LQE were tested to evaluate the capacity of generalization of the proposed models.

7.3.2 Experimental Trial

Algorithms for inertial sensor data fusion such as rate gyroscope integration [184], vector observation [185], Complementary Filtering (CF) [186] and Kalman filtering [187] resort to information from inertial measurement unit (IMU) – which measures linear acceleration, angular velocity and direction of magnetic field – to represent the human motion. Such algorithms, first, estimate the angles of segments and joints of human limb and, second, estimate the limb postures, which is a representation of the human limb angles (identified from a set of angles) [188]. There are two type of angles: i) angles of a non-static segment

("constituent parts into which a human body is divided or marked off by or as if by natural boundaries" [188]) of the human limb in relation to an anatomical plane or ii) angle between two contiguous segments to the joint, i.e. point of contact between segments.

Movements occur around and within axes aligned with respect to specific anatomical planes [188], [189], which are depicted in Figure 7.6.

Scenarios

The experimental trials carried out in this study occurred only in indoors (room), since this type of environments promotes small-scale fading (unlike outdoors) but not as aggressive as the magnitudes observed inside laboratories. The experiments follow a setup configuration (MAC configuration, network topology and packet scheduler) like the one carried out in Chapter 5. Since the goal is to develop a mechanism able to control the TPL and postpone the data packets transmission when required in static (TPC mechanisms based in models are only applicable in this type of scenarios) and dynamic scenarios, a radio channel characterization following a scenario-based approach was adopted, where the follow movements were considered:

A. Forearm Supination and Pronation – turning and revolving the forearm around a specific plane (Median, Transverse or Frontal plane of the hand), see Figure 7.7;

B. Shoulder Flexion and Extension – movement of the upper arm in Sagittal plane around a transverse axis, see Figure 7.8 a);

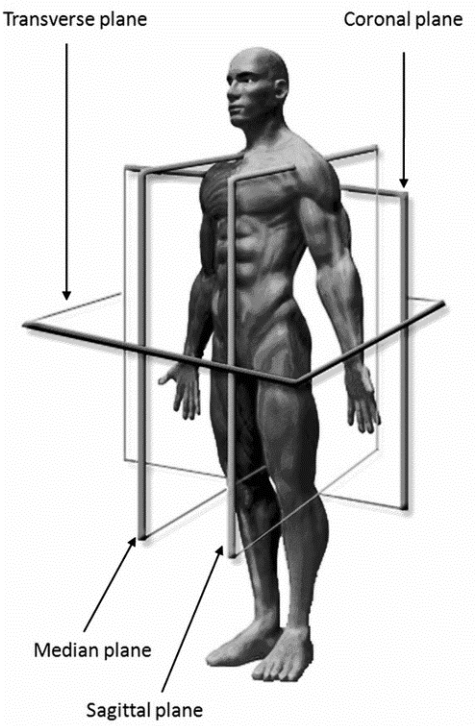

Figure 7.6. The main anatomical plans of the body, edited from [189].

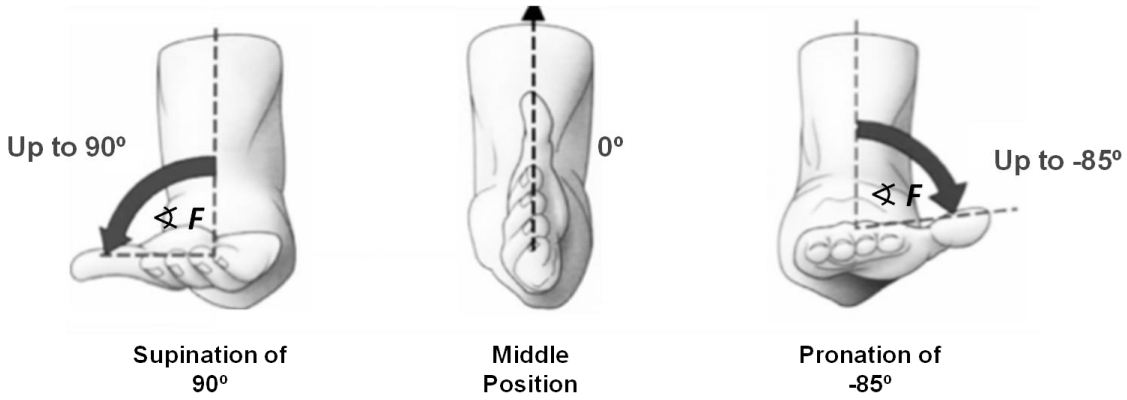

Figure 7.7. Pronation and Supination of forearm, edited from [189].

C. Elbow Flexion and Extension – movement of the forearm in Sagittal plane around a transverse axis, see Figure 7.8 b);

D. Shoulder Abduction and Adduction – movement of the arm in a Frontal plane around an anteroposterior axis, see Figure 7.8 c).

Up to a total of four arm angles (represented in Figure 7.7 and Figure 7.8) are estimated from readings obtained from IMU while the user performs any of the above mentioned movements. From readings up to four arm degrees of freedom are extracted:

- ∢*F*, angle of the type i) that reflects the angle of the forearm in relation to the forearm Middle Position. This angle permits the description of the movement *A.* in any plane;

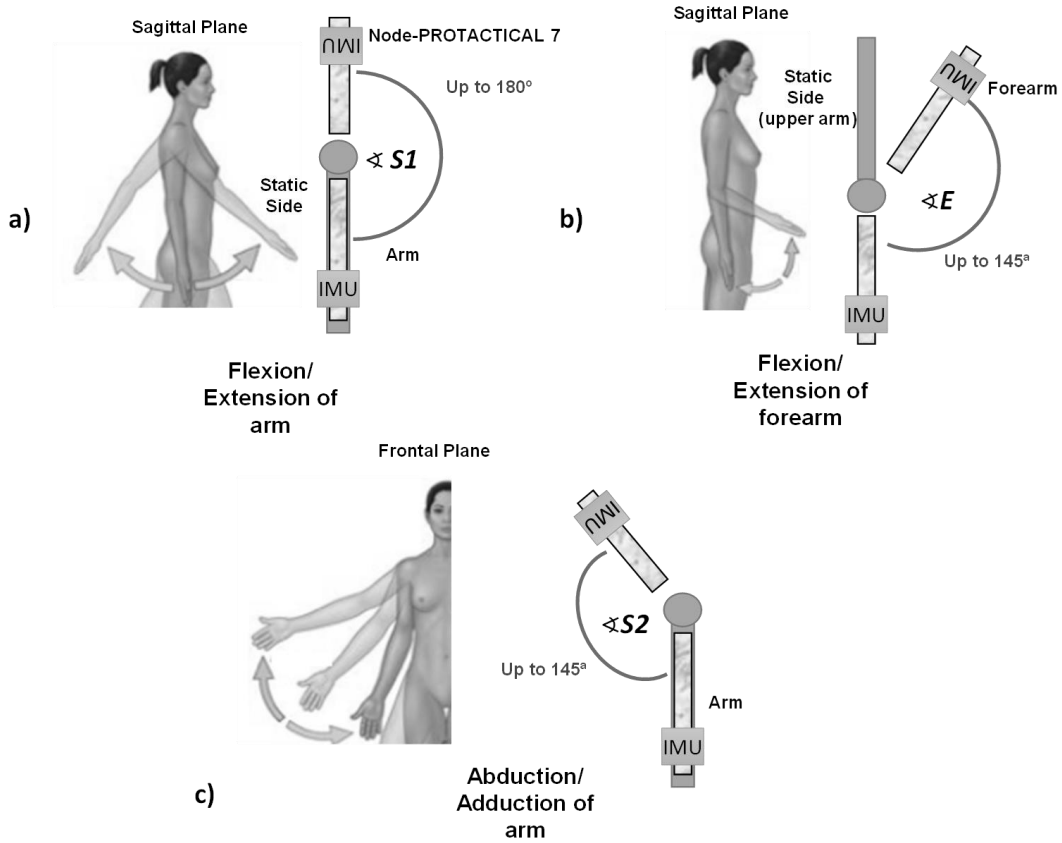

Figure 7.8. Angles of segments to estimate in experimental trial, edited from [188].

- ∢*S1*, angle, which is of the type i), of arm with respect to the Frontal plane, which helps us to describe the movement *B*;
- ∢*E*, angle of the type ii) that describes the angle formed by the upper arm segment and forearm. This angle permits the description of the movement *C*;
- ∢*S2*, this angle of the type i) and refers to the angle of the upper arm with respect to the Sagittal plane. This angle is important to identify the arm posture at any instant in movement *D*.

As can be seen in Figure 7.8, experiments are carried out in controlled environments, i.e. for each movement/experiment, only one of the angles varies over time while the three lefts are unchanged throughout the experiment. This approach simplifies the process of mapping the measured fading features samples (RSSI and PER) to the relative arm position, since our IMU will detect variations in only one of its axis (which varies depending on the performed movements). For example, in movement depicted in Figure 7.8 a) with ∢F angle of ≈85º, the x-axis of the IMU is aligned with the direction of the movement, while the rotations in the sagittal plane are sensed mainly by the y-axis of the gyroscope.

Figure 7.9 illustrates the pattern of the accelerometer and gyroscope signal (in this experiment shoulder Flexion/Extension angle ranged from 0º to 90º) sensed in the movement above described – c.f. Figure 7.8 a). Therefore, as the Node-PROTACTICAL 7 is attached in a fixed position and orientation, signal patterns enable the easy identification of which movement performed for each pair of movements. Also, this approach and the specific and static orientation of the IMU enables the use of simple algorithms to compute the angles by searching the data stream in one axis of the gyroscope. Additionally, as the majority of the movement is

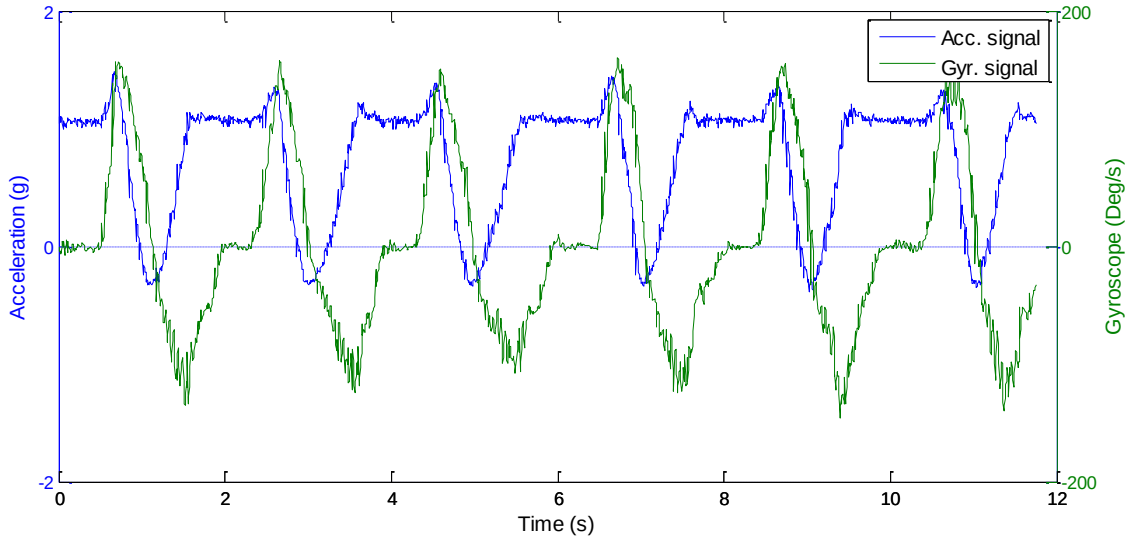

Figure 7.9. Raw accelerometer and gyroscope measurements for movement shoulder flexion/extension, collected from IMU embedded in Node-PROTACTICAL 7.

localized in one axis, initial IMU offsets or misalignments do not influence significantly the computed angles.

The angles under consideration are computed through the integration of the gyroscope signal over time. However, the gyroscope data is only reliable on the short term, since, on the long term, the measurement tends to drift. This means that when the arm returns to the original position, estimated angles will be different from expected angles for the original position. This is the main disadvantage of using gyroscope data to estimate rotations in localization and tracking system. The integration of the gyroscope signal shown in Figure 7.9 over time (interval in which 53 repetitions of movement B were executed) leads to the drift depicted in Figure 7.10. After 100 s, the drift error is close to -61º.

A technique designated Zero-Velocity Update (ZUPT), which is widely adopted to correct drift error in localization and tracking systems based on data fusion algorithms, provides the tilt from accelerometer as initial condition for the integration of the gyroscope, resetting every stride (IMUs are typically attached to ankle). This technique is especially important in data fusion algorithms, such as CF and Kalman filter. The former solution requires two estimates of the orientation (such as gyroscope integration and vector observation from the magnetometer and the accelerometers) while the latter solution is a very complex approach (tilt gives a pseudo measurement used to update the IMU orientations).

The proposed solution for relative arm position estimation is only executed after the IMU sensor calibration. For each experiment, the IMU readings are sampled at 100 Hz while data packets (carrying several IMU samples) are transmitted with an interval between transmissions

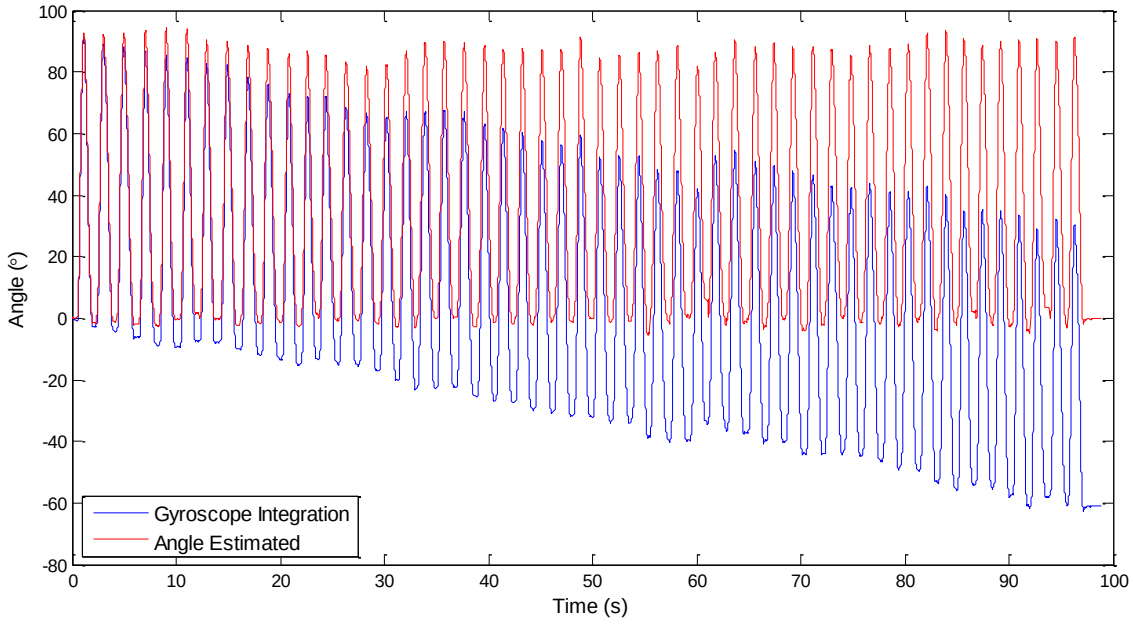

Figure 7.10. Estimation angles through the integration of the gyroscope signal with (red line) and without ZUPT method.

of 35 ms. To deal with the small offsets in the average signal output of both sensors, the proposed solution only starts transmitting the IMU readings after the first five minutes of IMU operation (sources of errors on estimations vary according to IMU temperature). The next IMU samples, which are collected before the arm moving, provide the bias error (averaging the IMU outputs while the Node-PROTACTICAL 7 is in a constant position for one minute). This source of estimation deviations is subtracted to future IMU readings. The scale factor (0.00078 g and 0.065º for accelerometer and gyroscope) is only compensated after bias compensations in IMU readings (computed bias errors relative to example of Figure 7.10 are 0.018844 g and 1.9023º for accelerometer and gyroscope respectively). After calibration, tilt is provided and set as the initial condition (initial value of the angle of interest in degrees) for gyroscope integration for each pair of movements.

The ZUPT method is executed every time that the arm returns to the original position, which is triggered through the condition: variations on absolute values of the acceleration and gyroscope samples greater than a threshold (0.09 g and 3º, respectively) for 0.4 s. As the accelerometer is only reliable on the long term, the resultant average acceleration (during the ZUPT) in the x-axis is used to compute the IMU tilt. This value is then set as the true angle value of the angle under consideration. The accuracy of the solution above described is computed every time that arm returns to the original position and is given as the difference between the estimations (gyroscope integration over time) and the tilt at each ZUPT.

The implementation of the ZUPT method allowed to reduce the error drift. In Figure 7.10, the red line represents the angle estimations through the proposed solution. The computed RMSE to an experiment depicted in Figure 7.10, which involved 53 shoulder flexion/extension movements, is 1.82º.

In summary, the arm posture is a representation of the orientation of the arm in which the Node-PROTACTICAL 7 is located, and it is identified from the four arm angles. In each experiment the user performs 53 repetitions of a specific movement. The movements above described were repeated for several static arm angles configurations. For instance, the flexion/extension of the arm was repeated for three different static $\measuredangle F$ angles, namely 90º, 0º and -90º and different $\measuredangle E$. To capture the effect of the TPL into the fading and outage, all TPL available in radio transceiver module were considered (experiments were repeated for each TPL). A total of 357500 RSSI samples were collected in the experimental trials.

Figure 7.11 depicts the measured RSSI samples for different forearm angles while user is standing with the arm stretched forward, forming a right angle with the Coronal plane. Experiments to an $\measuredangle F$ angle near to 90º resulted in a radio channel quality (RSSI) improvement

up to ≈12 dBm when compared to angles near to 0º. The effect of the arm angles is also felt in the PER metric, affecting the reliability of the system. For instance, considering the experiment where user is standing with the arm postures illustrated in Figure 7.7, it was observed a PER (100 data packets were transmitted) value of 70%, 2%, and 20% for forearm angle 0º, -85º and 90º respectively. The two examples above prove what was stated before, i.e. arm angles have a significant effect on the first- and second-order statistics of the signal.

7.3.3 ANFIS-LQE (RSSI)

The selection of the data used to training, checking and testing the models is extremely important. The training data, which was used to train the FIS model, must be fully representative of the features of system that the FIS is intended to model. To avoid a trivial checking and validation process, the testing data must be both representative of the features of the system that the FIS model is intended to evaluate and sufficient distinct from the training data. To avoid that ANFIS memorize the training data examples and to ensure that the ANFIS model have learned to generalize new situations the training, checking, and testing data do not contain repeated samples, since after randomly chosen the training data set, these samples are ignored during the selection of the remaining data sets. The training dataset used during the training process of the RSSI-prediction ANFIS models is composed by 27500 input and 27500 output vectors, corresponding to three quarters of the input data (19250); 4125 vectors were randomly chosen for the checking error; and the remaining 4125 vectors were selected for the testing dataset.

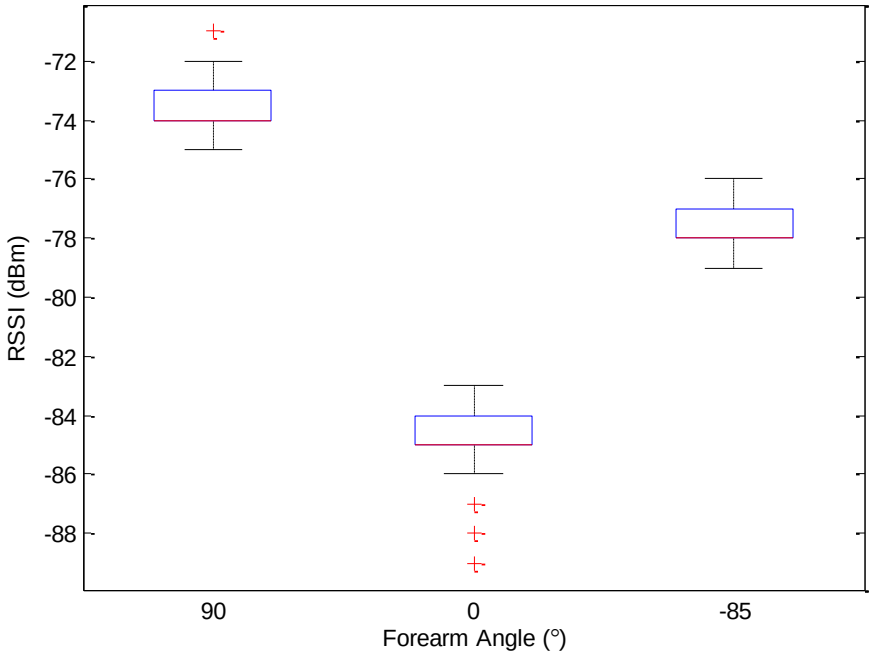

Figure 7.11. Influence of the forearm angle (∢F) on fading magnitude.

In order to find out the optimal FIS model, several experimental were carried out where different ANFIS model settings were tested. The factors that differ between ANFIS models are the input variables, fuzzy sets, MFs type and the hybrid learning technique adopted, whereas the length of the training and checking data set as well as the epoch number is the same. From the set of ANFIS models resultant of the methodology described above, the optimal ANFIS is the one that shows a better balance between its complexity, generalization ability to fit any sample space well, and RMSE values.

The resultant ANFIS models are identified through $ANFIS_{(i)}(j)$, where *i* is the number of inputs variables of the FIS model and *j* is the version of the ANFIS model under consideration. The input variables of the RSSI-prediction models must represent the arm limb angles through the description of the orientation angles in which the wearable system is setting at a time unit. A set of input variables required to describe the arm position at any instant form a pose vector designated *Arm Position*, which is expressed as P_{tx}={∢*Elbow*, ∢*Shoulder*, ∢*Forerm*}, which represents the elbow (*Elbow_F/E_Angle* ANFIS input represents the ∢*E* angle), the shoulder (*Shoulder_F/E_Angle* represents the ∢*S1* and *Shoulder_A/A_Angle* is the ∢*S2* angle) and the forearm (*Forearm_S/P_Angle* represents the ∢*F* angle) angles, respectively.

Two variables are given as inputs to the $ANFIS_{(2)}(j)$ model, namely ∢*S1* and ∢*S2* angles, and from the experiments four different initial ANFIS were generated: $ANFIS_{(2)}(1)$, $ANFIS_{(2)}(2)$ and $ANFIS_{(2)}(3)$ were structured through the Grid Partition technique and by selecting two inputs; defaulting values for MFs (9*6) and setting MFs as type Gaussian curve, triangular-shaped and generalised bell-shaped, respectively.

Figure 7.12 shows the RMSE of the initial $ANFIS_{(2)}(2)$ after carrying out the training process for 15 epochs. It is clear that the most relevant input variable into the description of the system under consideration is the *Shoulder_F/E_*Angle. Although the performance of the model increases with the increase of the number of fuzzy sets of each input variable, the difference is not significant (a RMSE 0.02 high than the RMSE of an ANFIS with the MF number 18*18). For that reason, the *Shoulder_F/E_Angle* and *Shoulder_A/A_Angle* inputs of all the models have 9 and 6 fuzzy sets respectively, which significantly reduces ANFIS structure complexity in relation to a potential ANFIS with two inputs and MFs number 18*18. Since the aim is to compare the initial ANFIS extracted from input output data by using different techniques, the $ANFIS_{(2)}(4)$ is the initial ANFIS extracted through the subtractive clustering technique.

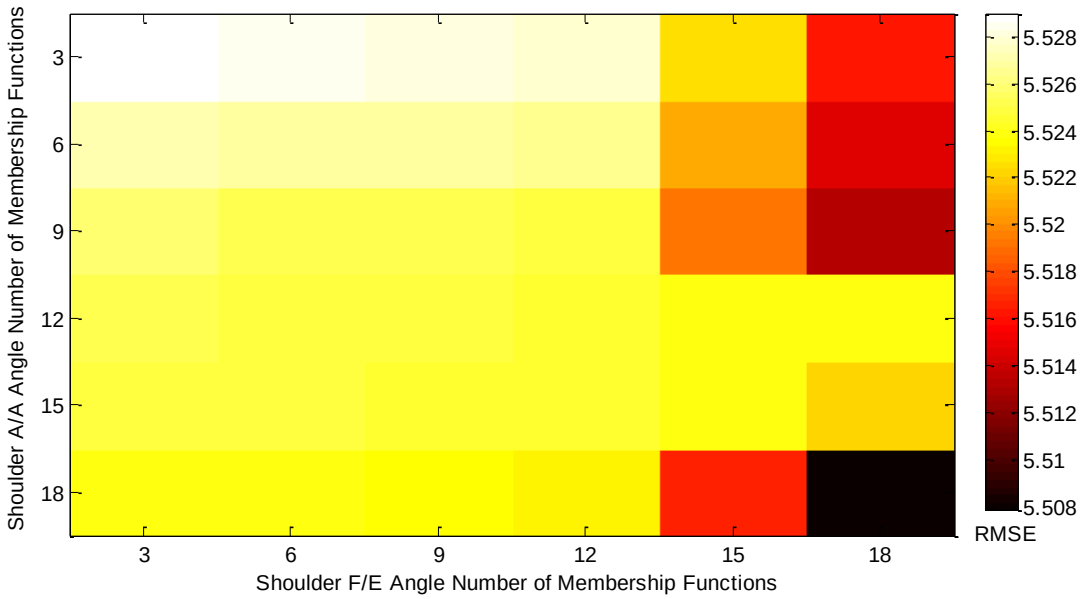

Figure 7.12. Training error measurement (RMSE) of ANFIS$_{(2)}$(*2*) inputs configured with different number of MFs.

Table 7.2 shows that the trained ANFIs model with the lowest RMSE is the model generated through Grid Partition technique that has two inputs, triangular-shaped MFs, MFs number (9*6). However, the effectiveness of this model is not outstanding compared to the remaining.

The ANFIS$_{(2)}$(*4*) ensures similar performance (training error is 5.5333 and while checking error is 5.98783). Since this initial model was generated by the Subtractive clustering technique, which has two inputs, namely *Shoulder_F/E_Angle; Shoulder_A/A_Angle*, with three MFs of the type Gaussian curve for each. Although the performance is slightly lower, the network complexity is much lower than the complexity of the ANFIS$_{(2)}$(*2*) (depicted in Figure 7.13,

Table 7.2. Information about the architectures of the set of ANFIS$_{(2)}$(*j*) models, which were generated through different initial model generation techniques and configured with different types of MFs.

ANFIS Parameter Type	**ANFIS$_{(2)}$ (*1*)**	**ANFIS$_{(2)}$ (*2*)**	**ANFIS$_{(2)}$ (*3*)**	**ANFIS$_{(2)}$ (*4*)**
Number of Inputs	2			
Generation technique	Grid Partition			Subtractive Clustering
Membership Function Type	Gaussian Curve	Triangular-Shaped	Generalised Bell-Shaped	Gaussian Curve
Number of MFs	9*6			3*3
Training Data Set	27500			
Checking Data Set	4125			
Epoch Number	15			
Number of Nodes	143	143	143	29
Number of Linear Parameters	162	162	162	12
Number of Nonlinear Parameters	45	45	45	16
Number of Fuzzy Rules	54	54	54	4
Input Combinations	*Shoulder_F/E_Angle*; *Shoulder_A/A_Angle*			
Training Error (RMSE)	5.52931	5.50861	5.51839	5.5333
Checking Error (RMSE)	5.97946	5.95267	5.97954	5.98783

where A_i is the MFs of the *Shoulder_F/E_Angle* and B_i is the MFs of *Shoulder_A/A_Angle* input), which is perfectly detectable through the number of NN architecture nodes (20 nodes compose the NN, against the 143 of the $ANFIS_{(2)}(j)$ structure), number of rules (4 against the 54 of the $ANFIS_{(2)}(j)$), linear and nonlinear parameters.

Table 7.3 summarizes the information about structure of the ANFIS generated by mean of different techniques and the performance of the models in terms of RMSE. The $ANFIS_{(3)}(j)$ models are similar to the previous models, the only difference is the inclusion of another input variable. The Sugeno FIS models are as depicted in Figure 7.14, having as inputs the variables *Shoulder_F/E_Angle*, *Shoulder_A/A_Angle* and *Forearm_S/P_Angle.*

The several generated models with three inputs have shown reduced performance variations. The $ANFIS_{(3)}(2)$, where every input is mapped as Triangular-shaped MFs, is the best-fit model to training and checking data, achieving the lowest RMSE value (5.16667), while $ANFIS_{(3)}(4)$ is the model that led to the lowest performance, it achieved a RMSE value of 5.18715. The model generated through the subtractive clustering, $ANFIS_{(3)}(4)$, is the less complex, since the number of rules and nodes is much lower than those that compose the structure of models generated through the Grid partition technique. Although $ANFIS_{(3)}(4)$ has more fuzzy sets per input variable, the generated fuzzy inference system structure only contains 10 rules, while the model that better describes the system under consideration, $ANFIS_{(3)}(2)$, has 162 rules. ANFIS models resulting from the Grid partition are expected to be more complex

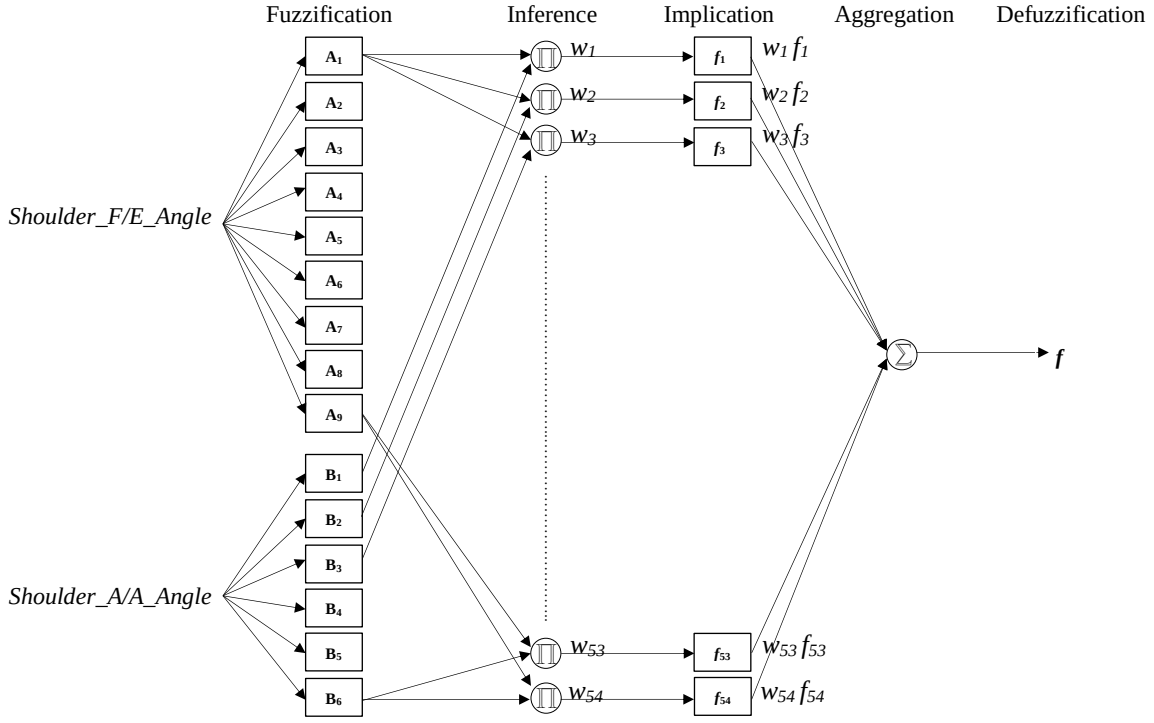

Figure 7.13. Structure of the $ANFIS_{(2)}$ for RSSI prediction.

Table 7.3. Information about the architectures of the set of ANFIS$_{(3)}$(*j*) models, which were generated through different initial model generation techniques and configured with different types of MFs.

ANFIS Parameter Type	**ANFIS$_{(3)}$(*1*)**	**ANFIS$_{(3)}$(*2*)**	**ANFIS$_{(3)}$(*3*)**	**ANFIS$_{(3)}$(*4*)**
Number of Inputs	3			
Generation technique	Grid Partition	Subtractive Clustering	Generation technique	Grid Partition
Membership Function Type	Gaussian Curve	Triangular-Shaped	Generalised Bell-Shaped	Gaussian Curve
Number of MFs	9*6*3			10*10*10
Training Data Set	27500			
Checking Data Set	4125			
Epoch Number	15			
Number of Nodes	378	378	378	86
Number of Linear Parameters	648	648	648	40
Number of Nonlinear Parameters	72	72	72	60
Number of Fuzzy Rules	162	162	162	10
Input Combinations	*Shoulder_F/E_Angle; Shoulder_A/A_Angle; Forearm_S/P_Angle*			
Training Error (RMSE)	5.17311	5.16667	5.17315	5.18715
Checking Error (RMSE)	5.6197	5.61323	5.61994	5.63132

than models generated through Subtractive clustering technique, since, in the former technique, any combination of MFs results in a rule. This complexity increment, which demands more computational resources, results in slight performance improvements.

Figure 7.15 illustrates the Membership functions shape after training the model ANFIS$_{(3)}$(*4*) for 15 epochs. Each input of this FIS model has ten MFs, which are called "Cluster 1", "Cluster 2", …, "Cluster 10" and ten rules are generated to describe the system. Each rule generated through the *genfis* MATLAB command has one value, since the output is of the type "*constant*" by default.

The ANFIS$_{(4)}$(*j*) relies in four inputs to describe the radio channel quality, namely *Shoulder_F/E_Angle*, *Shoulder_A/A_Angle*, *Forearm_S/P_Angle* and *Elbow_F/E_Angle.* The ANFIS$_{(4)}$(*4*) was generated through the Subtractive clustering and have MFs number (20*14*3*3) of the Gaussian type.

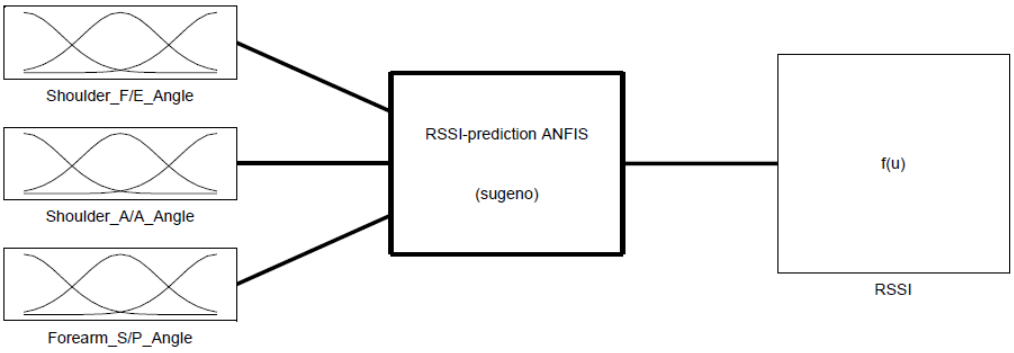

Figure 7.14. Sugeno Fuzzy Inference System with three inputs.

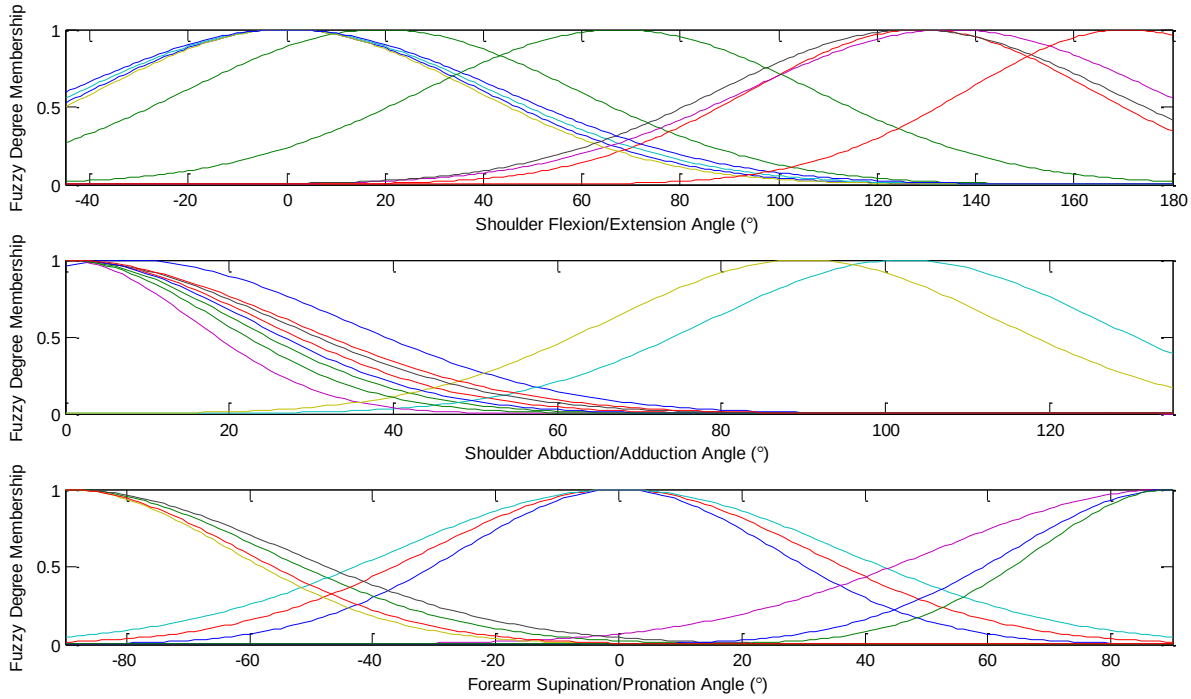

Figure 7.15. Membership Functions of the ANFIS$_{(3)}$(*j*) inputs after training.

Table 7.4 shows the ANFIS$_{(4)}$(*4*) information structure, demonstrating that twenty rules ensure a model performance that is acceptable and quite accurate to describe the system under consideration. The ANFIS$_{(4)}$(*j*) models performance demonstrated that the Triangular-shaped model is the best fit model with a RMSE value of 3.23473.

The lowest complexed model is the Subtractive clustering model that obtained 3.24985 and 3.87458 as training and checking RMSE's values, respectively. Several ANFIS models with different inputs, MFs number, and shapes were evaluated based on their performance in training and checking data sets in order to analyse the effect of their influence on model performance.

Table 7.4. The ANFIS$_{(4)}$(*4*) information structure.

ANFIS Parameter Type	**ANFIS$_{(4)}$(*4*)**
Number of Inputs	4
Membership Function Type	Gaussian Curve
Number of Membership Functions	20*14*3*3
Training Data Set	27500
Checking Data Set	4125
Epoch Number	15
Number of Nodes	127
Number of Linear Parameters	100
Number of Nonlinear Parameters	80
Number of Fuzzy Rules	20
Input Combinations	*Shoulder_F/E_Angle;* *Shoulder_A/A_Angle;* *Forearm_S/P_Angle;* *Elbow_F/E_Angle;*
Training Error (RMSE)	3.24985
Checking Error (RMSE)	3.87458

The performance of the best-fit models for each inputs combination and the Subtractive clustering models are shown in Table 7.5. It is clear that the ANFIS performance increase with the increase of the number of inputs, showing significant improvement variations.

Increasing the number of inputs means an increasing of model performance, however, increasing the number of MFs per input does not necessarily means an increase in the model performance or on the structure complexity. Grid partition models do not seem to be very sensitive to the type of MFs, as no significant difference between models has been reported. Summarizing, the subtractive clustering ANFIS models have much less rules and nodes, but ensure a model performance similar to the performance of Grid partition models.

Taking this observations into consideration, the $ANFIS_{(4)}(4)$ is chosen as the best-fit model. Even though this model is not the one with the best performance, it presents a lesser complex structure (four inputs, 20*14*3*3 - determined through trials -, and a NN that comprises 127 nodes and 20 rules) and performance is still satisfactory since an RMSE of 3.24985 and 3.87458 are the results of the model's evaluation against training and checking dataset, respectively.

The $ANFIS_{(4)}(4)$ was subjected to the steps (3), (4), (5), (6) and (7) of the methodology depicted in Figure 7.5. The training the ANFIS model for several interactions is very important not only to optimize the initial model as the maximum possible but also to handle with the problem of model overfitting. The overfitting problem can be identified by plotting the training and checking error. It occurs when error starts to increase with the number of epochs or when the performance on the training set is much lower than the performance on the checking set (because the model fits too much to seen data, and does not generalize well). The overfitting problem can be avoided through the identification of the last epoch before overfitting starts, i.e. epoch number where the RMSE is the lowest [177].

The training and checking errors for 100 epochs are depicted in Figure 7.16. The magnitude difference between the training and checking error is not significant. The optimal epoch number to the $ANFIS_{(4)}(4)$ is four.

Table 7.6 summarizes the performance results of the $ANFIS_{(4)}(4)$ model when it is assessed against the testing dataset. The performance results indicate that the model under consideration produces satisfactory results, namely a RMSE of 4.079, MAE of 2.24 and a R^2 of 0.83, showing

Table 7.5.Performance of the best-fit ANFIS models.

Model	**Inputs**	**Training Error (RMSE)**	**Checking Error (RMSE)**
$ANFIS_{(2)}(2)$	2	5.51661	5.97267
$ANFIS_{(2)}(4)$	2	5.5333	5.98783
$ANFIS_{(3)}(2)$	3	5.16667	5.61323
$ANFIS_{(3)}(4)$	3	5.18715	5.63132
$ANFIS_{(4)}(4)$	4	3.24985	3.87458

Table 7.6. Performance results of the ANFIS$_{(4)}$(*4*) when tested against the testing data set.

Model	**R^2**	**RMSE**	**MAE**
ANFIS$_{(4)}$(*4*)	0.83	4.07952	2.24

that this model can be successfully used to describe the system under consideration, i.e. the on-body link (Node-PROTACTICAL 7-Gateway-PROTACTICAL) quality). The testing RMSE result values are a bit higher than the training and checking RMSE values, but the error difference obtained suggest that this model might be able to generalize well unseen data sets.

Figure 7.17 shows an example of the ANFIS surface view. The three-dimensional curve was obtained through *gensurf* command provided by MATLAB. This graph represents the mapping from *Shoulder_F/E_Angle* and *Forearm_S/P_Angle* to the normalized ANFIS$_{(4)}$(*4*) output the (RSSI).

7.3.4 PER-prediction LQE

The methodology followed to find the best-fit RSSI-predicted model was also employed to find the model that best describe the outage probability of the system under consideration. Table 7.7 shows information related to training and checking error of the best-fit models after running the training methodology for 15 epochs.

These models were trained into a training data set composed by 2503 vectors (three quarters of the input data collected), while two groups of 537 vectors were randomly chosen for checking and testing data set.

The ANFIS$_{(5)}$(*4*) is the one with best performance, ensuring a training and checking RMSE values of 6.39227 and 6.76810, respectively. This ANFIS model has five inputs, namely *TPL,*

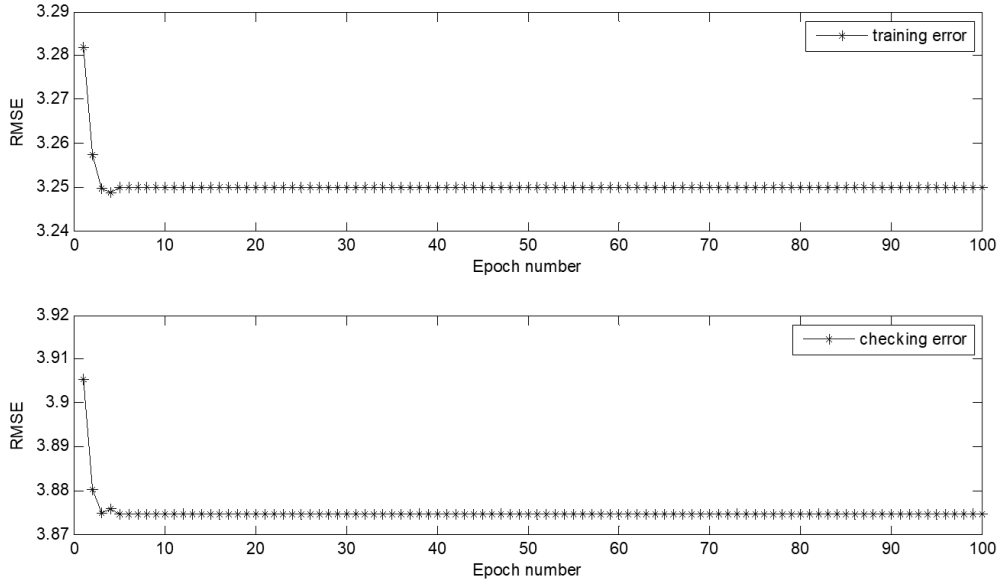

Figure 7.16. Training and checking error curve after training data into the ANFIS$_{(4)}$(*4*) Subtractive Clustering system (ANFIS) for 100 epochs with an error tolerance of 0.0001

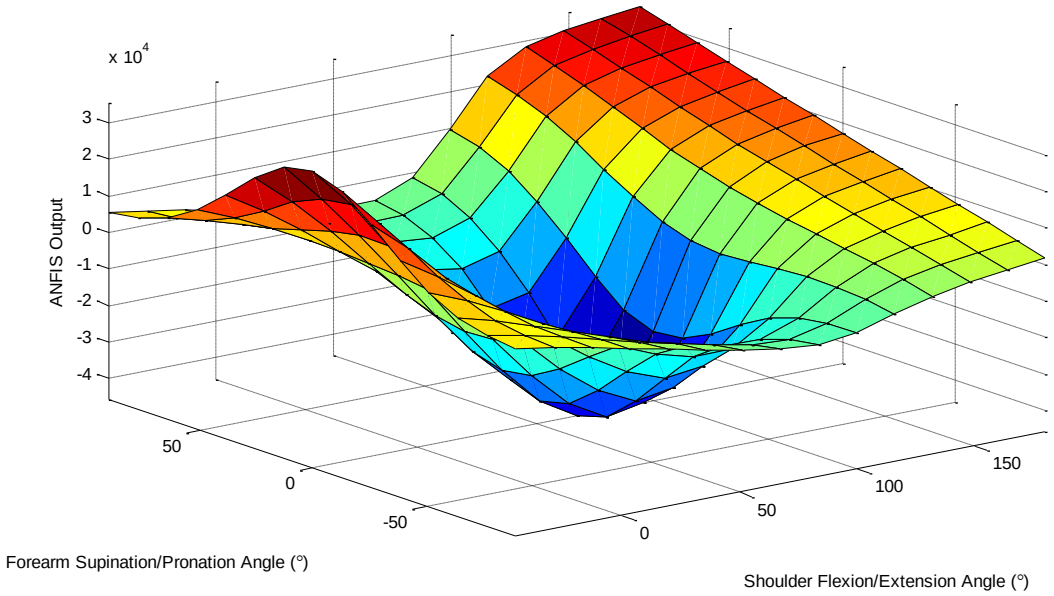

Figure 7.17. Surface view of the mapping between two model input and the ANFIS$_{(4)}$(*4*) output.

Shoulder_F/E_Angle, *Shoulder_A/A_Angle*, *Forearm_S/P_Angle*, and *Elbow_F/E_Angle* which have the MF number 35*35*35*35*35 with a Gaussian curve shape.

Table 7.8 summarizes the features of the ANFIS$_{(5)}$(*4*) structure, which consists of 428 nodes, 210 and 350 linear and nonlinear parameters respectively, where 35 rules are required to describe the system. This model was trained for 100 epochs in order to optimize the parameters of the several rules stored in the fuzzy rules database. As result of this process, the values of 6.35399 and 6.74908 were reported as the training and the checking error (RMSE).

The testing process shows that the error does not increase significantly in relation to the training error. Therefore, testing results suggest that the ANFIS$_{(5)}$(*4*) can be employed as a PER-prediction LQE. Figure 7.18 shows a three-dimensional curve that graphically describes the mapping from *Elbow_F/E_Angle* and *TPL* to the normalized ANFIS$_{(5)}$(*4*) output. This graph

Table 7.7. Performance of the best-fit ANFIS models when predicting the outage probability of WBAN-PROTACTICAL radio channels.

Model	**Inputs**	**MFs shape**	**Training Error**	**Checking Error**
ANFIS$_{(3)}$ (*2*)	*TPL, Shoulder_F/E_Angle, Shoulder_A/A_Angle;*	Triangular-shaped	7.41611	7.78093
ANFIS$_{(3)}$ (*4*)	*TPL, Shoulder_F/E_Angle, Shoulder_A/A_Angle;*	Gaussian Curve	7.44798	7.81321
ANFIS$_{(4)}$ (*2*)	*TPL, Shoulder_F/E_Angle, Shoulder_A/A_Angle, Elbow_F/E_Angle*	Triangular-shaped	7.11596	7.53910
ANFIS$_{(4)}$ (*4*)	*TPL, Shoulder_F/E_Angle, Shoulder_A/A_Angle, Elbow_F/E_Angle*	Gaussian Curve	7.15469	7.59917
ANFIS$_{(5)}$ (*4*)	*TPL, Shoulder_F/E_Angle, Shoulder_A/A_Angle, Elbow_F/E_Angle, Forearm_S/P_Angle*	Gaussian Curve	6.39227	6.76810

Table 7.8. The ANFIS$_{(5)}$(*4*) information structure.

ANFIS Parameter Type	**ANFIS$_{(5)}$(*4*)**
Number of Inputs	5
Membership Function Type	Gaussian Curve
Number of Membership Functions	35*35*35*35*35
Training Data Set	2503
Checking Data Set	537
Epoch Number	100
Number of Nodes	428
Number of Linear Parameters	210
Number of Nonlinear Parameters	350
Number of Fuzzy Rules	35
Training Error (RMSE)	6.35399
Checking Error (RMSE)	6.74908
Testing Error (RMSE)	7.0943
Testing Error (R^2)	0.89
Testing Error (MAE)	2.24

shows that the PER increase with the decrease of the TPL regardless of the angle between the upper arm and the forearm.

The accuracy of the RSSI- and PER-prediction model and their satisfactory performance when subjected to different data sets are ensured by the high values of R^2 and low values of RMSE and MAE. Table 7.9 summarizes some additional information relative to the complexity of each of the selected ANFIS models, where the number and types of mathematical operations required along the layers that compose the ANFIS model structure are shown.

7.4 PCPS Implementation

As stated before, the evaluation of any development on the WBANs field based on simulations is not common in the literature due to the fact that simulation models are based on simplified assumptions [24], [143]. As a consequence of the simulators not being able to model many of the characteristics of the real world, high discrepancies between the path-loss, radio channel quality temporal variations (fading) obtained through simulations and the on-body features obtained experimentally through the radio channel characterization performed are recurrent [143], [190].

In this regard, the selection of a simulator is extremely important. We have selected the software Simulink to implement and assess the PCPS mechanism.

7.4.1 Simulink Model

Although this Simulink is not a simulator for WBANs, WSNs or any other communication network, the path-loss and fading characteristics are introduced in our simulation implementation in the form of a database containing the data collected experimentally. Another

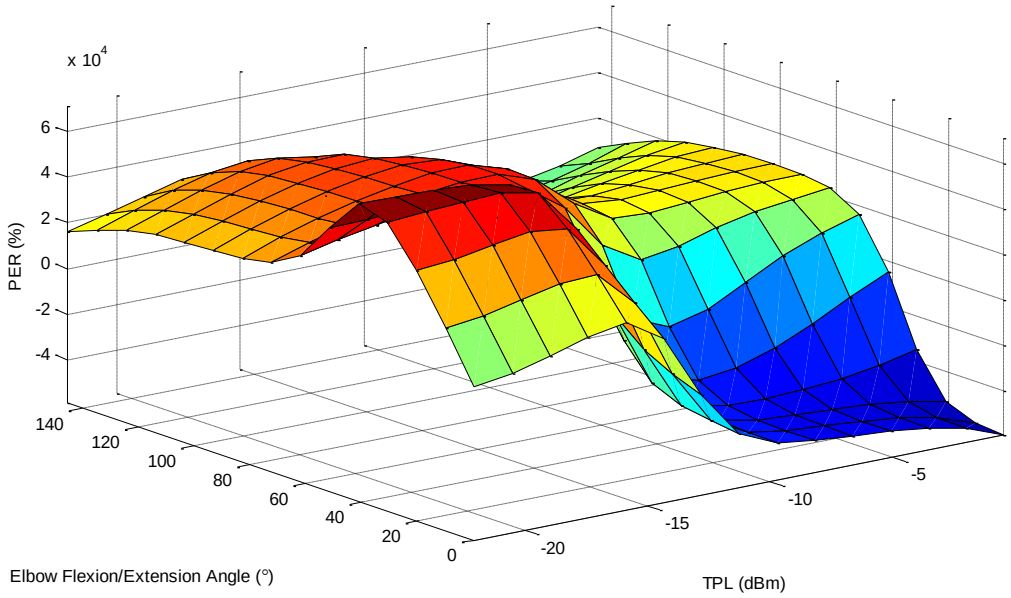

Figure 7.18. Surface view of the mapping between two inputs (*Elbow_F/E_Angle* and TPL) and ANFIS$_{(5)}$(*4*) output (PER).

limitation of this software package, is related to its incapacity of simulating the body movement. In order to overcome this limitation, the term *gesture* (*G*) was introduced, which is defined as "a movement of part of the body to express an idea or meaning" [Oxford English Dictionary, 2016], to represent a succession of movements of the upper limb. As a *posture* is a representation of several angles between two different segments of the upper limb, the arm motion is represented as a sequence of several *posture*, which can be defined as: $G = P(t)_{t_{0.035}}^{t_n} = \{P_{0.035}, P_{0.070}, P_{0,105}, \dots, P_n\}$, where P_{ti} is a posture in a time frame (time unit is 0.035 s).

Figure 7.19 depicts the PCPS mechanism implementation on Simulink where three main blocks can be seen: "ANFIS Model to RSSI Signal", represents the ANFIS model selected as RSSI-prediction LQE; "TPL_Control_Block", which is the equivalent to the TPL Control block illustrated in the PCPS mechanism structure overview (c.f. Figure 7.4); "ANFIS Model to PER Signal", which is the proposed PER-prediction ANFIS model; and a "While Iterator Subsystem".

The block "ANFIS Model to RSSI Signal" is a Fuzzy Inference System block that represents the implementation of the selected ANFIS model, the ANFIS$_{(4)}$(*4*), to operate as RSSI-prediction LQE. A set of Simulink blocks of the type "From Workspace" are linked to the RSSI-prediction LQE, namely "Shoulder_FlexionExtension",

Table 7.9. Number of operations of the selected ANFIS models to describe the system.

Model Output	Sums	Subtractions	Products	Divisions	Exponentials
RSSI	59	40	81	80	40
PER	351	350	176	350	175

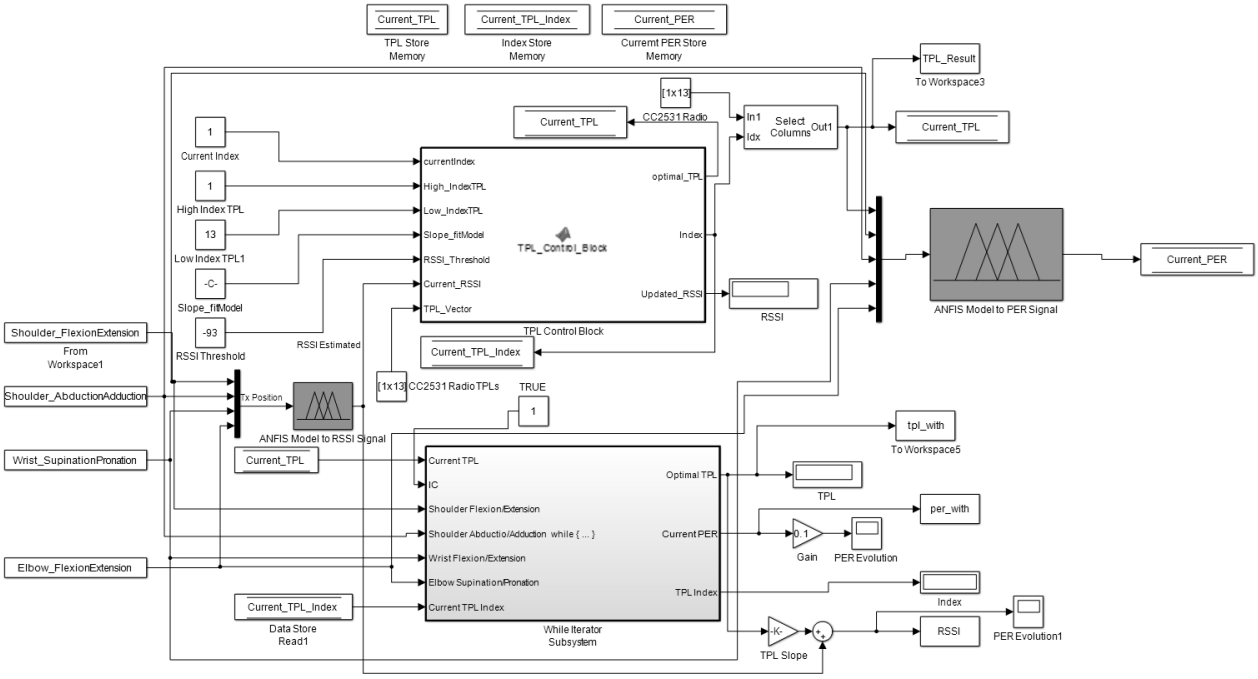

Figure 7.19. PCPS implementation in Simulink.

"Shoulder_AbductionAdduction", "Wrist_SupinationPronation" and "Elbow_FlexionExtension", which can only take one value at each time unit (Simulator are set to perform time steps of 0.035 s). Each of these blocks consist of time series, which are data vectors sampled over time (regular intervals of 0.035 s). Therefore, the combination scalar values (provided at any time instant by each block) form the *position* vector, whereas the sequence of rows of these blocks enable to determine the arm motion as a *gesture* (*G*).

Figure 7.20 shows an inside look at "ANFIS Model to RSSI Signal" block, illustrating the ANFIS structure implementation in Simulink in the form of layers equivalent to the $ANFIS_{(4)}(4)$ structure. The variables "in1", "in2", "in3", "in4" are the linguistic variables, referring to the *Shoulder_F/E_Angle*, *Shoulder_A/A_Angle*, *Elbow_F/E_Angle*, *Forearm_S/P_Angle* FIS inputs, respectively.

Figure 7.21 a) illustrates the "in1" input characteristics mapping through MFs process in the developed Simulink model. Figure 7.21 b) shows the sequence of blocks implemented to compute the "in1" degree of belongingness (Fuzzification step) to the fuzzy set via the associated membership function "in1cluster1", which is shaped through its associated parameters, which are here represented through "mu" (represents the MF centre) and "sigma" (determines the MF width) Constant blocks.

Figure 7.21 c) illustrates an implementation of a rule block, where inference and implication process are computed in order to calculate the rule output, which is the output of the layer 4 that given by expression (7.5). "andorMethod" block, depicted in depicted in Figure 7.21 c),

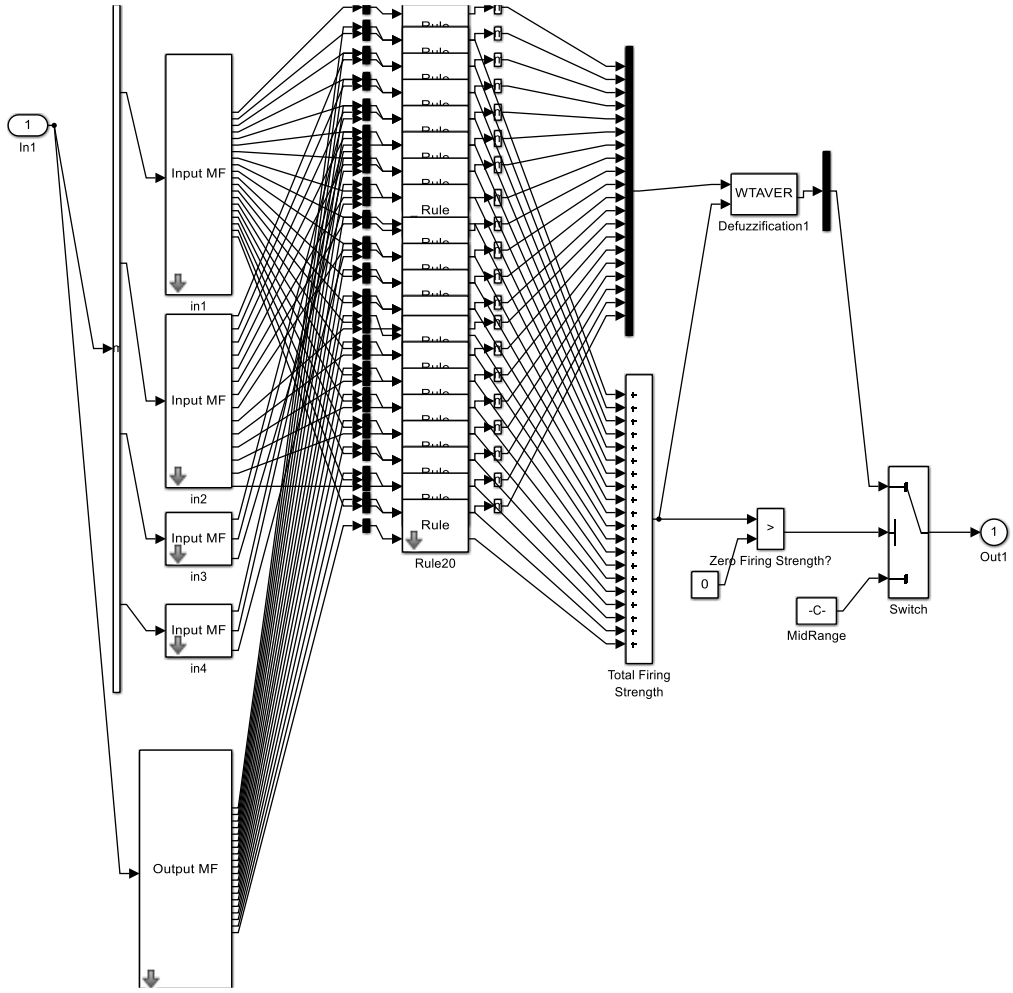

Figure 7.20. Simulink implementation of the ANFIS(4)(4) model.

performs the multiplication of all degrees of the fuzzy sets belongingness (antecedents) expressed by equation (7.3), providing a single number given by the antecedents (Layer 2 output in a Takagi-Sugeno FIS structure). The "weighting" block performs the product between the rule antecedent single value and the "weight" parameter, performing the expression (7.4), resulting the Takagi-Sugeno Layer 3 output: the normalized firing strength of the rule under consideration. The "impMethod" block performs a product, in our case the product of the equation (7.5), which consists in the multiplication between the normalized rule firing strength and the consequence parameter determined by the linear MF of the Fuzzy sets of the ANFIS output depicted in Figure 7.22.

Since the ANFIS$_{(4)}$(4) model has twenty rules, the number of MFs of the model output has to have exactly the same, since each MFs represents the consequent parameter. This is computed as a linear combination of the input variables added by a constant term, i.e. a_1"in1" + a_2" in2" + a_3"in3" + a_4"in4" + b ("in1", "in2", "in3" and "in4" the model inputs and a_i and b are the consequent parameters set, the linear and constant coefficient, respectively). The image on right side of Figure 7.22 shows the diagram of blocks implemented in Simulink to

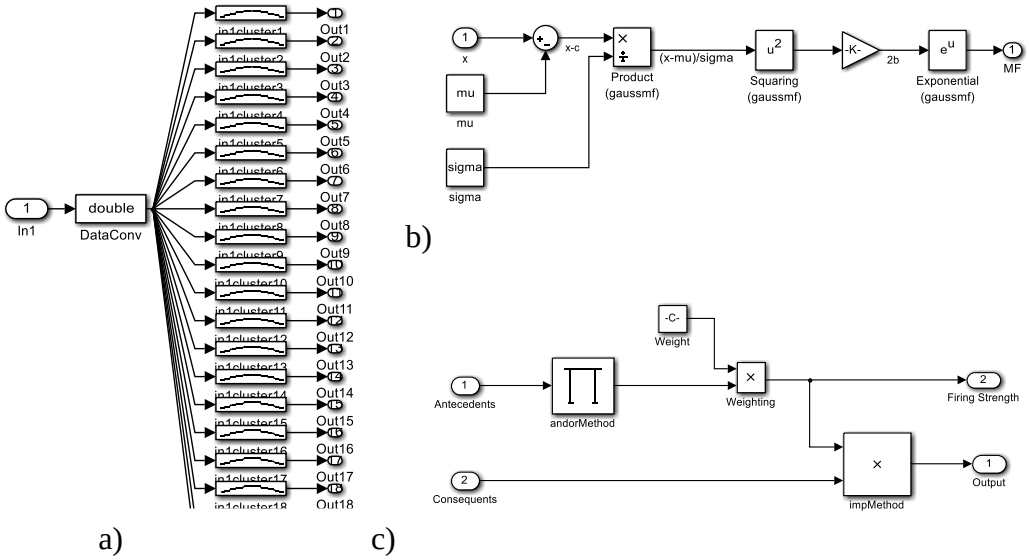

Figure 7.21. a) Representation of the Fuzzy sets of the "in1" (*Shoulder_F/E_Angle* FIS input), b) Simulink implementation of the Membership Function "in1cluster1", and c) rule 1 block implementation.

compute the linear equation, where the input of each "LinearMF" is a vector containing the values of each model input at the current simulation time. After computing the output "LinearMF" block, the result of this operation is the input on its respective "Rule" block (c.f. Figure 7.21). This input is called "consequents" and is the consequent parameter required to obtain the output given by expression (7.5).

Figure 7.23 shows the inside of the Defuzzification block that implements the defuzzification process of a Takagi-Sugeno ANFIS model, performing first the aggregation operator, which is the sum of all the incoming signals (multiplication between rule firing strength and consequent parameter). This value is then divided for the total firing strength in order to provide the $ANFIS_{(4)}(4)$ output as in equation (7.6). This output is the RSSI prediction of the RSSI-prediction LQE.

The "TPL_Control_Block" consists of a MATLAB Function block that enables the integration of the MATLAB algorithm in our Simulink model. The MATLAB script loaded by this block is a MATLAB function that performs the reactive-based TPL Control approach described in subsection 6.2.2. This bock requires as input the slope of the model given by expression (6.1) that describes the linear relation between TPL and RSSI. This slop is represented by a Constant Simulink block, designated "Slope_fitModel", that takes the value 0.8444, which is the RSSI decay rate found to subject 1 in chapter 5. Other important inputs of this block are the maximum and minimum TPL values (designated "High Index TPL" and "Low Index TPL, respectively"), these blocks limits the output block to the range [-0.5 dB, …, -22 dB].

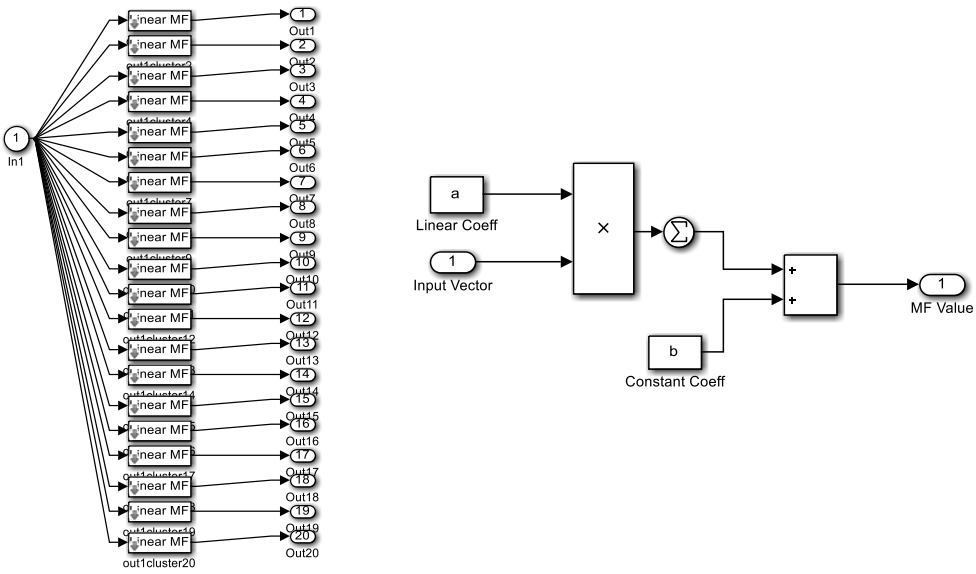

Figure 7.22. Set of MFs of the output variable (left image), which are computed as a linear equation, computed through the sequence of blocks illustrated in right image.

The "ANFIS Model to PER Signal" block consists of a Fuzzy Inference System block that implements the ANFIS$_{(5)}$(*4*). The "Shoulder_FlexionExtension", "Shoulder_AbductionAdduction", "Wrist_SupinationPronation", "Elbow_FlexionExtension" and "From Workspace blocks", namely "Current_TPL" are connected to the "ANFIS model to PER Signal" block, representing the *Shoulder_F/E_Angle*, *Shoulder_A/A_Angle*, *Elbow_F/E_Angle*, *Forearm_S/P_Angle* and *TPL* ANFIS$_{(5)}$(*4*) inputs. The "Current_TPL" is a Data Story Write block, which enables to write data to a data store, therefore the output of RSSI-prediction LQE, which is the optimal TPL, is stored in this block and later used by the PER-prediction LQE to estimate the PER according to the *position* vector at a given time. The output of the "ANFIS Model to PER Signal" is a PER value that is stored in "Current_PER" block.

The "While Iterator Subsystem" block (depicted in Figure 7.24) is the element in the Simulink model responsible for determining the TPL that might ensure a RSSI higher than the *RSSI Threshold* and with a higher chance of reaching de receiver (low OP). Although the

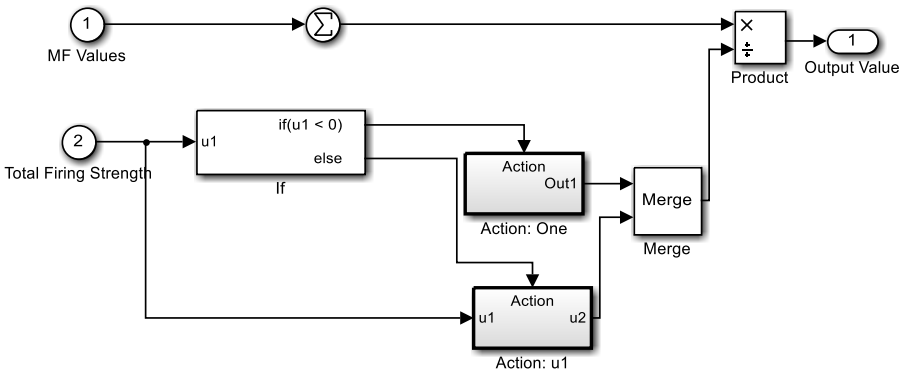

Figure 7.23. Defuzzification process implementation in Simulink.

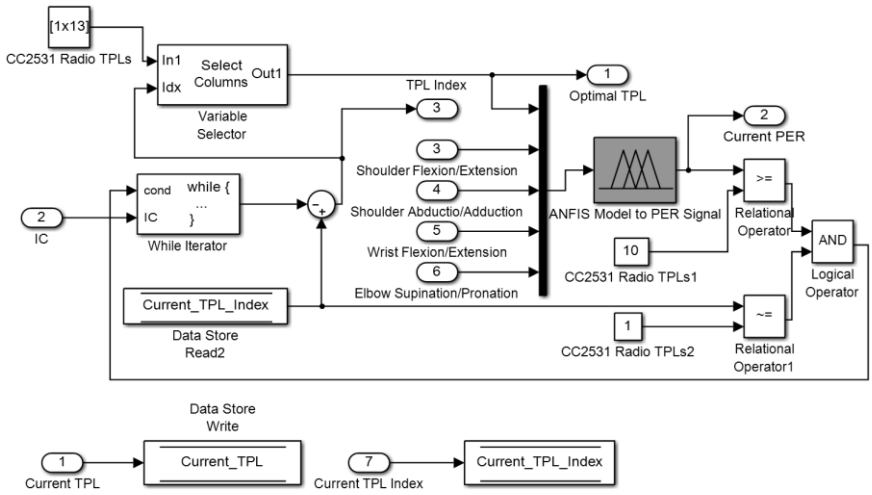

Figure 7.24. Inside look of the block called "While Iterator Subsystem" that comprises the ANFIS PER model and implements a While cycle in order to recalculate the optimal TPL.

computed RSSI of a potential data packet transmitted in the current scenario conditions at TPL given by the "ANFIS Model to RSSI Signal" block is higher than the receiver sensitivity (or another defined threshold), in terms of outage, this scenario conditions might not be favourable to successful transmissions. The "ANFIS Model to PER Signal" indicates this information through the computed PER as follows: high PER means that the optimal TPL must be increased in order to increase the hypotheses of the data packet be received in Coordinator node. Data packets are postponed when either the "ANFIS Model to RSSI" output is lower than the chosen threshold or no TPL ensures the criterion PER lower than a given threshold.

7.4.2 Simulation Results

In this subsection, the simulation results of the PCPS mechanism and the simulation results of other mechanisms are presented and compared. Besides the PCPS mechanism, the following mechanisms were assessed and the results analysed:

- Static TPL, in this approach all data packets transmission occurs at maximum TPL value allowable in on-body communications (-0.5 dBm);
- Offline PCPS, this mechanism has the same architecture of the proposed PCPS, as depicted in Figure 7.4. However, in this approach, the computation of the optimal TPL is performed off-line;
- Power Control (PC), this mechanism comprises the RSSI-prediction LQE and TPL Control blocks of the PCPS. However, it does not perform the PER-prediction LQE, implementing only the power control features of the PCPS mechanism;

- Power Scheduler (PS), similar to previous mechanism. However, only PER-prediction LQE mechanism is implemented. Thus, there is no output power control and this mechanism postpone when the PER is higher than a threshold value;
- Reactive Without Scheduler (RWS), it is a mechanism similar to the closed-loop control TPCs, where the optimal TPL is selected according to the measured RSSI of the previous transmitted data packet and following a dynamic-based TPL Control fashion;

The simulation of these mechanisms is only possible because the link created between the Node-PROTACTICAL 7 and the Gateway-PROTACTICAL was extensively characterized with respect to the RSSI and PER metrics in all the movements and for all the TPLs. Through the experimental data a Look-up Table (LUT) – it maps inputs (arm position angles and TPL) to an output (RSSI, PER and optimal TPL) – created in order to dictate the outcome of the execution of the mechanisms. In the Static TPL, Offline PCPS, and RWS mechanism the computation of the optimal TPL is done off-line and their outcome provided by the LUT. Unlike the PCPS mechanism that computes the optimal TPL online and his outcome (RSSI) is provided by the developed ANFIS models, the PC and PS mechanism use the RSSI-prediction LQE ("ANFIS Model to RSSI Signal" block of the PCPS's Simulink implementation) and the PER-prediction LQE ("ANFIS Model to PER Signal" block visible Figure 7.19) model, respectively, only to compute the optimal TPL ("TPL_Control_Block") and to determine the estimated PER (used to determine whether the current data packet transmission should be postponed or not), respectively. Their outcome (RSSI) is provided by the LUT.

The comparison of the performance results of all mentioned mechanisms enables the validation of each PCPS mechanism functionality, namely the power control and transmission scheduler. The various simulations performed during the evaluation process of the various mechanisms lasted the equivalent to the time required to perform 50 repetitions of any movement. Several movements and combinations have been considered during this process, such as:

1. Shoulder flexion (from angle -135º up to 180º) followed by extension (from 180º up to -135º) of upper limb at shoulder limb while the angle between upper arm and forearm is static (as well as the *Shoulder_AbductionAdduction* angle with value 0º), forming an angle of 0º. This movement was considered for three different simulation configurations, which differ in the forearm angle. Therefore, this movement is repeated

for scenarios where forearm angles are 90º, -90º and 0º (angle static during the simulation interval execution);

2. Shoulder abduction (from 0º up to 145º) followed by adduction (from 145º up to 0º) of left upper limb at shoulder joint while remaining angles are static (both *Shoulder_F/E_Angle* and *Elbow_F/E_Angle* with an angle of 0º) to static *Forearm_S/P_Angle* of -90º and 0º;
3. Elbow flexion (from 0º up to 145º) followed by extension (from 145º up to 0º) of the forearm at elbow joint while the remaining angles are static (*Shoulder_F/E_Angle* and *Shoulder_A/A_Angle* with an angle of 0º);
4. Walking movement is repeated for three different *Forearm_S/P_Angle* (90º, -90º and 0º) while *Elbow_F/E_Angle* remains static (0º).

In the first three upper limb movements the user is standing while he moves the upper limb as described above. Other important aspect, during the execution of the mechanism, is the *RSSI Threshold* (c.f. section 3.2) used by the TPL Control block (c.f. Figure 7.19) to estimate the optimal TPL. In this regard, the *OP Threshold* defined during simulations is 10%, whereas, regarding the *RSSI Threshold*, different values were chosen. To PCPS, offline PCPS and PC mechanism simulations the RSSI value -93 dBm was set as *RSSI Threshold*, whereas the RWS mechanism is configure with a *RSSI Threshold* value of -86 dBm.

The remaining section analyses the performance of the proposed mechanisms in terms of lost data/PER, average TPL and latency in transmissions, as well as the influence of the RSSI and PER limit on the mechanism performance.

In any simulation, the data packets transmission and the execution of the mechanism are trigger every 35 ms. Thus, the latency of any mechanism performance is in each simulation given by the multiplication of the interval between transmissions (35 ms) by the outcome of the division between the number of data packets not sent (data packet transmission postponed or data packets transmitted but never received by the receiver) and the number of data packets successfully transmitted to the receiver.

Performance Analysis

The analysis of the performance of a communication system that transmits data at the maximum power allowed in WBANs serves to prove that scaling mechanisms of data packet transmissions, as well as the power control schemes employed in each of these transmissions, are fundamental to a reliable communication system. The results obtained in terms of PER are shown in Figure 7.25 and they suggest that this mechanism (Static TPL) is not able to ensure

the reliability levels required in WBANs for part of the case studies considered. During the simulations of movements 1 and 4, this mechanism achieved PERs lower than the imposed limit, 7%, and 9% respectively. However, for the case study of movements 2 and 3, the PER was 15% and 13%, respectively.

The reported latency values of the Static TPL mechanism are lower than the limits of medical and non-medical applications. Average latency of 44.5 ms, 59.0 ms, 48.6 and 43 ms are reported for movement 1, 2, 3 and 4, respectively. These results, shows that outages occurs with high frequency but for a short period of time.

According to the performance results of the RWS mechanism, this mechanism ensures average RSSI values (-84 dBm, -85 dBm, -84 dBm, -82 dBm for movement 1, 2, 3 and 4 respectively) higher than the value imposed as *RSSI Threshold* (-86 dBm) in the performed simulations.

The performance results in terms of average RSSI of this mechanism and the others is shown in Table 7.10. It can be seen, from the average TPL used during simulations, that the TPL has suffered a significant reduction compared to the transmissions at the predefined power level (-0.5 dBm - c.f. Figure 7.26) performed by Static TPL and PS mechanism.

The RWS solution reduces the SAR, for movements 1, 2, 3 and 4, respectively. However, the performance of this mechanism, in terms of reliability is unsatisfactory. The observed PER values are higher than the maximum limits announced by working group TG6, and slightly

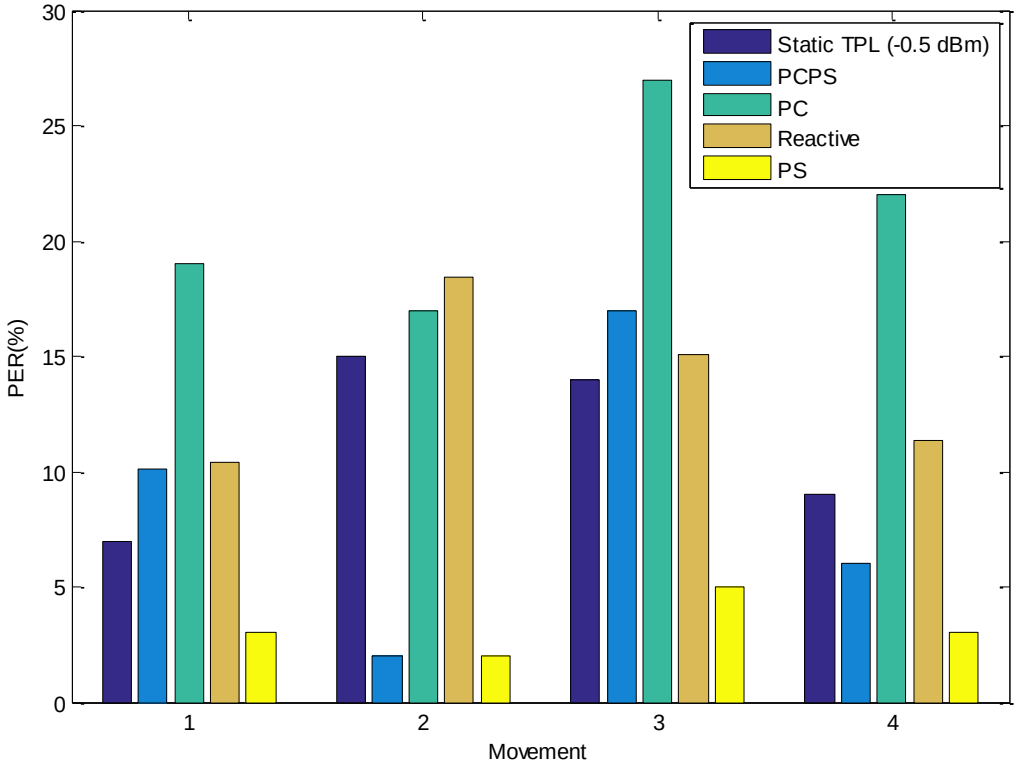

Figure 7.25. Packet Error Rate performance of several mechanisms in different movements.

Table 7.10. Simulation results in terms of average RSSI (dBm) for several mechanisms.

Mechanism	Movement 1	Movement 2	Movement 3	Movement 4
Static TPL (-0.5 dBm)	-77	-83.6	-82	-78
PCPS	-86	-90	-85	-84
Offline PCPS	-89	-91	-85	-85
PC	-89	-89	-90	-90
RWS	-84	-85	-84	-82
PS	-78	-84	-83	-76

worse than the results of Static TPL mechanism. The best performance of RWS in terms of PER occurs for simulations of movement 1, with a PER of 10.40%, while the worst case is movement 2 (PER is 18.45%).

Although the radio channel quality (when translated into the measured RSSI) suggests that the current radio channel conditions (RSSI values) are appropriate for performing data exchange between nodes, the amount of data lost during this process is quite significant. Thus, the use of the RWS mechanism for the study case under consideration would imply the degradation of the communication reliability, leading the system to lose data packets and to increase the latency and energy consumption on retransmissions of the lost data packets.

Although the above mechanism has proved to be inefficient in the quest to ensure the QoS requirements imposed by applications, this is not the one that has the worst performance. From the set of mechanisms considered for analysis, the PC mechanism is the one with the worst

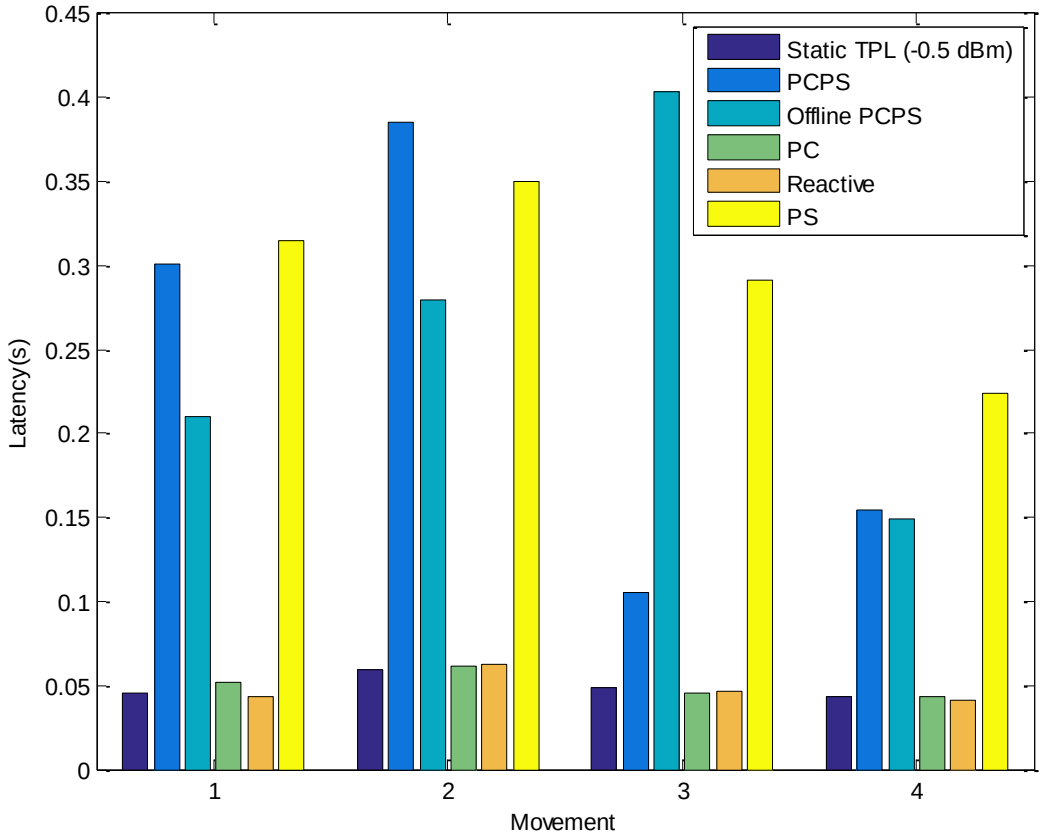

Figure 7.26. Latency performance of the several mechanism under consideration for different movements.

performance in terms of PER. With respect to the average PER, we can see that performance results of this mechanism are much higher than the *OP Threshold*. PER values of 19%, 17%, 27% and 22% were obtained for study case movements 1, 2, 3 and 4, respectively. The poor performance of this mechanism occurs due to the RSSI value set as a boundary in the TPL Control mechanism is quite close to the sensitivity of the radio module, neglecting the small-scale fading effect on the radio channel quality.

The average TPL values presented in Table 7.11 show that the PER values achieved by the PC mechanism are clearly lower than those achieved by the RWS mechanism. In summary, the *RSSI Threshold* is very important in the implementation of a solution that aims to control the signal power and ensure energy efficiency in the sending of the data packet.

The results of the performance of the PS mechanism proved the usefulness of the scheduling functionality of the proposed developments. From the reliability point of view, it can be seen that the PS mechanism shows the best result for all study cases considered. Through this functionality, the proposed mechanism might be able to reduce the amount of data packets lost, achieving PER values of 3%, 2%, 5% and 3% on average for movements 1, 2, 3 and 4, respectively. These values are below the minimum required PER value in WBAN applications as well as the values reached by other mechanism in the same test conditions. However, the PS mechanism performance in terms of latency was sacrificed to increase the reliability of the transmissions. Reported values, of 315 ms, 350 ms, 292 ms and 224 ms for movement 1, 2, 3 and 4 respectively, are above the limits maximums acceptable in medical and non-medical applications.

The *OP Threshold* parameter enables to deal with the trade-off between reliability and latency in the transmission. The performance results of the PS mechanism suggest that the "PER-prediction LQE" and "While Iterator Subsystem" blocks are key blocks in the proposed implementation of the PCPS mechanism, since permits to identify the instant in which data packets are not advisable and, as a consequence, these transmissions can be postponed to future instants.

Regarding the performance of the PCPS mechanism, the average values achieved in terms of the PER, TPL and RSSI values are between the results obtained by the PC and PS mechanism. This performance degradation can be explained by the inclusion of transmission power control functionality. The results of the PC mechanism suggest that the *RSSI Threshold* value is quite close to the sensitivity of the radio module, which reduces the communications' reliability. Therefore, situations in which the TPL Control suggests a TPL that leads to a PER lower than the *OP Threshold* without having to resort to the "While Iterator Subsystem" block

Table 7.11. Simulation results in terms of average TPL (presented in dBm) for several mechanisms.

Mechanism	**Movement 1**	**Movement 2**	**Movement 3**	**Movement 4**
Static TPL (-0.5 dBm)	-0.5	-0.5	-0.5	-0.5
PCPS	-10	-6	-5	-7
Offline PCPS	-12.4	-10	-7	-12
PC	-14	-7	-11	-15
RWS	-5.6	-3.8	-5.2	-7.7
PS	-0.5	-0.5	-0.5	-0.5

are propitious to failed transmissions due to the *RSSI Threshold* considered during the simulations. This mechanism respects the WBAN reliability requirement in movement 2 and 4, achieving a PER value of 2% of 6% respectively.

It can be seen, from the TPL, PER and latency point of view, that the offline PCPS shows better results than the PCPS mechanism for most of the study cases. However, the difference with the results given by the PCPS mechanism is relatively small in simulation of movement 4, while in movement 2 the PCPS mechanism shows better performance than offline PCPS in terms of average values of PER, TPL and RSSI. Relative to the remaining case studies, namely movement 1 and 3, unlike the PCPS mechanism, the offline PCPS meets the WBAN requirements in terms of reliability, with PER values lower than 10% (worst case occurs in movement 3, with a PER of 5% due to an error on ANFIS models prediction).

In summary, the Static TPL performance shows that the communication systems that do not rely in any TPC, scheduler or hybrid approach to optimize transmissions are not able to meet the QoS requirements of WBAN applications. The chosen *RSSI Threshold* for PC mechanism might be the explanation of the poor performance presented by PC mechanism in terms of PER for the majority of the study cases. Similar to PS, offline PCPS and PCPS mechanism, before outputting the optimal TPL and after the “RSSI-prediction LQE” and TPL Control output the optimal TPL this value is updated by the “While Iterator Subsystem” block, the average TPL is updated and, as a consequence, the number of lost data packets is lower.

The offline PCPS shows better results than all the other mechanisms, however, regarding the PER results of the mechanism, this outperforms the PS in only 1-3%.

The PS mechanism increases the latency on communications in order to reduce the amount of data packet lost. The larger latency (observed in simulations of movement 1) was 105 ms. Although the scheduler functionality of the proposed mechanism seems very efficient, the comparison between achieved PER of the offline PCPS and the PCPS mechanism (values chosen as *RSSI Threshold* and *OP Threshold* during the simulation was identical on both mechanisms) in simulations of movement 1 and 3 might suggest that the residual errors of the ANFIS models selected as RSSI- and PER-prediction LQE reduce the performance of the

proposed me. Therefore, the values set as *RSSI Threshold* and *OP Threshold* influences the performance of the PCPS mechanism.

Influence of the PCPS' configurable parameters on PCPS's performance

Figure 7.27 shows the results for PER in relation to the value chosen as *RSSI Threshold* of the proposed TPL Control block. These results relate to the simulation of movement 1, since the PCPS mechanism configuration (RSSI and *OP Threshold* with values -93 dBm and 10%, respectively) tested above in this study case leads to a PER value higher than maximum acceptable. During the simulations, a 10% PER value was assigned to the configurable parameter *OP Threshold*, which remained unchanged during all simulations while PCPS mechanism with different *RSSI Threshold* values were tested, starting with -78 dBm and incrementing by 2 dBm between simulations until the *RSSI Threshold* was equal to the received model sensitivity (-96 dBm). It can be seen that the value PER decreases with the increasing of the *RSSI Threshold*. It happens due to the fact that the margin between the *RSSI Threshold* and the receiver sensitivity increases, thus, the small scale fading is less likely to drive the radio channel to outage and, as a consequence, the number of data packets lost increases.

The minimum *RSSI Threshold* that enables the proposed mechanism to ensure a PER<10% is -92 dBm in the study case under consideration. The lower obtained PER value is 3.645% and occurs when - the *RSSI Threshold* value is set to -78 dBm. However, changing the *RSSI Threshold* also affects other performance metrics as shown in Table 7.12. This table presents the TPL, RSSI and latency in relation to the several *RSSI Threshold* values tested during the

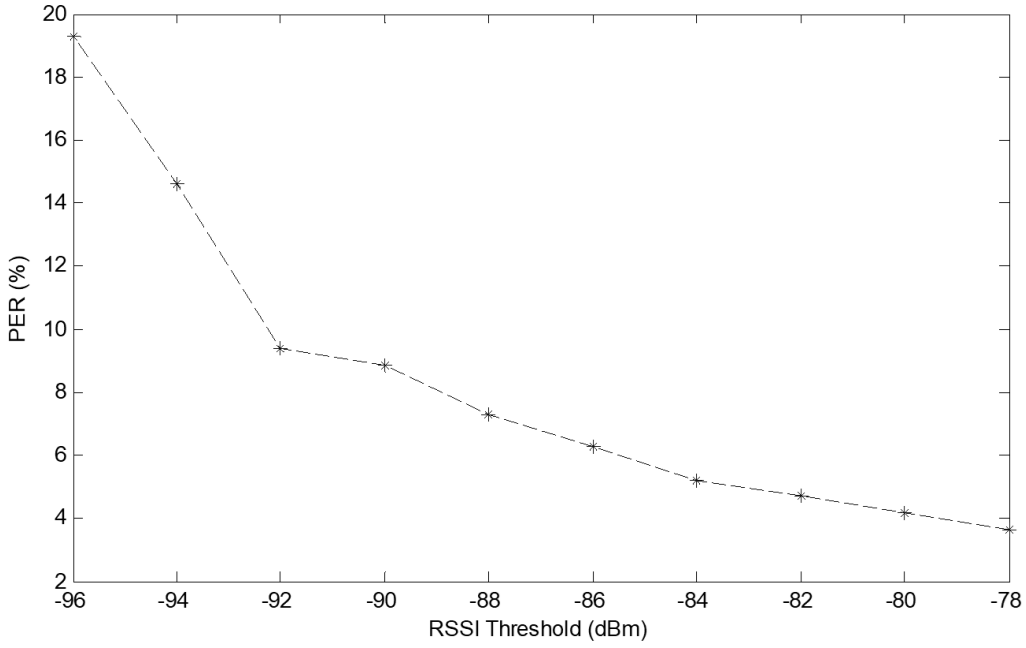

Figure 7.27. Performance of the PCSP in terms of PER for the simulation of the movement 1. PCPS mechanism is configured with 10% as *OP Threshold* while different *RSSI Threshold* were tested.

Table 7.12. PCPS mechanism performance results for metrics TPL, RSSI and latency in relation to the *RSSI Threshold* (*OP Threshold* is 10 % and remained unchanged between simulations).

***RSSI Threshold* (Movement 1)**	**TPL**	**RSSI**	**Latency**
-78	-1.31	-79.3002	0.294
-80	-1.95	-80.39	0.294
-82	-2.88	-80.91	0.294
-84	-3.92	-81.172	0.294
-86	-6.24	-82.742	0.28
-88	-6.35	-83.91	0.28
-90	-7.717	-84.384	0.28
-92	-9.266	-85.712	0.28
-94	-10.273	-86.772	0.28
-96	-11.5033	-87.159	0.28

simulations of the movement 1. It can be seen that the larger the *RSSI Threshold* value is, the lower the average TPL value is; increasing the *RSSI Threshold* value will translate into an increasing of the average RSSI value; the average latency value also increases with the increasing of the *RSSI Threshold* value. Therefore, increasing the *RSSI Threshold* value might positively affects the PER and RSSI values, but the TPL value increases, meaning that the SAR is negatively affected by high values of *RSSI Threshold*.

As the different in terms of TPL and RSSI of the minimum and maximum tested *RSSI Threshold* is significant (≈ -10 dBm and ≈ -8 dBm, respectively) a *RSSI Threshold* value that offers a satisfactory balance between metrics must be chosen. From this range of *RSSI Threshold* values, -86 dBm was the one selected for the *RSSI Threshold* since it is the one that offers the best balance between the several metrics. The observed average TPL and PER after execution of the PCPS mechanism configured with a *RSSI Threshold* of -86 dBm is shown in Table 7.13. Therefore, -86 dBm is the value chosen for the *RSSI Threshold* in the TPL Control block while different *OP Threshold* values must be tested until achieve his optimal value.

Several simulations for different *OP Threshold* values were executed to analyse the influence of this parameter on the performance of the proposed mechanism. Figure 7.28 shows the simulation average PER value for several movements. In summary, the PER value increases with the increasing of the *OP Threshold* value. Although the PER for low *OP Threshold* values is almost non-existent, these limits lead to less satisfactory results in terms of average TPL and latency values. High *OP Threshold* values result in average PER values higher than the PER reference value of 10 %, being the unique exception the PER value for the movement 3, where the maximum registered PER value is 9.8%, which occurs to the *OP Threshold* value of 18%. The maximum *OP Threshold* value that ensure average simulation PER values lower than 10% for each movement are 18%, 18%, 20% and 16% for movement 1, 2, 3 and 4, respectively.

Table 7.13. PCPS mechanism – configured with a *RSSI Threshold* and *OP Threshold* of -86 dBm and 10%, respectively – performance in terms of average TPL and PER.

Movement 1	**TPL (dBm)**	**PER (%)**
1	-6.24	6.32
2	-1.56	0
3	-4.208	7.84
4	-6.72	5.53

Regarding the latency, it can be seen in Figure 7.29 that low *OP Threshold* values result in higher latencies values, as the number of situations where both criterions (RSSI and PER higher than thresholds) are not met increase. An *OP Threshold* value of 2% leads to the maximum average latency values observed in this study, namely 0.5838 s, 0.5425 s, 0.455 s and 0.525 s for movement 1,2 ,3 and 4, respectively. At the same time, the minimum average latencies in communications are observed for simulations of the PCPS mechanism configured with *OP Threshold* value of 20%. Observed values are 0.175 s, 0.243 s, 0.202 s and 0.105 s respectively for movement 1, 2, 3 and 4.

The effect that the *OP Threshold* value has on TPL and RSSI metrics for movement 2 is represented in Table 7.14. It can be seen that both average TPLs and RSSI values decrease with the increase of the *OP Threshold* value. This trend is also observed in the remaining movements.

High *OP Threshold* values enable the "While Iterator Subsystem" block to choose from a higher range of TPL values at each time packet that might ensure a PER value lower than the *OP Threshold* value. Thus, the lowest values of this value range of TPL will be chosen as the optimal TPL value, which results on lower average simulations TPL values and, as a

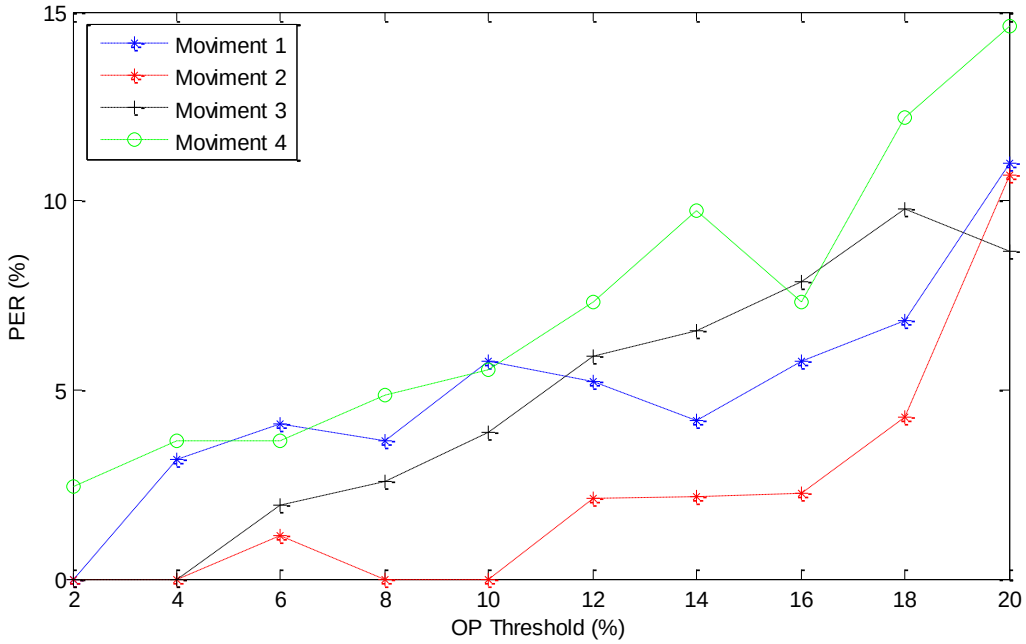

Figure 7.28. Simulation results, in terms of PER metric, of the PCPS configured with different *OP Threshold* values (2-20%).

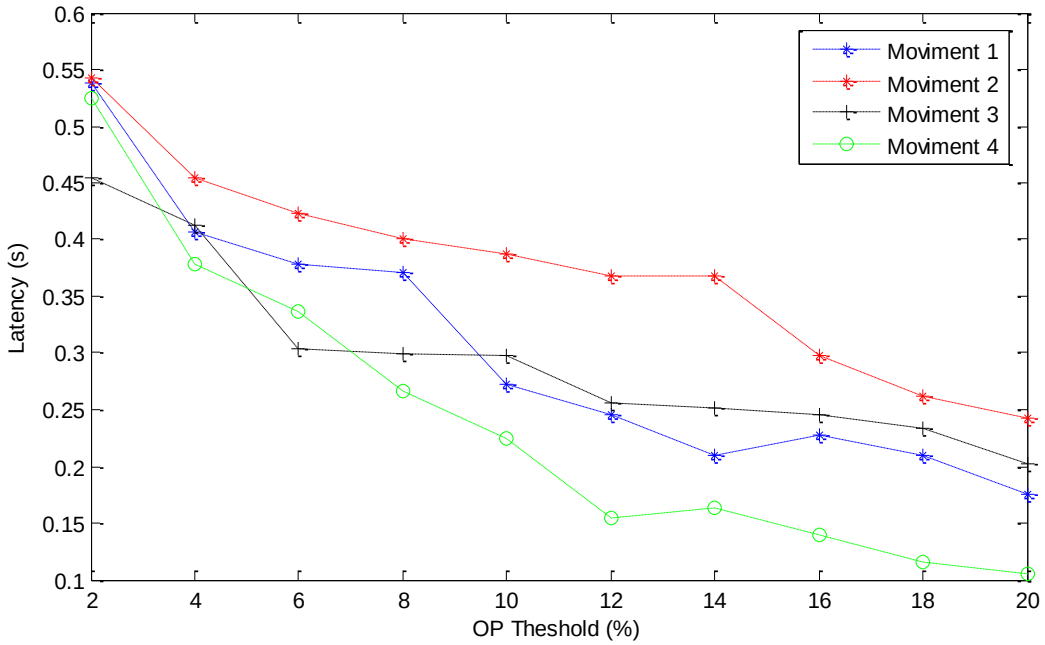

Figure 7.29. Latency for the PCPS mechanism configuration. *OP Threshold* values from the range 2-20%

consequence, on lower RSSI values. However, these chosen TPL values reduce the reliability of the communication system, by increasing the simulation average PER value.

A PCPS mechanism configured with a *RSSI Threshold* value of -86 dBm and an *OP Threshold* value of 12% can reach satisfactory results to all the metrics in all the study cases analysed. This configuration, for movement 1, show average values for PER, TPL, latency and RSSI of 5.24%, -6.8 dBm, 0.245 s and -84.4 dBm, respectively. For movement 2, the average values of 2.1%, -2.16 dBm, 0.36 s and -88.2 dBm were obtained for PER, TPL, latency and RSSI. The PCPS mechanism also provides benefits for movement 3, average values of 5.89%, -4.62 dBm, 0.303 s and -85.9 dBm were obtained for PER, TPL, Latency and RSSI, respectively. Finally, this PCPS mechanism configuration when employed to simulation of the movement 4 shows satisfactory performance in terms of the average values for PER (7.32%), TPL (-6.72 dBm), latency (0.154 s) and RSSI (-82.63).

Table 7.14. Latency and TPL values obtained after testing several PCPS mechanism configurations, differentiating in the *OP Threshold* value selected from the range 2-20%, in the simulation of movement 4.

***OP Threshold* (%)**	**TPL (dBm)**	**RSSI (dBm)**
2	-3.45	-79.22
4	-4.82	-80.45
6	-6.07	-81.21
8	-6.24	-81.78
10	-6.72	-82.29
12	-6.85	-82.63
14	-7.1	-82.66
16	-7.51	-82.79
18	-7.49	-83.12
20	-7.72	-83.93

The results above enabled to conclude that the PCPS mechanism with the previous mentioned configuration is able to improve the performance of the communications subsystem, while lower TPL values are used to transmit data packets. The PCPS mechanism shows a better PER value of 1 .76%, 12.9%, 8.11% and 2% for movements 1, 2, 3 and 4, respectively. However, the relation between simulation average PER and latency shows that the proposed PCPS mechanism is able to improve the reliability of the communications at the expense of latency. The PCPS mechanism shows an increase in latency of 0.196 s, 0.301 s, 0.255 s and 0.111 s for movement 1, 2, 3 and 4, respectively. The latency observed in Static TPL is due to the high number of data packets lost in transmissions, but the channel is on outage for short period of times, while the latency observed in PCPS mechanism is due to the delay assigned to data packets transmission, resulting in an increasing of reliability, reduced SAR and lower interferences with coexisting nodes or networks.

7.5 Summary

In this chapter, a solution, designated PCPS mechanism, is proposed to time-variant radio channel quality WBAN links, such us the Node-PROTACTICAL 7 of the WBAN-PROTACTICAL. This mechanism delays the data packets to instants in which the radio channel quality is more favourable to a successful data packet deliver. In addition, the PCPS mechanism can adjust the radio module output power whenever possible to make the communications more energy efficient.

Can the on-body radio channel quality (RSSI and Outage occurrences) be anticipated through a model?

The advantages of Neural Networks and Fuzzy Logic soft computing techniques to model the on-body channel were explored. Several ANFIS models were built, which were assessed and compared through analysis of their RMSE, MAE and R^2 results. Two models were selected to perform the task of RSSI- and PER-prediction LQEs in the PCPS mechanism (c.f. Figure 7.4). These ANFIS models show good fitting to the empirical data collected during the characterization of every user's movement, with a training error of 3.25 and 6.39, respectively. The checking and testing error values validate the generalization capability of these ANFIS models. Their values are not significantly different from the training error. By using the selected soft commuting techniques and following the methodology depicted in Figure 7.5, it was possible to build a model capable of describing the on-body channel in function of the relative position of the arm, the body posture and the scenario environment.

How can such a model be used to reduce the PER and minimize the energy consumption in on-body communications?

The proposed PCPS mechanism follows the operation principle depicted in Figure 7.4. It is based on three blocks: RSSI-prediction LQE, PER-prediction LQE and TPL Control. First, the PCPS mechanism (RSS-prediction LQE) estimates the RSSI value assuming that the next transmission is performed at -0.5 dBm output power. The TPL Control determines the optimal TPL value, implementing a dynamic-based approach and relying on the linear relation between RSSI and TPL values, analysed in section 6.2. Thereafter, the PCPS mechanism executes the PER-prediction LQE block. This block output suggests whether the transmission of data packets is advisable or not. If the PER-prediction LQE output value is larger than the *OP Threshold* value, the data packet transmission is postponed to a future instant. When the PER-prediction LQE output value is lower than the *OP Threshold* value, a closed-loop control based TPC approach is executed to determine the minimum TPL value that will ensure an outage probability and a predicted RSSI value inferior to the *RSSI Threshold* and *OP Threshold* value, respectively.

The proposed PCPS mechanism has shown to have a better performance than mechanisms that only exploit the multiple transmission levels provided by the current radio transceivers. The packet scheduler functionality of the proposed PCPS mechanism is simulated in several scenarios and its performance analysed through the simulation results of the PS mechanism. The PS mechanism implements the packet scheduler functionality without applying any power control. From the set of mechanisms tested, the PS is the one that has shown better simulation PER average values, ensuring PER values lower than 6% for all movements. The PCPS mechanism shows unacceptable PER average values in some scenarios, for instance, movement 1 and 3. By tuning of the RSSI and *OP Threshold* values in the TPL Control and "While Iterator Subsystem" block, respectively, the proposed PCPS mechanism's performance in terms of PER average value is improved. Increasing the *RSSI Threshold* value from -93 dBm to -86 dBm resulted in better PER average value of 3.87%. Moreover, by tuning the *OP Threshold* value the performance of the mechanism in terms of the PER metric is also improved at the expense of the latency, since the PCPS mechanism shows acceptable PER values for all the simulated movements (5.24%, 2.1%, 5.89% and 7.32% for movements 1, 2, 3 and 4, respectively).

The PCPS mechanism showed similar performance to the PS mechanism in terms of PER results, but with much lower TPL average values (less 6.3, 1.96, 4.12 and 6.25 dBm for movement 1, 2, 3 and 4, respectively) and similar latency values (the PCPS mechanism reduced the latency by 0.068 s, 0.01 s and 0.0684 s for movement 1, 2 and 4).

CHAPTER 8

CONCLUSION AND FUTURE WORK

One of the topics addressed by this thesis focused on the research objective (RO) 1- *Development of a WBAN for Firefighter Personal monitoring*. In chapter 4, a WBAN architecture to enhance the firefighter's occupational health and safety was proposed and described. This network enables its integration with other computational and control technologies within a Cyber Physical System. The communication within the WBAN-PROTACTICAL is performed using a wireless approach from the Edge of the Network nodes (Node-PROTACTICAL) to a Coordinator node, designated Gateway-PROTACTICAL in the context of the WBAN-PROTACTICAL. Several Edge of the Network nodes located at different parts of the garment using only wireless communication technologies were designed and developed, this approach is a unique solution among the state-of-the-art smart Personal Protective Equipment (PPE).

Although there are different communications scenarios in WBANs, the focus of this thesis is on RF communications among wearable nodes, since this type of nodes are not well studied for wireless communications. Several research works in the fields of the MAC layer and routing protocols for traditional networks such as WSNs have tried to apply different approaches to optimize the intra-WBAN reliability, but they have failed due to WBAN's quite unique features when compared to the traditional wireless networks. Therefore, before developing strategies to optimize the on-body communications, the second part of thesis was focused on the main source of communication unreliability: the fading of the transmission signal.

To achieve the RO 2 - *Establish a better understand of the impact that WBAN operation scenarios have on intra-WBAN communications*, an experimental radio channel characterization based on several scenarios was carried out. In comparison to other research works in this filed, this fading analysis covered a wider range of WBAN operation conditions and has followed a different approach, since a decomposing of the measured on-body signals into radio channel gain and large- and small-scale fading was adopted. The main conclusions, within the scope of chapter 5, for the proposed WBAN-PROTACTICAL are:

- User activity is the predominant effect to the time-variation of on-body communication channels;

- The on-body radio channel is a slow fading radio. The large-scale fading remains unchanged during each data packet transmission period and small magnitude differences between the fading magnitudes of two to three consecutive data packets were observed;
- Node-PROTACTICAL 4 is not subjected to variable path-loss (values near to -50 dB) and fading (magnitudes are low) regardless of the test scenario. The results in terms of these parameters are similar for all operation conditions. A static and pre-defined TPL can be adopted (for all covered scenarios) to this radio channel. Transmissions at a TPL of -22 dBm (resulting in ≈50% energy saving in relation to transmissions performed at -0.5 dBm) assure the reliability requirements in all considered scenarios;
- The Edge of the Network nodes located at the user's limbs, such as Node-PROTACTICAL 7, are the most affected by the user activity. A wide range of radio channel gain values and fading magnitudes above -18 dB were observed at all scenarios;
- As the Node-PROTACTICAL 2 is always in NLOS situation, it has the lowest radio channel gain values but with significant signal fading magnitudes. This node is not capable of meeting the WBAN application requirements in terms of reliability. So a multi-hop topology was explored;
- The large-scale signal fading effect is more substantial for the indoor scenarios, as proved by the obtained signal fading rates. Moreover, the energy contribution of the multi-path components on the signal increases the radio channel gain for some operation conditions.

Several TPC mechanisms have been addressed in the literature to optimize the Quality-of-Service (QoS) requirements in an energy-efficient way. The sate-of-the-art TPCs were addressed in chapter 3, the discussion proved that there are still several challenges and open issues in this field of study. There are two main types of TPC mechanisms: (1) Closed-Loop Control based and (2) Posture and Motion Detection. The most suitable solutions for updating the power control according to the radio channel conditions in dynamic scenarios are based on closed-loop control. However, due to the additional control packets required, there is a negative impact on the traffic overhead. The majority of the TPC mechanisms based on the posture and motion detection employ inertial sensors to estimate the radio channel conditions and select the optimal transmission power level (TPL). These solutions prove to be agile in

reaching the optimal TPL, however the current developments are only applicable to static scenarios (no user movement).

The remaining chapters of this thesis focused on mechanisms that have potential to improve the QoS requirements in an energy-efficient way were described and analysed and some scientific contributions have been provided.

In chapter 6 the RO 3 - *Mechanism to optimize the metrics of interest in the scope of this thesis in Emergency Traffic* was addressed and a novel TPC mechanism was proposed. The proposed solution aims to improve the Packet Reception Rate metric and minimize the energy consumption, without sacrificing the latency on data packets transmissions, for scenarios when the user is performing periodic movements such as walking or running, i.e., dynamic periodic scenarios. Daily routines involve significant amount of periodic movements, such as walking, running or jogging. For instance, according to [60], an adult walks on average one hour per day, which corresponds to between 6000 and 7000 steps.

Chapter 6 started by characterizing the fading signal while the user (tests with several users were carried out) was walking. The analysis of the collected empirical data drove the following conclusions:

- There is a significant temporal correlation between the user movements and the fading signal while the user performs periodic movements;
- The fading signal follows a regular pattern, with the fading magnitude showing significant fluctuations. A peak-to-peak fading magnitude between 20 and 25 dB and Link Margin gains (difference between fading magnitude and receiver sensitivity) between 25 dB and 30 dB, and between 5 dB and 15 dB were reported at outdoors and indoors respectively. While at indoor scenarios the Link Margin gains are inferior, and the fading signal is more unstable;
- For all the users and scenarios (i.e. for all the tests made) the number of data packets lost by the proposed P-TPC mechanism was very low;
- As the fading and acceleration signals follow a regular pattern, past samples can be used to forecast future fading signal values.

There are a few research works, such as [130], [137] and [145], that have addressed solutions for a similar operation scenario. However, their purpose is to detect the instant within a gait cycle that the maximum fading magnitude occurs. These mechanisms, which are very complex (preventing its implementation in resource constrained Edge of the Network nodes such the ones used on the proposed PPE), rely in local accelerometer information to track the

user's gait cycle period. A previous fading signal characterization allowed the identification of the gait cycle instant when the maximum fading signal amplitude occurs. Therefore, data packet transmission are delayed in order to be transmitted at that gait cycle instant since this moment offers more changes of a successfully deliver of the data packet. The Edge of the Network nodes receive control packets from the Coordinator node that contain the RSSI value of the last transmitted data packet. This RSSI value can be used in order to update the TPL by implementing a closed-loop control architecture.

Based on the above observations, a novel TPC mechanism was proposed employing a mixed operation principle (closed-loop control together with Posture and Motion detection) and targeting resource constrained nodes.

The proposed mechanism uses the on-body communication RSSI values to approximate the fading signal during the user's gait cycle and, simultaneously, the acceleration signal (from inertial sensors) is used to determine the instant within the gait cycle. By mapping the measured RSSI samples into the gait cycle, an interpolation function was derived, which is used to anticipate the fading signal magnitude for all instants of a gait cycle. The RSSI values are gathered based in the closed-loop control operation principle. Only 15 RSSI values are required to reach a satisfactory fading signal approximation. This approach results in an increasing of 3% on the traffic overhead. This results is insignificant when compared to the increases between 30 and 40% achieved by the closed-loop control based TPC mechanisms. A modified version of the DTW algorithm enabled to drastically reduce the complexity of the original DTW algorithm. The user's stride accelerations and gait cycle were computed using two anchors for each gait cycle, corresponding to the extremes of the acquired acceleration signal. By using the Euclidean distance, the proposed mechanism can identify and determine accelerations on the user's stride and identify how they affect the period of the on-going gait cycle. This approach proved to be of very low complexity, thus suitable to resource constrained devices, and very effective (please see results obtained in section 6.4). The proposed P-TPC mechanism was incorporated in the Z-stack (Texas Instruments communication stack) integrating the MAC and the PHY layers.

Experimental results show that the proposed TPC mechanism is capable of achieving an energy consumption reduction up to 30% per data packet transmitted, when compared to data packet transmissions performed at maximum TPL. Furthermore, this thesis research work shows that all WBAN application requirements identified by IEEE 802.15.6 TG can be ensured in an energy-efficient way without sacrificing the communications reliability and the latency (since data packets are not delayed). Even though this solution is limited to applications where

the user performs periodic movements, when no periodic movement is detected, the mechanism can follow a closed-loop control based TPC. The P-TPC solution meets all the features expected from TPC mechanisms: R1-R9 (c.f. chapter 3).

The last part of this thesis (chapter 7) addressed a packet scheduler mechanism denominated PCPS in order to answer the RO 4 - *Mechanism to optimize the metrics of interest in the scope of this thesis in Regular Traffic*. This solution also controls the TPL according to the current radio channel conditions. The radio channel characterization has shown that the relative position of the user arm (described as the combination of the angles of the different segments of the arm) has a significant influence on the RSSI value and the radio channel outage. In fact, for some arm postures successful data packets transmission is impossible (even at maximum allowed TPL), since radio channel conditions are not favourable. In such scenarios, the more wise action is to postpone the data packet transmission. This will increase the communication reliability, and the latency on transmissions. Therefore, two ANFIS models to estimate the RSSI value and outage probability of a transmission based on user information (arm posture, body posture and operation environment) were developed. This solution, which was assessed through simulations, was able to ensure the reliability (average PER is ≈4%, while static TPC transmissions is ≈12%) requirements and Specific Absorption Rate (since average TPL is between -10 to -5 dBm). An average increase in the order of 0.215 s in relation to the transmission at a static TPL (-0.5 dBm) were reported. The improvement in terms of energy consumption was not analysed since this solution was not experimentally tested. The PCPS mechanism have probed that unreliable links can be made reliable if data packets are transmitted in instants in which the radio channel quality is favourable to successful data packet delivery

Some future work must be performed in order to help WBAN applications overcoming some issues and challenges that have been hampering wearable systems of reaching their full potential.

In the context of the PROTACTICAL PPE, other tools can be developed for a better awareness of the firefighting challenges, as well as, to improve user safety by taking advantage of the proposed CPS approach. There are various examples of such tools: generation of escape routes, detection of flashover events and generation and analysis of biometric parameters.

The advent of CPS applicable to WBANs can also help TPC/Packet Scheduler mechanisms to improve their effectiveness in WBANs. As stated before, scenarios prone to inter-network interferences might drastically affect the efficiency of the proposed P-TPC and PCPS mechanisms, so mechanisms that explore channel-hopping schemes might be able to avoid

interference due to the radio channel sharing. This type of schemes are efficient in scenarios with low density of networks (they resort to cooperation between Coordinator nodes of different WBANs), but their performance decrease with the increasing of networks density. In this context, the CPS approach (which offers a holistic view over all the WBANs of a system) proposed in this research work and the location and tracking algorithm (addressed in [191] and developed in the context of the PROTACTICAL project) can be explored to develop a channel-hopping mechanism that consider the relative movement of WBANs with respect to each other. Thus, WBANs operating within a communication region around of each other (where potential transmissions are prone to fail) must manage their transmissions rate and TPLs to reach the maximum network utility and/or, wherever applicable, assign different radio channels to each of the coexisting WBANs to avoid RF interference.

Some research work must be carried out in order to ensure the applicability of the proposed PCPS mechanisms in a wide range of conditions. First, the generalizability of the results must be proven, thus, many more users should be considered during the radio channel characterization phase. Moreover, a very simplistic approach was adopted to determine the arm posture in real-time, thus not all degrees of freedom of the user's arm, as well as, user's postures were considered during the experimental trial (c.f. subsection 7.3.2). In this regard, the use of more than one inertial sensor is required. Processing of multiple sensor readings is a very challenging task, but it might allow the characterization of more user movements, enlarging the range of scenarios in which the proposed ANFIS model approach is able to efficiently describe the on-body radio channel.

BIBLIOGRAPHY

[1] G. Yi, D. Yu, and N. Kim, "Adjusting Control Packet Transmission Intervals in Low Power Sensor Systems," *Int. J. Distrib. Sens. Networks*, vol. 2014, pp. 1–8, 2014.

[2] D. Arbia, M. Alam, Y. Moullec, and E. Hamida, "Communication Challenges in on-Body and Body-to-Body Wearable Wireless Networks—A Connectivity Perspective," *Technologies*, vol. 5, no. 3, p. 43, Jul. 2017.

[3] "Statistics & Facts on Wearable Technology." [Online]. Available: https://www.statista.com/statistics/610447/wearable-device-revenue-worldwide/. [Accessed: 09-Sep-2017].

[4] S. Kim, S. Kim, and D.-S. Eom, "RSSI/LQI-Based Transmission Power Control for Body Area Networks in Healthcare Environment," *IEEE J. Biomed. Heal. Informatics*, vol. 17, no. 3, pp. 561–571, 2013.

[5] W. Lee and N. Kim, "Extended Dynamic Transmission Power Control Algorithm in Wireless Body Sensor Network Systems," *Int. J. Control Autom.*, vol. 6, no. 6, pp. 339–350, 2013.

[6] S. Patel, H. Park, P. Bonato, L. Chan, and M. Rodgers, "A review of wearable sensors and systems with application in rehabilitation," *J. Neuroeng. Rehabil.*, vol. 9, no. 1, p. 21, 2012.

[7] A. Pantelopoulos and N. G. Bourbakis, "A Survey on Wearable Sensor-Based Systems for Health Monitoring and Prognosis," *IEEE Trans. Syst. Man, Cybern. Part C (Applications Rev.*, vol. 40, no. 1, pp. 1–12, Jan. 2010.

[8] M. Chan, D. Estève, J.-Y. Fourniols, C. Escriba, and E. Campo, "Smart wearable systems: Current status and future challenges," *Artif. Intell. Med.*, vol. 56, no. 3, pp. 137–156, Nov. 2012.

[9] M. Quwaider, J. Rao, and S. Biswas, "Body-Posture-Based Dynamic Link Power Control in Wearable Sensor Networks," *IEEE Commun. Mag.*, vol. 48, no. 7, pp. 134–142, 2010.

[10] R. Kazemi, R. Vesilo, E. Dutkiewicz, and Ren Liu, "Dynamic power control in Wireless Body Area Networks using reinforcement learning with approximation," in *2011 IEEE 22nd International Symposium on Personal, Indoor and Mobile Radio Communications*, 2011, pp. 2203–2208.

[11] P. Lukowicz, A. Timm-Giel, M. Lawo, and O. Herzog, "WearIT@work: Toward Real-World Industrial Wearable Computing," *IEEE Pervasive Comput.*, vol. 6, no. 4, pp. 8–13, 2007.

[12] D. Curone *et al.*, "Smart garments for emergency operators: The ProeTEX project," *IEEE Trans. Inf. Technol. Biomed.*, vol. 14, no. 3, pp. 694–701, 2010.

[13] D. B. Smith, D. Miniutti, T. A. Lamahewa, and L. W. Hanlen, "Propagation Models for Body-Area Networks : A Survey and New Outlook," *IEEE Antennas Propag. Mag.*, vol. 55, no. 5, pp. 97–117, 2013.

[14] M. Homan, Y. Takeoka, T. Aoyagi, T. Ikegami, and R. Kohno, "IEEE P802.15 Working Group for Wireless Personal Area Networks etworks (WPANs): Channel model for Body Area Network (BAN)," 2008.

[15] N. Chevrollier and N. Golmie, "On the use of wireless network technologies in healthcare environments," in *Proceedings of the fifth IEEE workshop on Applications and Services in Wireless Networks (ASWN 2005)*, 2005, pp. 147–152.

[16] M. Marinoni, A. Biondi, P. Buonocunto, G. Franchino, D. Cesarini, and G. Buttazzo, "Real-Time Analysis and Design of a Dual Protocol Support for Bluetooth LE Devices," *IEEE Trans. Ind. Informatics*, vol. 13, no. 1, pp. 80–91, Feb. 2017.

[17] X. Lai, Q. Liu, X. Wei, W. Wang, G. Zhou, and G. Han, "A Survey of Body Sensor Networks," *Sensors*, vol. 13, no. 5, pp. 5406–5447, Apr. 2013.

[18] S. Movassaghi, M. Abolhasan, J. Lipman, D. Smith, and A. Jamalipour, "Wireless Body Area Networks: A Survey," *IEEE Commun. Surv. Tutorials*, vol. 16, no. 3, pp. 1658–1686, 2014.

[19] IEEE 802, "IEEE Standard for Local and metropolitan area networks - Part 15.6: Wireless Body Area Networks," 2012.

[20] Z. Wang *et al.*, "Cyber-physical systems for water sustainability: challenges and opportunities," *IEEE Commun. Mag.*, vol. 53, no. 5, pp. 216–222, May 2015.

[21] Z. Khan, N. Aslam, S. Sivakumar, and W. Phillips, “Energy-aware Peering Routing Protocol for indoor hospital Body Area Network Communication,” *Procedia Comput. Sci.*, vol. 10, pp. 188–196, Jan. 2012.
[22] M. Vallejo, J. Recas, P. G. del Valle, and J. L. Ayala, “Accurate human tissue characterization for energy-efficient wireless on-body communications.,” *Sensors (Basel).*, vol. 13, no. 6, pp. 7546–69, Jan. 2013.
[23] J. Ryckaert, P. De Doncker, R. Meys, and A. de Le Hoye, “Channel model for wireless communication around human body,” *Electron. Lett.*, vol. 40, pp. 533–544, 2004.
[24] L. Liu, R. D. Errico, L. Ouvry, P. De Doncker, and C. Oestges, “Dynamic Channel Modeling at 2.4 GHz for On-Body Area Networks,” *Adv. Electron. Telecommun.*, vol. 2, no. 4, pp. 18–27, 2011.
[25] F. Di Franco, C. Tachtatzis, B. Graham, D. Tracey, N. F. Timmons, and J. Morrison, “On-body to on-body channel characterization,” in *2011 IEEE SENSORS Proceedings*, 2011, pp. 908–911.
[26] M. Kim, J. Takada, and S. Member, “Characterization of Wireless On-Body Channel Under Specific Action Scenarios at Sub-GHz Bands,” *IEEE Trans. Antennas Propag.*, vol. 60, no. 11, pp. 5364–5372, 2012.
[27] G. A. Conway, W. G. Scanlon, S. L. Cotton, M. J. Bentum, A. H. Planar, and D. Medium, “An Analytical Path-Loss Model for On-Body Radio Propagation,” in *2010 URSI International Symposium on Electromagnetic Theory (EMTS)*, 2010, pp. 332–335.
[28] G. Lo, S. Gonzalez-Valenzuela, and V. C. M. Leung, “Wireless body area network node localization using small-scale spatial information.,” *IEEE J. Biomed. Heal. informatics*, vol. 17, no. 3, pp. 715–26, May 2013.
[29] Y. Zhang *et al.*, “Energy Efficient Design for Body Sensor Nodes,” *J. Low Power Electron. Appl.*, vol. 1, no. 3, pp. 109–130, Apr. 2011.
[30] C. He, A. Arora, M. E. Kiziroglou, D. C. Yates, D. O’Hare, and E. M. Yeatman, “MEMS Energy Harvesting Powered Wireless Biometric Sensor,” in *International Workshop on Wearable and Implantable Body Sensor Networks (BSN’09)*, 2009, pp. 207–212.
[31] F. Akhtar and M. H. Rehmani, “Energy Harvesting for Self-Sustainable Wireless Body Area Networks,” *IT Prof.*, vol. 19, no. 2, pp. 32–40, Mar. 2017.
[32] D. C. Hoang, Y. K. Tan, H. B. Chng, and S. Panda, “Thermal energy harvesting from human warmth for wireless body area network in medical healthcare system,” *Proceedings of the International Conference on Power Electronics and Drive Systems*. pp. 1277–1282, 2009.
[33] N. Barroca *et al.*, “Antennas and circuits for ambient RF energy harvesting in wireless body area networks,” in *2013 IEEE 24th Annual International Symposium on Personal, Indoor, and Mobile Radio Communications (PIMRC)*, 2013, pp. 532–537.
[34] M. H. Rehmani, A. Rachedi, S. Lohier, T. Alves, and B. Poussot, “Intelligent antenna selection decision in IEEE 802.15.4 wireless sensor networks: An experimental analysis,” *Comput. Electr. Eng.*, vol. 40, no. 2, pp. 443–455, 2014.
[35] M. H. Rehmani, T. Alves, S. Lohier, A. Rachedi, and B. Poussot, “Towards intelligent antenna selection in IEEE 802.15.4 wireless sensor networks,” in *Proceedings of the thirteenth ACM international symposium on Mobile Ad Hoc Networking and Computing - MobiHoc ’12*, 2012, p. 245.
[36] R. Sruthi, “Medium Access Control Protocols for Wireless Body Area Networks: A Survey,” *Procedia Technol.*, vol. 25, no. Raerest, pp. 621–628, 2016.
[37] S. Anand Gopalan and Jong-Tae Park, “Energy-efficient MAC protocols for wireless body area networks: Survey,” in *International Congress on Ultra Modern Telecommunications and Control Systems*, 2010, pp. 739–744.
[38] a Rahim, N. Javaid, M. Aslam, Z. Rahman, U. Qasim, and Z. A. Khan, “A Comprehensive Survey of MAC Protocols for Wireless Body Area Networks,” in *2012 Seventh International Conference on Broadband, Wireless Computing, Communication and Applications*, 2012, no. August, pp. 434–439.
[39] M. A. Shah, Y. Li, and A. H. Sodhro, “Energy-efficient adaptive transmission power control for wireless body area networks,” *IET Commun.*, vol. 10, no. 1, pp. 81–90, Jan. 2016.
[40] J. Bangash, A. Abdullah, M. Anisi, and A. Khan, “A Survey of Routing Protocols in Wireless Body Sensor Networks,” *Sensors*, vol. 14, no. 1, pp. 1322–1357, Jan. 2014.

[41] S. Ullah *et al.*, "A Comprehensive Survey of Wireless Body Area Networks," *J. Med. Syst.*, vol. 36, no. 3, pp. 1065–1094, Jun. 2012.
[42] B. Latré, B. Braem, I. Moerman, C. Blondia, and P. Demeester, "A survey on wireless body area networks," *Wirel. Networks*, vol. 17, no. 1, pp. 1–18, Jan. 2011.
[43] R. Kazemi, R. Vesilo, E. Dutkiewicz, and G. Fang, "Inter-network interference mitigation in Wireless Body Area Networks using power control games," in *2010 10th International Symposium on Communications and Information Technologies*, 2010, pp. 81–86.
[44] G. Fang, E. Dutkiewicz, K. Yu, R. Vesilo, and Y. Yu, "Distributed Inter-Network Interference Coordination for Wireless Body Area Networks," in *2010 IEEE Global Telecommunications Conference GLOBECOM 2010*, 2010, pp. 1–5.
[45] S. Movassaghi, A. Majidi, A. Jamalipour, D. Smith, and M. Abolhasan, "Enabling interference-aware and energy-efficient coexistence of multiple wireless body area networks with unknown dynamics," *IEEE Access*, vol. 4, pp. 2935–2951, 2016.
[46] W. Lee, B. Lee, and N. Kim, "Hybrid Transmission Power Control for Wireless Body Sensor Systems," *Int. J. Distrib. Sens. Networks*, vol. 2014, p. 9, 2014.
[47] S. Xiao, A. Dhamdhere, V. Sivaraman, and A. Burdett, "Transmission Power Control in Body Area Sensor Networks for Healthcare Monitoring," *IEEE J. Sel. Areas Commun.*, vol. 27, no. 1, pp. 37–48, Jan. 2009.
[48] M. Quwaider, A. Muhammad, J. Choi, and S. Biswas, "Posture-Predictive Power Control in Body Sensor Networks Using Linear-Quadratic Gaussian Control," in *2009 First International Conference on Networks & Communications*, 2009, pp. 52–59.
[49] M. Nabi, T. Basten, M. Geilen, M. Blagojevic, and T. Hendriks, "A robust protocol stack for multi-hop wireless body area networks with transmit power adaptation," in *Proceedings of the Fifth International Conference on Body Area Networks - BodyNets '10*, 2010, p. 77.
[50] D. B. Smith, T. Lamahewa, L. W. Hanlen, and D. Miniutti, "Simple Prediction-Based Power Control for the On-Body Area Communications Channel," in *2011 IEEE International Conference on Communications (ICC)*, 2011, pp. 1–5.
[51] M. Nabi, M. M. C. W. Geilen, and T. A. A. Basten, "An empirical study of link quality estimation techniques for disconnection detection in WBANs," in *Proceedings of the 16th ACM international conference on Modeling, analysis & simulation of wireless and mobile systems - MSWiM '13*, 2013, pp. 219–228.
[52] E. B. Hamida, R. D'Errico, and B. Denis, "Topology Dynamics and Network Architecture Performance in Wireless Body Sensor Networks," in *2011 4th IFIP International Conference on New Technologies, Mobility and Security*, 2011, pp. 1–6.
[53] M. Quwaider and S. Biswas, "Probabilistic routing in on-body sensor networks with postural disconnections," in *ACM international symposium on Mobility management and wireless access - MobiWAC '09*, 2009, p. 149.
[54] L. Liang, Y. Ge, G. Feng, W. Ni, and A. A. P. Wai, "Experimental study on adaptive power control based routing in multi-hop Wireless Body Area Networks," in *IEEE Global Communications Conference (GLOBECOM)*, 2012, pp. 572–577.
[55] N. Baccour *et al.*, "Radio link quality estimation in wireless sensor networks," *ACM Trans. Sens. Networks*, vol. 8, no. 4, pp. 1–33, Sep. 2012.
[56] S. Ullah and K. S. Kwak, "An Ultra Low-power and Traffic-adaptive Medium Access Control Protocol for Wireless Body Area Network," *J. Med. Syst.*, vol. 36, no. 3, pp. 1021–1030, Jun. 2012.
[57] R. D'Errico and L. Ouvry, "Time-variant BAN channel characterization," in *2009 IEEE 20th International Symposium on Personal, Indoor and Mobile Radio Communications*, 2009, pp. 3000–3004.
[58] R. D. Errico and L. Ouvry, "Delay Dispersion of the On-Body Dynamic Channel," in *2010 Proceedings of the Fourth European Conference on Antennas and Propagation (EuCAP)*, 2010, pp. 1–5.
[59] S. L. Cotton and W. G. Scanlon, "An Experimental Investigation into the Influence of User State and Environment on Fading Characteristics in Wireless Body Area Networks at 2.45 GHz," *IEEE Trans. Wirel. Commun.*, vol. 8, no. 1, pp. 6–12, 2009.
[60] J. Hauer, "Towards Reliable Communication in Low-Power Wireless Body Area Networks,"

Technische Universität Berlin, 2014.
[61] A. Alomainy and Y. Hao, “Modeling and Characterization of Biotelemetric Radio Channel From Ingested Implants Considering Organ Contents,” *IEEE Trans. Antennas Propag.*, vol. 57, no. 4, pp. 999–1005, 2009.
[62] D. B. Smith, L. W. Hanlen, J. (Andrew) Zhang, D. Miniutti, D. Rodda, and B. Gilbert, “First- and second-order statistical characterizations of the dynamic body area propagation channel of various bandwidths,” *Ann. Telecommun. - Ann. des télécommunications*, vol. 66, no. 3–4, pp. 187–203, Apr. 2011.
[63] N. Yamamoto, N. Shirakata, D. Kobayashi, and K. Ogawa, “BAN Communication Quality Assessments Using an Arm-Waving Dynamic Phantom Replicating the Walking Motion of a Human,” in *2011 IEEE International Conference on Communications (ICC)*, 2011, pp. 1–6.
[64] T. E. Hewett, S. L. Di Stasi, and G. D. Myer, “Current Concepts for Injury Prevention in Athletes After Anterior Cruciate Ligament Reconstruction,” *Am. J. Sports Med.*, vol. 41, no. 1, pp. 216–224, Jan. 2013.
[65] D. Fernandes *et al.*, “On-body signal propagation in WBANs for firefighters personal protective equipment: Statistical characterization and performance assessment,” in *2017 IEEE International Conference on Industrial Technology (ICIT)*, 2017, pp. 1360–1365.
[66] D. Fernandes, A. G. Ferreira, R. Abrishambaf, J. Mendes, and J. Cabral, “A Low Traffic Overhead Transmission Power Control for Wireless Body Area Networks,” *IEEE Sens. J.*, vol. P-P, no. 99, pp. 1–1, 2017.
[67] D. Fernandes, A. Ferreira, J. Mendes, and J. Cabral, “A Wireless Body Sensor Network based on Dynamic Power Control and Opportunistic Packet Scheduling Mechanisms,” in *IEEE International Conference on Industrial Technology*, 2015, no. 1, pp. 1–6.
[68] G. V. Crosby, T. Ghosh, R. Murimi, and C. A. Chin, “Wireless Body Area Networks for Healthcare: A Survey,” in *International Journal of Ad hoc, Sensor & Ubiquitous Computing (IJASUC)*, 2012, vol. 3, no. 3, pp. 1–26.
[69] M. Patel and J. Wang, “Applications, challenges, and prospective in emerging body area networking technologies,” *IEEE Wirel. Commun.*, vol. 17, no. 1, pp. 80–88, Feb. 2010.
[70] H. Cao, V. Leung, C. Chow, and H. Chan, “Enabling technologies for wireless body area networks: A survey and outlook,” *IEEE Commun. Mag.*, vol. 47, no. 12, pp. 84–93, Dec. 2009.
[71] R. Cavallari, F. Martelli, R. Rosini, C. Buratti, and R. Verdone, “A Survey on Wireless Body Area Networks: Technologies and Design Challenges,” *IEEE Commun. Surv. Tutorials*, vol. 16, no. 3, pp. 1635–1657, 2014.
[72] C. Liolios, C. Doukas, G. Fourlas, and I. Maglogiannis, “An overview of body sensor networks in enabling pervasive healthcare and assistive environments,” in *Proceedings of the 3rd International Conference on PErvasive Technologies Related to Assistive Environments - PETRA ’10*, 2010, p. 1.
[73] M. Chen, S. Gonzalez, A. Vasilakos, H. Cao, and V. C. M. Leung, “Body Area Networks: A Survey,” *Mob. Networks Appl.*, vol. 16, no. 2, pp. 171–193, Apr. 2011.
[74] R. .G.K and K. Baskaran, “A Survey on Futuristic Health Care System: WBANs,” *Procedia Eng.*, vol. 30, no. 2011, pp. 889–896, 2012.
[75] M. Salayma, A. Al-Dubai, I. Romdhani, and Y. Nasser, “Wireless Body Area Network (WBAN),” *ACM Comput. Surv.*, vol. 50, no. 1, pp. 1–38, Mar. 2017.
[76] J. Wilson, V. Bhargava, A. Redfern, and P. Wright, “A Wireless Sensor Network and Incident Command Interface for Urban Firefighting,” in *2007 Fourth Annual International Conference on Mobile and Ubiquitous Systems: Networking & Services (MobiQuitous)*, 2007, pp. 1–7.
[77] F. Felisberto, N. Costa, F. Fdez-Riverola, and A. Pereira, “Unobstructive Body Area Networks (BAN) for Efficient Movement Monitoring,” *Sensors*, vol. 12, no. 12, pp. 12473–12488, Sep. 2012.
[78] U. Mitra, B. A. Emken, S. Lee, M. Li, and S. California, “KNOWME: A Case Study in Wireless Body Area Sensor Network Design,” *IEEE Commun. Mag.*, vol. 50, no. 5, pp. 116–125, 2012.
[79] D. Malan and T. Fulford-Jones, “Codeblue: An ad hoc sensor network infrastructure for emergency medical care,” in *Proceeding on the MobiSys 2004 Workshop on Applications of Mobile Embedded Systems*, 2004, pp. 12–14.
[80] A. Ferreira, D. Fernandes, S. Branco, J. Cabral, and A. M. Rocha, “A smart wearable system for

sudden infant death syndrome monitoring," in *2016 IEEE International Conference on Industrial Technology (ICIT)*, 2016, pp. 1920–1925.
[81] "WASP - Wearable Advanced Sensor Platform," 2016. [Online]. Available: http://globeturnoutgear.com/innovation/wasp. [Accessed: 27-Jan-2016].
[82] D. C. Teles, M. F. M. Colunas, J. M. Fernandes, I. C. Oliveira, and J. P. S. Cunha, "iVital: A Real Time Monitoring System for First Response Teams," in *Mobile Networks and Management: Third International ICST Conference (MONAMI)*, vol. 97, Aveiro, Portugal, 2012, pp. 396–404.
[83] M. Batalin, E. Yuen, B. Dolezal, D. Smith, C. Cooper, and J. Mapar, "PHASER: Physiological Health Assessment System for emergency responders," in *2013 IEEE International Conference on Body Sensor Networks*, 2013, pp. 1–6.
[84] V. Amendolare *et al.*, "WIP Precision personnel locator system: Inertial navigation supplementation," in *Record - IEEE PLANS, Position Location and Navigation Symposium*, 2008, pp. 350–357.
[85] W. Hawkinson *et al.*, "GLANSER: Geospatial location, accountability, and Navigation System for Emergency Responders - system concept and performance assessment," in *Proceedings of the 2012 IEEE/ION Position, Location and Navigation Symposium*, 2012, pp. 98–105.
[86] S. Feese, B. Arnrich, G. Troster, M. Burtscher, B. Meyer, and K. Jonas, "CoenoFire," in *Proceedings of the 2013 ACM international joint conference on Pervasive and ubiquitous computing - UbiComp '13*, 2013, p. 83.
[87] "i-PROTECT," 2016. [Online]. Available: https://www.i-protect.pl/. [Accessed: 27-Jan-2016].
[88] R. Soukup, T. Blecha, A. Hamacek, and J. Reboun, "Smart textile-based protective system for firefighters," in *Proceedings of the 5th Electronics System-Integration Technology Conference, ESTC 2014*, 2014.
[89] S. K. Ghosh, S. Chakraborty, A. Jamthe, and D. P. Agrawal, "Comprehensive monitoring of firefighters by a Wireless Body Area Sensor Network," in *IFIP International Conference on Wireless and Optical Communications Networks, WOCN*, 2013.
[90] "ProFiTex - Advanced Protective Firefighting Equipment," 2016. [Online]. Available: https://www.ims.tuwien.ac.at/projects/profitex. [Accessed: 27-Jan-2016].
[91] G. Magenes, D. Curone, M. Lanati, E. L. Secco, and A. Overview, "Long-Distance Monitoring of Physiological and Environmental Parameters for Emergency Operators," in *31st Annual International Conference of the IEEE EMBS*, 2009, pp. 5159–5162.
[92] C. Schonauer, E. Vonach, G. Gerstweiler, and H. Kaufmann, "3D building reconstruction and thermal mapping in fire brigade operations," in *2013 IEEE Virtual Reality (VR)*, 2013, pp. 1–2.
[93] M. Klann, "Tactical navigation support for firefighters: The LifeNet ad-hoc sensor-network and wearable system," in *Lecture Notes in Computer Science (including subseries Lecture Notes in Artificial Intelligence and Lecture Notes in Bioinformatics)*, 2009, vol. 5424 LNCS, pp. 41–56.
[94] M. Klann *et al.*, "LifeNet: an Ad-hoc Sensor Network and Wearable System to Provide Firefighters with Navigation Support," in *Adjunct Proc Ubicomp 2007*, 2007, vol. M, no. 1, pp. 124–127.
[95] A. W. ASTRIN, H.-B. LI, and R. KOHNO, "Standardization for Body Area Networks," *IEICE Trans. Commun.*, vol. E92–B, no. 2, pp. 366–372, 2009.
[96] IEEE 802, "IEEE P802.15 TG6 (Body Area Network) Call For Applications," 2008.
[97] and A. A. Bin Zhen, Maulin Patel, SungHyup Lee, EunTae Won, "TG6 technical requirements document," 2009.
[98] A. Astrin, A. Radio, and A. Palo, "TG6 Call for Proposals (CFP)," 2009.
[99] A. Boulis, D. Smith, D. Miniutti, L. Libman, and Y. Tselishchev, "Challenges in body area networks for healthcare: the MAC," *IEEE Commun. Mag.*, vol. 50, no. 5, pp. 100–106, May 2012.
[100] J. Y. Khan, M. R. Yuce, G. Bulger, and B. Harding, "Wireless Body Area Network (WBAN) Design Techniques and Performance Evaluation," *J. Med. Syst.*, vol. 36, no. 3, pp. 1441–1457, Jun. 2012.
[101] A. F. G. Ferreira, D. M. A. Fernandes, A. P. Catarino, and J. L. Monteiro, "Localization and Positioning Systems for Emergency Responders: A Survey," *IEEE Commun. Surv. Tutorials*, vol. 19, no. 4, pp. 2836–2870, 2017.

[102] M. Rosu and S. Pasca, “A WBAN-ECG approach for real-time long-term monitoring,” in *2013 8Th International Symposium on Advanced Topics in Electrical Engineering (Atee)*, 2013, pp. 1–6.
[103] Bluetooth SIG, “Specification of the Bluetooth System: Master Table of Contents & Compliance Requirements,” 2010.
[104] M. Siekkinen, M. Hiienkari, J. K. Nurminen, and J. Nieminen, “How low energy is bluetooth low energy? Comparative measurements with ZigBee/802.15.4,” in *2012 IEEE Wireless Communications and Networking Conference Workshops (WCNCW)*, 2012, pp. 232–237.
[105] C. Gomez, J. Oller, and J. Paradells, “Overview and Evaluation of Bluetooth Low Energy: An Emerging Low-Power Wireless Technology,” *Sensors*, vol. 12, no. 12, pp. 11734–11753, Aug. 2012.
[106] E. Mackensen, M. Lai, and T. M. Wendt, “Performance analysis of an Bluetooth Low Energy sensor system,” in *2012 IEEE 1st International Symposium on Wireless Systems (IDAACS-SWS)*, 2012, pp. 62–66.
[107] E. . Yazdi, “Adaptive Resource Allocation for Wireless Body Sensor Networks,” University of Canterbury, New Zeland, 2014.
[108] R. Kazemi, R. Vesilo, and E. Dutkiewicz, “A Novel Genetic-Fuzzy Power Controller with Feedback for Interference Mitigation in Wireless Body Area Networks,” in *2011 IEEE 73rd Vehicular Technology Conference (VTC Spring)*, 2011, pp. 1–5.
[109] Cheng Leong Lim, M. Bolt, A. Syed, P. Ng, C. Goh, and Yun Li, “Dynamic performance of IEEE 802.15.4 devices under persistent WiFi traffic,” in *2015 International Conference on Recent Advances in Internet of Things (RIoT)*, 2015, pp. 1–6.
[110] M. S. Akbar, H. Yu, and S. Cang, “Delay, Reliability, and Throughput Based QoS Profile: A MAC Layer Performance Optimization Mechanism for Biomedical Applications in Wireless Body Area Sensor Networks,” *J. Sensors*, vol. 2016, pp. 1–17, 2016.
[111] S. van Roy *et al.*, “Dynamic Channel Modeling for Multi-Sensor Body Area Networks,” *IEEE Trans. Antennas Propag.*, vol. 61, no. 4, pp. 2200–2208, Apr. 2013.
[112] E. Reusens *et al.*, “Characterization of on-body communication channel and energy efficient topology design for wireless body area networks.,” *IEEE Trans. Inf. Technol. Biomed.*, vol. 13, no. 6, pp. 933–45, Nov. 2009.
[113] N. Katayama, K. Takizawa, and T. Aoyagi, “Channel model on various frequency bands for wearable Body Area Network,” in *2008 First International Symposium on Applied Sciences on Biomedical and Communication Technologies*, 2008, pp. 1–5.
[114] Y. Chen and A. Terzis, “On the Implications of the Log-normal Path Loss Model : An Efficient Method to Deploy and Move Sensor Motes,” in *SenSys ’11 Proceedings of the 9th ACM Conference on Embedded Networked Sensor Systems*, 2011, pp. 26–39.
[115] L. Roelens, “Path loss model for wireless narrowband communication near biological tissue,” in *6th UGent-FirW Doctoraatssymposium, Interactive poster session, paper nr. 120*, 2005, no. 120, pp. 5–6.
[116] L. Roelens, S. Vand den Bulcke, W. Joseph, and G. Vermeeren, “Path loss model for wireless narrowband communication above flat phantom,” *Electron. Lett.*, vol. 42, no. 1, pp. 10–11, 2006.
[117] Theodore S. Rappaport, *Wireless Communications Principles And Practice 2Nd Edition*, 2nd ed. Prentice Hall PTR Upper Saddle River, NJ, USA, 2002.
[118] A. ; Y. H. Alomainy, “Radio channel models for UWB body-centric networks with compact planar antenna,” in *IEEE Antennas and Propagation Society International Symposium 2006*, 2006, pp. 2173–2176.
[119] R. D’Errico and L. Ouvry, “A Statistical Model for On-Body Dynamic Channels,” *Int. J. Wirel. Inf. Networks*, vol. 17, no. 3–4, pp. 92–104, Sep. 2010.
[120] K. Y. Yazdandoost, “IEEE P802.15 working group for wireless personal area networks (WPANs): channel model for body area network (BAN),” IEEE802. 15. 6 technical contribution, document ID: 15-08-078i0-09-0006, 2009.
[121] S. L. Cotton and W. G. Scanlon, “Characterization of the On-Body Channel in an Outdoor Environment at 2 . 45 GHz,” in *EuCAP 2009. 3rd European Conference on Antennas and Propagation*, 2009, pp. 722–725.
[122] D. Smith, L. Hanlen, D. Miniutti, J. Zhang, D. Rodda, and B. Gilbert, “Statistical characterization

of the dynamic narrowband body area channel," in *2008 First International Symposium on Applied Sciences on Biomedical and Communication Technologies*, 2008, pp. 1–5.
[123] V. G. Chaganti, S. Member, D. B. Smith, and L. W. Hanlen, "Second-Order Statistics for Many-Link Body Area Networks," *IEEE Antennas Wirel. Propag. Lett.*, vol. 9, pp. 322–325, 2010.
[124] S. L. Cotton, G. A. Conway, and W. G. Scanlon, "A Time-Domain Approach to the Analysis and Modeling of On-Body Propagation Characteristics Using Synchronized Measurements at 2 . 45 GHz," *IEEE Trans. Antennas Propag.*, vol. 57, no. 4, pp. 943–955, 2009.
[125] D. B. Smith, J. Zhang, L. W. Hanlen, and D. Miniutti, "Temporal correlation of dynamic on-body area radio channel," *Electron. Lett.*, vol. 45, no. 24, pp. 1212–1213, 2009.
[126] D. B. Smith, D. Miniutti, and L. W. Hanlen, "Characterization of the Body-Area Propagation Channel for Monitoring a Subject Sleeping," *IEEE Antennas Propag. Mag.*, vol. 59, no. 11, pp. 30–34, 2011.
[127] S. L. Cotton, R. D'Errico, and C. Oestges, "A Review of Radio Channel Models for Body Centric Communications," *Radio Sci.*, vol. 49, no. 6, pp. 371–388, May 2014.
[128] K. S. Prabh and J. Hauer, "Opportunistic Packet Scheduling in Body Area Networks," in *Proceeding EWSN'11 Proceedings of the 8th European conference on Wireless sensor networks*, 2011, pp. 1–16.
[129] Y. I. Nechayev, P. S. Hall, I. Khan, and C. C. Constantinou, "Wireless channels and antennas for body-area networks," in *2010 Seventh International Conference on Wireless On-demand Network Systems and Services (WONS)*, 2010, pp. 137–144.
[130] J. Hauer, "Leveraging Human Mobility for Communication in Body Area Networks," *J. ACM Trans. Sens. Networks*, vol. 10, no. 3, 2014.
[131] R. Fu, Y. Ye, and K. Yang Ning, Pahlavan, "Doppler spread analysis of human motions for Body Area Network applications," in *2011 IEEE 22nd International Symposium on Personal, Indoor and Mobile Radio Communications*, 2011, pp. 2209–2213.
[132] M. Kim and J.-I. Takada, "Statistical Model for 4.5-GHz Narrowband On-Body Propagation Channel With Specific Actions," *IEEE Antennas Wirel. Propag. Lett.*, vol. 8, pp. 1250–1254, 2009.
[133] C. Oliveira and L. M. Correia, "A Statistical Model to Characterize User Influence in Body Area Networks," in *2010 IEEE 72nd Vehicular Technology Conference - Fall*, 2010, pp. 1–5.
[134] M. Lauzier, P. Ferrand, and A. Fraboulet, "Full Mesh Channel Measurements on Body Area Networks under Walking Scenarios," in *European Conference on Antennas and Propagation (EuCAP)*, 2013, pp. 3508–3512.
[135] M. Vallejo, J. R. Piorno, and J. L. A. Rodrigo, "A Link Quality Estimator for Power-Efficient Communication Over On-Body Channels," in *2014 12th IEEE International Conference on Embedded and Ubiquitous Computing*, 2014, pp. 250–257.
[136] C. Guo, R. V. Prasad, and M. Jacobsson, "Packet Forwarding with Minimum Energy Consumption in Body Area Sensor Networks," in *2010 7th IEEE Consumer Communications and Networking Conference*, 2010, pp. 1–6.
[137] weilin Zang and Y. Li, "Gait Cycle Driven Transmission Power Control Scheme for Wireless Body Area Network," *IEEE J. Biomed. Heal. Informatics*, vol. 2194, no. c, pp. 1–1, 2017.
[138] B. Moulton, L. Hanlen, J. Chen, G. Croucher, L. Mahendran, and A. Varis, "Body-Area-Network transmission power control using variable adaptive feedback periodicity," in *2010 Australian Communications Theory Workshop (AusCTW)*, 2010, pp. 139–144.
[139] T. Guan, C. Yi, D. Qiao, L. Xu, and Y. Li, "PID-Based Transmission Power Control For Wireless Body Area Network," in *International Conference on Signal Processing (ICSP)*, 2014, pp. 1643–1648.
[140] W. Gao, B. Jiao, G. Yang, W. Hu, and J. Liu, "Transmission Power Control for IEEE 802.15.6 Body Area Networks," *ETRI J.*, vol. 36, no. 2, pp. 313–316, 2014.
[141] F. Di Franco, Y. Ge, and I. Tinnirello, "On-body and Off-body Transmit Power Control in IEEE 802.15.6 Scheduled Access Networks," in *International Symposium on Personal, Indoor, and Mobile Radio Communication (PIMRC)*, 2014, pp. 1254–1258.
[142] F. Di Franco, C. Tachtatzis, I. Tinnirello, R. C. Atkinson, and I. A. Glover, "Channel estimation and transmit power control in wireless body area networks," *IET Wirel. Sens. Syst.*, vol. 5, no. 1, pp. 11–19, Feb. 2015.

[143] M. Vallejo, J. Recas, and J. Ayala, “Proactive and Reactive Transmission Power Control for Energy-Efficient On-Body Communications,” *Sensors*, vol. 15, no. 3, pp. 5914–5934, Mar. 2015.
[144] D. Fernandes *et al.*, “Energy Saving Mechanism for a Smart Wearable System : Monitoring Infants during the Sleep,” in *IEEE International Conference on Industrial Technology*, 2016, pp. 1932–1937.
[145] W. Zang, S. Zhang, and Y. Li, “An Accelerometer-Assisted Transmission Power Control Solution for Energy-Efficient Communications in WBAN,” *IEEE J. Sel. Areas Commun.*, vol. 34, no. 12, pp. 3427–3437, Dec. 2016.
[146] D. B. Smith, L. W. Hanlen, and D. Miniutti, “Transmit power control for wireless body area networks using novel channel prediction,” in *2012 IEEE Wireless Communications and Networking Conference (WCNC)*, 2012, pp. 684–688.
[147] J. Dong and D. Smith, “Joint relay selection and transmit power control for wireless body area networks coexistence,” in *2014 IEEE International Conference on Communications (ICC)*, 2014, pp. 5676–5681.
[148] R. Kazemi, R. Vesilo, E. Dutkiewicz, and Ren Ping Liu, “Reinforcement learning in power control games for internetwork interference mitigation in Wireless Body Area Networks,” in *2012 International Symposium on Communications and Information Technologies (ISCIT)*, 2012, pp. 256–262.
[149] Z. Zhang, H. Wang, C. Wang, and H. U. A. Fang, “Interference Mitigation for Cyber-Physical Wireless Body Area Network System Using Social Networks,” *IEEE Trans. Emerg. Top. Comput.*, vol. 1, no. April, pp. 121–132, 2013.
[150] L. Zou, B. Liu, C. Chen, and C. W. Chen, “Bayesian game based power control scheme for inter-WBAN interference mitigation,” in *2014 IEEE Global Communications Conference*, 2014, pp. 240–245.
[151] E. Spanakis, V. Sakkalis, K. Marias, and A. Traganitis, “Cross Layer Interference Management in Wireless Biomedical Networks,” *Entropy*, vol. 16, no. 4, pp. 2085–2104, Apr. 2014.
[152] M. Mittal and D. K. Chauhan, “Cost Effective Security Solutions for Mobility in Wireless Body Area Networks,” *Int. J. New Innov. Eng. Technol.*, vol. 3, no. 3, pp. 31–37, 2015.
[153] J. I. E. Dong, D. B. Smith, L. W. Hanlen, and N. Ict, “Socially Optimal Coexistence of Wireless Body Area Networks Enabled by a Non-Cooperative Game,” *ACM Trans. Sens. Networks*, vol. 12, no. 4, pp. 1–26, 2016.
[154] S. Xiao, V. Sivaraman, and A. Burdett, “Adapting Radio Transmit Power in Wireless Body Area Sensor Networks,” in *Proceedings of the 3rd International ICST Conference on Body Area Networks*, 2008, p. 14.
[155] D. B. Smith, D. Miniutti, L. W. Hanlen, D. Rodda, and B. Gilbert, “Dynamic Narrowband Body Area Communications: Link-Margin Based Performance Analysis and Second-Order Temporal Statistics,” in *2010 IEEE Wireless Communication and Networking Conference*, 2010, pp. 1–6.
[156] T. H. Cormen, C. E. Leiserson, R. L. Rivest, and C. Stein, *Introduction to Algorithms*, 3r ed. The MIT Press, 2009.
[157] D. E. Knuth, *The Art of Computer Programming, Volume 3: Sorting and Searching*, 3rd ed. Addison-Wesley, 1998.
[158] M. Cheffena, “Time-varying on-body wireless channel model during walking,” *EURASIP J. Wirel. Commun. Netw.*, vol. 2014, no. 1, p. 29, Dec. 2014.
[159] K. G. Dangi and S. P. Panda, “Challenges in Wireless Body Area Network-A survey,” in *2014 International Conference on Reliability Optimization and Information Technology (ICROIT)*, 2014, pp. 204–207.
[160] L. H. a. Correia, D. F. Macedo, A. L. dos Santos, A. a. F. Loureiro, and J. M. S. Nogueira, “Transmission power control techniques for wireless sensor networks,” *Comput. Networks*, vol. 51, no. 17, pp. 4765–4779, 2007.
[161] D. Gavidia and M. van Steen, “A probabilistic replication and storage scheme for large wireless networks of small devices,” in *IEEE International Conference on Mobile Ad Hoc and Sensor Systems*, 2008, pp. 469–476.
[162] Hongwei Zhang, A. Arora, and P. Sinha, “Link Estimation and Routing in Sensor Network Backbones: Beacon-Based or Data-Driven?,” *IEEE Trans. Mob. Comput.*, vol. 8, no. 5, pp. 653–

667, May 2009.
[163] G. R. Tsouri, A. Prieto, and N. Argade, “On Increasing Network Lifetime in Body Area Networks Using Global Routing with Energy Consumption Balancing,” *Sensors*, vol. 12, no. 12, pp. 13088–13108, Sep. 2012.
[164] Y. T. Y. Tan, M. C. Vuran, and S. Goddard, “Spatio-Temporal Event Model for Cyber-Physical Systems,” in *2009 29th IEEE International Conference on Distributed Computing Systems Workshops*, 2009, pp. 44–50.
[165] A. P. Catarino, A. M. Rocha, H. Carvalho, and M. J. Dias, “Electrodes based on textile substrates,” EP2671506 B1, Sep-2013.
[166] J. Lage, A. Catarino, H. Carvalho, and A. Rocha, “Smart Shirt with Embedded Vital Sign and Moisture Sensing,” in *The First International Conference on Smart Portable, Wearable, Implantable and Disability-oriented Devices and Systems*, 2015, no. c, pp. 25–30.
[167] H. Carvalho, a. P. Catarino, A. Rocha, and O. Postolache, “Health monitoring using textile sensors and electrodes: An overview and integration of technologies,” in *2014 IEEE International Symposium on Medical Measurements and Applications (MeMeA)*, 2014, pp. 1–6.
[168] S. L. Cotton, S. Member, and W. G. Scanlon, “Higher Order Statistics for Lognormal Small-Scale Fading in Mobile Radio Channels,” *IEEE Antennas Wirel. Propag. Lett.*, vol. 6, pp. 540–543, 2007.
[169] C. Ferrer, D. Torres, and M. E. Hernández-Dı´az, “Using dynamic time warping of T0 contours in the evaluation of cycle-to-cycle Pitch Detection Algorithms,” *Pattern Recognit. Lett.*, vol. 31, no. 6, pp. 517–522, Apr. 2010.
[170] Texas Instruments, “A USB-Enabled System-On-Chip Solution for 2.4-GHz IEEE 802.15.4 and ZigBee Applications,” 2010.
[171] M. Buragohain, “Adaptive Network based Fuzzy Inference System (ANFIS) as a Tool for System Identification with Special Emphasis on Training Data Minimization,” Indian Institute of Technology Guwahati, 2008.
[172] I. Heazlewood, J. Walsh, M. Climstein, J. Kettunen, K. Adams, and M. DeBeliso, “A Comparison of Classification Accuracy for Gender Using Neural Networks Multilayer Perceptron (MLP), Radial Basis Function (RBF) Procedures Compared to Discriminant Function Analysis and Logistic Regression Based on Nine Sports Psychological Constructs t,” in *10th International Symposium on Computer Science in Sports (ISCSS). Advances in Intelligent Systems and Computing*, vol. 392, P. Chung, A. Soltoggio, C. W. Dawson, Q. Meng, and M. Pain, Eds. Cham: Springer International Publishing, 2016, pp. 93–101.
[173] L. A. Zadeh, “Fuzzy sets,” *Inf. Control*, vol. 8, no. 3, pp. 338–353, 1965.
[174] L. A. Zadeh, “Outline of a New Approach to the Analysis of Complex Systems and Decision Processes,” *IEEE Trans. Syst. Man. Cybern.*, vol. SMC-3, no. 1, pp. 28–44, 1973.
[175] J.-S. R. Jang, C.-T. Sun, and E. Mizutani, “Neuro-Fuzzy and Soft Computing—A Computational Approach to Learning and Machine Intelligence,” *IEEE Trans. Automat. Contr.*, vol. 42, no. 10, pp. 1482–1484, 1997.
[176] Y. Chai, L. Jia, and Z. Zhang, “Mamdani Model Based Adaptive Neural Fuzzy Inference System and its Application in Traffic Level of Service Evaluation,” in *2009 Sixth International Conference on Fuzzy Systems and Knowledge Discovery*, 2009, vol. 3, no. 3, pp. 555–559.
[177] A. Al-Hmouz, Jun Shen, R. Al-Hmouz, and Jun Yan, “Modeling and Simulation of an Adaptive Neuro-Fuzzy Inference System (ANFIS) for Mobile Learning,” *IEEE Trans. Learn. Technol.*, vol. 5, no. 3, pp. 226–237, Jul. 2012.
[178] A. M. Abdulshahed, A. P. Longstaff, and S. Fletcher, “The application of ANFIS prediction models for thermal error compensation on CNC machine tools,” *Appl. Soft Comput.*, vol. 27, pp. 158–168, Feb. 2015.
[179] J.-S. R. Jang, “ANFIS: adaptive-network-based fuzzy inference system,” *IEEE Trans. Syst. Man. Cybern.*, vol. 23, pp. 665–685, 1993.
[180] R. Pereira, A. Fagundes, R. Melício, V. M. F. Mendes, J. Figueiredo, and J. C. Quadrado, “Fuzzy Subtractive Clustering Technique Applied to Demand Response in a Smart Grid Scope,” *Procedia Technol.*, vol. 17, pp. 478–486, 2014.
[181] A. Priyono, M. Ridwan, A. J. Alias, R. A. O. K. Rahmat, A. Hassan, and M. A. Mohd. Ali, “Generation of Fuzzy Rules with Subtractive Clustering,” *J. Teknol.*, vol. 43, no. 1, pp. 143–153,

Dec. 2005.
[182] S. L. Chiu, “Selecting Input Variables for Fuzzy Models,” *J. Intell. Fuzzy Syst.*, vol. 4, no. 4, pp. 243–256, 1996.
[183] J.-S. R. Jang, “Input selection for ANFIS learning,” in *IEEE International Conference on Fuzzy Systems*, 1996, pp. 1493–1499.
[184] W. Hu, E. Charry, M. Umer, A. Ronchi, and S. Taylor, “An inertial sensor system for measurements of tibia angle with applications to knee valgus/varus detection,” in *2014 IEEE Ninth International Conference on Intelligent Sensors, Sensor Networks and Information Processing (ISSNIP)*, 2014, pp. 1–6.
[185] F. L. Markley, “Fast Quaternion Attitude Estimation from Two Vector Measurements,” *J. Guid. Control. Dyn.*, vol. 25, no. 2, pp. 411–414, Mar. 2002.
[186] A. D. Young, “Comparison of Orientation Filter Algorithms for Realtime Wireless Inertial Posture Tracking,” in *2009 Sixth International Workshop on Wearable and Implantable Body Sensor Networks*, 2009, pp. 59–64.
[187] D. Simon, “kalman Filtering,” *Embed. Syst. Program.*, vol. 14, no. 6, pp. 72–79, 2001.
[188] I. H. Lopez-Nava and A. Munoz-Melendez, “Estimation of Angles from Upper and Lower Limbs for Recognition of Human Gestures using Wireless Inertial Sensors,” Puebla, Mexico, 2015.
[189] K. J. Chin, M. K. Karmakar, and P. Peng, “Ultrasonography of the Adult Thoracic and Lumbar Spine for Central Neuraxial Blockade,” *Anesthesiology*, vol. 114, no. 6, pp. 1459–1485, Jun. 2011.
[190] T. Aoyagi, Iswandi, M. Kim, J. Takada, K. Hamaguchi, and R. Kohno, “Body motion and channel response of dynamic body area channel,” in *Proceedings of the 5th European Conference on Antennas and Propagation EUCAP*, 2011, pp. 3138–3142.
[191] A. Ferreira, D. Fernandes, A. Catarino, and J. Monteiro, “Performance Analysis of ToA-Based Positioning Algorithms for Static and Dynamic Targets with Low Ranging Measurements,” *Sensors*, vol. 17, no. 8, p. 1915, Aug. 2017.
[192] D. Hasenfratz, O. Saukh, S. Sturzenegger, and L. Thiele, “Participatory Air Pollution Monitoring Using Smartphones,” in *2nd International Workshop on Mobile Sensing*, 2012, pp. 1–5.
[193] D. Keenan, J. Mastrotoraro, and G. Voskanyan, “Delays in Minimally Invasive Continuous Glucose Monitoring Devices :,” *Diabetes Sci Technol.*, vol. 3, no. 5, pp. 1207–1214, 2009.
[194] A. Woo and D. Culler, “Evaluation of Efficient Link Reliability Estimators for Low-Power Wireless Networks,” *Ad Hoc Networks*, vol. 27, no. C, pp. 1–20, 2003.
[195] O. Prakash, V. Laguri, A. Pandey, A. Kumar, and A. Kumar, “Review on various modelling techniques for the solar dryers,” *Renew. Sustain. Energy Rev.*, vol. 62, pp. 396–417, Sep. 2016.